Preparation of cellulose oligomers by acid hydrolysis

Wei Li

THÈSE

Pour obtenir le grade de

DOCTEUR DE L'UNIVERSITE GRENOBLE ALPES

Spécialité : **Chimie Physique Moléculaire et Structurale**

Arrêté ministériel : 25 mai 2016

Présentée par

Wei LI

Thèse dirigée par **Yoshiharu NISHIYAMA, CNRS**
et co-encadrée par **Yu OGAWA, CNRS**

préparée au sein du **Laboratoire CEntre de Recherche sur les Macromolécules Végétales**
dans **l'École Doctorale Chimie et Sciences du Vivant**

Préparation d'oligomères de cellulose par hydrolyse acide

Preparation of cellulose oligomers by acid hydrolysis

Thèse soutenue publiquement le **26 juillet 2021**,
devant le jury composé de :

Monsieur Redouane BORSALI
DIRECTEUR DE RECHERCHE, CNRS délégation Alpes, Président du jury

Monsieur Akira ISOGAI
PROFESSEUR, The University of Tokyo, Rapporteur

Monsieur Eero KONTTURI
PROFESSEUR ASSOCIE, AALTO Yliopisto, Rapporteur

Madame Antje POTTHAST
PROFESSEUR, Universität für Bodenkultur Wien, Examinatrice

Madame Christine CHIRAT
PROFESSEUR DES UNIVERSITES, Grenoble INP, Examinatrice

Acknowledgements

Primarily, I would like to thank my two esteemed supervisors Dr. Yoshiharu Nishiyama and Dr. Yu Ogawa who give me the chance to work on this project. I am grateful for all their valuable supervision, support and tutelage throughout my PhD study.

My gratitude extends to Dr. Issei Otsuka, Prof. Gérard Mortha, Mr. Killian Barry and Mr. Jessie Muamba for the helps in carbanilation reactions and size exclusion chromatography measurements. Additionally, I would like to thank Dr. William Helbert, Dr. Isabelle Morfin and Prof. Gérard Mortha for being the members of my thesis CSI committee and the illuminating discussions, and to Dr. Isabelle Morfin also for the help in synchrotron. My appreciation also goes out to Dr. Karim Mazeau for building the molecular models. Thanks to Dr. Henri Chanzy for the help in literatures and nice discussions. I also thank Dr. Christine Lancelon-Pin for the microscopy tests. Thanks to Prof. Emily Cranston and Dr. Fangbo Lin for providing some cellulose nanocrystals to estimate the sulfate content. I would like to thank Dr. Jean-luc Putaux for the correction of thesis in French and the helpful discussions. In addition, I want to express my gratitude to Prof. Pan Chen and Dr. Bruno Jean for their help and nice advices during my study. I also thank Ms. Stéphanie Pradeau, Mr. Pierre Sailler and Ms. Patricia Chaud for helping me in sample preparation and technical support. Many thanks to Ms. Isabelle Jeacomine for helping me with NMR test, Ms. Laure Fort for the help in mass spectrometry, Ms. Laurine Buon and Mr. Eric Bayma for measuring dn/dc values, and Dr. Javier Perez for the help in SOLEIL synchrotron.

In addition, I would like to express my sincere gratitude to Prof. Akira Isogai, Prof. Antje Potthast, Prof. Eero Kontturi, Prof. Christine Chirat and Dr. Redouane Borsali for participating my defence jury, reviewing this thesis and offering massive valuable comments and suggestions.

Thanks to my lovely friends, team members and colleagues — Pierangelo Mora Castille, Jun Zhang, Wanqiu Liu, Chunjing Ma, Ge Zhu, Hong Li, Shun Yao, Dr. Fangcheng Liang, Dr. Yoko Otsuka, Jean Sebastian, Dr. Cong-Anh-Khanh Le, Dr. Julien Leguy, Dr. Yotam Navon, etc. for their encouragement and support all through my studies, and a cherished time spent together in the lab. Specially, I am deeply grateful to Dr. Christine Lancelon-Pin and Dr. Henri Chanzy for the helps when my leg was broken. Finally, I would like to express my gratitude to my parents and my rest family members for their tremendous understanding, support and encouragement.

In the end, I want to thank China Scholarship Council and Polynat for the financial support that allow me to conduct this study.

Table of Content

List of abbreviations **1**
Summary **3**
Résumé des travaux de thèse **7**
Chapter I. Introduction **17**
I.1. Sources and applications of cellulose 17
I.2. Chemical and crystalline structure of cellulose 18
I.3. Cellulose oligomers 19
I.4. Preparation of cellulose oligomers 20
I.4.1. Synthetic methods 20
I.4.1.1. Chemical synthesis 21
I.4.1.2. Enzymatic synthesis 21
I.4.2. Depolymerization methods 22
I.4.2.1. Enzymatic depolymerization 23
I.4.2.2. Acetolysis 23
I.4.2.3. Pyrolysis 24
I.4.2.4. Mechanical depolymerization 24
I.4.2.5. Acid hydrolysis 24
I.4.3. Fractionation of cellulose oligomers 27
I.5. Determination of degree of polymerization of cellulose oligomers 29
I.5.1. Derivatization of cellulose 30
I.5.2. Characterization methods of molecular weight 32
I.5.2.1. End group method 33
I.5.2.2. Mass spectroscopy 33
I.5.2.3. Viscometry 34
I.5.2.4. Static light scattering 35
I.5.2.5. Size exclusion chromatography 36
I.6. Solvents for cellulose 37
I.7. Cellulose-complex crystals 39
I.7.1 Cellulose/alkaline complex 39
I.7.2. Cellulose/ammonia complex 42
I.7.3. Cellulose/ammonium hydroxides complex 43
I.7.4. Cellulose/amine complex 43
I.7.5. Cellulose hydrate complex 46
I.7.6. Cellulose/ionic liquid complex 47
I.7.7. Other cellulose complexes 47
I.8. Motivation and purpose 48

Chapter II. Materials and methods 53
II.1. Materials 53
II.2. Preparation of cellulose oligomers..... 53
II.2.1 Dissolution and hydrolysis of cellulose in phosphoric acid 54
II.2.2 Dissolution and hydrolysis of cellulose in sulfuric acid..... 54
II.2.3 Regeneration 55
II.2.3.1 Regeneration of cellulose in water and in organic solvents 55
II.2.3.2. Neutralization of the regeneration mixtures..... 55
II.3. Carbanilation of cellulose 56
II.3.1. Carbanilation in DMF 56
II.3.2. Purification of cellulose carbanilates by washing with methanol 56
II.3.3. Purification of cellulose carbanilates by dialysis 56
II.3.4. Carbanilation for DP mearsurement..... 57
II.4. Characterization..... 57
II.4.1. Polarized light microscopy..... 57
II.4.1.1. Principle..... 57
II.4.1.2. Experimental procedure..... 58
II.4.2. X-ray diffraction 58
II.4.2.1. Principles 58
II.4.2.2. Experimental procedure..... 61
II.4.3. Size exclusion chromatography 63
II.4.3.1. Principle..... 63
II.4.3.2. Experimental procedure..... 67
II.4.4. Elemental analysis..... 68
II.4.4.1. Principles 68
II.4.4.2. Experimental procedure..... 69
II.4.5. Nuclear magnetic resonance spectroscopy..... 69
II.4.5.1. Principle..... 69
II.4.5.2. Experimental procedure..... 73
II.4.5.3 Measurement of degree of polymerization by NMR 73
II.4.5.4 Measurement of degree of substitution by NMR..... 74
II.4.6. Fourier-transform infrared spectroscopy..... 74
II.4.6.1. Principle..... 74
II.4.6.2. Experimental procedure..... 75
II.4.7. Mass spectroscopy 76
II.4.7.1. Principle..... 76
II.4.7.2. Experimental procedure..... 76
Chapter III. Dissolution and swelling of cellulose in acid..... 81

III.1. Introduction 81
III.2. Dissolution of cellulose in acid 82
III.3. Swelling of cellulose in acid by X-ray diffraction 84
III.4. Conclusions 93
Chapter IV. Derivatization of cellulose 97
IV.1. Introduction 97
IV.2. Methods 97
IV.2.1. Preparation of fraction A 97
IV.2.2. Nitration of cellulose 98
IV.2.3. Carbanilation of cellulose 98
IV.3. Comparison between nitration and carbanilation 98
IV.4. Study on carbanilation and determination of substitution degree 101
IV.4.1. Determination of substitution degree of cellulose carbanilate 102
IV.4.1.1. Side products 103
IV.4.1.2. DS estimation based on elementary analysis 106
IV.4.1.3. DS estimation based on ^{1}H NMR spectroscopy 107
IV.4.2. Carbanilation with different concentrations of phenylisocyanate 110
IV.4.3. Optimization of carbanilation 119
IV.4.3.1. Carbanilation time 119
IV.4.3.2. State of phenylisocyanate & usage of argon gas 121
IV.5. Conclusions 122
Chapter V. Comparison of characterization techniques for DP determination 127
V.1. Introduction 127
V.2. Liquid-state ^{1}H NMR spectroscopy 128
V.3. Quantitative DP analysis by Solid-state ^{13}C CP/MAS NMR 129
V.4. Mass spectroscopy 134
V.5. Size exclusion chromatography 140
V.6. Conclusions 146
Chapter VI. Tunable DP and DP distribution of cellulose oligomers 149
VI.1. Introduction 149
VI.2. Effect of hydrolysis conditions on fraction A 150
VI.3. Effect of regeneration conditions on fraction B 155
VI.3.1. Fraction B from phosphoric acid hydrolysis 155
VI.3.2. Fraction B precipitated from isopropanol and methanol 160
VI.4. Effect of regeneration conditions on fraction A 167
VI.4.1. Solution/precipitant ratio 168
VI.4.2. Regeneration temperature and pH 169

VI.4.3. Regeneration time 172
VI.5. Substitution of phosphoric acid by sulfuric acid 174
VI.5.1. Fraction A from sulfuric acid hydrolysis 175
VI.5.2. Fraction B from sulfuric acid hydrolysis 178
VI.5.3. Fraction A regenerated in salt solutions 185
VI.6. Conclusions 188
Chapter VII. Mechanism on producing monodisperse cellulose oligomers 193
VII.1. Introduction 193
VII.2. Hypothesis-1 about how regenerated cellulose become monodisperse 193
VII.3. Crystalization of cellulose during regeneration 195
VII.3.1. Synchrotron X-ray scattering 195
VII.3.2. Lab source X-ray diffraction 197
VII.4. Hypothesis-2 about how regenerated cellulose become monodisperse 202
VII.5. Conclusions 205
Chapter VIII. Conclusions and perspectives 209
VIII.1. General conclusions 209
VIII.2. Perspectives 211
Appendix 1. Supporting information of Chapter II & IV 225
Appendix 1.1. Comparison between two phenylisocyanate 225
Appendix 2. Supporting information of Chapter III 227
Appendix 2.1. Exhaustive search of unit cell parameters 227
Appendix 3. Supporting information of Chapter V 231
Appendix 3.1 Kinetics of cross-polarization between ^{1}H and ^{13}C 231
Appendix 4. Supporting information of Chapter VI 235
Appendix 4.1. Formation of cellulose IV_{II} 235
Appendix 4.2. Estimation of sulfur content based on ATR-FTIR. 236
Appendix 4.3. ^{1}H-NMR of Fraction B-p and Fraction B-s in DMSO-d6 239
Appendix 4.4. DP information of fraction A regenerated from salt solutions 241
References 245

List of abbreviations

DP: Degree of polymerization

DS: Degree of substitution

NMR: Nuclear magnetic resonance

SP/MAS: Single pulse magic angle spinning

CP/MAS: Cross polarization magic angle spinning

ATR-FTIR: Attenuated total reflectance fourier-transform infrared spectroscopy

MALDI-TOF: Matrix assisted laser desorption ionization-time of flight

MS: Mass spectrometry

SEC: Size exclusion chromatography

WAXS: Wide angle X-ray scattering

SAXS: Small angle X-ray scattering

XRD: X-ray diffraction

LS: Light scattering

EA: Elemental analysis

H_3PO_4: Phosphoric acid

H_2SO_4: Sulfuric acid

DMSO: Dimethylsulfoxide

HCl: Hydrochloric acid

LiCl: Lithium chloride

NaCl: Sodium chloride

KCl: Potassium chloride

Na_2SO_4: Sodium sulfate

DMF: Dimethylformamide

PI: Phenylisocyanate

MCC: Microcrystalline cellulose

DMAc: Dimethylacetamide

AGU: Anhydroglucopyranose

Đ: Polydispersity index

Summary

Cellulose oligomer has a high potential in various fields such as food and cosmetic industries, and also as a model substance of cellulose. However, so far, its use is very limited due to its poor availability. Only oligomers with a limited molecular weight range are commercially available in small quantities mostly for research purposes. The main reason of this situation is the lack of an efficient production method of cellulose oligomers. An ideal production method should be simple and scalable, so that the oligomers can be produced in bulk quantities. Furthermore, the physicochemical properties of oligomers depend largely on their molecular weights, so a good control of the molecular weight distribution is desirable in such a method.

In this thesis, concentrated acid hydrolysis-based method is investigated for cellulose oligomer production. The method is simple, scalable and aqueous-solution based. The molecular weight distribution can be controlled by solubility-based fractionation during the regeneration of cellulose oligomers. In particular, there are three goals in this thesis: (1) having a better understand of the mechanisms in the swelling, dissolution, hydrolysis and regeneration processes; (2) preparing cellulose oligomers with controlled molecular weight and molecular weight distribution by acid hydrolysis; (3) establishing characterization methods of molecular weight distribution of cellulose oligomers.

In Chapter III, the swelling behaviors of cellulose in sulfuric acid were followed at -20 ˚C using X-ray diffraction. At low temperature, cellulose-sulfuric acid crystalline complex was found as the first example of cellulose-acid crystallosolvate. This crystalline complex had an orthorhombic unit cell (a = 18.24 Å, b = 25.98 Å, c = 25.05 Å) that was composed of 4 cellulose chains, 48 sulfuric acid molecules and 144 water molecules. This complexation is acid-concentration dependent and occurs only above 62 wt%, indicating that the lack of water

molecules drives the complexation to form a stable hydration state of sulfuric acid.

In Chapters IV and V, to characterize the molecular weight of cellulose oligomers, derivatization methods of cellulose and the different characterization methods were compared. Compared to nitration, carbanilation was more suitable for SEC since light scattering is more sensitive to cellulose carbanilate than to cellulose nitrate. For determining the DS of cellulose carbanilate the liquid state ^{1}H NMR-based method using N-H proton intensity was found more reliable due to its smaller error than other methods such as the elemental analysis. As for characterization methods for DP and DP distribution, four different methods were compared, namely liquid state ^{1}H and solid-state ^{13}C CP/MAS NMR, MALDI-TOF MS spectroscopies and SEC. SEC was found to be suitable for relatively higher molecular weight oligomer fractions, while other three spectroscopic methods were suitable for lower molecular weight fractions.

In Chapter VI, the effects of various hydrolysis conditions, regeneration conditions, and acid species were investigated on the DP and DP distribution of cellulose. Different conditions provide oligomers with different DP values ($5<DP_w<37$) and distributions as well as yields. For instance, H_3PO_4 hydrolysis, high temperature hydrolysis significantly shortens the preparation time: the cellulose oligomers obtained from hydrolysis at 23 ˚C for 42 days exhibited almost the same average DPs and yield as the cellulose oligomers from hydrolysis at 40 ˚C for 3 days. Cellulose solution regenerated in the same weight of water with the regeneration time of 24 hours showed a little change in average DP and DP distribution but a higher yield. Regeneration in an acidic environment at 70 ˚C resulted in narrower DP distribution, smaller average DP and smaller yield.

In Chapter VII, the resulting DP distribution from this oligomer production method is tentatively explained by a model based on random chain scission and a fractionation cutoff

based on the solubility of cellulose oligomers in a given solvent.

This thesis serves a solid basis for a better control of molecular weight distribution of cellulose oligomers from acid hydrolysis. The knowledge of characterization of cellulose oligomers in this thesis would also be useful for further investigations and utilization of cellulose oligomers in both industries and academic research communities.

Résumé des travaux de thèse

La cellulose est un homopolymère linéaire composé de résidus de β-D-glucopyranose liés par des liaisons glycosidiques β-(1-4). Elle est largement répandue dans la nature, principalement en tant que composant structurel des tissus de divers organismes, des plantes et des algues aux animaux et aux micro-organismes. Elle est largement utilisée dans notre vie quotidienne sous diverses formes telles que le papier, les fibres textiles et les additifs alimentaires. Les oligomères de cellulose sont des chaines de faible masse moléculaire dont le degré de polymérisation (DP) est généralement compris entre 2 et 30. Par rapport à la cellulose de masse moléculaire élevée, les oligomères de cellulose présentent une meilleure aptitude au traitement en raison de leur plus haute solubilité et de leur faible viscosité dans les solvants usuels. Ils sont également considérés comme une substance modèle de la cellulose pour étudier ses relations structure-propriété à la fois expérimentalement et *in silico*. Outre ces avantages, les oligomères de cellulose monodisperses ont un grand potentiel en tant qu'élément constitutif de nanomatériaux fonctionnels en raison de leurs extrémités réductrices réactives abondantes. Cependant, l'utilisation des oligomères de cellulose dans l'industrie est très limitée, principalement en raison de leur faible disponibilité et des méthodes de production fastidieuses.

Les méthodes de préparation des oligomères de cellulose peuvent être classées en méthodes synthétiques et méthodes de dégradation. Les méthodes de synthèse, y compris les synthèses chimique et enzymatique, sont des voies ascendantes pour produire des oligomères de cellulose à partir d'unités monomères ou dimères. Même si les méthodes de synthèse peuvent produire des oligomères de cellulose d'un DP ciblé avec une grande pureté, les processus de préparation impliquent généralement de

nombreuses étapes sophistiquées et longues, ce qui rend ces méthodes inadaptées à la production industrielle à grande échelle. Les méthodes de dégradation sont des voies permettant de produire des oligomères à partir de cellulose de haute masse moléculaire, notamment la dégradation enzymatique, l'acétolyse, la pyrolyse, la dépolymérisation mécanique et l'hydrolyse acide. Parmi elles, l'hydrolyse acide est une méthode de production simple et évolutive qui convient aux applications industrielles. Les acides minéraux concentrés, tels que les acides sulfurique et phosphorique, sont des réactifs d'hydrolyse intéressants pour la production d'oligomères de cellulose. Étant donné qu'ils sont des solvants directs de la cellulose de masse moléculaire élevée, la cellulose peut être efficacement hydrolysée lors de sa dissolution dans ces solutions aqueuses d'acide concentré. Isogai et Usuda [1] ont décrit une méthode d'hydrolyse à l'acide phosphorique et ont obtenu deux fractions d'oligomères de cellulose presque monodisperses avec, respectivement, des DP moyens de 15 (fraction insoluble dans l'eau, fraction A) et 7 (fraction insoluble dans le méthanol, fraction B). Inspiré par ce travail, l'objectif primordial de cette thèse était de produire des oligomères de cellulose avec une masse moléculaire moyenne et une distribution de masse moléculaire contrôlées, reposant sur une hydrolyse acide concentrée suivie d’un fractionnement basé sur la solubilité. En particulier, cette thèse avait trois objectifs : (1) mieux comprendre les mécanismes des processus de gonflement, de dissolution, d'hydrolyse et de régénération de la cellulose ; (2) contrôler la distribution de la masse moléculaire des oligomères de cellulose obtenus en faisant varier les conditions de préparation ; (3) établir des méthodes de caractérisation robustes de la distribution de la masse moléculaire des oligomères de cellulose.

Pour étudier le mécanisme moléculaire du gonflement et de la dissolution de la cellulose dans des solutions acides concentrées, l'évolution structurale de la cellulose immergée dans l'acide sulfurique durant séquences de traitements thermiques spécifiques a été suivie par diffusion des rayons X sur la ligne de lumière SWING du synchrotron SOLEIL (Gif-sur-Yvette). Nous avons constaté que la cellulose formait un complexe cristallin avec l'acide sulfurique à -20 ˚C à une concentration supérieure à 62 % en poids. Le complexe cristallin possède une maille élémentaire orthorhombique dont les paramètres sont a = 18,24 Å, b = 25,98 Å, c = 25,05 Å. Cette grande maille élémentaire contient 4 chaînes de cellulose, 48 molécules d'acide sulfurique et 144 molécules d'eau. La périodicité de 25 Å selon l'axe de fibre indique une conformation hélicoïdale d'ordre 5 des molécules de cellulose, qui est un cas assez rare. Les molécules d'acide sulfurique sont organisées de manière similaire à celle du cristal d'acide sulfurique tétrahydraté. Les groupements hydroxyles des chaines de cellulose sont susceptibles de participer à l'hydratation des molécules d'acide sulfurique avec les molécules d'eau dans la maille cristalline. La complexation ne se produit qu'au-dessus d'une concentration critique d'acide de 62 % en poids. Cette dépendance du gonflement des cristaux avec la concentration indique que le manque de molécules d'eau dans le système entraîne la complexation pour former un état d'hydratation stable de l'acide sulfurique.

La dérivatisation de la cellulose est essentielle pour caractériser la masse moléculaire puisque la cellulose est insoluble dans la plupart des solvants usuels. La carbanilation et la nitration sont deux méthodes de dérivatisation fréquemment utilisées pour mesurer la masse moléculaire de la cellulose. Elles ont d'abord été comparées en termes d'amélioration de la caractérisation des oligomères de la

cellulose. D'après les signaux de diffusion de la lumière et le rendement issu de la chromatographie d'exclusion de taille (SEC), la cellulose microcristalline nitrée (MCC, DP autour de 200) était plus soluble et stable dans le diméthylformamide (DMF) que dans le tétrahydrofurane (THF). Nous avons ensuite comparé les résultats SEC des oligomères de cellulose nitrés et carbanilés. Les oligomères de cellulose carbanilés ont donné des signaux de diffusion de la lumière beaucoup plus intenses que les oligomères de cellulose nitrés en raison de leur taille moléculaire et de leur valeur dn/dc plus élevées. Ainsi, la carbanilation a été choisie comme méthode de dérivatisation pour caractériser la masse moléculaire des oligomères de cellulose. Le degré de substitution (DS, ou le nombre de groupes phénylcarbamates par résidu de glucose) affecte la solubilité du carbanilate de cellulose et la précision de la mesure du DP de la cellulose par SEC. Nous avons comparé les deux méthodes les plus fréquemment utilisées pour détecter le DS, l'analyse élémentaire et la spectroscopie RMN ^{1}H. Il s'est avéré que l'estimation basée sur la RMN ^{1}H à l'état liquide est la plus fiable lorsqu'elle utilise les intensités intégrales du proton du carbamate (N-H) et du proton H1 attaché au carbone C1, par rapport à la méthode basée sur la RMN ^{1}H utilisant les protons aromatiques et le proton H1 combiné à l'analyse élémentaire. Ensuite, une carbanilation avec différentes concentrations de phénylisocyanate a été effectuée pour obtenir des carbanilates de cellulose avec trois valeurs DS différentes. Les carbanilates de cellulose avec des DS inférieurs à 2 contenaient encore des cristaux de cellulose de type I, ce qui rend ces carbanilates de cellulose à faible DS insolubles dans les solvants usuels. Les spectroscopies ^{13}C SP/MAS NMR et FT-IR à l'état solide se sont avérées efficaces pour estimer le DS de ces carbanilates de cellulose faiblement substitués. En outre, la cellulose entièrement carbanilisée a été

obtenue via une réaction de carbanilation dans le DMF avec du phénylisocyanate frais et l'utilisation d'argon gazeux.

Quatre méthodes analytiques (SEC, spectroscopie de masse par désorption ionisation laser assistée par matrice/temps de vol (MALDI-TOF MS), RMN du liquide et du solide), ont été comparées pour la détermination des oligomères de cellulose par DP. La RMN ^{1}H à l'état liquide, la RMN ^{13}C CP/MAS à l'état solide et la spectroscopie MALDI-TOF MS conviennent mieux à la caractérisation des oligomères de cellulose de faible masse moléculaire et de distribution de DP étroite. Alors que pour les oligomères de cellulose avec une masse moléculaire relativement élevée et une large distribution de DP, la SEC est un choix préférable par rapport aux autres méthodes spectroscopiques.

Enfin, nous avons tenté de contrôler le DP moyen et de la distribution de DP en faisant varier les conditions d'hydrolyse et de régénération/fractionnement. Pour l'hydrolyse à l'acide phosphorique, l'augmentation de la température d'hydrolyse de 23 à 40 ˚C pourrait considérablement raccourcir le temps de préparation. Avec une température d'hydrolyse à 23 ˚C, il a fallu 42 jours pour obtenir la fraction A avec un rendement de 44 %, un DP_w de 17,3 et un indice de polydispersité (PDI) de 1,21. Il n'a fallu que 3 jours pour l'hydrolyse à 40 ˚C pour obtenir une fraction similaire avec un rendement de 45 % avec un DP_w de 17,5 et une valeur PDI de 1,29. En faisant varier le rapport solution/précipitant, le mélange de régénération solution de cellulose/eau 1:1 a permis d'obtenir la fraction A avec un rendement supérieur de 7 % avec un DP moyen inférieur de 13 % par rapport au mélange solution de cellulose/eau 1:10. Le pH du mélange de régénération a également été modifié. Lors de la régénération à 23 ˚C, le rendement, le DP moyen et la distribution du DP ont peu

changé entre les environnements de régénération acide et neutralisé. Cependant, lorsqu'elle a été régénérée à 70 ˚C en milieu acide, la fraction A a été obtenue avec un rendement plus faible de 53 % avec un DP_w de 14,5 et un PDI de 1,26, tandis que l'environnement de régénération neutre a donné un rendement de 51 %, un DP_w de 26,0 avec un PDI de 1,69. La fraction A avec un temps de régénération de 24 h a été obtenue un rendement plus élevé que celle récupérée et lavée immédiatement après le mélange de la solution et de l'eau. Cependant, ces deux fractions n'ont présenté que peu de changement dans le DP moyen et la distribution du DP. L'acide sulfurique s'est avérée être un réactif d'hydrolyse plus puissant que l'acide phosphorique à la même température, et le temps d'hydrolyse requis à température ambiante était beaucoup plus court dans l'acide sulfurique que dans l'acide phosphorique. La fraction B hydrolysée par l'acide sulfurique a pu être dissoute dans le DMSO, avec pratiquement le même DP moyen que la fraction B hydrolysée par l'acide phosphorique avec un rendement légèrement supérieur et une distribution DP plus étroite. Les rendements de la fraction A régénérée à partir de différentes solutions salines ont été classés comme suit : Na_2SO_4 > KCl > NaCl > LiCl > HCl.

Sur la base de ces observations, nous avons discuté de la manière dont la cellulose régénérée devient monodisperse en utilisant une hydrolyse acide concentrée et un fractionnement basé sur la solubilité. La monodispersité de la fraction A préparée à température ambiante peut être expliquée par une hypothèse basée sur la scission aléatoire des chaînes et une limite de fractionnement due à la solubilité des oligomères de cellulose dans un solvant donné. Les résultats de la simulation basés sur cette hypothèse concordent bien avec les résultats expérimentaux en termes de DP moyens, de PDI et de rendement de la fraction A. Ainsi, nous considérons

provisoirement que la deuxième hypothèse offre une explication plausible à la question de savoir comment la cellulose régénérée est devenue monodisperse, bien que plusieurs hypothèses de la simulation puissent ne pas être correctes et doivent être étudiées plus en détail. Une hydrolyse supplémentaire après la régénération et la cristallisation des molécules de cellulose explique la plus grande monodispersité de la fraction A obtenue à 70 ˚C dans un environnement acide. Le mécanisme proposé met en lumière le contrôle ultérieur de la masse moléculaire et de la distribution de la masse moléculaire de la cellulose.

Les connaissances de la caractérisation des oligomères de cellulose dans cette thèse seront également utiles pour d'autres études et l'utilisation des oligomères de cellulose dans des contextes industriels et académiques.

Chapter I

Chapter I. Introduction

Cellulose, a renewable, biodegradable and biocompatible polysaccharide, is applied in the daily life of human beings throughout history. Sufficiently purified plant tissues with molecular formula as $C_6H_{10}O_5$ were discovered by Payen in 1838 [2], and it was first named as “cellulose” in a report from French Academy in 1839 [3]. Recently, cellulose has attracted considerable interest due to its good mechanical properties, low thermal expansion and high potentials in developing a more economic and sustainable substitution of materials based on fossil energy resources.

I.1. Sources and applications of cellulose

Cellulose widely exists in plants (such as wood, cotton etc.), algae, animals like tunicates, and microorganisms (bacteria, amoeba etc.). The annual production of cellulose by nature is estimated to be approximately 75 billion tons, and the annual industrial global production of cellulose pulp is about 180 million tons [4-6]. The cellulose market includes not only pulp, but also fibers, microcrystalline cellulose (MCC), nanocellulose, cellulose esters, cellulose ethers and other derivatives [7]. Cellulose pulp and cellulose fibers occupy the majority of the market share owing to their significant applications in textiles, paper & pulp, construction materials, pharmaceuticals and food industry. MCC, partially depolymerized cellulose with the size less than 5 μm, finds applications in medicine production, food products and cosmetics as an emulsifier, binder and fat replacement [8, 9]. Nanocelluloses, including bacterial cellulose, cellulose nanofibrils, and cellulose nanocrystals, are used in food, cosmetics, paints, oil & gas, construction and pharmaceutical industries [10]. Cellulose ethers form gel-like consistency when mixed with water and can be suitable for applications in food, paint, coating and construction industries [11]. Cellulose esters are

used in tobacco industry, yarns, LCD screens, paints and coatings [12-16].

I.2. Chemical and crystalline structure of cellulose

Cellulose is a linear homopolymer and consists of β-D-glucopyranose residues bound via β-(1-4) glycosidic bonds [17], as shown in Figure I.1a. The two opposite chain ends are chemically different: the so-called reducing end is in equilibrium between the open form of a free aldehyde and closed ring hemiacetal in both α and β anomeric configurations. The reducing end is more reactive compared to the other hydroxyl groups on the cellulose molecule. The non-reducing end has only one hydroxyl group at C4 whose reactivity is limited. The length of one β-anhydroglucopyranose (AGU) along the chain axis is about 5 Å. The molar mass of an AGU unit is 162. If the degree of polymerization (DP) of cellulose is a positive

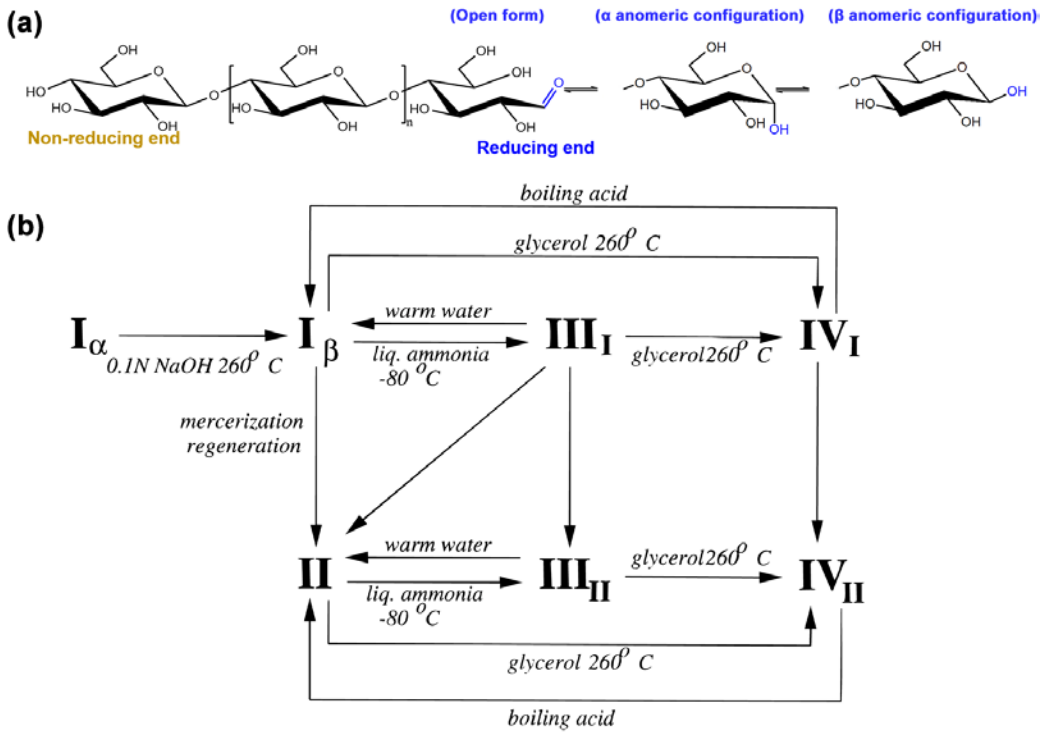

Figure I.1. *(a) Molecular structure of cellulose chain where the reducing end is highlighted by blue color; (b) Conversions of various cellulose crystalline allomorphs [20].*

integer *n*, the molecular weight of cellulose is (162×*n*+18).

Native cellulose occurs mostly in a fibrous crystalline form. In such a crystal, cellulose molecules are organized in a parallel chain arrangement due to its directional biosynthesis. There are two crystalline polymorphs in native cellulose, cellulose Iα with a one-chain triclinic unit cell and cellulose Iβ with a two-chain monoclinic unit cell [18, 19]. Cellulose from different sources has different ratios of these two allomorphs. After regeneration or mercerization, cellulose II with antiparallel chains in a two-chain monoclinic unit cell can be obtained. With the treatment of liquid ammonia, cellulose III_I and cellulose III_{II} are formed from cellulose I and cellulose II, respectively. Cellulose III_I of parallel chain packing and cellulose III_{II} with antiparallel chain packing can be converted by heat treatment to cellulose I and cellulose II, respectively. Heat treatment of cellulose III in glycerol for 20 min at 260 ˚C results in cellulose IV_I and IV_{II} with reference to the starting materials cellulose I and cellulose II, respectively. The conversions between the various cellulose crystalline polymorphs are summarized by Kroon et al. and shown in Figure I.1b [20].

I.3. Cellulose oligomers

Cellulose oligomers are low-molecular-weight cellulose comprising a small number of repeat units of β-D-glucopyranose, typically with a degree of polymerization from 2 to 30. The physical properties of cellulose oligomers significantly depend on their DP. The cellulose oligomers with the DP in the range of 2-7 are water-soluble and also named as cellodextrins [21]. Cellulose oligomers are more soluble in common solvents than high molecular-weight cellulose, which greatly increases the processibility. Cellulose oligomers can be used as the feedstock for biofuel production and bio-based surfactants and its immediate applications include

biomedicine and food nutrients [22-26]. Furthermore, cellulose oligomers are an ideal model substrate to study complex physicochemical properties of cellulose. For instance, conformation studies using atomistic simulations of high-DP cellulose are severely hindered by its slow relaxation of a long polymer chain [27]. This problem can be avoided by using the oligomers which relax much faster compared to the high molecular-weight counterpart. Thus, monodisperse cellulose oligomers can be used as model molecules for a better understanding of structure-property relationships of cellulose [28]. In addition, oligomers are more feasible to form defined regular structures than polymers with relatively high molecular weight [29]. With other multiple advantages, such as abundant reducing ends and molecular directionality, monodisperse cellulose oligomers have great potential in making new types of functional nano-objects by crystallization and self-assembly processes. However, the applications of cellulose oligomers as functional materials are rare in daily life, mainly due to its poor availability and the time-consuming production methods originating from the poor processability of cellulose.

I.4. Preparation of cellulose oligomers

An efficient and easy-to-implement production process of cellulose oligomers is essential for advancing their scientific and technological applications. Various methods for the production of cellulose oligomers have been proposed and classified as two categories: synthetic methods and depolymerization methods. Together with these two methods, the fractionation methods for preparing monodisperse cellulose oligomers will be introduced in detail in the following sections.

I.4.1. Synthetic methods

Synthetic methods of cellulose oligomers are bottom-up pathways to produce them

mostly from monomer units and are categorized into chemical and enzymatic syntheses.

I.4.1.1. Chemical synthesis

Cellulose oligomers with DP less than 4 are synthesized by multi-step chemical synthesis in the 1980s [30, 31]. Nakatsubo and coworkers synthesized cellulose oligomers with higher DP by ring-opening polymerization [32]. Firstly, commercially available 1,2:5,6-di-*O*-isopropylidene-*α*-D-glucopyranose was used to synthesize the starting monomer, (3-*O*-benzyl-6-*O*-pivaloyl-*α*-glucopyranose) with a yield of around 60% via an eight-step reaction pathway. Then the polymerization in dichloromethane with triphenylcarbenium tetrafluoroborate at 20 ˚C for 2 hours generated a DP of around 20 and yield of 62%. If the initial monomer concentration was half, a DP of around 10 and yield of 93% were obtained after the polymerization at 20 ˚C for 14 hours. Afterwards, the protecting groups were removed to obtain cellulose oligomers. Another protocol to synthesize cellulose oligomers involves the use of a glycosyl donor and a glycosyl acceptor [33-37]. This type of reaction is time-consuming because the hydroxyl groups other than that of the 4th position have to be protected by functionalization with acetate or benzyl groups, or by the use of protecting reagents such as boronic acids [37, 38]. The chemical reaction steps are directly proportional to the targeted DP of cellulose oligomers [39, 40]. The main advantage of this protocol is that a specific DP can be targeted with a good purity.

I.4.1.2. Enzymatic synthesis

Enzymes, such as hydrolases, phosphorylases and glycosyltransferases, are used to synthesize cellulose through reverse reactions [41-45]. For instance, hydrolases catalyze a glycosylation reaction to produce saccharide chains by using fluorinated

monosaccharides as the donors. Phosphorylases elongates saccharide molecules by consuming monosaccharide phosphate. Leloir glycosyltransferases are used in the *in vivo* synthesis of oligosaccharides with sugar nucleotides (e.g. UDP glucose). Transglycosidases can catalyze chain elongation reactions using non-activated saccharide molecules such as sucrose.

An example of *in vitro* enzymatic synthesis of cellulose catalyzed by hydrolases was reported in 1991 [46]. The substrate was β-cellobiosyl fluoride, in a mixed solvent of acetonitrile and acetone buffer with the pH of 5 at 30 ˚C for 12 h [47, 48]. Cellulose oligomers with an average DP of around 22 and yield of 54% could be obtained, while at higher concentrations of substrate and acetonitrile, the average DP of the obtained cellulose oligomers was 8 with a yield of 70% [46]. For phosphorylases catalyzed synthesis of cellulose oligomers, commercial α-D-glucose-1-phosphate was used as the donor and glucose or cellobiose acted as the acceptor. Cellulose oligomers with DP in the range of 3-13 could be obtained, and the obtained DP and DP distribution depended on the reaction time and also the cellobiose concentration [49, 50]. By using cellulolytic enzyme, endoglucanase I, the transglycosylation of cellobiose or cellotriose took place to produce cellulose oligomers with a DP in a range of 4-16 and yield of 30% [51]. The synthesis using a mutated cellulase, a so-called glycosynthase, required fluorinated cellobiose as an activated donor, and in the end, methylated cellulose oligomers with DP in the range of 3-6 could be obtained with high purity [52].

I.4.2. Depolymerization methods

Considering the sophisticated and time-consuming processes of synthetic methods, the depolymerization methods are more applicable for industrial production. The depolymerization methods are pathways to produce cellulose oligomers from high

molecular-weight cellulose, including enzymatic depolymerization, acetolysis, pyrolysis, mechanical depolymerization and acid hydrolysis.

I.4.2.1. Enzymatic depolymerization

The studies on enzymatic depolymerization of cellulose have been developed for more than a century [53]. In the recent years many works on enzymatic depolymerization of cellulose focus on their potential applications in bio-fuel production [54]. There are three major classes of cellulase enzymes: endoglucanases, exoglucanases and beta-glucosidases [55, 56]. Endoglucanases hydrolyze soluble and insoluble cellulose chains in a random mode [57]. Cellobiohydrolase, a typical example of exoglucanases, preferentially hydrolyzes cellulose from chain ends of cellulose chains to give cellobiose [58]. Beta-glucosidases hydrolyze soluble cellodextrins into D-glucose [59]. Pretreatments of cellulose increase the surface area accessible by water and cellulases, resulting in an improvement in hydrolysis kinetics [60, 61]. The pretreatments include acidic [62], alkaline [63-65], enzymatic [66], mechanical treatments [67, 68], as well as electron beam irradiation [69] ammonia expansion [70]. One of the most studied pretreatments is ionic liquid treatment [71-75]. However, Turner et al. reported that [bmim]Cl appeared to disactivate cellulase [76]. Known examples of ionic liquids reported to solubilize cellulose and be compatible with cellulase are 1-ethyl-3-methylimidazolium acetate, choline acetate and tris(2-hydroxyethyl)methylammonium methylsulfate [77, 78].

I.4.2.2. Acetolysis

Acetolysis, first proposed by Hess and Dziengel in 1935 [79], introduces acetyl group at the reducing end while cleaving the glycosidic linkage. This reaction consists of acetic anhydride together with solvents and sulfuric acid as a catalyst [80, 81]. When the

reaction condition is at 50 ˚C for 2 hours, the average DP of the obtained cellulose oligomers is around 9 with the yield of only 2% [82]. Akpinar and Penner achieved the yield of 32% and an average DP of 5 by an acetolysis reaction at room temperature for 60 hours [83].

I.4.2.3. Pyrolysis

Pyrolysis of cellulose include a random cleavage reaction of glycosidic linckage [84, 85], which causes depolymerization of high molecular-weight cellulose chain to cellulose oligomers. Oligomers with DP of 2-7 and yield of about 20% are produced by treating cellulose at 1000 ˚C for 50 milliseconds [85]. Oligomers with DP of 1-10 and a yield of only 3% are obtained at a lower temperature of 100-350 ˚C for 30 mins [86].

I.4.2.4. Mechanical depolymerization

Depolymerization of cellulose also occurs upon mechanical treatments such as ball milling. With impregnation with sulfuric acid followed by ball milling process at 300 rpm for 15 mins, MCC are degraded into cellulose oligomers with an average DP of 7 and a yield of about 92% [87]. During this reaction, re-organization of molecular structure can occur, causing α-1,6 linked glucose branch structures [88]. Although such ramification increases solubility of the depolymerized product, they are not purely cellulose oligomers.

I.4.2.5. Acid hydrolysis

Acid hydrolysis degrades cellulose to cellulose oligomers, and this process can be accompanied with the formation of furanic by-products due to the acidic dehydration of glucose. Acid hydrolysis primarily takes place on the surface of cellulose crystals in the case of heterogeneous reactions. Thus, cellulose solvents are often used to efficiently hydrolyze cellulose by making the chain scission sites more accessible. Li

and Zhao reported efficient acid hydrolysis of cellulose from several sources in ionic liquid 1-butyl-3-methylimidazolium ([C_4mim]Cl) [89]. Some mineral acids like concentrated sulfuric acid and phosphoric acid are common cellulose solvents that simultaneously hydrolyze cellulose. These acids attract scientific attention for making cellulose oligomers in the past decades. Table I.1 summarizes acid hydrolysis-based preparation methods of cellulose oligomers. The acid nature significantly influences the yield of cellulose oligomers. For heterogeneous acid hydrolysis like using fuming HCl, the yield of cellulose oligomers is around 5 %, much smaller than that by homogenous acid hydrolysis using concentrated sulfuric or phosphoric acid. A mixture of 80:20 HCl/H_2SO_4 at room temperature is found to increase the yield compared to the pure fuming HCl. Precipitants also have an impact on the polydispersity and yield of the obtained oligomers.

Table I.1. Parameters and results of producing cellulose oligomers by acid hydrolysis.

Ref.	Cellulose	Hydrolysis conditions	Precipitant	DP_w	Đ	Yield (%)
[90]	Avicel PH-101	80% H_2SO_4, 70 ˚C, 14 mins	Ethanol	1-8	nd[a]	1.8
[91]	Avicel PH-105	4:1 of fuming HCl : 98% H_2SO_4, 22 ˚C, 4-6 mins	Acetone	1-8	nd	45
[92]	Whatman cellulose	Fuming HCl, room temperature	Water then neutralized	3-7	nd	5

	CF-11					
[93]	Cellulose APX [b]	Fuming HCl, 25 ˚C, 2-3 hours	Isopropanol	1-12	nd	5
[94]	Whatman cellulose CF-11	Fuming HCl, 25 ˚C, 2-3 hours	Isopropanol	1-6	nd	3
[95]	Avicel PH-101	85% H_3PO_4, 55 ˚C, 20 h	Ethanol	5.7	1.3	47
		85% H_3PO_4, 55 ˚C, 20 h	Isopropanol	14.6	1.9	56
		85% H_3PO_4, 55 ˚C, 20 h	Acetone	19.1	4.0	53
		85% H_3PO_4, 55 ˚C, 20 h	Tetrahydrofuran	14.6	2.1	68
[96]	Whatman cellulose CF-11	85% H_3PO_4, room temperature, 6 weeks	Water	8-15	2.0	52
[1]	Whatman cellulose CF-11	85% H_3PO_4, room temperature, 6-8 weeks	Water	15	1.15	40
		85% H_3PO_4, room	Methanol	7	1.07	15

	temperature, 6-8 weeks	

[a] nd means no data;

[b] APX cellulose was produced in Serva, Heidelberg, F.R.G.. No further information was found.

I.4.3. Fractionation of cellulose oligomers

Most of the above-mentioned depolymerization methods generate a mixture of oligomers with a wide DP distribution. Although cellulose oligomers with a uniform chain length can be directly obtained synthetically as mentioned in the Chapter I.4.1, these methods are not suitable for a larger scale production due to their complicated and time-consuming procedures. Hence, the isolation/fractionation methods have been developed to obtain monodisperse oligomer fractions from crude oligomer mixtures obtained from the depolymerization methods.

Chromatography is the most employed method for fractionation of cellulose oligomers. Thomas et al. used normal phase-high performance liquid chromatography to separate peracetylated cellulose oligomers and prepared monodisperse cellulose oligomers up to a DP of 20 [97]. The principle of column chromatography is using gravity or a pump to move a solution of compounds of interest through a column filled with absorbent. Compounds with different affinities to stationary phase move through the column at different rates and thus can be separated into fractions. Flugge and co-workers reported the isolation of cellulose oligomers with DP from 2 to 8 by column chromatography [98]. They used a column based on activated charcoal and celite and a gradient of water/ethanol as eluent. Zhang and Lund used a two-column system based on fine polyacrylamide beads and cation exchange resins for the separation of cellulose oligomers with higher efficiency [91]. Cation exchange resins are

found efficient for separating cellulose oligomers, because they have strong affinity with hydroxyl groups of cellulose [99]. The most commonly used column is based on calcium cation as it is eluted with water alone without co-solvents [100]. Another example is a silver-based column that provides an increased retention and resolution compared with the calcium ones [101]. Diethylaminoethyl derivatives of Spheron, a synthetic anion exchange resin, is also known as an effective absorbent and use borate buffer as an eluent [102].

Another method to fractionate cellulose oligomers is based on the different solubility in various solvents. For instance, cellulose oligomers with DP of 5 and 6 are insoluble in ethanol/water solution when the ethanol concentration exceeds 80% [94]. Isogai and Usuda reported two fractions of nearly monodisperse cellulose oligomers with the DP of 15 and 7, respectively, based on such a solubility-based fractionation [103]. A fraction with an average DP of 15 comes from the precipitates of cellulose/phosphoric acid solution mixing with water, and the supernatant mixing with methanol results in a fraction with an average DP of 7. Another study by Billès et al. introduced a similar but more complicated procedure to get nearly monodisperse cellulose oligomers [22]. After hydrolysis in phosphoric acid at 50 ˚C for 20 hours, the regenerated cellulose oligomers are obtained by precipitation in THF, then the regenerated cellulose oligomers are mixed with water to extract a water-soluble fraction. After neutralization and drying, the water-soluble oligomers are further separated by mixing with methanol. The methanol-insoluble fraction contains 41.5% of cellotetraose, 35.7% of cellopentaose, 5.9% of cellotriose, 11.7% of glucose and cellobiose, and 5.2% of cellohexaose.

I.5. Determination of degree of polymerization of cellulose oligomers

Degree of polymerization (DP) describes the number of glucose units in cellulose. Molecular weight is the mass of an individual molecule. Polydispersity index (Đ) is a measure of the molecular weight distribution and calculated based on the number-average molecular weight (M_n) and weight-average molecular weight (M_w) as follows.

$$\overline{M_n} = \frac{\sum c_i \times M_i}{\sum c_i}$$

$$\overline{M_w} = \frac{\sum c_i \times {M_i}^2}{\sum c_i}$$

$$Đ = \frac{\overline{M_w}}{\overline{M_n}}$$

where c_i is the concentration of molecules with the molecular weight M_i. The number-averaged molecular weight is the total mass of cellulose divided by the total number of molecules. The weight average molecular weight is calculated as the sum of all molecular weights multiplied by weight fractions, so this molecular weight average is weighted towards the larger molecules in the system. The Đ value is never smaller than 1 without theoretical upper limit because M_w is always equal to or larger than M_n. The closer the Đ value is to 1, the more homogenous the chain length of cellulose is.

Established methods of DP determination of cellulose include size-exclusion chromatography (SEC), light scattering (LS) and viscometry. These solution-based methods require dissolution of cellulose. It can be achieved via direct dissolution of cellulose in cellulose solvents or derivatization of cellulose to make it dissolve in common solvents. The later choice is usually employed for cellulose oligomers with DP larger than 7, since the cellulose oligomers with DP smaller than 7 can directly

dissolve in common solvents such as DMSO and water. In the following sections, the derivatization methods of cellulose and the characterization techniques for DP determination are described.

I.5.1. Derivatization of cellulose

Carbanilation and nitration are the most studied methods for solubilizing cellulose in common solvents for DP determination.

Nitration method is developed in the 1940s for measuring the DP of cellulose viscometrically [104]. Alexander and Mitchell reported a nitration method for rapid measurement of cellulose viscosity but with shorter reaction time and high reproductivity of DP values of which measurement error is within 1%. Cellulose is treated in a mixture of nitric acid, phosphoric acid, and phosphorus pentoxide in the weight ratio of 64:26:10 at room temperature for 20 mins [105]. The moisture is strictly excluded during the nitration, and neutralization is necessary in the very beginning of the washing process. Claisse used nitration to derivatize cellulose oligomers for measuring their DP by size exclusion chromatography without light scattering detectors [106]. However, there is still a debate about the validity of nitration method used in the DP determination due to possible hydrolysis of cellulose during derivatization and instability of the cellulose trinitrates.

Cellulose tricarbanilate, obtained by the reaction of cellulose with phenyl isocyanate, is another cellulose derivative for DP determination [107-110]. Carbanilation of cellulose can be conducted in heterogeneous and homogenous conditions, depending on the solvents used for reactions. It is reported that cellulose is oxidized and degraded during the carbanilation in DMSO as a solvent [111-113]. Thus, DMSO is

not recommended as the solvent for carbanilation. Carbanilation was also performed on the partially substituted cellulose ethers or esters to obtain organic-soluble products for the analysis of molecular weight [114, 115]. Carbanilation is widely used in SEC for its several advantages over other choices, such as nitration and direct dissolution in cellulose solvents. First, the carbanilation of cellulose with solvents like pyridine and DMF is considered non-destructive due to its mild and neutral reaction condition. Nitration and acetylation are performed in acidic conditions and thus can degrade cellulose via hydrolysis with the presence of trace amount of water. Second, the cellulose carbanilates are stable in most common eluents of SEC, such as THF and DMF. This is practically beneficial compared to the direct dissolution of cellulose in multicomponent solvents, for example LiCl/DMAc, which are less available as a SEC eluent. Third, the increase of molar mass by carbanilation and the large refractive index increment (dn/dc) contribute to the enhanced sensitivity of light scattering and refractive index detection. Furthermore, the introduction of aromatic groups makes it UV detectable.

Degree of substitution (DS), a number of aromatic carbamate groups per glucose unit, affects the properties of cellulose carbanilates and the accuracy of the DP determination of cellulose. Table I-2 summarizes the carbanilation with different reaction conditions in relation to the resulting DS and the techniques that are used to determine the DS values. The characterization techniques include elemental analysis (EA), Fourier-transform infrared spectroscopy (FTIR) and liquid state ^{1}H nuclear magnetic resonance (^{1}H-NMR) spectroscopy.

Table I.2. Carbanilation conditions in relation to the DS of obtained cellulose carbanilates.

Ref.	Solvent	Phenylisocyanate content[a]	Temperature (°C)	Time (hours)	Detection method of DS	DS
[116]	$[C_4mim]^+Cl^-$	10	80	2	EA[b]	3
[117]	pyridine	3.7	80	48	-	-
[118]	Pyridine	2	100	4-8	EA	3
[119]	$[C_4mim]^+Cl^-$	10	80	2	EA	2.25
[120]	DMF	4.2	95-100	8	EA	3
	DMF	10.08	95-100	8	EA	3
	DMF	25.2	95-100	8	EA	3
[121]	DMF	28	100	168	Incomplete reaction	
	pyridine	28	80	29	EA	2.8
[122]	5%LiCl/DMAc	13.7	60-70	2	EA	3
[123]	Pyridine	28	80	48-72	FTIR	3
[124]	AmimCl	5	100	2	^{1}H-NMR	2.38

[a] molar equivalent to anhydroglucose unit.
[b] EA, elemental analysis.

I.5.2. Characterization methods of molecular weight

In this section, the main methods for characterizing molecular weight of cellulose

are described.

I.5.2.1. End group method

As mentioned above, a cellulose chain has a reducing end. It is in the equilibrium between the open form aldehyde and the hemiacetals of α and β configurations. The aldehyde content can be measured by titration [125]. One can also estimate the content of reducing ends using NMR spectroscopy, since the chemical environment of anomeric carbon and its bonded hydrogen at the reducing end is different from those involved in glycosidic linkage. By measuring the total number of glucose units (N_G) and reducing ends (N_R), the number-averaged DP can be calculated as follows,

$$DP_n = \frac{N_G}{N_R}$$

The biggest challenge of this method is the decreasing sensitivity with increasing chain length. It is generally accepted that the peak intensities in liquid state ^{1}H-NMR can be used for quantitative analysis, but it is less straightforward for liquid- and solid-state ^{13}C-NMR, especially when molecules with different dynamics co-exist.

I.5.2.2. Mass spectroscopy

Mass spectrometry is an analytical tool for measuring the molecular mass. The results are presented as an intensity spectrum as a function of the mass-to-charge ratio, and each molar mass gives a distinct signal in the mass spectrum. Matrix assisted laser deposition/ionization time-of-flight (MALDI-TOF) mass spectroscopy has been used to investigate biological macromolecules since MALDI technique allows ionization of large molecules while minimizing fragmentation. However, there are two major known problems in MALDI of molecules with a large polydispersity index, namely mass discrimination and molecular mass distribution inaccuracies [126-128]. Mass

discrimination is a problem related to high-molecular weight molecules mainly due to a detector saturation caused by matrix-related ions and low-mass oligomers [129]. Other factors, such as use of different matrixes, multimer formation, cation inclusion and instrumental factors, also contribute to the mass discrimination problem. The molecular mass distribution is found to be remarkably sensitive to ionization conditions and detector conditions. Differences in ionization efficiency have been observed between low- and high-molecular weight molecules, leading to different sensitivity to different molar masses [129].

I.5.2.3. Viscometry

Viscometry is a major method for determining average molecular weight in industrial applications. Hermann Staudinger was the first to report an empirical relationship between the relative magnitude of the increase in viscosity and the molecular weight of polymer in 1930 [130]. Intrinsic viscosity [η], describes the contribution of a solute to the viscosity η of a solution, is used for calculating molecular weight M in polymer chemistry through the Mark-Houwink equation (or Landau-Kuhn-Mark-Houwink-Sakurada equation) [131].

$$[\eta] = KM^{a}$$

where K and α are the Mark-Houwink parameters for a given polymer, solvent and temperature, and normally calculated based on calibration with polymers of known molecular weights. The most common solvent used for viscometry method of cellulose is cupriethylenediamine hydroxide, also named as Cuen. One drawback of this solvent is the high alkalinity that may cause depolymerization of cellulose molecule. Classical viscometric measurements are performed using an Ubbelohde capillary viscometer.

The accuracy of Mark-Houwink equation also depends on an expected DP range. To the current knowledge, there is no equation available for cellulose with a large oligomeric portion, in this case, the cuen-DP values may have a considerable error due to a low viscosity. It is standard practice to use linear fits for a log[η] against log[M] plot, but it is questionable whether such a fit is applicable for cellulose oligomers [132, 133].

I.5.2.4. Static light scattering

Static light scattering (SLS) is a technique for measuring molecular weight by using light scattering of solute molecules in a solution. SLS determines the scattered light intensity at a given scattering angle by averaging the fluctuating intensity over a long-time scale compared with the time scale of the intensity fluctuation. The increase in the intensity of scattered light is linear with molecular weight but non-linear with respect to molecular size.

There are several kinds of light scattering instruments: right-angle light scattering (RALS), low-angle light scattering (LALS) and multi-angle light scattering (MALS). RALS measures the scattered light intensity at 90˚ to the incident beam. In this condition, any flare or noise created by the change in refractive index is minimized, thus resulting in the best signal-to-noise ratio and sensitivity. LALS measures at an angle that is as close to 0 ˚ as possible, which gives the calculated molecular weight the highest accuracy. RALS/LALS hybrid detectors combined the advantages that use RALS to maximize sensitivity for weak scatterers and use LALS to maximize the accuracy for anisotropic scatterers. The molecular size can be estimated but with a limited accuracy. MALS measures the scattered light intensity at multiple angles that the molecular weight of all molecules from small to large is calculated, and an

accurate molecular size can be obtained.

I.5.2.5. Size exclusion chromatography

Most of the methods above can only provide average molecular weight information. In order to access the molecular weight distribution of cellulose, size exclusion chromatography (SEC) is the most used method. SEC, also known as gel permeation chromatography (GPC), is a special type of column chromatography that the analyte is assumed to have no enthalpic interactions with the stationary phase. The sample in a solvent the same as used in the mobile phase with a dilute concentration, normally around 3 mg/mL, is injected into a series of columns that are continuously flowed with the mobile phase. The large molecules elute from the columns first, followed by molecules with decreasing molecular size.

An appropriate column calibration is necessary for establishing a relation between the elution volume and the molar mass of the eluting molecules. A straightforward calibration method is based on a set of well-characterized polymer standards with as narrow a molecular weight distribution as possible. This calibration technique is regarded as a relative, but not absolute calibration because the obtained molecular weight values are of the calibrant. For example, if the column is calibrated with polystyrene standards and cellulose tricarbanilate is a sample, the obtained molecular weight values is not accurate for cellulose tricarbanilate. In contrast, universal calibration can provide accurate molecular weight of the analyte by determining the molecular weight at each slice of elution time through a viscometer detector together with the dRI detector. The combination of SEC with light scattering detectors is a powerful tool for providing absolute molecular weight information, especially when standards are missing, as is the case for cellulose.

However, cellulose oligomers have not received much attention in cellulose analytics [133]. Thus, one of our goal is to investigate the characterization of cellulose oligomers by some of these methods mentioned above.

I.6. Solvents for cellulose

Dissolving cellulose is one critical step to bring homogeneous modifications for analytical purposes. A dissolution process is a transition from two phases to one phase where cellulose chains are dispersed at molecular level in a solvent. In contrast, through a swelling process cellulose remains as solid phase, though the physical properties significantly change and the volume increases due to uptake of the solvent. The strong cohesion among cellulose chains involves different molecular interactions, such as hydrogen bonding and hydrophobic interactions [134, 135]. There are limited choices of solvents since cellulose is insoluble in most of common solvents. The effort to develop efficient solvents for cellulose has been made for more than a century. The solvents that can derivatize cellulose are categorized as “derivatizing” solvents. These solvents dissolve cellulose by altering molecular interactions between cellulose molecules via derivatization of their hydroxyl groups. For example, the viscose process includes successive treatment of cellulose with caustic soda and carbon disulfide, which results in cellulose xanthate derivative. Regeneration of this dissolved cellulose derivative in acid solution makes the derivative revert to cellulose. In contrast, the “non-derivatizing” solvents dissolve cellulose by strong intermolecular interactions between cellulose and solvent molecules [136]. Examples of non-derivatizing solvents include lithium chloride (LiCl)/N, N-dimethylacetamide (DMAc), N-methylmorpholine-N-oxide (NMMO)/water, ionic liquids, alkaline/urea, sulfuric acid, phosphoric acid. Factors that influence the dissolution of cellulose in

solvents includes mixing temperature, mixing time, the crystallinity of cellulose, and the DP of cellulose [137].

Isogai and Atalla reported that the solubility of cellulose decreases with the increasing DP of cellulose [138]. It indicates that the dissolution of cellulose can be strictly controlled by the DP value, and this phenomenon is consistent with the majority of polymers. Cellotetraose can be readily dissolved in water. Dimethylsulfoxide (DMSO) can dissolve the regenerated cellulose oligomers with the average DP of 7. With increasing DP, water and DMSO alone cannot solubilize cellulose any more.

When considering the preparation of cellulose oligomers, acid solutions are the preferred solvents because the dissolution of cellulose in acidic media is typically accompanied by hydrolysis process [139]. The possibility to dissolve cellulose in sulfuric acid and phosphoric acid has been known for a long time, already described in a patent in 1925 for phosphoric acid, while sulfuric acid has been known as a cellulose solvent since the middle of the 19th century and has been investigated in the 20th century [140-144]. It is found that at room temperature or lower, the sulfuric acid and phosphoric acid with concentrations over 62% and 83%, respectively, cause dissolution of cellulose [145, 146]. Some early investigations show that increased temperature of the acidic treatment promotes the hydrolysis and dissolution of cellulose [145, 147, 148]. However, high temperature of acidic treatment makes the control of molecular weight of resulting oligomers more difficult because the depolymerization happens too quick. Recently Huang and co-workers reported that 64% H_2SO_4 at -20 ˚C could rapidly dissolve high molecular weight spruce cellulose without a drastic change in its molecular weight [149]. It is beneficial for some

applications where higher molecular weights or more precise control of DP are required. Phosphoric acid belongs to the "non-derivatizing" solvent while sulfuric acid can partially derivatize the hydroxyl groups of cellulose and form sulfate half esters [150-152].

I.7. Cellulose-complex crystals

As aforementioned, cellulose occur as a crystalline compound in nature. The first step of dissolution of cellulose is often a penetration of solvent molecules into its crystalline core. During such a swelling process, it is found that cellulose can form complex crystals with solvent molecules. The crystal structure analysis can provide insight into the spatial arrangement of cellulose and solvent molecules as well as intermolecular interactions among them[153]. A better understanding of the polymer-solvent interactions can lead to optimized solvent design and processing of cellulose.

I.7.1 Cellulose/alkaline complex

During the swelling process of native cellulose in alkaline solutions, some intermediate crystalline structures called alkali-celluloses are formed. The first alkali-cellulose complex with caustic soda, namely Na-cellulose, is reported by Hess and Trogus in 1931 [154]. Sobue et al. reported a phase diagram of Na-cellulose complexes, including Na-cellulose I, Na-cellulose II, Na-cellulose-III and Na-cellulose IV, as a function of temperature and NaOH concentration (Figure I.2) [155].

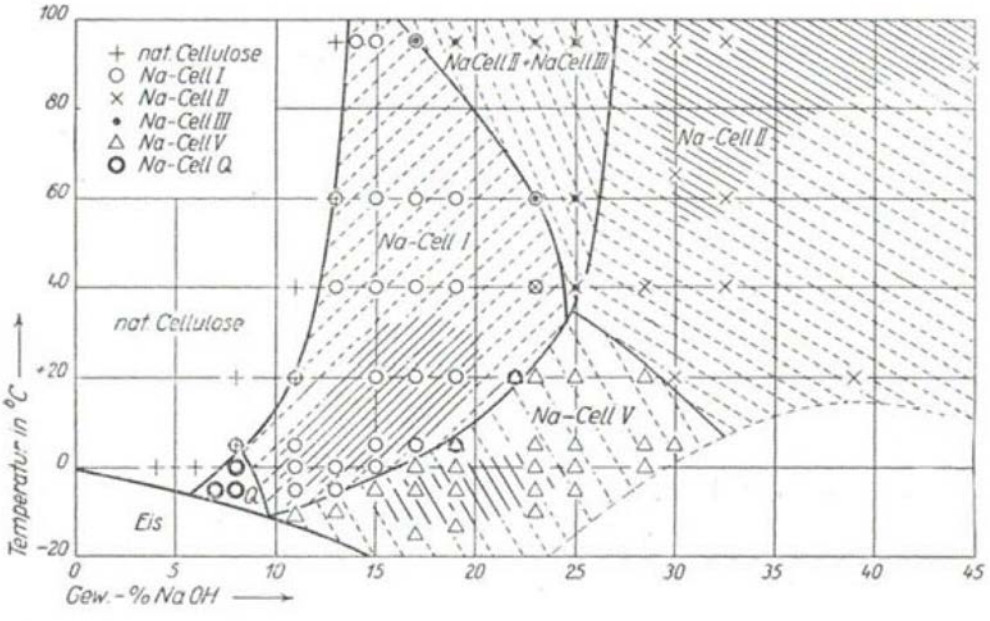

Figure I.2. *Formation diagram of different Na-cellulose as a function of NaOH concentration and temperature* [155].

Na-cellulose I can be obtained by immersing cellulose in NaOH aqueous solution with a concentration greater than 10 wt% at room temperature. The unit cell of Na-cellulose I is determined as a space group $P2_1$ with the unit cell parameters of a = 8.83 Å, b = 25.28 Å, c (fiber axis) = 10.29 Å, $\alpha = \beta = \gamma = 90^\circ$ by Nishimura et al [156]. Na-cellulose I converts to Na-cellulose III upon drying. Compared with Na-cellulose I, Na-cellulose III exhibits similar unit cell parameters and NaOH content in unit cell, only with minor changes in the molecular packing [157]. They both share a 10-Å fiber repeat with the cellulose allomorphs, indicative of two-fold helical conformation of cellulose chains in the complexes. Na-cellulose IIA, a complex obtained with a NaOH solution of higher concentration, has a 15-Å fiber repeat, implying the presence of three-fold helical conformation of cellulose chains. Na-cellulose IIB, another crystal structure with a 15-Å fiber repeat, was initially considered a pure alkali-cellulose

complex but later found as a complex of cellulose, soda and Cu(II) ions [157, 158]. Na-cellulose IV is obtained via water-rinsing of Na-cellulose I, Na-cellulose IIA, Na-cellulose III to eliminate NaOH. Despite its name, Na-cellulose IV is a complex of cellulose and water alone. This complex easily converts to cellulose II upon drying or heating in water. Nishimura and Sarko revealed that Na-cellulose IV has a monoclinic unit cell containing two antiparallel chains, with space group $P2_1$ and cell parameters of a = 9.57 Å, b = 8.72 Å, c (fiber axis) = 10.35 Å, α = β = 90˚, γ = 122.0˚ [159]. Projections of Na-cellulose IV on the a-b plane in the 0 0 1 direction and on the b-c place in the 1 0 0 direction are shown in Figure I.3.

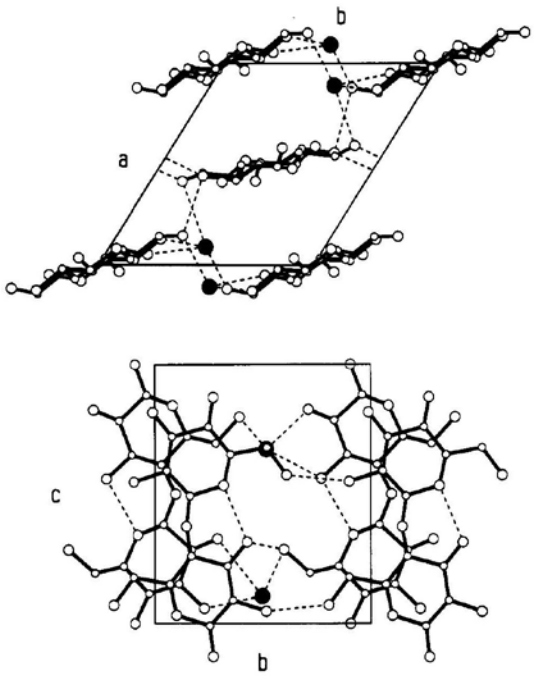

Figure I.3. *Projections of Na-cellulose IV with water molecules on the a-b plane in the 0 0 1 direction (top) and on the b-c plane in the 1 0 0 direction (down)* [159].

I.7.2. Cellulose/ammonia complex

The intake of ammonia into crystal lattice of cellulose results in cellulose/ammonia complexes with different crystalline structures, depending on the temperature [160-162]. Native ramie cellulose with anhydrous liquid ammonia can form the cellulose I-

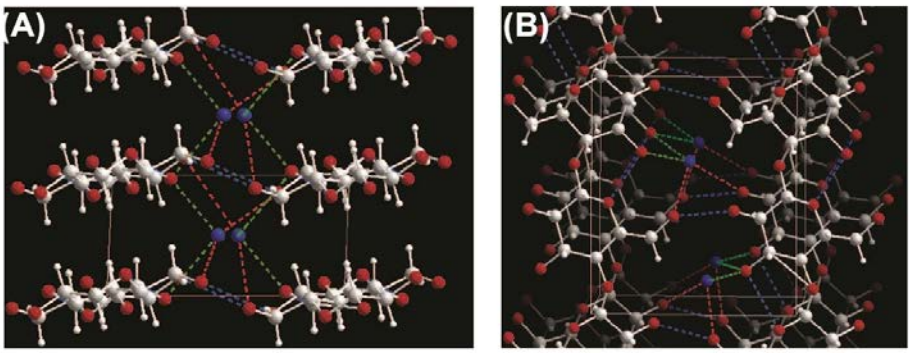

Figure I.4. *Projection of cellulose I-ammonia I with NH_3 molecules (A) on the a-b plane in the direction along the c axis and (B) on the b-c plane in the direction perpendicular to the c axis [163].*

ammonia I complex at a temperature above -20 to -30 ˚C and the cellulose I-ammonia II complex at a lower temperature [160]. The crystalline structure of cellulose I-ammonia I complex has been determined by Wada et al., as one chain monoclinic unit cell with space group $P2_1$ and unit cell parameters of a = 4.47 Å, b = 8.81 Å, c = 10.34 Å, α = β = 90˚, γ = 92.7˚. The stoichiometry between cellulose and guest ammonia is found to be 1:1 for glucose and ammonia units. The projections of cellulose I-ammonia I complex with NH_3 molecules are shown in Figure I.4 [163]. Cellulose I-ammonia II is characterized to have a hexagonal unit cell of a = b = 14.50 Å, c = 15.20 Å, α = β = 90˚, γ = 120˚ [160]. Sawada and co-workers prepared a different low-temperature phase cellulose/ammonia complex by freeze-trap cellulose at 150 K with a pretreatment of liquid ammonia, and the crystal structure was revealed as two-chain and about ten ammonia molecules within a unit cell of a = 15.49 Å, b = 11.35 Å, c = 10.42 Å, α = β

= 90˚, γ = 143.5˚. The diffraction pattern of the cellulose ammonia complex from the starting material of mercerized cellulose II is identical with that of cellulose I-ammonia I complex [164].

I.7.3. Cellulose/ammonium hydroxides complex

Cuprammonium hydroxide is long-known as a solvent for cellulose as early as in 1857 [165]. Hess and Trogus reported that Na-cellulose I/ Cuprammonium hydroxide crystalline complex crystals had longer fiber period when the absorbed concentration of copper was higher [154]. The equilibrium molar ratio of absorbed copper to glucopyranose unit of cellulose is 0.65, which is almost the same value with that of cellulose/cuprammonium solution system [166]. Wayne and Willian found the tetramethyl-, trimethylethyl-, trimethylbenzyl- and dimethyldibenzyl-ammoinium hydroxides changed the lattice of both native and mercerized cellulose, and the lattice extension was not proportional to the size of the substituted groups [167].

I.7.4. Cellulose/amine complex

Immersion of cellulose in both cellulose I or cellulose II allomorphs in amines provides various cellulose-amine complexes from hydrazine and ethylenediamine (EDA) to tetramethylenediamine [168]. The cellulose/diamine complexes are found more stable than the cellulose/monoamine complexes against heating or extraction of excess amine by non-oxygen containing solvents [169-171]. In these complexes, amines exist between molecular sheet structures of cellulose. The spacing between the molecular sheets the cellulose/diamine complexes increases about 1.1 Å per carbon atom increased in the diamine chain [172].

The crystalline cellulose I-ethylenediamine (EDA) complex can be obtained by

swelling native cellulose in EDA, and the complex converts to cellulose III_1 after washing in anhydrous methanol [173-175]. Wada et al. revealed the structure of cellulose I-EDA complex as a one-chain monoclinic unit cell in space group $P2_1$: a = 4.55 Å, b = 11.33 Å, c = 10.37 Å, α = β = 90˚, γ = 94.02˚, with one glucosyl residue and one EDA molecule forming an asymmetric unit [175]. Sawada and co-workers studied the location of proton atoms in the cellulose I-EDA complex, and the hydrogen bonding networks of naturally occurring cellulose I were disrupted by the formation of

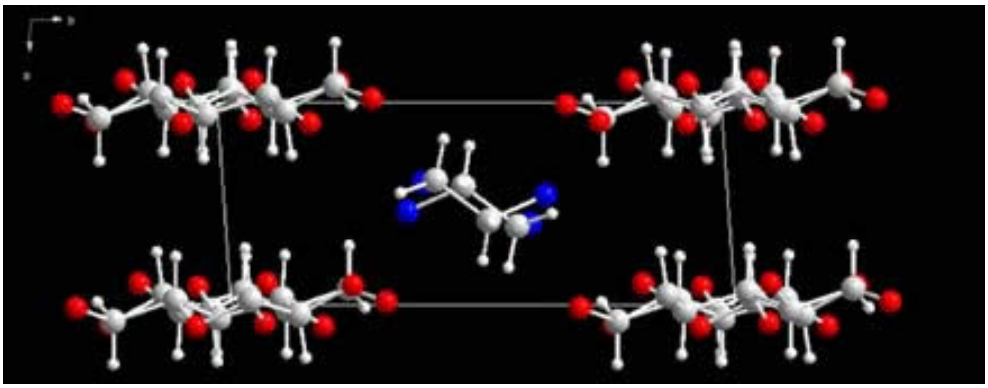

Figure I.5. *Projection of the cellulose I-EDA complex on the a-b plane along the fiber axis direction [175].*

hydrogen bonds between O6/O3 and EDA [176]. Projections of the crystalline cellulose I-EDA complex in 0 0 1 direction on the a-b plane and in the 1 0 0 direction on the b-c plane are shown in Figure I.5.

Native cellulose I is capable of forming complex crystal with hydrazine, and the structure can be explained by a two-chain monoclinic unit cell in space group $P2_1$ of a

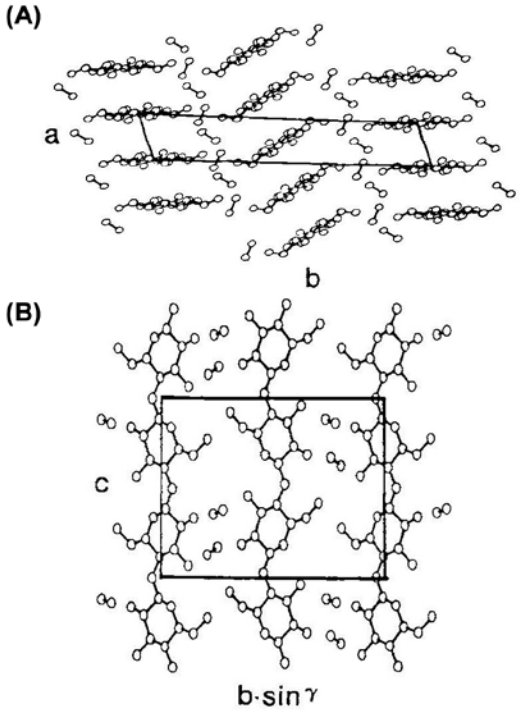

Figure I.6. *Projection of cellulose II hydrazine complex (A) on the a-b plane in the direction along the c axis and (B) on the b-c plane in the direction along the a axis* [178].

= 8.79 Å, b = 10.76 Å, c = 10.38 Å, α = β = 90˚, γ = 122˚ [177]. Two cellulose II-hydrazine complexes have been reported based on two starting materials of mercerized and regenerated cellulose. When hydrazine form a complex with mercerized cellulose II, the cellulose II hydrazine complex has a two-chain monoclinic unit cell in space group $P2_1$ with a = 10.42 Å, b = 10.46 Å, c = 10.38 Å, α = β = 90˚, γ = 129.7˚ [177]. With the starting material of regenerated cellulose, Lee et al. reported that the cellulose II-hydrazine complex had a monoclinic unit cell of a = 9.37 Å, b = 19.88 Å, c = 10.39 Å, α = β = 90˚, γ = 120˚, containing 8 glucose residues with stoichiometry of one hydrazine per glucose residue. The projections of crystalline

cellulose II-hydrazine complex in the 001 direction on the a-b plane and in the 1 0 0 direction on the b-c plane are shown in Figure I.6 [178]. They demonstrated that the interaction of cellulose II with hydrazine involves scission of intermolecular hydrogen bonds and reorganization of the stacks of quarter-staggered chains along the chain direction [178].

I.7.5. Cellulose hydrate complex

Crystalline cellulose hydrates are only formed with cellulose II and proposed by Sakurada and Hutino in 1936 for the first time [179]. There are three forms in term of different preparation methods: cellulose hydrate A, cellulose hydrate B and cellulose C. Cellulose hydrate A is formed by steaming the cellulose II [180]. Cellulose hydrate B is an intermediate form after removal of the mercerizing agent, and thus corresponds to Na-cellulose IV [179]. Cellulose hydrate C is prepared by swelling cellulose II in hydrazine and then washing with water [181]. The unit cell dimensions for these structures are given in Table I-3. Kobayashi et al. studied the crystal transition from cellulose II hydrate C to cellulose II [182]. The most significant change in d-spacing is the 1-10 crystalline plane, 8.86 Å for cellulose hydrate complex and 7.36 Å for cellulose II. The d-spacings of 1 1 0, 0 2 0 and 0 0 2 crystalline planes remain almost constant on drying from cellulose hydrate complex to cellulose II. The transition mechanism is explained that the molecular sheets along the 1$\bar{1}$0 plane become closer due to the release of water molecules.

Table I.3. Unit cell dimensions for cellulose hydrates A, B and C.

	a (Å)	b (Å)	c (Å)	γ (°)

Hydrate A [180]	8.58	9.38	10.30	121
Hydrate B [179]	10.03	9.98	10.30	128
Hydrate C [181]	9.02	9.63	10.34	116

I.7.6. Cellulose/ionic liquid complex

Ionic liquids, composed of an organic cation (pyridinium, imidazolium cations etc.) and an inorganic anion (OAc^-, $HCOO^-$, $(MeO)_2\ PO_2^-$, Cl^- anions etc.), are capable of dissolving cellulose in high concentration up to 25 wt% [61, 137]. Song et al. prepared lamellar complex crystals in form of spherulites by placing 19 wt% microcrystalline cellulose/1-allyl-3-methylimidazolium chloride ([Amim]Cl) solution in a moisture-controlled chamber (relative humidity of about 10%) at constant temperature of room temperature and 100 K [183]. The unit cell dimension is tetragonal with a = b = 12.92 Å, c = 10.40 Å at room temperature in space group $P2_12_12_1$ [153]. The unit cell contains 4 glucose residues, 4 ionic liquid molecules and 4-8 water molecules [153]. Endo et al found several complex crystals of cellulose with 1-methyl-3-propylim-diazolium ([C3mim]+) paired with dimethylphospate ($[DMP]^-$) and chloride (Cl^-) with or without water molecules, but the crystal structures are not revealed yet [184].

I.7.7. Other cellulose complexes

In addition to above mentioned cellulose complex crystals, several other cellulose complexes have been reported, including cellulose/NMMO complex, cellulose oligomers/DMSO complex and cellulose/alcohol complex. Nishiyama et al. studied the wide-angle X-ray scattering profiles of 10% cellulose/NMMO solution after addition of water, and the diffraction peaks at q = 1.4 and 1.5 $Å^{-1}$ were probably due

to an intermediate cellulose/NMMO complex before converting to cellulose II [185]. Cellulose oligomers with the average DP of 7 are able to dissolve in DMSO [186]. Zhang et al. presented an oligomeric cellulose (DP 7)/DMSO complex crystal at the APS conference (Boston) in 2019, and the X-ray diffraction data showed a monoclinic unit cell with parameters of a = 9.29 Å, b = 21.72 Å, c = 10.28 Å, α = β = 90˚, γ = 87.89˚ [187]. Warwicker and Wright prepared a serious of cellulose/alcohol complexes by washing cotton/caustic soda samples in methanol, ethanol, n-propanol and n-butanol, and the unit cell parameters of the complexes with or without different drying methods were presented [188].

I.8. Motivation and purpose

As described above the cellulose oligomers have high potentials in different fields but yet underused due to their poor availability. So far, there is no established affordable and scalable method of cellulose oligomer production that allows precise control over their molecular weight distribution.

The aim of this thesis work is to produce cellulose oligomers with controlled average molecular weight and molecular weight distribution, based on concentrated acid hydrolysis inspired by Isogai and Usuda [1]. To achieve this goal, I first investigated the molecular mechanism in the swelling, dissolution, hydrolysis and regeneration processes of cellulose in concentrated acid solutions. I also compared different characterization methods to accurately determine the average molecular weight and molecular weight distribution of resulting cellulose oligomers.

In particular, sulfuric acid and phosphoric acid were used for solubilize and hydrolyze microcrystalline cellulose. The swelling behavior of cellulose in acid

solutions were studied using wide-angle X-ray scattering experiments (Chapter 3). For better characterization of molecular weight, two derivatization methods of cellulose, nitration and carbanilation, were compared and the carbanilation method was further investigated and optimized (Chapter 4). For the DP estimation methods, the molecular weight of cellulose oligomers from the SEC with RALS and LALS detectors, MALDI-TOF mass spectrometry, liquid-state ^{1}H NMR and solid-state ^{13}C NMR spectroscopy were compared (Chapters 5). Finally, the preparation conditions of cellulose oligomers were varied to control the molecular weight and its distribution (Chapter 6). Based on the obtained information in the Chapter 6, the key parameters and mechanisms for the production of cellulose oligomers were discussed (Chapter 7).

Chapter II

Chapter II. Materials and methods

II.1. Materials

Microcrystalline cellulose (MCC) Vivapur®101 (batch number 561014060606) is derived from purified wood pulp and purchased from JRS Pharma, Germany. Dimethylformamide (DMF) and dimethyl sulfoxide (DMSO) were bought from Fisher Chemicals, UK. 96 wt% Sulfuric acid (H_2SO_4) was purchased from Acros Organics, France. 37% of Hydrochloric acid (HCl) was bought from Carlo Erba Reagents, France. Sodium sulfate (Na_2SO_4) was from Honeywell Fluka, France. Sodium hydroxide (NaOH) and potassium chloride (KCl) were purchased from VWR, France. Isopropanol, methanol and acetone was purchased from Biosolve Chimie, Netherlands. Deuterated acetone was from Eurisotop, France. Phosphoric acid (H_3PO_4), sodium chloride (NaCl), lithium chloride (LiCl) and deuterated chloroform ($CDCl_3$) were obtained from Sigma-Aldrich, the U.S.A. There were two bottles of phenylisocyanate used in this thesis. Both were purchased from Sigma-Aldrich, the U.S.A. One was stored in a shelf for about 3 years after it was opened, and the other one was newly bought, named here as PI-old and PI-new, respectively. The comparison of PI-new and PI-old is given in Appendix 1.1.

II.2. Preparation of cellulose oligomers

The general strategy for preparation of cellulose oligomers is based on the method proposed by Isogai and Usuda [1]. As schematized in the Scheme II.1. the method consists of three steps: (i) dissolution and hydrolysis of cellulose in concentrated phosphoric or sulfuric acid solution, (ii) regeneration of water-insoluble cellulose fraction (fraction A) and (iii) regeneration of organic solvent-insoluble cellulose

fraction (fraction B). In the following, a typical example of preparation conditions is given. The preparation conditions for the actual samples can vary for each experiment as specified in each chapter.

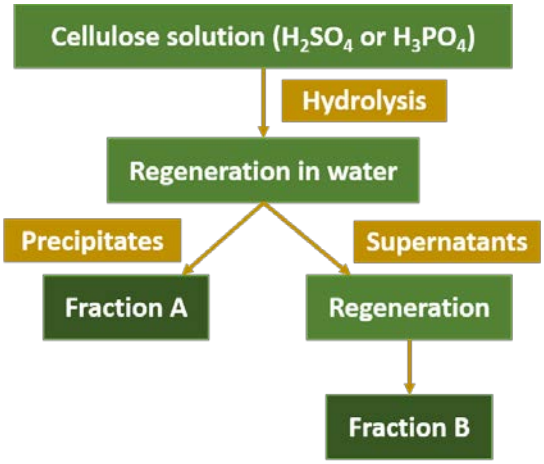

Scheme II.1. *Scheme of preparing regenerated cellulose fraction A and B by sulfuric acid or phosphoric acid.*

II.2.1 Dissolution and hydrolysis of cellulose in phosphoric acid

MCC was mixed with 85 wt% phosphoric acid aqueous solution, and stirred with a magnetic stirrer at room temperature until the solution became homogenous and clear. The final concentration of cellulose and phosphoric acid was 3 wt% and 83 wt%, respectively. The hydrolysis took place at different temperature (23 ˚C and 40 ˚C) for different duration of time.

II.2.2 Dissolution and hydrolysis of cellulose in sulfuric acid

MCC was mixed with distilled water in a flask and placed in an ice bath. Then 96% sulfuric acid was slowly added into the mixture with agitation. The final concentrations of cellulose and sulfuric acid were 9 wt% and 62-64 wt%, respectively. The reaction mixture was stored in a freezer at -20 ˚C for 1 h, after which a clear solution was obtained. The hydrolysis took place at different temperature (15 ˚C and

40 ˚C) for different duration of time.

II.2.3 Regeneration

II.2.3.1 Regeneration of cellulose in water and in organic solvents

The cellulose phosphoric and sulfuric acid solutions after the hydrolysis were mixed with an equal or 10 times its weight of water at different temperature (4 ˚C, 23 ˚C and 40 ˚C) for different decantation time (0 or 24 hours). Then the mixture was centrifugated at 15892 g for 10 mins. The precipitate was named as fraction A. It was washed with water by centrifugation to neutrality. The first supernatants were filtered with filter paper, mixed with three times their volume of isopropanol or methanol, and stored at 4 ˚C for 24 hours. Then this precipitate was named as fraction B and washed with the respective solvents (methanol and isopropanol) by centrifugation until pH reached neutral. The fraction A and B were freeze-dried, and the yield was calculated as follow,

$$Yield\ (\%) = \frac{m}{m_0} \times 100$$

where m was the mass of freeze-dried regenerated cellulose fractions A or fractions B, and m_0 was the mass of air-dried MCC.

II.2.3.2. Neutralization of the regeneration mixtures

Cellulose phosphoric and sulfuric acid solutions were prepared according to II.2.1 and II.2.2 and placed in an ice bath. Solid NaOH was slowly added to the cellulose solution in an ice bath until the pH reached neutral. After decantation for 24 hours, the precipitate was collected by centrifugation and washed with water for four times. Then the precipitate was freeze-dried and the yield was calculated as in the Chapter II.2.3.1.

II.3. Carbanilation of cellulose

In chapter IV, carbanilation was done with DMF as a solvent. However, it turned out that the derivatization efficiency was higher in pyridine, so DMF was replaced by pyridine in Chapter V and VI. Both of the reaction conditions together with a purification method are described below.

II.3.1. Carbanilation in DMF

Cellulose (MCC, fractions A and B) was dried overnight in a single-neck flask at 110 ˚C, then mixed with dry DMF+0.01 M LiCl. The flask was closed with a rubber plug and purged with argon gas for about 3 min. Then phenyl isocyanate was injected to the flask using a syringe. The reaction mixture was kept at 90 ˚C for 48 hours. The reactions were stopped by adding excess methanol to the mixtures.

II.3.2. Purification of cellulose carbanilates by washing with methanol

After carbanilation, the reaction mixtures were poured into a large amount of methanol. After decantation for one day, the precipitate was washed with methanol for four times by centrifugation and freeze-dried. The yield of MCC carbanilates was around 60 %, and the yield of carbanilated cellulose oligomers was around 10 %.

II.3.3. Purification of cellulose carbanilates by dialysis

After carbanilation, the reaction mixture was dialyzed against acetone using a dialysis membrane (Spectra/Por® 7 RC dialysis membrane tubing, cutoff = 1 kD, MWCO) for two weeks to remove the side products, then the cellulose carbanilates/acetone solutions were concentrated in a 50 ˚C oven until acetone was evaporated. The yield of MCC carbanilates after the purification was around 65 %, and that of carbanilated cellulose oligomers was around 20 %.

II.3.4. Carbanilation for DP mearsurement

About 20 mg (0.1 mmol) of cellulose samples were vacuum-dried overnight at 100 ˚C, then mixed with 200 μL dry pyridine or DMF+0.01 M LiCl. Then the cellulose suspension was mixed with 100 μL of PI-new (0.9 mmol, 3.0 molar equiv. to the -OH groups of cellulose). The reactions were kept at 90 ˚C for 48 hours, then stopped by the addition of 100 μL methanol.

II.4. Characterization

In the following, the principles and typical manipulations of characterization methods used in this thesis are described. The measurement conditions may vary among different experiments as specified in each chapter.

II.4.1. Polarized light microscopy

II.4.1.1. Principle

Polarized light microscopy is an optical microscopy method to image optically anisotropic (or birefringent) specimens, such as uniaxial and biaxial crystals. The image contrast arises from interference effect generated by interactions between polarized light and birefringent specimen. In a polarized light microscope, there are usually two polarizing filters, the polarizer and the analyzer as shown in the scheme. The polarizer is located between the light source and the specimen. It filters non-polarized white light into plane-polarized light before it hits the specimen. The polarized light passes through the specimen, which produces two individual wave components that are each polarized in mutually perpendicular planes (Figure II.1). The analyzer is placed after the specimen but before detector and eyepieces. It combines the two wave components to generate the final image contrast.

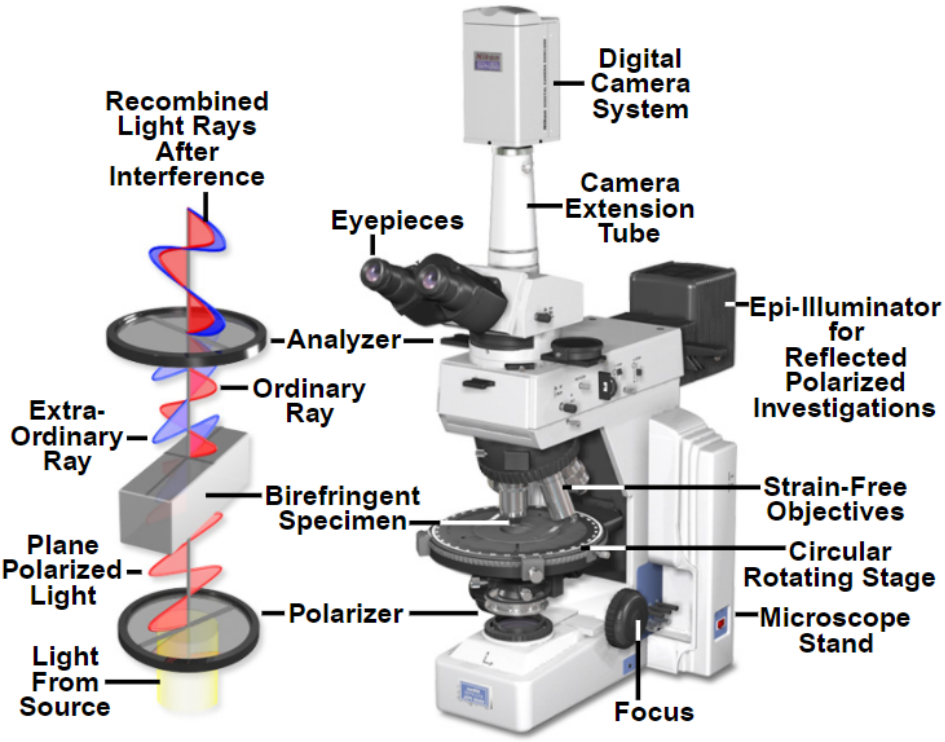

Figure II.1. *Polarized light microscopy configuration* [189].

II.4.1.2. Experimental procedure

The specimens were deposited on a glass slide and covered with a glass slip, and observed using a Zeiss Axiophot II microscopy (Zeiss, Germany) equipped with a crossed polarizer and a lambda plate. The images were recorded with an Olympus SC50 digital camera operated with an Olympus Stream software.

II.4.2. X-ray diffraction

II.4.2.1. Principles

X-rays are electromagnetic waves with a wavelength ranging from 0.01 nm to 10 nm. Since the wavelength of X-rays is comparable to the size of atoms and molecules, they are used to probe atomic and molecular structures of materials through different types of interactions between X-rays and materials. In this thesis, I mainly used X-ray

diffraction technique which is elastic scattering of X-rays by crystalline compounds.

Scattering of X-ray photons by matter is roughly equivalent to the scattering by the electrons within the matter, because the nuclei have little contribution to the scattering of X-rays. When X-rays with a λ wavelength interact with a crystalline sample, they are scattered by a constituent atom in a specular fashion with a specific scattering angle. When these scattered X-rays constructively interfere, so-called Bragg diffraction occurs and strong reflection spots are observed at the detector. Here, the parallel lattice planes are spaced with a distance of *d* (d-spacing), and the angle between the incident beam and the lattice plane is θ. The waves reflected by the two lattice planes have an optical path difference of 2dsinθ. The condition to have the

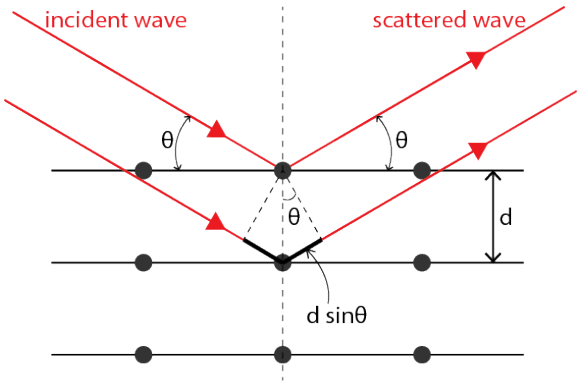

Figure II.2. *Illustration for Bragg's law.*

constructive interference is given as 2dsinθ = nλ, (n is an integer) which is called Bragg's law. Each diffraction peak in a diffraction pattern corresponds to a specific crystalline lattice plane in real space. For three-dimensional crystal system, the smallest repeating unit in a crystal is a unit cell which is defined by three vectors a, b, and c, and the interaxial angles between them, α, β, and γ. Lattice planes in the crystal system are described by Miller indices (h, k and l). A (h k l) plane denotes the family

of planes vertical to the ha*+kb*+lc*, where a*, b*, and c* are reciprocal lattice vectors of the unit cell. The d-spacing, d_{hkl} of given lattice plane (h k l) is calculated using h, k, l and lattice parameters. For instance, in the orthorhombic system ($a \neq b \neq c$, $\alpha = \beta = \gamma = 90°$), which I investigated in Chapter III, d-spacing of (h k l) plane is given as:

$$\frac{1}{{d_{hkl}}^2} = \frac{h^2}{a^2} + \frac{k^2}{b^2} + \frac{l^2}{c^2}$$

The diffraction intensity of each diffraction spot is proportional to the square of amplitude of structure factor which is a function describing the amplitude and phase of the wave diffracted from a corresponding crystalline lattice plane. X-ray crystallography uses the information of structure factor to determine the three-dimensional electron density and hence the atomic coordinates in the crystal system.

In this thesis, two different X-ray sources are used for diffraction experiments: synchrotron radiation X-rays and lab-source X-rays which is based on a rotating X-ray tube. One of the main differences between synchrotron radiation X-ray and the lab source is the much higher brilliance in the Synchrotron one. The synchrotron X-ray beam is at least several orders of magnitude brighter than the lab-source X-rays. Synchrotron radiation is electromagnetic radiation generated when a charged particle, such as an electron, is radially accelerated. Such a situation is obtained using a bending magnet and an undulator in a Synchrotron facility. An undulator is a device inserted in the orbit of electrons in the synchrotron storage ring and can generate strong and highly oriented X-ray beams. An undulator consists of a series of magnets with alternating polarities, which makes the electron orbit literally undulate. Each time a moving electron changes direction, strong radiation is generated. The electrons

are travelling very close to the speed of light within a synchrotron, so the emitted energies are at X-ray range. One of the benefits of using such high energy, high-brilliance X-rays is a shorter measurement time to obtain X-ray diffraction patterns of good signal-to-ratio compared to a lab-source X-ray machine. This allows a time-resolved diffraction measurement. Another benefit is a smaller attenuation thanks to the high-energy of X-rays, which allows one to measure thicker samples or those composed of high-Z elements. This is particularly important in this thesis as it is only possible with synchrotron X-rays to obtain diffraction pattern of cellulose in sulfuric acid solution as shown in Chapter III.

II.4.2.2. Experimental procedure

The wide-angle X-ray scattering (WAXS) and small-angle X-ray scattering (SAXS) experiments in Chapter III (Dissolution and swelling of cellulose in acid) were conducted with X-rays (λ = 0.77489 Å) at SWING beamline of SOLEIL Synchrotron (Paris, France). For its good uniaxial orientation of the cellulose crystals along the fiber axis, flax fiber was used to investigate the swelling process in concentrated H_2SO_4 aqueous solutions (60 wt%, 62 wt% and 64 wt%). 2-cm tips of glass pipettes were cut off and their one ends were closed by flame. They were used as glass sample tubes with an outer diameter of about 1.3 mm and a wall thickness of 0.15 mm. 3.75 mg of flax fiber and about 15 mg of H_2SO_4 solution were put into the tube. These glass tubes were centrifuged to fully immerse the fibers in H_2SO_4 solution and remove air bubble from the tube. The tube with the sample was then placed in a temperature-controlled specimen holder (Linkam THMS 600). It took approximately 15 min from the addition of the acid solution to the measurement of the first scattering pattern. The specimen was cooled down from the room temperature (23 ˚C) to -20 ˚C with a

cooling rate of about 8 ˚C/min. The specimen was kept at -20 ˚C for an hour and warm up to 20 ˚C. During this process, two-dimensional scattering patterns were recorded every 5 mins with an exposure time of 2 s. The experiments were repeated twice for each acid concentration with different sample-to-detector distance to cover both small-angle and wide-angle regions.

The SAXS and WAXS in Chapter VII (Mechanism on producing monodisperse cellulose oligomers) were measured with X-rays of 18 keV (λ = 0.6888 Å) at D2AM beamline of European Synchrotron Radiation Facility (Grenoble, France). The cellulose phosphoric or sulfuric acid solutions were put in glass capillaries (outer diameter of 3 mm, thickness of 200 μm) for the measurements. The silicon pixel detector with a central hole "WOS" (imXPAD, France) was placed at about 7 cm from the samples. A rectangular detector "XPAD-D5" (imXPAD, France) was placed at 1.5 m from the samples. The exposure time was 10 s for each frame. The scattering data were calibrated by the scattering patterns of silver behenate and chromium trioxide.

The incident and the transmitted beam intensities were monitored by scintillation counters placed before and behind the samples respectively. After the scattering signal from the empty capillary was subtracted, the scattered intensity was normalized with the transmitted intensity. The scattering intensities are presented as a function of the magnitude of the scattering vector

$$q = \frac{4\pi sin\theta}{\lambda} (\text{Å}^{-1})$$

where 2θ is the angle between the incident beam and the scattered beam.

For lab-source X-ray diffraction experiments, X-rays was generated by a Philips PW3830 generator operating at 30 kV and 20 mA (Ni filtered CuKα radiation, λ =

1.5418 Å). X-ray diffraction (XRD) patterns were recorded on Fujifilm imaging plates in a Warhus vacuum chamber, read by a Fujifilm BAS 1800-II bioimaging analyser. The diffraction data were calibrated using a diffraction pattern of calcite powder.

II.4.3. Size exclusion chromatography

II.4.3.1. Principle

The SEC instruments used in this thesis are comprised of an injection system, a series of columns, two light scattering detectors (RALS and LALS), differential refractive index (dRI) detectors or ultraviolet (UV) detectors. The sample, in the form of a dilute solution in the same solvent used as the mobile phase, is injected into the columns that have a continuous flow of the mobile phase. The large molecules elute from the columns first, followed by molecules with decreasing molecular size. The concentration of molecules eluting from the column outlet is monitored by a concentration detector, a dRI detector or a UV detector. The two light scattering detectors detect the scattered light intensity at two different angles, and the ratio of scattered light intensity to incident light intensity is measured as the Rayleigh ratio R_Θ. The relationship between the intensity of the light scattered by a sample and its size and molecular weight is described by Rayleigh theory:

$$\frac{\mathrm{Kc}}{R_\theta} = \frac{P_\theta}{M_w} + 2A_2c + 3A_3c^2 + \cdots$$

where c is the concentration of the separated fraction calculated from the dRI detectors or UV detectors; Θ is the measurement angle; M_w is the molecular weight of the sample; $2A_2c + 3A_3c^2 + \cdots$ is the virial equation of states. This virial expansion relates to intermolecular interactions. Under a dilute condition where there is no

intermolecular interaction, the virial coefficients can be regarded as zero. K is a constant and P_Θ is the scattering function, and they are defined as follows,

$$K = \frac{4\pi^2}{\lambda_0{}^4 N_A}(n_0 \frac{d_n}{d_c})^2$$

where λ_0 is the laser wavelength; N_A is the Avogadro's number; n_0 is the refractive index of the solvent; and dn/dc is the refractive index increment of the sample in the corresponding solvent;

$$P_\theta = 1 + \frac{16\pi^2 n_0{}^2 R_g{}^2}{3\lambda_0{}^2}\sin^2(\frac{\theta}{2})$$

where R_g is the molecule's radius of gyration. From the Rayleigh equation, the intensity of scattered light at a given angle is dependent on many factors including molecular weight and molecular size. The increase in the intensity of scattered light is

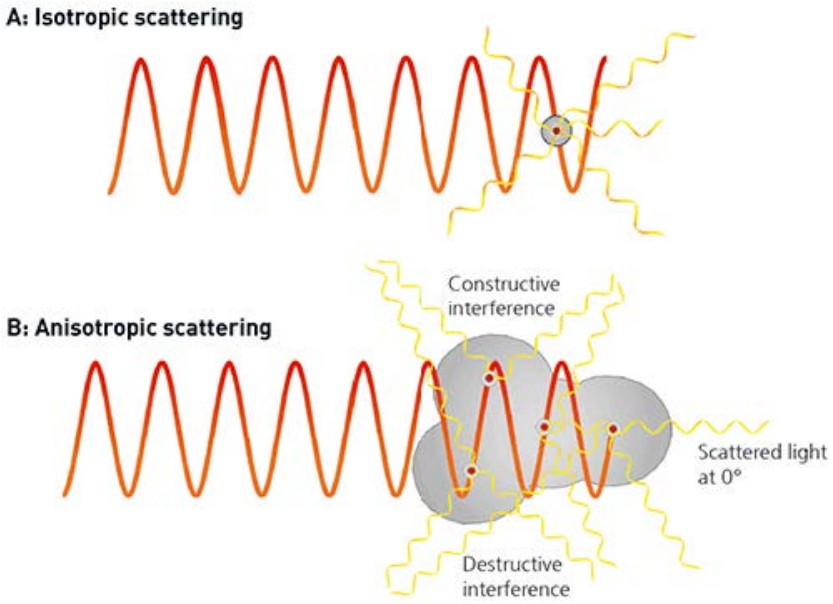

Figure II.2. *(A) An isotropic scatterer is small relative to the wavelength of the light and scatters light evenly in all directions; (B) An anisotropic scatterer has significant size compared with the wavelength of the incident light and scatters light in different directions with different intensities* [184].

linear with molecular weight but non-linear with respect to molecular size.

As seen in the scattering function P_Θ, the scattered light intensity varies as a function of measurement angle. Molecules with the size much smaller than the wavelength of incident light isotropically scatter the laser light as shown in the Figure II.2A [190]. On the other hand, for large molecules whose molecular size is significant compared to the wavelength of the incident light, the photons no longer scatter independently but interfere with each other as shown in Figure II.2B. If the scattered light intensity at $\Theta = 0^\circ$ could be measured, then P_Θ would be 1 and the molecular weight could be calculated without influenced by the angular dependence. Unfortunately, it is unrealistic because the incident laser light is so much stronger than the scattered light that the signals from scattered light is simply overwhelmed by the incident light. To extrapolate the intensity at 0˚, a Guinnier plot, Kc/ R_Θ as a function of $\sin^2(\Theta/2)$ is used. The slope of the angular dependence plot is expressed as follows,

$$\frac{dy}{dx} = \frac{16\pi^2 {n_0}^2 {R_g}^2}{3{\lambda_0}^2 M_w}$$

The molecular size R_g can be determined from this plot. However, at small molecular size, the slope is very small and hidden in the noise of the data. Only when the molecule reaches a size large enough to behave as an anisotropic scatter will the slope be large enough to get a reliable R_g value. Thus, the light scattering method may not be suitable for cellulose oligomers with too small molecular size as discussed in Chapter V.

An appropriate column calibration is necessary to establish a relation between the elution volume and molar mass of the eluting molecules. A straightforward calibration method is based on a set of well-characterized polymer standards with as narrow a

molecular weight distribution as possible. This calibration technique is regarded as a relative calibration because the obtained molecular weight values are relative to the calibrant. For example, if the column set is calibrated with polystyrene narrow standards and cellulose tricarbanilate is run as a sample, the obtained molecular weight values is based on polystyrene, and inaccurate for cellulose tricarbanilate. In contrast, universal calibration can provide accurate molecular weight of the analyte by determining the molecular weight of each slice through a viscometer detector along with the dRI detector.

The addition of light scattering detectors to an SEC system allows to directly measure the molecular weight of the sample without column calibration. However, it still requires instrument calibration to relate the signal from the photo detector to the magnitude of scattered light intensity and then to the molecular weight of the sample. With a standard sample with known concentration, injected volume, molecular weight (M_{std}) and dn/dc, the calibration constant (K_{ls}) can be calculated and also can be performed on every angle in the light scattering detector simultaneously.

$$Calibration\ constant\ K_{ls} = \frac{I_{std}}{M_{std} \times \left(\frac{dn}{dc}\right)_{std}^{2} \times m_{std}}$$

where I_{std} is the measured light scattering intensity of the standard, and the m_{std} is the injected mass of the standard that is calculated by multiplying the concentration with injected volume. Once the calibration constant is determined, the molecular weight for any sample (M_w) can be measured.

$$M_w = \frac{I}{K_{ls} \times \left(\frac{dn}{dc}\right)^2 \times m}$$

where *I* is the measured light scattering intensity of the sample, *dn/dc* is the refractive index increment of the sample, and m is the injected mass of the sample.

II.4.3.2. Experimental procedure

Two SEC instruments have been used in this thesis and named as SEC-1 and SEC-2, respectively. The SEC-1 was performed at 40 °C using an Agilent Technologies 1260 Infinity system (1260 quaternary pump, 1100/1200 thermostatted column compartment, 1260 MDS RI detector, 1260 variable wavelength detector (UV wavelength = 280 nm), 1260 infinity multi detector suite with low-angle light scattering at 15^{o} and right-angle light scattering at 90^{o}) equipped with a Shodex GF-1G 7B pre-column, a Shodex GF-310 HQ column (linear, 7.6 mm × 300 mm; pore size, 20 nm; bead size, 5 μm; exclusion limit, 4 × 10^4) and a Shodex GF-7 M HQ column (linear, 7.6 mm × 300 mm; pore size, 20 nm; bead size, 9 μm; exclusion limit, 4 × 10^7) in DMF containing lithium chloride (0.01 mol L^{-1}) at a flow rate of 0.6 mL min^{-1}. The calibration was using monodisperse standard polystyrene samples with different molecular weight (from 1000 to 320000). Cellulose was carbanilated in DMF+0.01 M LiCl according to the Chapter II.3.4, and the clear solution after carbanilation was diluted to a concentration of about 3 mg/mL, then directly injected for the SEC test. Cellulose trinitrates were dissolved in DMF+0.01 M LiCl with a concentration of about 3 mg/mL and injected for the SEC test.

The SEC-2 was performed at 40 °C using an Viskotek TDAmax system (VE 2001 GPC Solvent/Sample module, UV detector model 2501 with deuterium lamp and UV wavelength = 280 nm, TDA 302 Triple array detectors includes RI detector, viscometer detector and light scattering detectors with low-angle light scattering at 7^{o} and right-angle light scattering at 90^{o}) equipped with a Shodex GF-1G 7B pre-column,

a Shodex GF-310 HQ column (linear, 7.6 mm × 300 mm; pore size, 20 nm; bead size, 5 μm; exclusion limit, 4×10^4) and a Shodex GF-7 M HQ column (linear, 7.6 mm × 300 mm; pore size, 20 nm; bead size, 9 μm; exclusion limit, 4×10^7) in THF at a flow rate of 0.4 mL min^{-1}. The calibration used the universal calibration method. Cellulose was carbanilated in pyridine according to the Chapter II.3.4. After carbanilation, pyridine and the excess methanol in the mixtures were removed by a vacuum condenser. Then the precipitates were dissolved in THF with the concentration of about 3 mg/mL for cellulose tricarbanilates, then injected for the SEC test. For nitrated samples, cellulose trinitrates were dissolved in THF with a concentration of about 3 mg/mL and injected for the SEC test. The polydispersity index (Đ) and recovery are calculated as follows,

$$Đ = \frac{Mw}{Mn}$$

$$Recovery\ (\%) = \frac{c_{RI}}{c_0} \times 100\%$$

where the *Mw* is the weight average molecular weight, Mn is the number average molecular weight, C_{RI} is the concentration of samples that is calculated based on the RI signals, and C_0 is the injected concentration of samples.

II.4.4. Elemental analysis

II.4.4.1. Principles

An elemental analyzer include three major zones of the system: the combustion area, the gas control area, and the separation and detection area. It requires high temperature combustion in an oxygen-rich environment. In the combustion process, carbon is converted to carbon dioxide; hydrogen to water; nitrogen to nitrogen gas or

oxides of nitrogen; and sulphur to sulphur dioxide. If other elements such as chlorine are present, they will be converted to combustion products such as hydrogen chloride. A variety of absorbents are used to remove these additional combustion products as well as some of the principal elements, for example sulphur, if determination of these additional elements is not required. Catalysts are usually added to the combustion section to aid complete combustion. The combustion gases can be separated on a GC column and normally quantified using a thermal conductivity detector. Quantification of the elements requires calibration for each element by using high purity micro-analytical standard compounds such as acetanilide and benzoic acid.

II.4.4.2. Experimental procedure

In our case, elemental analysis was conducted on an elemental analyser (Vario MICRO Cube, Elementar) for C and N determination. The sample was put in a tin capsule and catalytic combusted at a temperature of 1150 °C in the first furnace. Then the reduction of gases was conducted on a hot copper in the second furnace at 850 °C. The formed gases (N_2, CO_2, H_2O and SO_2) were in a stream of carrier gas (He). The gaseous mixture was separated in a Temperature Programmed Desorption (TPD) column, then detected by a catharometer.

II.4.5. Nuclear magnetic resonance spectroscopy

II.4.5.1. Principle

NMR spectroscopy exploits the nuclear magnetic resonance phenomenon of magnetically active nuclei, such as ^{13}C and ^{1}H, to investigate local magnetic environment of such nuclei. The nuclei in an external magnetic field are excited from a lower-energy (equilibrium) to high energy spin state by radiofrequency irradiation (RF pulse). The energy corresponding to the energy gap between two states is

absorbed [191]. This high-energy state is relaxed to the initial equilibrium, with the low energy spin state, during which NMR signals are generated as free induction decay (FID). Nuclei with different environments, depending on the local magnetic environment like binding partners, bond length, bond angle, etc., correspond to different energies and hence resulting in different NMR signals. An NMR frequency spectrum is obtained via Fourier transformation of FID signals. The variation of the resonance frequency of a nucleus relative to a standard is called a chemical shift. Molecular motions depending on the rate and type of intra- and intermolecular reorientations greatly influence the observed spectral features, such as the line widths and shapes, chemical shifts, spin-spin coupling constants, quadrupolar splitting, dipolar couplings and relaxation time.

Generally speaking, the magnetic environment around a nucleus is anisotropic. In liquid-state NMR, such anisotropic information is averaged out due to a fast and random molecular tumbling, and only a single isotropic chemical shift value is observed with a narrow peak with a Lorentz distribution. On the other hand, in solid-state, molecules are immobile and oriented in random directions with respect to the external magnetic field, which gives rise to a very broad line shape for each nucleus due to the chemical shift anisotropy. This peak broadness makes it virtually impossible to interpret solid-state NMR spectrum obtained in a static state measurement. To overcome this challenge, the anisotropic NMR interactions are suppressed by macroscopically rotating the samples at 54.7˚, known as the magic angle, with respect to the magnetic field [192]. This method is called magic angle spinning (MAS). The magic angle corresponds to the angle between a space diagonal of a cube and its edge. This rotation mimics molecular motion in liquid state, which

makes the line shape narrower and the resolution improved. A faster MAS rate results in a narrower peak. However, even at 12 kHz rotation, which is a standard MAS rate in our spectrometer, the line width is significantly broader than those of liquid-state NMR. Cross polarization (CP) is another important technique in solid-state NMR, which transfers the polarization of abundant spins (such as ^{1}H) to the dilute spin (for example ^{13}C) during a so-called contact time. The CP allows to detect dilute spins efficiently with an enhanced repetition rate. ^{13}C has a 1% natural abundance and much longer spin-lattice relaxation time, so the CP technique is very useful and indeed a standard method for ^{13}C NMR in the solid state. In contrast to CP, the direct excitation of dilute spins, named as single-pulse (SP) NMR, requires much longer acquisition times due to the long ^{13}C spin-lattice relaxation time. This technique is further discussed below and also in Chapter IV. Since cellulose has difficulty in being dissolved in common solvents, the combination of CP and MAS techniques is a powerful analytical tool for solid cellulose.

The longitudinal relaxation time, or spin-lattice relaxation time, denoted as T1, is a time constant describing a rate at which excited nuclei return to equilibrium. T1 values for ^{1}H nuclei in medium-size molecules typically range from 0.5 to 4 seconds, and it is feasible for ^{1}H nuclei to have all the signals relaxed fully during the recycled delay between pulses. However, T1 values for ^{13}C can range from 0.1 to tens of seconds for quaternary carbons. Normally, it will take too long for all the ^{13}C nuclei in the tested sample to relax fully between pulses. It means that carbons with different dynamics may relax in different extents during a recycle delay time. Thus, it is generally accepted in the liquid state NMR that ^{1}H NMR signals can be used for quantitative analysis, but not the case for the ^{13}C NMR signals without applying pulse

sequences specifically designed for a quantitative analysis.

^{13}C CP/MAS NMR spectrum should also be considered semi-quantitative. In the solid-state CP experiment, the ^{13}C signal detection does not depend on the slow ^{13}C spin-lattice relaxation, but on ^{1}H spin lattice relaxation time, thanks to the cross polarization. However, a solid-state NMR spectrum loses its quantitative nature due to the kinetics effect involved in the cross-polarization process. In the cross-polarization event, three constants of time are involved: T_{1H}, proton spin-lattice relaxation time, T_{CH}, magnetization transfer time constant from ^{1}H spin reservoir to ^{13}C spin reservoir, and T_{1C}, carbon spin-lattice relaxation time. respectively. The rate of change of ^{13}C magnetization (M_s) in the CP experiment as function of a contact time t is given as follows [193],

$$M_s(t) = \frac{M_0}{T_{CH}} \times \left(\frac{1}{T_{CH}} + \frac{1}{T_{1C}} - \frac{1}{T_{1H}}\right) \times \left(e^{-\frac{t}{T_{1H}}} - e^{-t\times\left(\frac{1}{T_{CH}}+\frac{1}{T_{1C}}\right)}\right)$$

where M_0 is the initial ^{1}H spin temperature, corresponding to the maximum magnetization. Generally, T_{1C} is very long compared with T_{1H} and T_{CH}, as well as CP contact time, and its influence on the relaxation dynamics during the cross-polarization can be ignored. If the conditions of (1) $T_{1C} \gg T_{1H}$ and (2) $T_{1H} \gg T_{CH}$ can be satisfied, the above equation can be simplified as follows,

$$M_s(t) = M_0 \times \left(e^{-\frac{t}{T_{1H}}} - e^{-\frac{t}{T_{CH}}}\right)$$

This indicates that, for instance, apparent intensity of mobile methylene carbon should be smaller than that of rigid ring carbon due to the different ^{1}H spin-lattice relaxation time. Quantitative analysis based on ^{13}C CP/MAS spectra is possible only when one compares M_0 values based on the above-mentioned consideration of the CP kinetics.

II.4.5.2. Experimental procedure

The ^{1}H NMR spectra were recorded on a Bruker Avance III 400 spectrometer at 298 K. The relaxation delay was set as 10 s, and the number of scans was 16 times. The solid-state ^{13}C CP/MAS (cross-polarization magic-angle spinning) NMR spectra were measured with a Bruker Avance III 400 spectrometer operating at 100 MHz for ^{13}C. The MAS rate was set at 12 kHz, the sweep width at 29761 Hz, the recycle delay at 2 s and the cross-polarization contact at 2 ms. The ^{13}C chemical shifts were calibrated with the glycine carboxyl group at 176.03 ppm.

II.4.5.3 Measurement of degree of polymerization by NMR

For solid-state ^{13}C CP/MAS NMR analysis, after calculating the M_0 of C1 on all anhydroglucose units (denoted as I_1) and C1 on the reducing ends (denoted as I_R) are integrated, the number-averaged DP can be calculated as follows,

$$DP_n = \frac{I_1}{I_R}$$

For cellulose oligomers with DP less than 7, liquid state ^{1}H NMR can be used for calculation of the number-averaged DP by dissolving cellulose oligomers in deuterated DMSO or 2% NaOD/D_2O. Given the quantitative measurements of ^{1}H resonance intensity from specific positions on cellulose chains, the number-averaged DP can be calculated as follows,

$$DP_n = \frac{I_\alpha + I_\beta + I_i}{I_\alpha + I_\beta}$$

where I_α and I_β are the integrated intensities of peaks corresponding to H1 of reducing ends, while I_i is the integrated intensity of peak assigned to H1 of other anhydroglucose units except reducing ends.

II.4.5.4 Measurement of degree of substitution by NMR

Liquid-state and solid-state NMR techniques were also used for measuring the DS values of cellulose carbanilates. For liquid-state NMR, about 30 mg of cellulose carbanilates were dissolved in 0.6 mL of deuterated acetone (acetone-d6). The DS values were calculated as follows,

$$DS = \frac{A_{NH}}{A_{C1}}$$

where A_{NH} is the integrated peak area assigned to the NH groups (peaks in the range from 7.4 ppm to 8.0 ppm) and A_{C1} is the integrated peak area corresponded to the C1 (around 4.2 ppm). For solid state SP/MAS (single-pulse magic-angle spinning) NMR experiments, the ^{13}C 90° pulse width was 4 μs with a delay time of 64 s, while all other acquisition parameters were the same as for the CP/MAS experiments. The DS values were calculated as follows,

$$DS = \frac{A_{CO}}{A_{C1}}$$

where A_{NH} is the integrated peak area assigned to the carbonyl groups (around 153 ppm) and A_{C1} is the integrated peak area corresponded to the C1 (around 105 ppm).

II.4.6. Fourier-transform infrared spectroscopy

II.4.6.1. Principle

Molecules absorb energy of photon of a wavelength that matches to a frequency of molecular vibration, which induces excitation of the vibration from the ground state to the excited state. The range of molecular vibration frequency lies in the infrared region (wavelength of 2.5 to 25 μm). Thus, when a sample is irradiated with infrared light, only photons with specific wavelengths are absorbed depending on the vibration

modes existing in the sample. Such spectral information can be used to investigate structure and physicochemical environment of molecules.

Note that infrared absorption only occurs when the vibrations of bonds involve a change in dipole moment. Take CO_2 as an example, symmetric stretching vibrations do not absorb infrared light but asymmetric stretching vibrations do absorb infrared light because the dipole moment changes. In addition to stretching vibrations, infrared absorption also occurs for bending and rotation vibrations, as long as the dipole moment changes. The infrared spectrum is a plot of measured infrared light absorbance or transmittance vs. frequency (sec^{-1}), wavelength (cm) or wavenumber (cm^{-1}).

Attenuated total reflectance (ATR) is a subset of FTIR spectroscopy technique which enables samples to be examined directly in liquid- or solid-state. It is a form of absorption spectroscopy with a small, defined path length. The ATR crystal is made of an optical material with a high refractive index such as diamond. The infrared light is steered towards the ATR crystal at a specific angle, usually around 45˚. When the light reflects off the crystal at this angle, some of the light occurs as an evanescent wave on the surface of the crystal. If there is a sample on the surface of the ATR crystal, the light will enter the sample and reflect back down, and be collected by a detector. The penetration depth of the wave into the sample is typically 0.5-2 μm.

II.4.6.2. Experimental procedure

ATR-FTIR spectra were recorded with a Perkin-Elmer spectrometer in the wavenumber from 4000 to 400 cm^{-1} with a resolution of 1 cm^{-1}. The wet sample or dry sample was directly amounted on an optically dense crystal with a high refraction

index and the data was collected. Then the sample was removed and the crystal surface was cleaned by pure ethanol.

II.4.7. Mass spectroscopy

II.4.7.1. Principle

In mass spectrometry, a charged particle passing through a magnetic field is deflected along a circular path on a radius that is proportional to the mass-to-charge ratio, m/e. Ionization efficiency is the key factor in development of mass spectrometry for macromolecules as it significantly decreases with increasing molecular weight. Matrix-assisted laser desorption/ionization (MALDI) is a common ionization technique for the analysis of biomolecules like proteins. In MALDI, the sample is mixed with a suitable matrix material, for instance, 2,5-dihydroxybenzoic acid (DHB), and then irradiated by a pulsed laser to trigger ablation and desorption of the sample and matrix material. The analyte molecules are ionized by being protonated or deprotonated and accelerated into spectrometer for analysis. Time of flight (TOF) mass spectrometer is widely used with MALDI to increase the resolution. MALDI-TOF MS is capable of creating singly charged ions or multiply charged ions depending on the nature of the matrix, the laser intensity, and the voltage used. The charged ions consist of the initial neutral molecule [M] with ions added or removed, for example, $[M+Na]^+$ and $[M-H]^-$. The results are presented as a plot of intensity as a function of the mass-to-charge ratio, and each molar mass gives a distinct signal in the mass spectrum.

II.4.7.2. Experimental procedure

Cellulose oligomers in DMSO and cellulose carbanilates in DMF with concentration of about 0.02 mol L^{-1} were for MALDI-TOF measurements. The

measurements were performed on a Bruker Daltonics Autoflex Speed apparatus using DHB as a matrix. High resolution mass spectrometry was carried on a Thermo Scientific LTQ Orbitrap XL (quadrupole hybrid with orthogonal acceleration time-of-flight) mass spectrometer. The integration of peak areas that belongs to the same DP were perform on an in-house program.

Chapter III

Chapter III. Dissolution and swelling of cellulose in acid

III.1. Introduction

Dissolving cellulose is one critical step for homogeneous modifications or analytical purposes. There are limited choices since cellulose is insoluble in most common solvents, with each of them having their advantages and disadvantages [134]. Be it aqueous or non-aqueous solvents, all cellulose solvents share in common that at least one component strongly interacts with the hydroxyl groups of cellulose, otherwise cellulose tend to form crystals with regular hydrogen bond networks. The strong interactions and the regularity of cellulose chains often result in crystalline complex involving solvent constituents [194, 195]. Crystal structures of these so-called crystallosolvates have been extensively studied to understand solute-solvent interactions at the atomic resolution. Among such "complexable" molecules, ammonia [196] and ethylenediamine [175] are the major ingredients in the historical cellulose solvents. For cuprammonium hydroxide and cupriethylenediamine hydroxide, they receive strong hydrogen bonding from the hydroxymethyl groups of cellulose leading to highly stable complexes even above the boiling temperature of the solvents [175]. Sodium hydroxide, a promising aqueous solvent of cellulose is known to form a variety of complex crystal with cellulose depending on concentration and temperature [155, 156]. Both N-methylmorpholine N-oxide used in Lyocell process and a new ionic liquid solvent, 1-allyl-3-methylimidazolium chloride, form complex crystals with cellulose [153, 185]. Even non-solvents of cellulose such as water and alcohol can be trapped in the crystalline lattice to form intercalated crystals [159, 188].

Concentrated mineral acids such as sulfuric acid and phosphoric acid are another

class of cellulose solvents well-known for more than a century [144]. Sulfuric acid swells paper to obtain parchment-like substance as already mentioned in 1846[197] and is able to make cellulose dope of very high concentration without much degradation if the temperature is kept low [198]. However, to date, no complex structure of cellulose with any acid has been reported. Recently, Huang and co-workers reported that sulfuric acid solution precooled at -20 ˚C dissolves cellulose at a lower concentration (64 wt%) compared to that of the room-temperature system (i.e. 72 wt%) [149]. Based on this observation, we followed the structural evolution of cellulose immersed in sulfuric acid under temperature perturbation using X-ray scattering, and found the existence of new type of complex at low temperature.

III.2. Dissolution of cellulose in acid

Figure III.1 shows the dissolution or swelling of MCC in sulfuric acid. For about 62 wt% sulfuric acid, 9 wt% MCC are swelled at room temperature, while at -20 ˚C, 9 wt% are dissolved. At -20 ˚C, 9 wt% MCC are not dissolved in the 61 wt% sulfuric

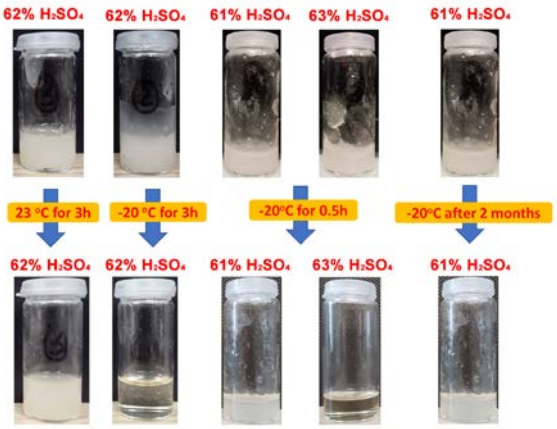

Figure III.1. *Change in appearance of 9 wt% MCC in sulfuric acid aqueous solution of different concentrations at different temperature.*

acid, but in 63 wt% sulfuric acid, it forms a clear solution in 0.5 h. In brief, MCC can

be swiftly dissolved in concentrated sulfuric acid of above 62 wt% at low temperature.

For its good uniaxial orientation of the cellulose crystals along the fiber axis, flax cellulose was selected to observe the dissolution or swelling in sulfuric acid at different acid concentration and temperature. 60 wt%, 61 wt%, 62 wt%, 63 wt% and 64 wt% sulfuric acid were put at -20 ˚C, 19 ˚C and 70 ˚C for about 20 mins before the

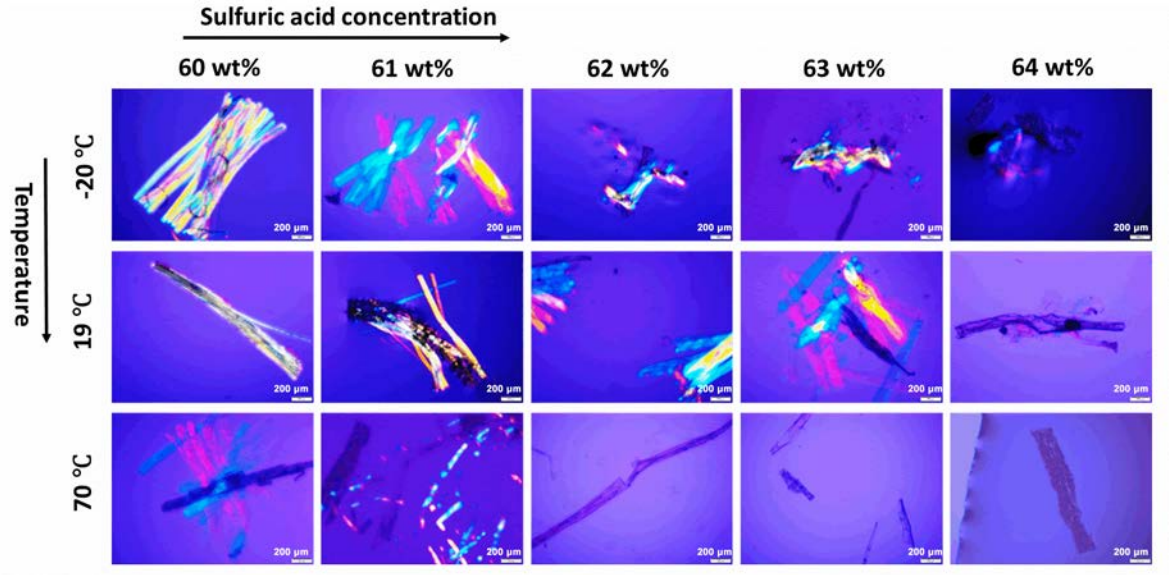

Figure III.2. *The polarized light micrographs of the flax fibers after immersing for 3 mins in 60 wt% - 64 wt% of sulfuric acid acqueous solutions at -20 ˚C, 19 ˚C and 70 ˚C.*

experiment. Flax cellulose fibers were put in sulfuric acid with different temperature and acid concentration for 3 mins, then the morphologies were observed by the polarized light microscopy and shown in Figure III.2. At 19 ˚C, flax fibers maintain the original morphology in the 60 wt% sulfuric solution and begin to swell as the acid concentration increased, and almost dissolve in the 64 wt% sulfuric solution. For -20 ˚C, flax fibers swell in the 60 wt% sulfuric solution, start to dissolve from 61 wt% sulfuric acid. As for 70 ˚C, flax fibers swell and dissolve in the 60 wt% sulfuric acid solution, degrade into fragments in the 61 wt% sulfuric acid solution, as the acid concentration continued increasing, the flax fibers are almost dissolved in the solution.

In brief, the swelling and dissolution of flax fibers prefer the temperature of -20 ˚C and 70 ˚C than 19 ˚C. That high temperature like 70 ˚C contributes to quicker dissolution is due to the quick decomposition of cellulose chains, and shorter cellulose chains are more facile for dissolution.

III.3. Swelling of cellulose in acid by X-ray diffraction

Experiments.

Swelling is regarded as the first stage of dissolution. In this section, to understand how low temperature and acid concentration affect the swelling of cellulose in sulfuric acid, flax fibers with a small amount of sulfuric acid (cellulose concentration of about 20 wt%) were subjected to the WAXS experiments. We put well-aligned dry flax fiber in glass tube, and added 64 wt% sulfuric acid solutions, then eliminated the trapped air bubble by centrifugation. The tubes were mounted on a temperature-controlled sample holder (Linkam Shcientific instruments, UK) for diffraction measurements with an X-ray beam of 16 keV (λ = 0.77489 Å) at the SWING beamline of SOLEIL synchrotron facility (Paris, France). The specimens were cooled from the ambient temperature (23 ˚C) to -20 ˚C, then kept at -20 ˚C for 1 hour, and warmed up back to the ambient temperature. Two-dimensional wide-angle X-ray diffraction patterns were recorded on a hybrid pixel detector (EigerX4M, Dectris, Switzerland) every five minutes through the entire temperature process. The obtained 2D diffraction patterns were processed using in-house programs for further analyses.

Results and discussion.

Figure III.3 shows fiber diffraction diagrams of flax cellulose in 64 wt% sulfuric acid solution at 23 ˚C (Figure III.3a) and -20 ˚C (Figure III.3b). The isotropic background scattering was numerically subtracted [199], which originated mainly from the sulfuric acid solution. The diagram at 23 ˚C shows a diffraction pattern of native cellulose allomorph, cellulose I, with three characteristic equatorial reflections and one strong meridional reflection, 0 0 2, at d-spacing of 0.26 Å [200]. The diagram was taken approximately 15 mins after the flax fiber was immersed in the acid solution, so the room temperature immersion did not affect the cellulose crystal. The cooling gave rise to a series of new sharp reflections (Figure III.3b). These reflections have similar azimuthal angular intensity distributions to those of the original cellulose crystals, and it means that there is no large change in the orientation distribution along the fiber axis. The d-spacings of observed reflections do not match to those of known sulfuric acid crystals. The new reflections were significantly sharper than the original crystals. The crystal dimension estimated

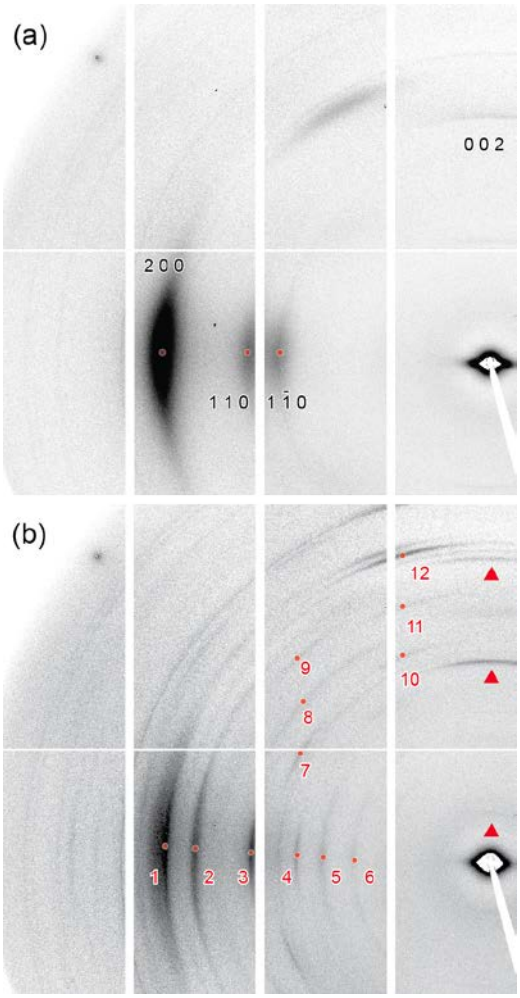

Figure III.3. *Fiber X-ray diffraction patterns of flax cellulose fibers in 64 wt% sulfuric acid aqueous solution at (a) 23 °C and (b) -20 °C. Arrowheads in (b) indicate meridional reflections. Numbered reflections in (b) are used in the exhaustive search of the unit cell parameters.*

from the peak width, 7 nm, is roughly double the initial crystallite size of cellulose I but does not correspond to typical mineral crystalline diffractions that are even sharper. It indicates that the new reflections belong to the cellulose complex in swollen crystalline fibers.

Since three visible meridional reflections appeared at multiples of d* = 0.04 $Å^{-1}$, we assigned these peaks, from the innermost to the utmost, to 0 0 1, 0 0 4 and 0 0 6 with the c-axis being 25.08 Å. Then we searched for a unit cell by an exhaustive approach, assuming an orthorhombic unit cell (α = β = γ = 90°) and using d-spacings of 12 strong and well separated reflections marked in Figure 1b. The detailed procedure of this exhaustive search is described in the supporting information. The obtained parameters were a = 9.12 Å and b = 12.99 Å. The reflection positions calculated using this unit cell are superimposed on the diffraction pattern remapped in cylindrical reciprocal space coordinate (Figure III.4a). They are generally in good agreement, while there are four observed reflections, including a strong

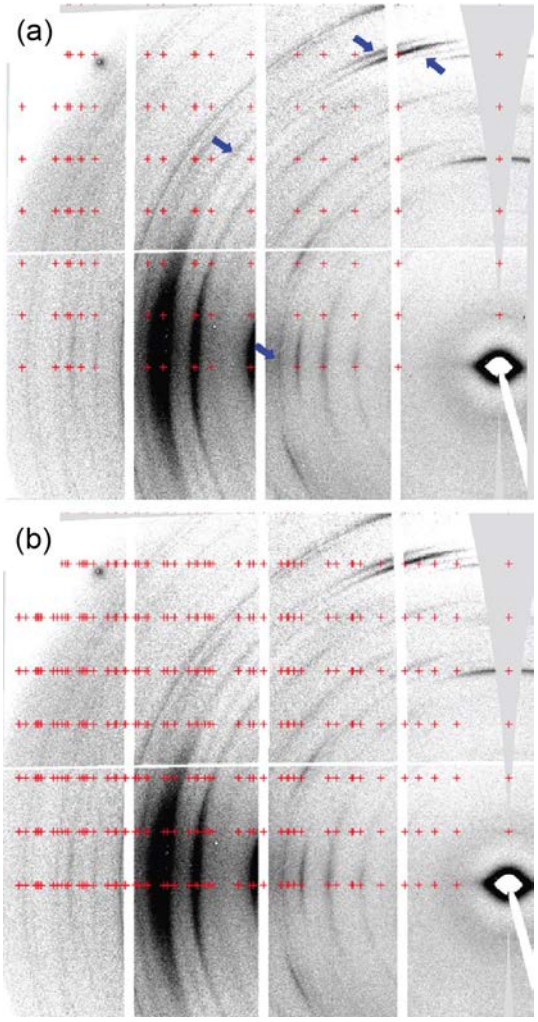

Figure III.4. *Predicted reflection position superimposed on the diffraction pattern of the cellulose-sulfuric acid complex remapped in cylindrical reciprocal space coordinate. (a) a = 9.12 Å and b = 12.99 Å, c = 25.05 Å (b) a = 18.24 Å, b = 25.98 Å, c = 25.05 Å. Blue arrows indicates the observed reflections that are not predicted by the unit cell.*

one on the sixth layer line, that are not predicted from the unit cell.

The lattice constant along the fiber axis, c = 25 Å, corresponds to five times the length of glucose residue, 5 Å. On the meridian, the strongest reflection is 0 0 4, indicating the presence of a periodicity of 6.27 Å along the fiber axis. Such a periodicity is not expected from the cellulose structure, but sulfuric acid tetrahydrate crystal has a tetragonal unit cell with a lattice constant of c = 6.35 Å [201]. This length corresponds to a distance between two sulfuric acid molecules. Considering the similar spacings between 0 0 4 of this complex and c-axis of the tetrahydrate, sulfuric acid molecules in this complex are likely organized along the fiber axis in a similar manner to those in the tetrahydrate crystal. In a 64 wt% sulfuric acid solution, the molar ratio between sulfuric acid and water is 1:3. To form a tetrahydrate-like organization, hydroxyl groups of cellulose would replace one hydration site of sulfuric acid tetrahydrate structure in the complex.

The stoichiometric ratio between each component in the complex is thus glucose residue: sulfuric acid: water = 5n: 4m: 12m. The volume of the unit cell is 2971 $Å^3$ and those of each component are 164 $Å^3$ for glucose residue based on cellulose I_β crystal structure [18], 88 $Å^3$ for sulfuric acid based on the density at 0 ˚C, and 30 $Å^3$ for water. When n and m are 1 and 3, the sum of the component volumes is 2956 $Å^3$, reasonably close to the unit cell volume. Thus, the unit cell contains one cellulose chain, 12 sulfuric acid molecules and 36 water molecules, yielding a density of 1.46 g/cm^3.

To understand the molecular organization in the complex crystal, we first built a packing model based on the unit cell dimensions and the stoichiometry (Figure III.5a). Along the c-axis, four sulfuric acid molecules stack up as in the tetrahydrate crystal.

According to the structure of sulfuric acid tetrahydrate, the distance between sulfur atoms should be around 6 Å [201]. A way to place three molecular stacks of sulfuric acid in the a-b projection while leaving space for the cellulose chain would be to place them on the border, two on the long b axis and one on the short a axis. This will leave space in the middle of the unit cell to host a cellulose chain. These molecular stacks should be shifted to each other along the c-axis, so the inter-sulfur distance is kept around 6 Å. This indicates that the real unit cell should be larger than the current cell. Doubling both a and b dimensions allows to accommodate all the stacks in the different z-positions, resulting in the unit cell dimensions of a = 18.24 Å, b = 25.98 Å, c = 25.05 Å. This unit cell provides a better prediction of diffraction positions compared to the smaller one (Figure III.5b). In this packing model four sulfuric acids between cellulose chains are organized in a similar way to two center and two corner molecules in the tetrahydrate crystal, as indicated with squares in Figures III.5a and 5b. Thus, the orientation of sulfuric acid molecules in this quadruplet presumably conforms that of the tetrahydrate.

Based on the above-mentioned consideration, we constructed a molecular model shown in Figures III.5c and 5d. The 25-Å periodicity along the fiber axis implies an occurrence of five-fold helical conformation of cellulose molecules. This is the first example of cellulose adapting this conformation since, so far, the five-fold conformation has been reported only for one cellulose derivative crystal, cellulose trinitrate, among known cellulosic crystal structures [202]. The inter-sulfur distances in this structure are maintained approximately at 6.1 Å, similar to those of the tetrahydrate crystal. The orientation of sulfuric acid molecules is determined according to their organization in the tetrahydrate crystal. Each SO_4 molecule is

surrounded by three water molecules and one hydroxyl group of cellulose. The intermolecular distance between cellulose chains is 9 Å, which is slightly more than twice the initial intermolecular distance in cellulose I, 3.9 Å [18]. This indicates that the peak sharpening upon complexation, where the full width half maximum of the diffraction peak becomes about a half, is mainly due to this swelling effect rather than crystal growth or co-crystallization.

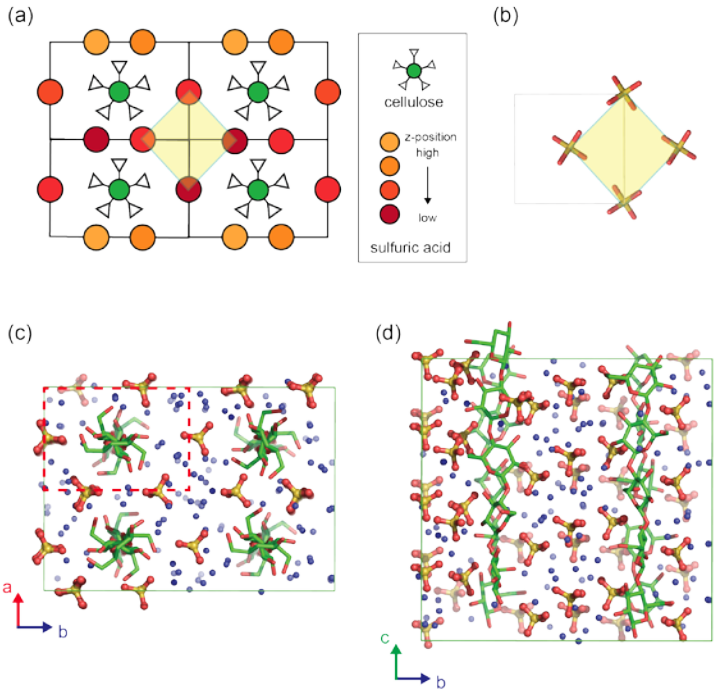

Figure III.5. *(a) Schematic packing model of the cellulose-sulfuric acid complex in ab projection. Circles with different colors denote sulfuric acid molecules in different z-position (along c-axis). A yellow romb indicates the quadruplet formation of sulfuric acid. (b) Organization of sulfuric acid molecules in the tetrahydrate crystal. Water molecules are removed for clarity. (c, d) Molecular model of the cellulose-sulfuric acid complex in (c) ab and (d) bc projections.*

We further investigated the formation and stability of the cellulose-sulfuric acid complex in terms of time, temperature and acid concentration. Figure III.6 shows equatorial diffraction profiles of flax cellulose in sulfuric acid at a concentration of 60, 62 and 64 wt% during the cooling and warming temperature schedule as described

above. At room temperature, the equatorial profiles at all concentrations remain identical to that of cellulose I after 15 min of immersion in the solutions. In the 64 wt% solution, the complexation occurred c.a. 5 min after the specimen temperature reached -20 ˚C. At the 25th minute, reflections of the complex became visible at q = 1.19 and 1.47 Å^{-1}, while the intensity of cellulose I reflections became weaker. Sharp reflections of the complex became stronger over time. Minor part of the cellulose crystal might still exist as cellulose I after 1 hour at -20 ˚C since the 2 0 0 reflection was seen as a shoulder peak in the profile at the 80th min. A similar but much slower complexation was observed in the 62 wt% solution, where the features of the crystallosolvate appeared only after the 40th minute. The reflections of the complex were weaker compared to those of the 64 wt% specimen. A greater portion of cellulose I remained unswollen in the 62 wt% solution as the 2 0 0 reflection of cellulose I (q = 1.6 Å^{-1}) was clearly visible at -20 ˚C. On the other hand, the complex did not form in the 60 wt% solution. Although the reflection intensities became weaker at the low temperature, all the reflection of cellulose I was present and no trace of complexation was observed during the cooling experiment. Upon warming to room temperature, the reflections of the complex immediately disappear in the 62 wt% solution, while in the 64 wt % solution, the trace of them remained for more than 1 hour at room temperature. The intensities of cellulose I reflections became weaker after warming in all the samples, indicating partial dissolution or amorphization of cellulose. This trend is more pronounced in the higher concentrated solutions: the intensity of 2 0 0 decreased by about 70 % in the 64 wt% solution, 50 % in the 62 wt% solution, and 30 % in the 60 wt% solution, respectively. These observations show that the formation of cellulose-sulfuric acid complex occurred at the low temperature and

with a critical concentration at above 62 wt%.

This observed acid-concentration and temperature dependence reflects the mechanism behind the complexation. The crystallization of sulfuric acid tetrahydrate occurs in aqueous sulfuric acid solution below -36 ˚C [203]. Thus, the tetrahydrate-like molecular organization of sulfuric acid is favored in the current system upon cooling. When the number of water molecules is sufficiently low compared to that in the tetrahydrate structure (sulfuric acid concentration is 57.6 wt% in the tetrahydrate crystal), the hydroxyl groups of cellulose would be necessary for hydration of sulfuric acid to form a stable tetrahydrate-like hydration state. Such a water-lacking situation would lead to effective swelling of cellulose fibers and the complexation between sulfuric acid and cellulose. This implies that complexation with different hydration numbers of sulfuric acid might be possible by exploring a wider acid concentration range.

After complexation in the 64 wt% sulfuric acid solution at -20 ˚C, we washed the swollen flax fibers with cold water. The washed flax fibers were subjected to lab-source X-ray diffraction and solid-state ^{13}C NMR spectroscopy. As shown in Figure

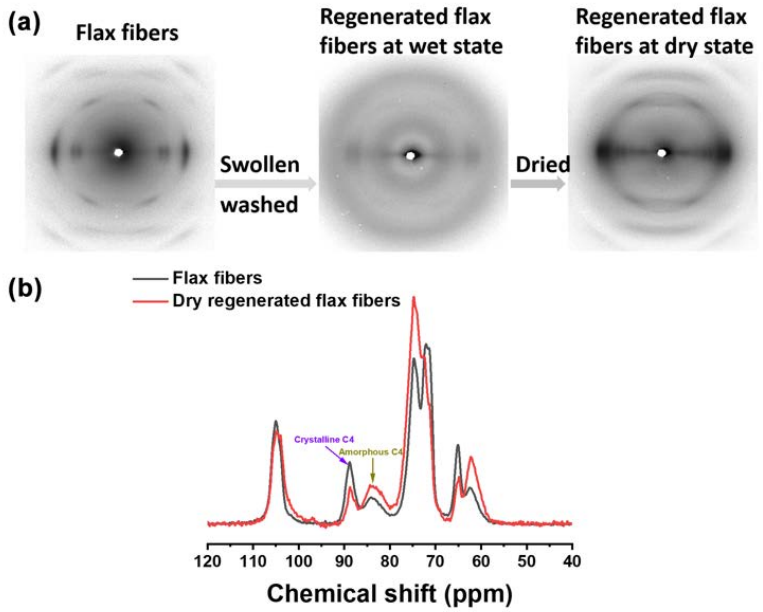

Figure III.7. *(a) Two-dimensional X-ray diffraction patterns of flax fibers, the regenerated flax fiber at wet and dry state. (b) Solid state CP/MAS ^{13}C NMR spectra of flax fibers and the regenerated flax fibers at dry state.*

III.7, the X-ray diffraction patterns of both wet and dry fibers show blurry scattering, indicating the amorphous nature of cellulose in the sample. The solid-state NMR spectrum also shows features of low crystalline cellulose, in accordance with the X-ray diffraction results. This is distinctive from cellulose-alkali complexes which convert to crystalline cellulose II upon water rinsing and drying [204]. This different behavior suggests, on one hand, that cellulose chains are likely in parallel chain arrangement in the complex as in cellulose I. On the other hand, complexation with cellulose II might provide a similar crystal structure but with cellulose molecules in anti-parallel chain arrangement.

III.4. Conclusions

The dissolution of cellulose in acid was confirmed more efficient with lower temperature and higher acid concentration. Cellulose was found to form a crystalline complex with sulfuric acid at -20 ˚C and above the acid concentration of 62 wt%. The complex crystal has an orthorhombic unit cell with dimensions of a = 18.24 Å, b = 25.98 Å, c = 25.05 Å. This large unit cell contains 4 cellulose chains, 48 sulfuric acid molecules and 144 water molecules. The fiber repeat of 25 Å indicates the rare occurrence of five-fold helical conformation of cellulose molecules. Sulfuric acid molecules are organized in a similar manner to that in the sulfuric acid tetrahydrate crystal. Hydroxyl groups of cellulose molecules are likely to participate to the hydration of sulfuric acid molecules together with water molecules in the crystalline lattice. The complexation occurs only above the critical acid concentration, 62 wt%. This concentration dependence of crystal swelling indicates that the lack of water molecules in the system drive the complexation to form a stable hydration state of sulfuric acid. The observed complexation behavior between cellulose and sulfuric acid will serve a basis for better understanding of low temperature swelling and dissolution of cellulose in sulfuric acid and ultimately the process optimization of sulfuric acid-based cellulose solvent systems.

Chapter IV

Chapter IV. Derivatization of cellulose

IV.1. Introduction

Most of the techniques for characterizing molecular weight of polymers, such as SEC and MALDI-TOF MS, require samples in the solution state. The determination of molecular weight and molecular weight distribution is not straightforward for cellulose because cellulose is insoluble in most common solvents. Derivatization methods of cellulose are used to make cellulose solubilized in common solvents. As reviewed in Chapter I.5.1, the most frequently used derivatization methods are nitration and carbanilation. So far, these two methods have not been evaluated or compared in the context of molecular weight measurement of low molecular-weight cellulose.

In this chapter, nitrated and carbanilated cellulose oligomers are first compared using SEC. Then, I further investigated cellulose carbanilate in terms of the degree of substitution (DS). The DS of cellulose carbanilate *i.e.* the average number of aromatic carbamate groups bound per glucose unit, affects the properties of cellulose derivatives (*e.g.* solubility) and the estimation accuracy of degree of polymerization (DP) of cellulose by SEC. Different methods for characterizing the DS values were compared in this chapter, including elemental analysis and several NMR techniques. In the end, the carbanilation method was optimized to get fully substituted cellulose.

IV.2. Methods

IV.2.1. Preparation of fraction A

3 wt% MCC was hydrolyzed in 83 wt% H_3PO_4 at room temperature for 5 weeks (Chapter II.2.1), then regenerated in water according to the Chapter II.2.3.1.

IV.2.2. Nitration of cellulose

Nitrating acid mixture was prepared by mixing 12.12 g of phosphorus pentoxide with 30 g fuming nitric acid in ice bath. Dry MCC or hydrolyzed cellulose specimens (10 mg) were added in the prepared nitrating acid mixture (400 mg). The nitration was proceeded for 20 minutes at room temperature (*c.a.* 23 ˚C). The reaction mixture was neutralized with sodium carbonate together with ice, then washed successively with distilled water and ethanol by vacuum suction filtration.

IV.2.3. Carbanilation of cellulose

20 mg of MCC and the cellulose oligomers in IV.2.1 were carbanilated by PI-new with the usage of argon gas in 0.01M LiCl/DMF according to the Chapter II.3.1.

IV.3. Comparison between nitration and carbanilation

Method.

The SEC experiments were conducted with the nitrated and carbanilated cellulose. 2.9 mg/mL of nitrated MCC/THF and DMF solutions and 3.2 mg/mL of nitrated MCC/DMF solution were injected into the SEC-2 and SEC-1 instruments (Chapter

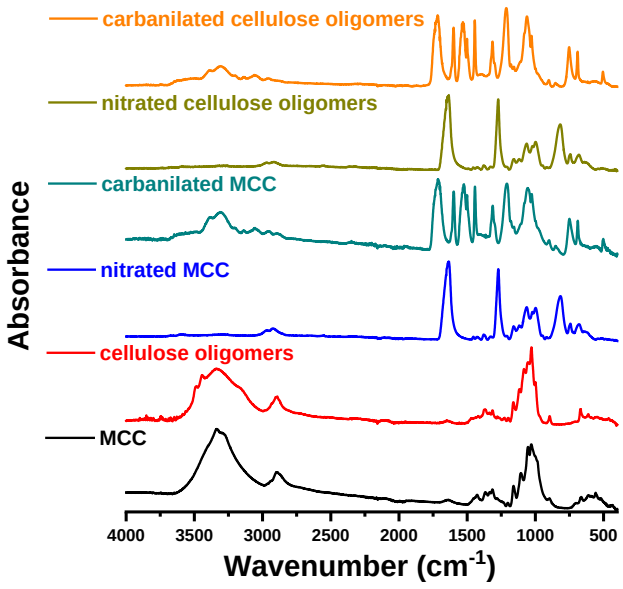

Figure IV.1. *ATR-FTIR spectra of MCC, regenerated cellulose oligomers that hydrolyzed for 5 weeks, and the nitrated and carbanilated MCC and cellulose oligomers that hydrolyzed for 5 weeks.*

II.4.3.2), respectively. Carbanilated cellulose was subject to SEC without purification. ATR-FTIR measurement of the nitrated and carbanilated cellulose were done according to the Chapter II.4.6. Cellulose carbanilates were washed by methanol (Chapter II.3.2).

Results and discussion.

Figure IV.1 shows FT-IR spectra of the nitrated and carbanilated MCC and cellulose oligomers, together with those of non-derivatized MCC and the oligomer. The spectra of MCC and the cellulose oligomers show several bands between 3000 cm^{-1} and 3600 cm^{-1}, which correspond to stretching vibrations of O-H of cellulose. These bands disappear in the spectra of nitrated and carbanilated celluloses. It indicates the cellulose are trinitrated or tricarbanilated. The spectra of the carbanilated MCC and oligomers show absorbance bands at 3382 cm^{-1}, 3301 cm^{-1} and 1716 cm^{-1} that are assigned to the N-H and C=O stretching vibrations [205]. The peaks at 1599 cm^{-1} and 1524 cm^{-1} are due to the C-C stretching vibrations of aromatic rings [206] in the phenylcarbamate

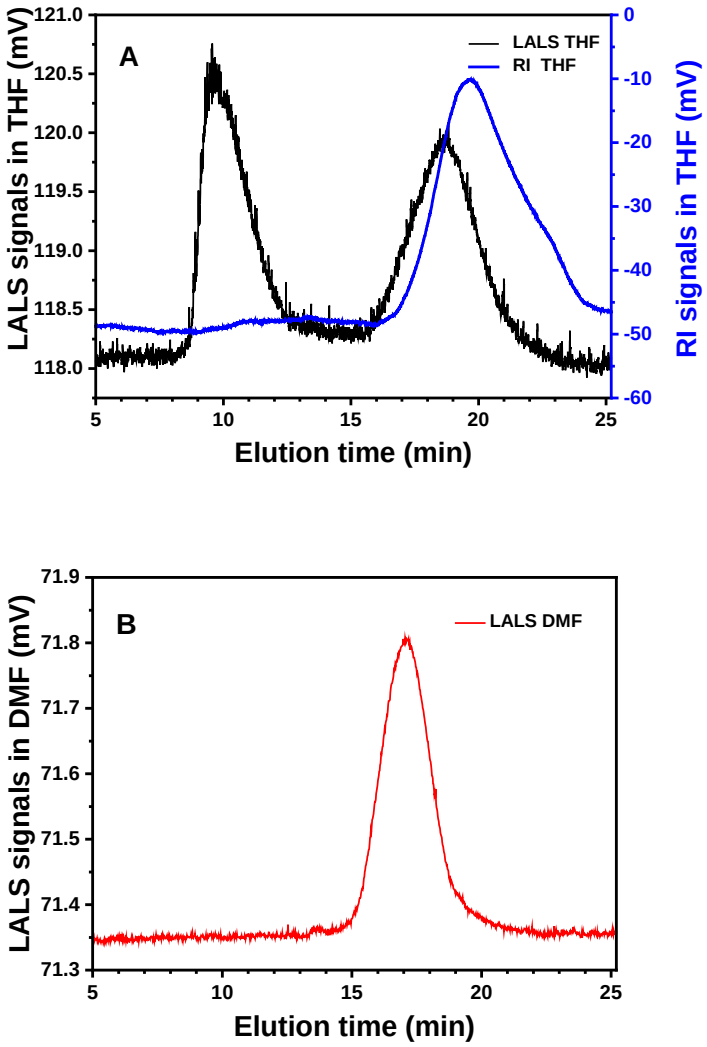

Figure IV.2. *(A) Low-angle light scattering (LALS) and refractive index (RI) signals of nitrated MCC in*

moiety. For the spectra of nitrated MCC and cellulose oligomers, the strong band at 1272 cm^{-1} is due to the N-O stretching vibration [207].

Figure IV.2A shows the low-angle light scattering (LALS, black) signals and refractive index (RI, blue) signals of the nitrated MCC in THF. For the LALS signals, there are two peaks located at 10.0 min and 15.6 min, respectively. However, for RI signals, there is no peak around 10.0 min, which indicates the peak at 10.0 min in the LALS signals is due to aggregates in the solution. Considering the peak position of the RI signal curve, the peak at 15.6 min in the LALS signals is attributed to the fully dissolved nitrated MCC molecules. Figure IV.2B presents the LALS signals of the nitrated MCC in DMF. There is only one peak corresponding to the well dissolved nitrated MCC molecules. The recovery (Chapter II.4.3.2) of the nitrated MCC in the SEC-2 instrument with the solvent of THF and the SEC-1 instrument with the solvent of DMF is 56 % and 92 %, respectively. It indicates that the nitrated cellulose molecules were prone to aggregate in THF, and the aggregates would be filtered before the injection or by the filtration system in the SEC instruments. In brief, the nitrated cellulose is more soluble and stable in DMF than THF.

The tricarbanilated and trinitrated cellulose oligomers are compared in terms of the light scattering responses of SEC-1 in the solvent of 0.01M LiCl/DMF. The SEC profiles are shown in Figure IV.3. The light scattering signals at 90˚ and 15˚ of the tricarbanilated cellulose oligomers were detectable with a large singal-to-noise (S/N) ratio. The main peak around 20 min is attributed to the tricarbanilated cellulose oligomeric molecules, and a couple of peaks at larger elution times are assigned to the side products, phenylisocyanate trimer and dimer (Scheme IV.1). In contrast, the light scattering signals at 90˚ and 15˚ of the trinitrated cellulose oligomers are weak and

almost hidden in the background. The difference in the S/N ratio is striking between the nitrated MCC and oligomer (Figs. IV.2B and IV.3), indicating the low sensitivity of LS to the low-molecular weight cellulose nitrate. The low LS sensitivity is particularly problematic with cellulose oligomers compared to the higher molecular

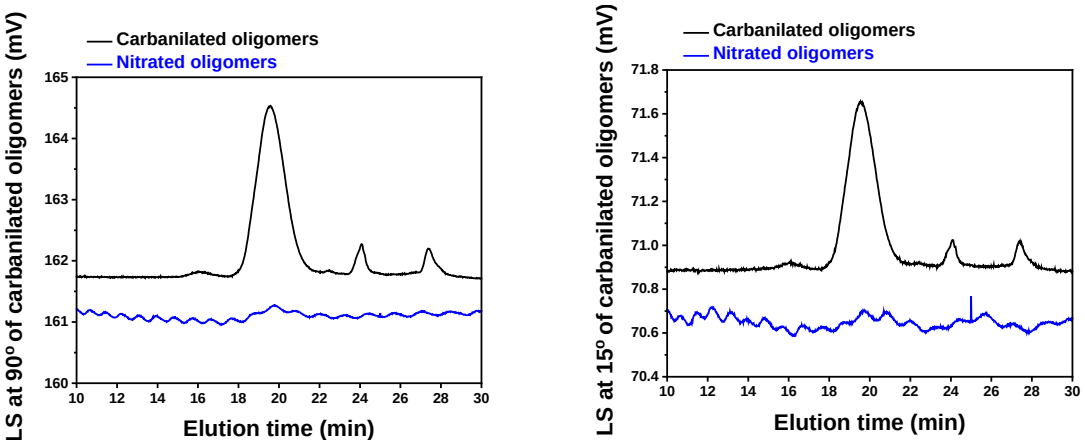

Figure IV.3. *Light scattering signals at 90˚ and 15˚ of carbanilated and nitrated cellulose oligomers that were hydrolyzed at room temperature for 5 weeks, and the solvent was DMF+0.01M LiCl.*

weight counterpart, because the light scattering intensity decreases with decreasing particle size when the refractive indexes of particles are the same. The dn/dc of cellulose trinitrates and cellulose tricarbanilates in 0.01M LiCl/DMF is 0.055 cm^3/g and 0.131 cm^3/g, respectively. A higher dn/dc value results in higher magnitude of light scattering responses. In conclusion, for cellulose oligomers, carbanilation is a better derivatization method than nitration for its better performance in light scattering detection.

IV.4. Study on carbanilation and determination of substitution degree

Based on the results from IV.3, the carbanilation was chosen as the derivatization method for the molecular weight analysis of cellulose oligomers. The carbanilation

reaction of cellulose is shown in Scheme IV.1. The hydroxyl groups of cellulose are substituted with phenylcarbamate molecules in anhydrous DMF. There are several side products, for example, the phenylisocyanate dimer and trimer. Unless the reacting system is completely dry, phenylisocyanate will react with water and form

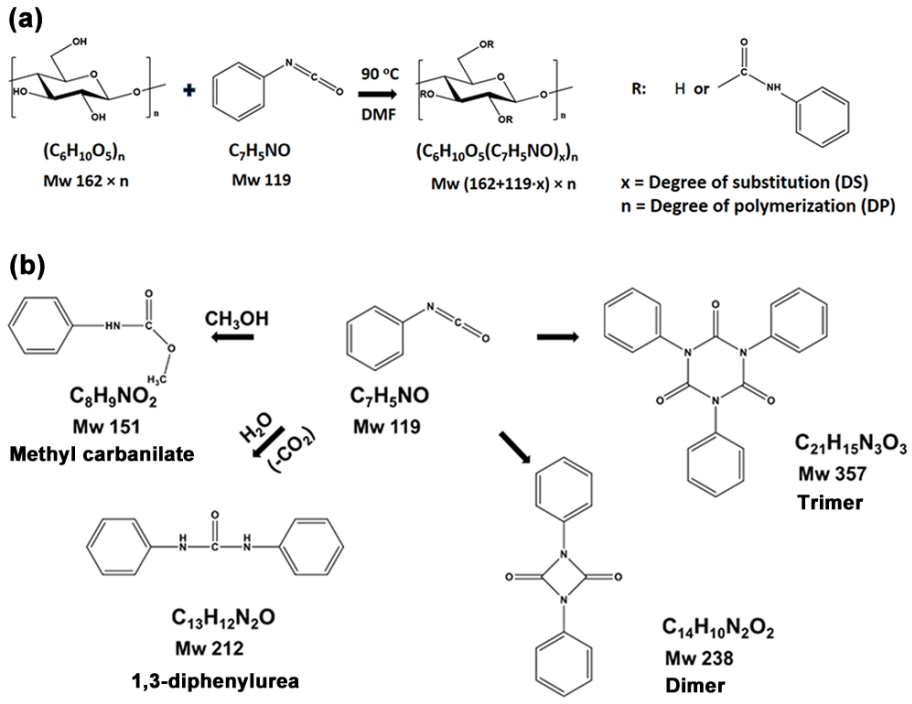

Scheme IV.1. *The carbanilation of cellulose and the side products during the carbanilation.*

1,3-diphenylurea. The carbanilation of cellulose is normally terminated by the addition of methanol, and the excess phenylisocyanate reacts with methanol to generate methyl carbanilate. The cellulose carbanilates are isolated by precipitation in methanol or dialysis against acetone (Chapters II.3.2 and II.3.3).

IV.4.1. Determination of substitution degree of cellulose carbanilate

Majority of the publications use elemental analysis to detect the DS value of cellulose carbanilate, and there is only a small number of papers where the DS values

of cellulose carbanilate are estimated based on other methods such as NMR spectroscopy (Table I.2). In this section, the DS values of cellulose carbanilates from elemental analysis and ^{1}H NMR spectroscopy were compared.

IV.4.1.1. Side products

Samples.

1 g (about 0.6 mmol) of MCC was subject to carbanilation reaction with 2 mL of PI-old (18.3 mmol, 10.0 molar equivalent to the -OH groups of cellulose) without the usage of argon flow for different durations of time, 0.5, 2.3, 7, 24 and 52 hours (Chapter II.3.1). Then the obtained carbanilated MCC were purified by washing with methanol (Chapter II.3.2).

Results and discussion.

Figure IV.4 presents the UV signals of SEC eluent curves of the carbanilated MCC. The main peak with the retention time at 17.2 min belongs to the carbanilated MCC, and the other minor peaks correspond to the side products that are shown in Scheme

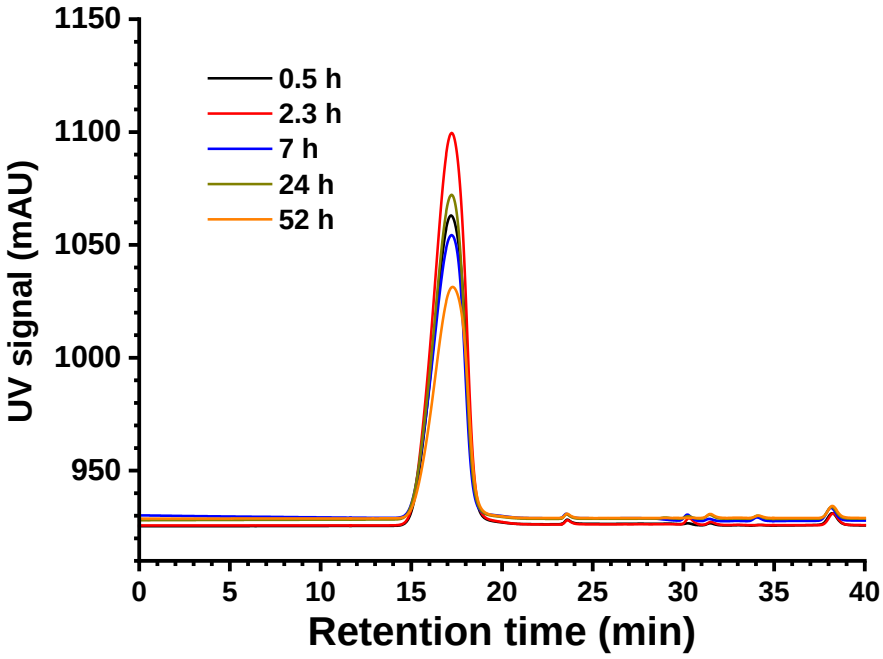

Figure IV.4. *UV signals of SEC eluent curves of the carbanilated MCC samples that were carbanilated by PI-old for 0.5 hour, 2.3 hours, 7 hours, 24 hours and 52 hours*

IV.1. In SEC, molecules with smaller molecular size elute later than the ones with larger molecular size, so the peaks at 23.6, 30.3, 31.5, 34.1 and 38.2 min are assigned

to trimers, dimers, 1,3-diphenylurea, methyl carbanilate and phenylisocyanate, respectively. The area of each peak is shown in Table IV.1. Since the UV detection is done at 280 nm, the peak area of the absorbance of aromatic ring is assumed

Table IV.1. *The Area and the normalized area (Area') of the peaks in Figure IV.4, and the estimated percentages of cellulose carbanilates and different side prducts in the samples. The samples were the carbanilated MCC that were carbanilated by PI-old for 0.5 hour, 2.3 hours, 7 hours, 24 hours and 52 hours.*

Retention time (min)		**17.2**	**23.6**	**30.3**	**31.5**	**34.1**	**38.2**
Assignment		**MCC carbanilates**	**Trimers**	**Dimers**	**1,3-diphenylurea**	**Methyl carbanilates**	**PI**
0.5 h	Area	284.5	0.9	0.3	0.4	0.0	3.8
	Area'	118.5	0.3	0.1	0.2	0.0	3.8
	Molar ratio (%)	96.4	0.3	0.1	0.2	0.0	3.0
2.3 h	Area	353.7	0.8	1.5	0.8	0.0	3.3
	Area'	141.5	0.3	0.7	0.4	0.0	3.3
	Molar ratio (%)	96.8	0.2	0.5	0.3	0.0	2.3
7 h	Area	254.5	0.9	1.3	0.5	1.1	3.7
	Area'	101.8	0.3	0.6	0.3	1.1	3.7
	Molar ratio (%)	94.5	0.3	0.6	0.2	1.0	3.4
24 h	Area	284.7	0.7	0.4	0.7	0.6	3.4
	Area'	109.5	0.3	0.2	0.4	0.6	3.4
	Molar ratio (%)	95.9	0.2	0.2	0.3	0.5	3.0
52 h	Area	215.2	0.7	0.0	0.8	0.5	3.4
	Area'	76.9	0.2	0.0	0.4	0.5	3.4
	Molar ratio (%)	94.4	0.3	0.0	0.5	0.6	4.2

proportional to the content of aromatic rings in each component. The measured peak area (Area) is first normalized by the number of aromatic rings per molecule (Area').

The DS values of cellulose carbanilate in this estimation are taken from the ^{1}H NMR analysis described below. The molar ratio of each component in the samples is calculated based on the normalized area values. From Table IV.1, the molar ratio of the side products in the samples is estimated about 3-5 %. While the peak of PI appears approximately in the expected position (38.2 min), it is unclear why the side products still contained about 72 % of phenylisocyanate after the addition of excess methanol and the washing process.

IV.4.1.2. DS estimation based on elementary analysis

The results of elementary analysis of the carbanilated MCC with different carbanilation time are summarized in Table IV.2. The DS values of cellulose carbanilates are calculated as follows,

$$DS = \frac{36}{7 \times (R_{c/n} - 6)}$$

where $R_{c/n}$ is the percentage of C divided by the percentage of N in the samples. All the DS values of the carbanilated MCC are in the range of 2.6-3.0 and do not show a

Table IV.2. *Elemental analysis (EA) of cellulose calbanilate.*

	C [%]	N [%]	DS	Errors of DS from experiments
0.5 h	61.8±0.2	8.0±0.1	3.0	0.1
2.3 h	61.2±0.2	7.8±0.0	2.9	0.1
7 h	61.5±0.0	7.7±0.3	2.7	0.5
24 h	61.4±0.0	7.9±0.1	2.8	0.1
52 h	61.5±0.1	7.9±0.0	2.8	0.0

tendency with increasing reaction time. The errors in Table IV.2 are measurement errors calculated based on three repeated experiments. Another possibility of error can come from the presence of side products. The $R_{c/n}$ of phenylisocyanate (monomer, dimer, and trimer) is 6.00, and those of 1,3-diphenylurea, methyl carbanilate are 5.57 and 6.85, respectively. The average ratios of the PI (monomer, dimer, and trimer), 1,3-diphenylurea, and methyl carbanilate are estimated as 85.1 %, 6.8 %, and 8.1 % based on the five sets of data in Table IV.1. Here, the composition of side products is assumed constant regardless of the reaction time. Based on this average composition, the $R_{c/n}$ of the entire side products is 6.04. When assuming the DS value of cellulose carbanilate being 3, the error from the presence of side products is estimated in a range between 0.1 (3% side products) and 0.2 (5% side products). The sum of the measurement error and the error from the side product is thus 0.1-0.7, which was a 5-23 % error for cellulose carbanilates of DS 3.

IV.4.1.3. DS estimation based on ^{1}H NMR spectroscopy

The ^{1}H-NMR spectrum of the cellulose carbanilates with reaction time of 52 hours

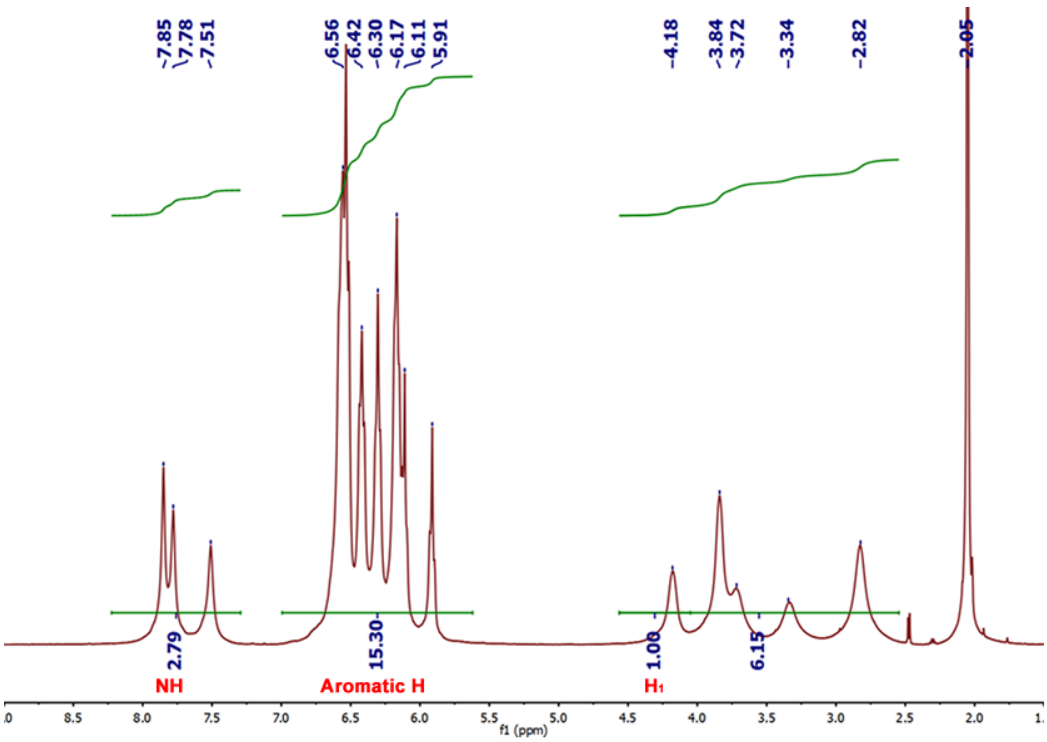

Figure IV.5. *Liquid state ^{1}H NMR of the carbanilated MCC that were carbanilated by PI-old for 52 hours with the solvent of deuterated acetone.*

is shown in Figure IV.5. The peaks in 7.3-8.2 ppm are assigned to the proton of NH on the phenylcarbamate moieties (named as NH). The peaks in 5.8-6.8 ppm correspond to the protons on the aromatic rings (named as aromatic H). The protons on the cellulose backbones appear in the region of 2.6-4.5 ppm, among which the peak at 4.18 ppm is due to the protons on C1 (named as H_1). The integrated peak area of all the protons on the cellulose backbones (2.6-4.5 ppm) is slightly higher than 6 times of the integrated peak area of H_1 (4.1-4.5 ppm) (1:6.15), which can be attributed to the contamination of methanol at 3.31 ppm and 3.12 ppm in deuterated acetone because the carbanilated cellulose was purified by washing with methanol. Two methods are used to calculate the DS values based on the ^{1}H NMR spectra: using the integrated areas of NH and aromatic H peaks as follows,

$$DS(\mathrm{NH/H_1}\ method) = \frac{Area(NH)}{Area(H_1)}$$

$$DS\ (\text{aromatic H}/\mathrm{H_1}\ method) = \frac{Area(Aromatic\ H)}{5 \times Area(H_1)}$$

The DS values of cellulose carbanilates with the carbanilation time of 52 hours from NH/H_1 and aromatic H/H_1 methods are 2.8 and 3.1, respectively. First of all, it is physically impossible to reach DS larger than 3 for cellulose derivatives. The overestimated DS value is mainly due to the defects of method or impurities, and this rule is the same for the later DS results. In the chemical structures of PIs (monomer, dimer and trimer), protons only exist on the aromatic rings. For the NH/H_1 method, thus, an error from side products arises only from 1,3-diphenylurea and methyl carbanilate, while the aromatic H/H_1 method has an influence from all the side products including PIs. 3-diphenylurea and methyl carbanilate take up about 20 % of

the side products, which gives an estimation of an error of 1.1% on the DS value. The error from all the side products is estimated as 5.6 % on the DS value. The DS value from the aromatic H/H_1 method should be always larger than the one from the NH/H_1 method in ^1H NMR due to a larger effect from the presence of the side product. However, the composition of the side products (Table IV.1) did not fully explain the large observed difference of two DS values (2.8 vs 3.1). The reason that caused such a big difference is unknown.

The DS values of carbanilated MCC from the elemental analysis and liquid state ^1H-NMR spectroscopy are plotted in Figure IV.6. For the results from ^1H-NMR by NH/H_1 method, the DS values of carbanilated MCC show a monotonical increase

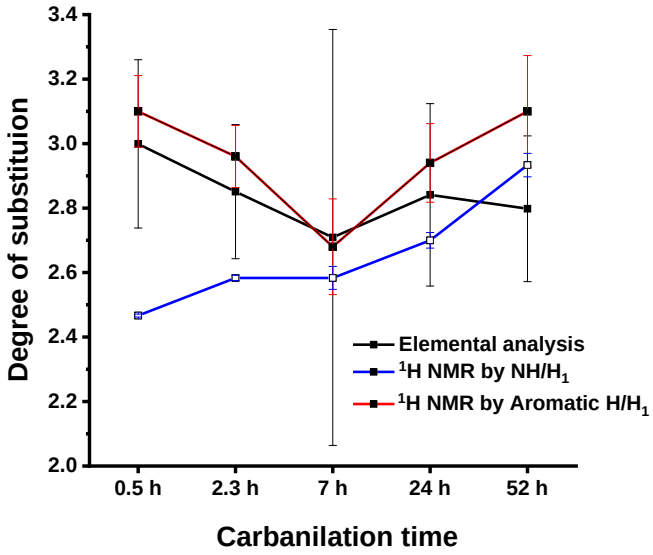

Figure IV.6. *The comparison of DS values of the carbanilated MCC obtained from elemental analysis, liquid-state ^1H NMR by the NH/H_1 method and the aromatic H/H_1 method. The carbanilated MCC samples were obtained from the carbanilation of MCC by PI-old for 0.5 hour, 2.3 hours, 7 hours, 24 hours and 52 hours.*

with the increasing reaction time. The DS values from the aromatic H/H_1 method and the elemental analysis show high DS values without any clear tendency with respect

to the reaction time. Based on the above considerations, the DS values from ^{1}H-NMR by NH/H_1 method should have a smaller error and thus should be more reliable than the DS values from elemental analysis and the aromatic H/H_1 method. Therefore, the DS values in the following sections are based on NMR NH/H_1 method.

IV.4.2. Carbanilation with different concentrations of phenylisocyanate

Samples.

0.5 g (about 3 mmol) of MCC reacted with 0.4 mL (3.6 mmol, 0.4 molar equivalent to the -OH groups of cellulose), 0.7 mL (6.4 mmol, 0.7 molar equivalent to the -OH groups of cellulose) and 1.1 mL (10.1 mmol, 1.1 molar equivalent to the -OH groups of cellulose) of PI-new with the usage of argon gas according to the Chapter II.3.1, and named as cmcc1, cmcc2 and cmcc3, respectively. The maximum achievable DS values are 1.2 for cmcc1, 2.1 for cmcc2, and 3 (3.3) for cmcc3,

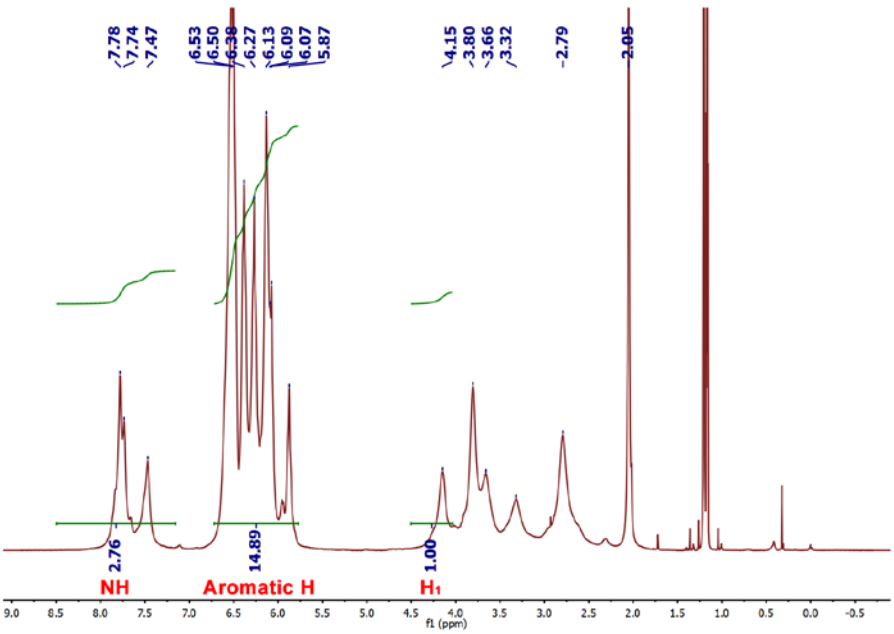

Figure IV.7. *^{1}H NMR spectrum of cmcc3.*

respectively, based on the amount of PI in the system. After carbanilation, the cmcc1, cmcc2 and cmcc3 were purified by dialysis against acetone (Chapter II.3.3).

Results and discussion.

To better understand the process of the heterogeneous carbanilation, different amount of PI was used for carbanilation of MCC. The DS and solid-state structure of carbanilated products were investigated using liquid- and solid-state NMR, FT-IR and X- day diffraction.

Figure IV.7 shows the liquid-state ^{1}H NMR spectrum of cmcc3. By using NH/H_1 method described above, the DS value of cmcc3 is calculated as 2.8. When using the aromatic H/H_1, the DS value of cmcc3 is estimated as 3.0. On the other hand, the other two samples, cmcc1 and cmcc2 could not be analysed using ^{1}H NMR spectroscopy as they did not dissolve in common NMR solvents such as DMSO and acetone, apparently due to the low DS values.

We then used the solid-state NMR spectroscopy to investigate these low-DS cellulose carbanilate specimens. Solid-state ^{13}C CP/MAS NMR spectra of MCC, cmcc1, cmcc2 and cmcc3 are shown in Figure IV.8. While the spectrum of MCC displays spectral features of cellulose I, the carbanilated cellulose samples show additional peaks corresponding to the carbamate moiety. The peak at 153.3 ppm is assigned to the carbon atom of carbamate group. The peak at 137.6 ppm and those in the range from 133.6 ppm to 113.6 ppm correspond to the carbon atoms of C-N and the other five aromatic carbon atoms, respectively. In the spectrum of MCC, the peak at 104.9 ppm is the resonance of C1, and the C4 carbon is observed as two peaks: a sharp peak at 88.7 ppm (cellulose I crystal) and a weak and broad one at 84.1 ppm

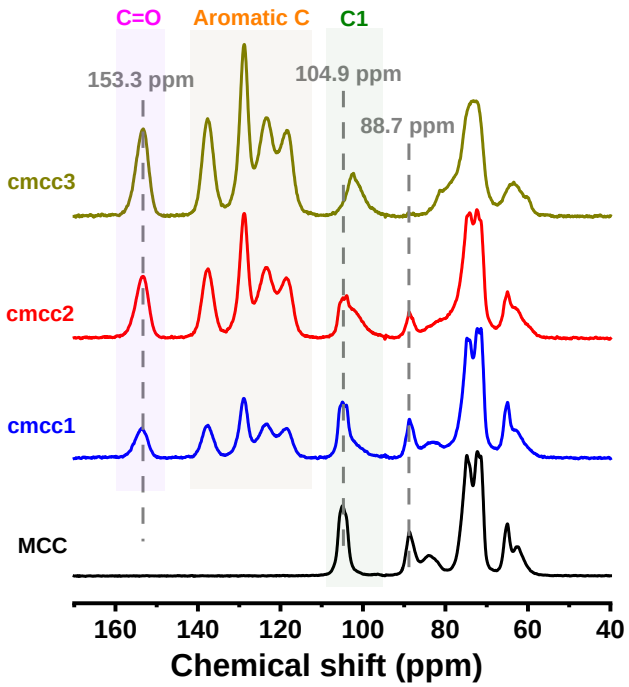

Figure IV.8. *Solid-state ^{13}C CP/MAS NMR spectra of MCC, cmcc1, cmcc2 and cmcc3, respectively.*

(amorphous, surface). The peaks in the range of 79.6-67.6 ppm are assigned to the C2, C3 and C5 carbons. C6 is seen as a sharp peak centred at 64.9 ppm corresponding to the crystalline C6 at trans-gauche conformation and a broader peak around 62.4 ppm which should be from C6 of the surface chains. In the spectra of cmcc1, cmcc2 and cmcc3, an additional upfield broad peak appears in the C1 region. The position is shifted by about 2.7 ppm with respect to the initial C1 position of MCC. The sharp peak at 88.7 ppm in the C4 region gets weaker with increasing PI content and almost disappears in the spectrum of cmcc3. C4 peaks are mostly likely shifted upfield and merged with the C2, C3, C5 composite peaks near 81.1 ppm in the spectrum of cmcc3. The C6 region becomes less resolved and the crystalline C6 peak turns significantly weaker in the carbanilated samples. In the spectrum of cmcc3, the crystalline C6 peak is not visible and a broad peak centred at around 62 ppm becomes dominant.

All the above-mentioned changes indicate gradual loss of crystallinity of cellulose I with increasing amount of PI in the reaction mixture. The rise of the new set of peaks correspond to the formation of cellulose carbanilate. The upfield shifts of C1 and C4 of cmcc3 indicate that the carbanilated cellulose is no longer in a two-fold helix conformation. The spectra of cmcc1 and cmcc2 still show the spectral features of cellulose I, indicating the non-reacted part of cellulose remains crystalline without swelling.

By integrating the peak area of carbonyl group and C1 on the cellulose rings, the DS values of cmcc1, cmcc2 and cmcc3 are calculated as 0.5, 1.0 and 1.7, respectively. When using integrated peak areas of aromatic carbons and C1 on the cellulose rings, the DS of cmcc1, cmcc2 and cmcc3 are calculated as 0.4, 0.8 and 1.4, respectively. For cmcc3, the DS values based on the solid-state NMR are significantly lower than that from ^{1}H NMR. As described in Chapter II.4.5.1, the signal intensities of CP/MAS ^{13}C NMR is biased towards carbons of slow dynamics compared to more flexible ones due to the ^{1}H spin-lattice (T1) relaxation. This is likely the case for cellulose carbanilate as the cellulose backbone is expected to have higher rigidity compared to the carbamate side chain, leading to the significant underestimation of DS.

One can obtain quantitative information of carbons of different dynamics with a ^{13}C single-pulse experiment when using a sufficiently long recycle delay comparable to the slowest ^{13}C spin-lattice relaxation time in the system. The ^{13}C SP/MAS NMR spectra of cmcc3 with the delay times of 2, 8, 16, 32, 64 and 96 s are shown in Figure IV.9a. With the increasing delay time, the intensities of all the peaks increase. After delay time of 64 s, the intensities are saturated for the carbonyl groups, aromatic rings and C1. It indicates the magnetization of carbons on the carbonyl groups, aromatic

rings and C1 on the cellulose rings are all fully relaxed in 64 s. The solid-state ^{13}C SP/MAS NMR spectra of MCC and carbanilated MCC with the delay time of 64 s are shown in Figure IV.9b. By integrating the peak area of carbonyl carbon and C1, the

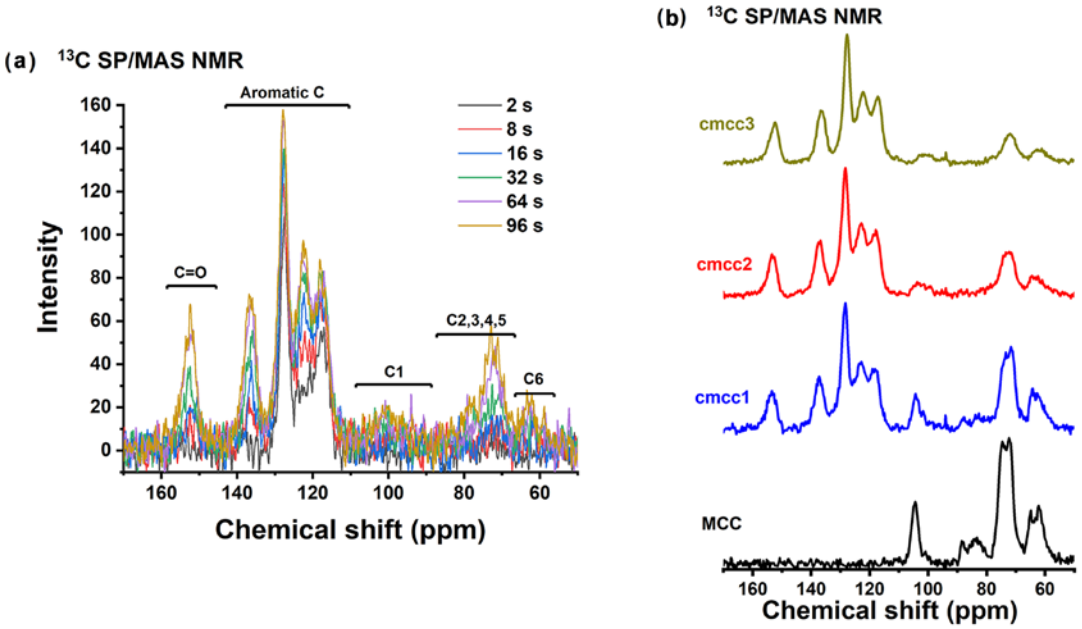

Figure IV.9. *(a) ^{13}C SP/MAS NMR spectra of cmcc3 with the ^{13}C spin lattice relaxation times T_{1C} of 4 s, 8 s, 16 s, 32 s, 64 s and 96 s; and (b) Solid-state ^{13}C SP/MAS NMR spectra of MCC, cmcc1, cmcc2 and cmcc3.*

DS values of cmcc1, cmcc2 and cmcc3 are calculated as 0.9, 1.8 and 2.9, respectively. However, by integrating the peak areas that correspond to aromatic carbons and C1 on the cellulose rings, the DS of cmcc1, cmcc2 and cmcc3 are calculated as 1.3, 2.5 and 3.7, respectively.

The comparison of DS values from ^{13}C CP/MAS NMR, ^{1}H NMR, and ^{13}C SP/MAS NMR are summarized in Table IV.3. As mentioned previously, the DS values calculated by the NH/H_1 method are affected less from the side products than that by the aromatic H/H_1 method. The DS value of cmcc3 by the NH/H_1 method (2.8) is very close to that by the C=O/C1 method of ^{13}C SP/MAS NMR (2.9), almost twice of the

DS values calculated by ^{13}C CP/MAS NMR, which indicates the DS value calculated by the C=O/C1 method of ^{13}C SP/MAS NMR is reasonable. For the aromatic C/C1 method of ^{13}C SP/MAS NMR, the DS values of cmcc1, cmcc2 and cmcc3 were 1.3, 2.5 and 3.7, respectively. However, according to the amounts of phenylisocyanate that were added for carbanilation, the DS values for cmcc1, cmcc2 and cmcc3 should not be larger than 1.2, 2.1 and 3 (3.3), respectively. Thus, these high values are due to erroneous estimations. One possible reason of this error is that the recycle delay of 64

Table IV.3. *Comparison in DS values of cmcc1, cmcc2 and cmcc3 from ^{13}C CP/MAS NMR, ^{1}H NMR, and ^{13}C SP/MAS NMR.*

	^{13}C CP/MAS NMR		^{1}H NMR		^{13}C SP/MAS NMR	
	C=O/C1	Aromatic C/C1	NH/H1	Aromatic H/H_1	C=O/C1	Aromatic C/C1
cmcc1	0.5	0.4	-	-	0.9	1.3
cmcc2	1.0	0.8	-	-	1.8	2.5
cmcc3	1.7	1.4	2.8	3.0	2.9	3.7

s might not have been long enough for the relaxation of magnetization of all carbons. Even though we observed the intensity saturation after 64 s in Fig. IV.9a, the low S/N ratio might have affected the apparent intensity values. Separate experiments for ^{13}C T1 characterization of cmcc3 is necessary to check if this causes the overestimation of DS.

Figure IV.10 shows the XRD patterns of cellulose and carbanilated cellulose. MCC shows a typical cellulose I pattern. The peaks around 15º, 16.5º and 22.5º are as 1 $\bar{1}$ 0, 1 1 0 and 2 0 0, respectively. The diffraction pattern of cmcc1 still has the cellulose I features together with a new peak at 2θ=5.8°. The peaks of cellulose I become less obvious with the increasing DS value, and not visible in the diffraction pattern of

cmcc3. It implies that the carbanilation alters the cellulose I crystalline structure, and the carbanilated cellulose is less crystalline with the increasing DS. The observed

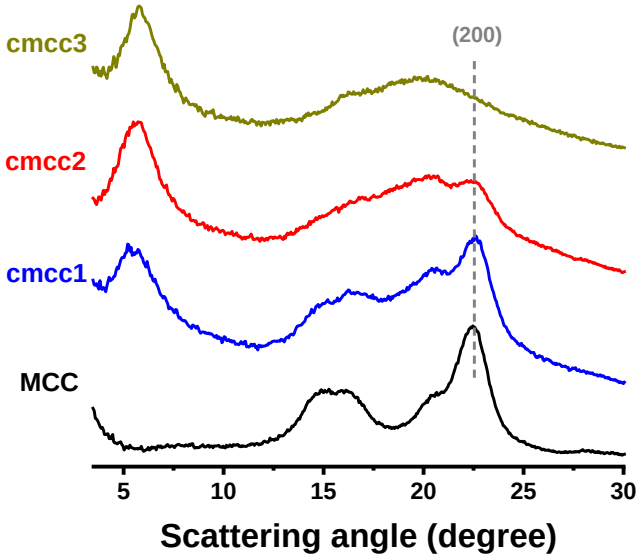

Figure IV.10. *XRD profiles of MCC, cmcc1, cmcc2 and cmcc3.*

gradual loss of crystallinity agrees with the results of solid-state NMR spectroscopy. The carbanilation reaction is thus considered to heterogenously proceed from the outside of cellulose crystal without swelling the crystalline core of cellulose, resulting in a binary system of cellulose carbanilates and crystalline cellulose I in the intermediate stage. The remaining crystalline cellulose I in cmcc1 and cmcc2 is likely the reason why cmcc1 and cmcc2 are insoluble in DMSO and acetone.

The FTIR spectra of MCC, cmcc1, cmcc2 and cmcc3 are shown in Figure IV.11a. Characteristic absorbance bands of phenylcarbamate moiety are indicated in the figure and assigned to the N-H (3382 and 3301 cm^{-1}), C=O vibrations (1716 cm^{-1}) [205], 1599 cm^{-1} and C-C strenching vibrations of aromatic rings (1524 cm^{-1}) [206]. The spectrum of MCC shows a broad band of OH groups in the range from 3600 cm^{-1} to 3000 cm^{-1}, which becomes weaker with increasing DS value. The absorbance bands from 1271-

1172 cm^{-1} and 1138-923 cm^{-1} correspond to the C-N stretching and the C-O-C stretching vibrations and are named as peak A and peak B, respectively. These two peaks are used to estimate the DS value of cellulose carbanilate. Integral areas and heights of peak A and peak B were calculated as illustrated as in Figure IV.11a by using Origin 2019. The ratios between areas and peak height of MCC, cmcc1, cmcc2 and cmcc3 are shown as a function of the DS values from SP/MAS NMR by the C=O/C1 method in Figure IV.11b and 11c, respectively. Both area and height plots could be fit with linear functions as indicated in the figures. However, these functions do not go through the origin or the value estimated from the spectrum of MCC. Thus, they cannot be used for the entire DS range from 0 to 3. One explanation is that the peak intensities and shapes might be altered not just by chemical structure but also by the physical environment around cellulose molecules such as dense molecular packing in cellulose crystal or mechanical constraint of cellulose molecules at the interface between cellulose crystal and carbanilate. Nevertheless, these functions seem usable between the DS values from 1 to 3.

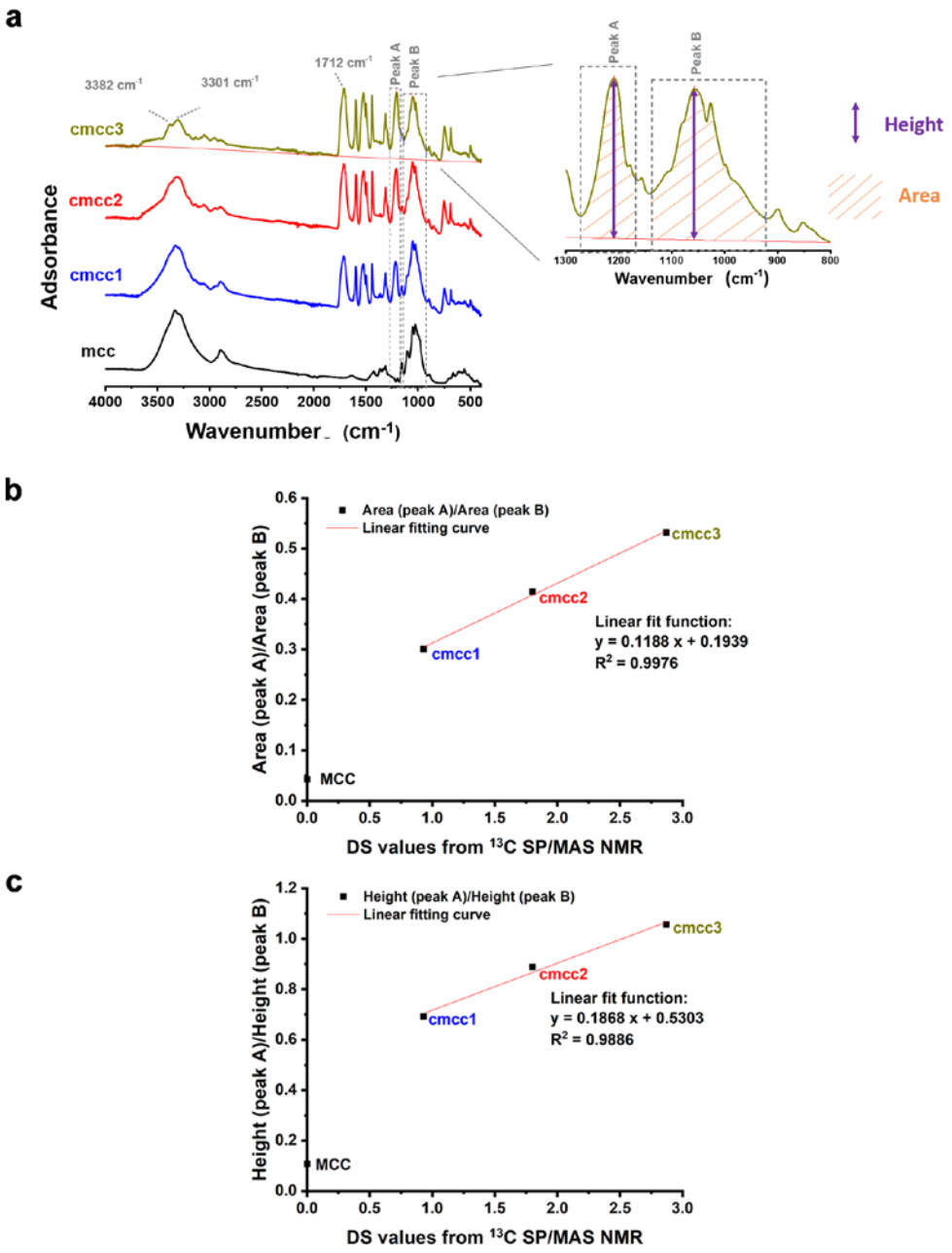

Figure IV.11. *(a) ATR-FTIR spectra of MCC, cmcc1, cmcc2 and cmcc3, and the illustration of calculating the area and height of peak A and peak B. DS values of MCC, cmcc1, cmcc2 and cmcc3 from ^{13}C SP/MAS NMR by C=O/C1 method as function of (b) the area ratios and (c) the height ratios of peak A/peak B.*

IV.4.3. Optimization of carbanilation

From Figure IV.5, the carbanilated MCC by excess PI-old was not cellulose tricarbanilates even after the carbanilation time of 52 h. However, the DS value of the carbanilated MCC (cmcc3) reached 2.8 when the amount of PI-new was only 1.1 equivalent to the -OH group of cellulose. Thus, in this section, the DS values of cellulose carbanilates were compared in terms of the reaction time, the state of phenylisocyanate (i.e., PI-old and PI-new), and the usage of argon gas. The amount of phenylisocyanate was set as 2.0 equivalent to the -OH group of cellulose.

IV.4.3.1. Carbanilation time

Samples.

Based on the Chapter II.3.1, 0.5 g (about 3 mmol) of MCC was carbanilated by 2 mL of PI-new (18.3 mmol, 2.0 molar equivalent to the -OH groups of cellulose) after purging with argon gas at 90 ˚C. About 100 μL of the reacting mixtures were taken for ATR-FTIR measurements after the reaction time of 6.5 hours, 28.5 hours and 48 hours without further purification. After reacting for 48 hours, the reaction was stopped by adding excess emthanol. The carbanilated MCC was purified by dialysis according to Chapter II.3.3. The purified carbanilated MCC were dissolved in deuterated DMSO with concentration of 50 mg/mL for ^{1}H NMR measurement.

Results and discussion.

From Figure IV.12, the absorbance of O-H stretching vibrations from 3000 cm^{-1} to 3600 cm^{-1} get weaker as the reaction proceeds. After 48 h of the carbanilation reaction, the N-H (3382, 3301 cm^{-1}) and C=O vibrations (1716 cm^{-1}) become very strong, and

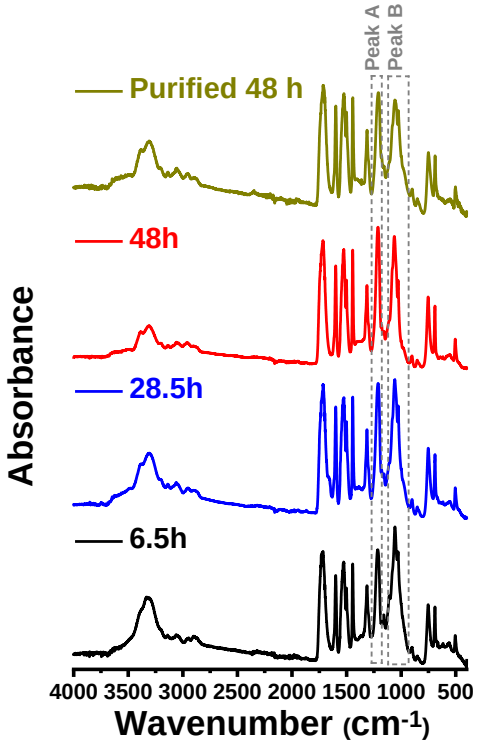

Figure IV.12. *ATR-FTIR spectra of the reaction mixture that MCC were carbanilated by PI-new with the usage of argon gas for 6.5 h, 28.5 h and 48 h, and the purified carbanilated MCC with carbanilation time of 48 h.*

there is almost no -OH group in the sample, indicating cellulose is converted into cellulose tricarbanilate. Based on the fitted functions in Figure IV.11, the DS values of the carbanilated MCC with the carbanilation time of 6.5 hours, 28.5 hours and 48 hours are estimated and shown in Table IV.4. The DS values estimated based on ^{1}H NMR and ATR-FTIR are summarized in Table IV.4. The IR-height and the ^{1}H-NMR methods provide the similar DS value for the purified 48 hours sample. The sample before purification has higher DS values based on IR-height compared to the purified one, indicating the per-carbanilation of cellulose in this sample. This tendency is more

pronounced with the IR-area method. The overestimation from the 48 hours sample before purification should be due to the presence of the side products in the reaction mixture that affects the intensity and shape of the C-N stretching vibration. The similar overestimation of DS values is expected for the samples of 6.5 and 28.5 hours. Thus, the reaction time in the rest of this thesis was set to 48 h to obtain tricarbanilated cellulose.

IV.4.3.2. State of phenylisocyanate & usage of argon gas

Samples:

0.5 g (about 3 mmol) of MCC was carbanilated by 2 mL of PI-new or PI-old (18.3 mmol, 2.0 molar equivalent to the -OH groups of cellulose) with or without argon purge gas at 90 ˚C for 48 hours (Chapter II.3.1). The carbanilated MCC was purified by dialysis according to II.3.3. The purified carbanilated MCC were subjected to ATR-FTIR tests. The purified carbanilated MCC were dissolved in deuterated DMSO with concentration of 50 mg/mL for ^{1}H NMR measurement.

Table IV.4. *Comparison in DS values of carbanilated MCC that were carbanilated by PI-new for 6.5 hours, 28.5 hours and 48 hours before purification. The DS values estimated from ATR-FTIR were based on the functions in Figure IV.10.*

DS values from	IR-Area	IR-Height	^{1}H NMR (NH/H1)	^{1}H NMR (Aromatic H/H_1)
48 hours	3.8	3.2	-	-
purified 48 hours	3.4	3.0	3.0	3.1
28.5 hours	2.9	2.4	-	-
6.5 hours	2.1	1.6	-	-

Results and discussion.

Table IV.5 summarizes the DS values of the carbanilated MCC based on ^{1}H-NMR and FT-IR estimations. The DS values of carbanilated MCC with argon purge are higher than the DS values of carbanilated MCC without the purge gas. One reason of this tendency is that the removal of humidity in air by the argon purge increases the reaction efficiency of carbanilation. From the ^{1}H NMR NH/H_1 method, the DS values of carbanilated MCC with PI-new are higher than that with PI-old. The purity of the PI-old was doubtable, and the impurities inside the PI-old might decrease the effective concentration of phenylisocyanate, thus the reaction efficiency of the carbanilation might be lower with PI-old.

Table IV.5. *Comparison in DS values of the carbanilated MCC with various carbanilation conditions.*

PI-new	PI-old	Usage of argon	^{1}H-NMR (NH/H_1)	^{1}H-NMR (aromatic H/H_1)	IR-Area	IR-Height
+	-	+	3.0	3.1	3.4	3.0
-	+	+	2.7	3.0	3.2	3.0
+	-	-	2.6	2.7	3.0	2.7
-	+	-	2.6	2.9	nd	nd

"+" means the condition was used, "-" means the condition was not used, "nd" means no data.

IV.5. Conclusions

In this chapter, firstly the two common derivatization methods of cellulose were compared in terms of SEC signals. The tricarbanilated cellulose oligomers showed higher light scattering signals than the trinitrated cellulose oligomers due to its larger

molecular size and dn/dc value. Thus, the carbanilation of cellulose was chosen as the derivatization method of cellulose oligomers. For the estimation of DS values of the carbanilated cellulose, the NH/H_1 method using ^1H NMR spectrum was found more accurate due to the limited influence from the side product compared to the aromatic H/H_1 method and the elemental analysis. When the content of phenylisocyanate in the reaction mixture was below the molar equivalence to OHs of cellulose, the resulting specimen contained cellulose I crystal. Solid-state ^{13}C SP/MAS NMR and FT-IR spectroscopies were found effective to estimate the DS of such low-substituted cellulose carbanilates in the solid-state. In addition, fully carbanilated cellulose could be obtained via carbanilation reaction in DMF with fresh phenylisocyanate and the usage of argon gas.

Chapter V

Chapter V. Comparison of characterization techniques for DP determination

V.1. Introduction

The characterization techniques for DP determination of cellulose and their principles have been described in the Chapter I.5 and Chapter II.4. The characterization techniques for the high-molar-mass cellulose may not always be suitable for cellulose oligomers. For examples, static light scattering requires molecules large enough to behave as an anisotropic scatter for an accurate measurement. It is impossible to get a reliable R_g and hence a molecule weight information when the molecular size is too small. In viscometry, it is still under debate whether the linear fits of log[η] against log[M] are applicable to cellulose oligomers [132, 133]. On the other hand, some characterization techniques, such as mass spectroscopy and the end group method based on NMR spectroscopy, can be used only with the low-molecular weight molecules.

In this chapter, four analytical methods (liquid and solid-state NMR, SEC, MALDI-TOF MS) were applied for DP determination of two cellulose oligomer fractions (fractions A and B) with different DP distributions. The benefits and drawbacks of these methods were described and compared.

Samples

Two fractions of cellulose oligomers, namely fraction A and fraction B, were prepared according to the paper from Isogai and Usuda [1] with minor modification and used in this chapter. Briefly, the fraction A was obtained as water-insoluble

precipitation from the cellulose phosphoric acid solutions (3 wt% MCC / 83 % H_3PO_4 solution stored at 23 ˚C for 8 weeks) mixed with the same weight of water as described in the Chapter II.2.3.1. For fraction B, 3 wt% MCC / 83 % H_3PO_4 solution was stored at 23 ˚C for 6 weeks and mixed with the same weight of water at 23 ˚C with decantation time of 24 hours. Supernatant of this mixture was mixed with 3 times its volume of isopropanol to obtain isopropanol-insoluble fraction B. Then these fractions were washed with respective solvents until pH reached neutral.

V.2. Liquid-state ^{1}H NMR spectroscopy

The ^{1}H NMR spectrum of fraction B in deuterated DMSO is shown in Figure V.1.

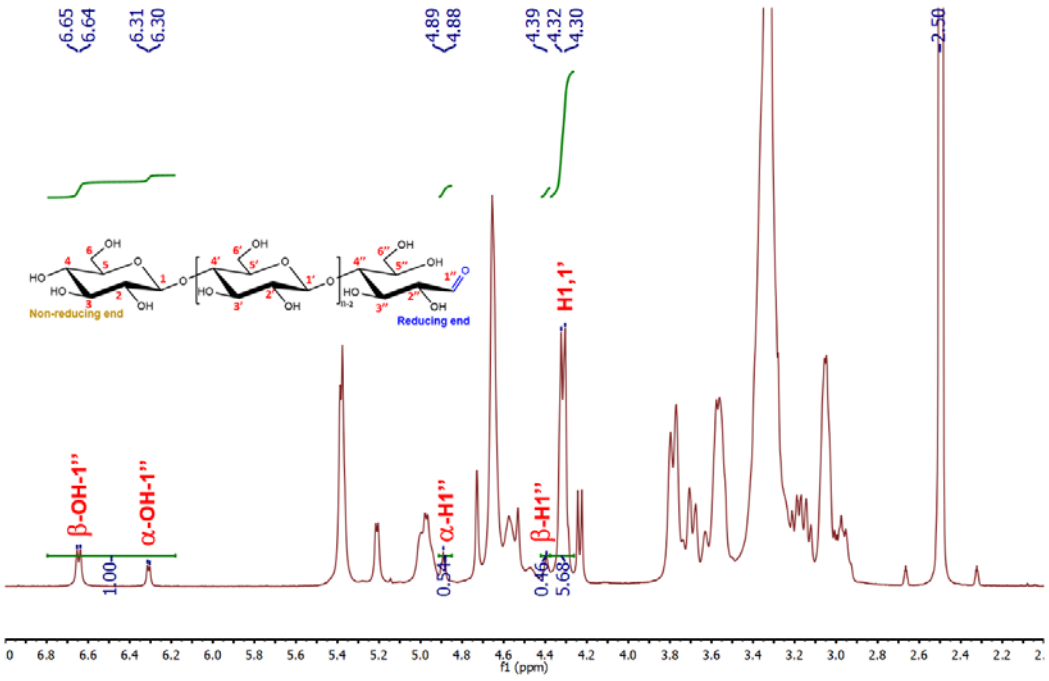

Figure V.1. *^{1}H-NMR spectrum of fraction B in deuterated DMSO. Characteristic chemical shifts corresponding to specific bonds are annotated on the chemical structure of the cellulose molecule in the inset.*

Peak assignments were done according to the previous studies [98, 186, 208-210]. The peaks at 4.89 ppm and 4.39 ppm are attributed to the α- and β-anomeric protons at the

reducing ends of cellulose oligomers, respectively. Those at 6.31 ppm and 6.65 ppm are assigned to the hydroxyl protons of α- and β-anomers of the reducing ends. The peaks at 4.31 ppm and 4.33 ppm are from the protons from the H1 and H1' (inset of Figure V.1). Given the quantitative measurement of ^{1}H resonance intensity from specific positions on cellulose chains, the number-averaged DP could be calculated as follows,

$$DP_n = \frac{I_\alpha + I_\beta + I_i}{I_\alpha + I_\beta}$$

where I_α and I_β are the integrated intensities of peaks corresponding to OH-1'' or H1'' of reducing ends, while I_i is the integrated intensity of peak assigned to H1 and H1'. A number-averaged DP is calculated as 6.7, identical between two estimations based on O-H and C-H signals.

V.3. Quantitative DP analysis by Solid-state ^{13}C CP/MAS NMR

Fraction A is reported to have a DP of about 15 [1]. Unlike Fraction B, it is insoluble in common mono-component solvents like DMSO, making it more difficult to be characterized with liquid-state NMR. Thus, solid-state ^{13}C CP/MAS NMR technique is a more straightforward method for Fraction A. However, the peak intensities in ^{13}C CP/MAS NMR spectroscopy are not quantitative due to difference in magnetization relaxation behavior and cross polarization efficiency of each carbon. To overcome this problem, one can use SP/MAS method as described in the Chapter IV. However, the quantitative SP/MAS is time consuming as the recycle delay should be set equal to ^{13}C T1 of the slowest carbon in the system which is in a range from tens to a hundred of seconds for crystalline cellulose. Thus, its application is rather limited to a case where a number of samples are relatively small. Alternatively, one can restore the

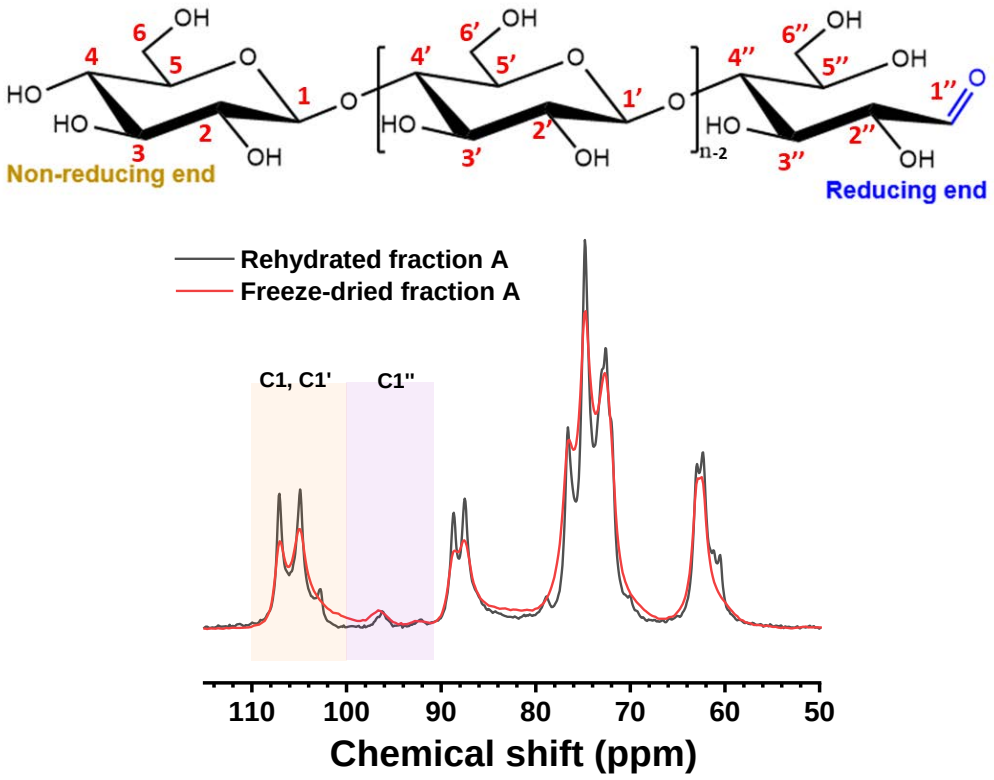

Figure V.2. *Solid state ^{13}C CP/MAS NMR spectra of rehydrated fraction A and freeze-dried fraction A. The colored regions correspond to specific carbon bonds that are annotated on the chemical structure of the cellulose molecule.*

quantitative nature of peak intensities of ^{13}C CP/MAS spectra by taking the kinetics effect into account as described in Chapter II.4.5.1. In this chapter, such a correction was made to estimate the DS of Fraction A.

Figure V.2 shows the solid-state ^{13}C CP/MAS NMR spectra of the freeze-dried fraction A and rehydrated fraction A. Both of the spectra show typical spectral features of cellulose II crystal [211]. The resonance lines of the rehydrated sample were narrower without change in chemical shifts when compared with those of freeze-dried one. The reason behind this phenomenon was previously described by Horii et al. [212]. Water might relax mechanical constraints of cellulose crystals caused by drying and

the non-crystalline or surface chains to a relatively ordered state. Peak deconvolution is easier with sharper and more obvious peaks, so all the sample is in a rehydrated state in this consideration. Fraction A was immersed in water and then centrifuged to remove the excess water. On the other hand, Fraction B is partially soluble in water, so this method might cause a partial loss of low-molecular weight oligomers. Fraction B was thus rehydrated in a desiccator of 97 % RH for one week.

The C1 and C1’ region in the rehydrated fraction A was deconvoluted into five ^{13}C signals as shown in Figure V.3. The two major peaks at 107.2 ppm and 105.0 ppm with the same integrated peak area are assigned to the C1 of the center and corner chains of the cellulose II crystal. The peaks at 106.1 ppm and 102.9 ppm are attributed

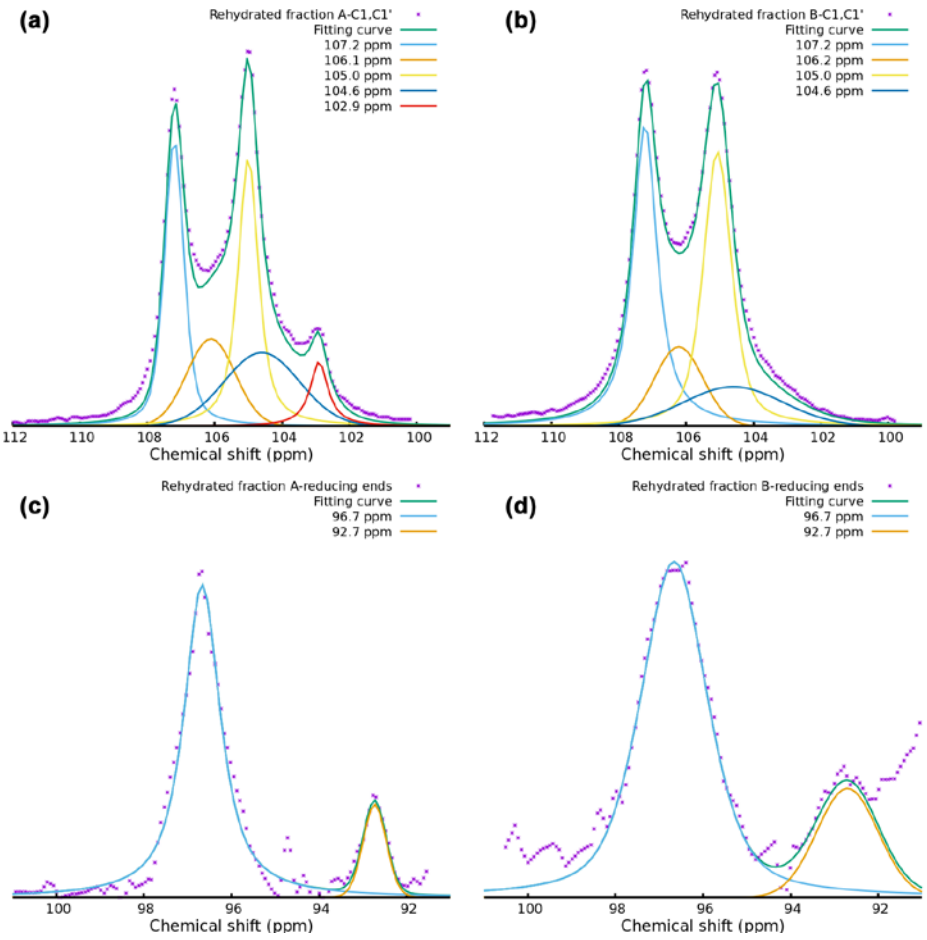

Figure V.3. *(a, b) C1 & C1’ region and (c, d) reducing end C1’’ region of solid state ^{13}C CP/MAS NMR spectra together with their spectral deconvolutions of rehydrated fraction A and B.*

to the crystalline surface signals as they have much faster ^{1}H T1 relaxation. The amorphous signals correspond to the broad peak centered at 104.6 ppm [213, 214]. For rehydrated fraction B, the resonance region of C1 and C1’ is deconvoluted into four

^{13}C signals: two peaks of crystalline cellulose II C1 at 107.2 ppm and 105.0 ppm, one broad amorphous signal at 104.6 ppm, and only one crystalline surface signal at 106.2 ppm. The regions of reducing end C1 in rehydrated fraction A and B are both deconvoluted into two peaks at 96.7 ppm and 92.7 ppm, corresponding to C1 of β- and α-conformers, respectively [215]. While the two fractions share general spectral features, there are several differences between two spectra in both the C1-C1' and reducing end regions. The two reducing-end peaks of rehydrated fraction B are

Table V.1. *^{13}C chemical shift assignments and the results of fitting the ^{13}C CP dynamics for rehydrated fraction A and B.*

Samples	Assignment	Shift (ppm)	M_0	T_{1H} (ms)	T_{CH} (ms)	M_s	M_s / M_0
Fraction A	C1 & C1'	107.2	88012	27.2	0.1	66275	0.8
		106.1	61558	21.9	0.1	49371	0.8
		105.0	88068	27.0	0.1	66313	0.8
		104.6	72368	29.1	0.1	64030	0.9
	Reducing ends	102.9	22369	7.9	0.4	8244	0.4
		96.7	26583	11.5	0.1	23245	0.9
		92.7	9963	2.8	0.1	8709	0.9
Fraction B	C1 & C1'	107.2	111665	13.7	0.2	78056	0.7
		106.2	53766	17.6	0.1	43002	0.8
		105.0	112017	13.6	0.2	78290	0.7
		104.6	89153	2.5	0.1	72613	0.8
	Reducing ends	96.7	41942	4.5	0.1	37699	0.9
		92.7	18870	2.2	0.1	14663	0.8

broader than that of rehydrated fraction A. The surface peak at 102.9 ppm is only visible in the fraction A but not in the fraction B. These differences might arise from

the different rehydration method. The fraction A would contain more water than rehydrated fraction B as the fraction A was immersed in bulk water.

Based on the principles described in the Chapter II.4.5.1 that use the solid-state ^{13}C CP/MAS NMR, Appendix 3.1 presents the result of peak fitting. In the cross-polarization experiment, three constants of time are involved: T_{1H}, the proton spin-lattice relaxation time; T_{CH}, magnetization transfer time constant from ^{1}H spin reservoir to ^{13}C spin reservoir; and T_{1C}, carbon spin-lattice relaxation time. As expected from the Appendix 3.1, three constants of time are in a following order: T_{1C} » T_{1H} » T_{CH}. Since the ^{13}C T1 (tens to a hundred of seconds) is much longer than other two constants (in a millisecond order), the rate of change of ^{13}C magnetization (M_s), hence the signal intensity, as a function of a CP contact time t can be simplified as:

$$M_s(t) = M_0 \times (e^{-\frac{t}{T_{1H}}} - e^{-\frac{t}{T_{CH}}})$$

The calculated T_{1H}, T_{CH}, and M_0 are shown in Table V.1. The M_s/M_0 represented how much the intensity decreased at a given contact time with respect to the extrapolated maximum magnetization M_0. Then the number-averaged DP was calculated as follows,

$$DP_n = \frac{\sum M_0(C1\&C1') + \sum M_0(Reducing\ ends)}{\sum M_0(Reducing\ ends)}$$

Based on the spectra shown in Fig. V3 and the constants in Table V.1, the DP_n of fraction A and fraction B are estimated as 10.1 and 7.0, respectively.

V.4. Mass spectroscopy

The MALDI-TOF MS spectroscopy was applied to the fractions A and B. The

fraction B could be directly subjected to the experiment after dissolving in DMSO. The fraction A is insoluble in DMSO. Thus, the fraction A was carbanilated before the MS measurement. The fraction B is also carbanilated for a comparison. Figure V.4 shows MALDI-TOF MS spectra of the fraction B, carbanilated fraction B and carbanilated fraction A as a function of mass-to-charge (m/z) ratio in the positive-ion mode. In the spectrum of fraction B (Fig V.4a), the major peaks are separated by m/z of 162, corresponding to one anhydroglucose repeating unit. The m/z values of major peaks are the sum of the mass of one cellulose molecule and one sodium ion, which can be expressed in the following equation,

$$M(n) = 162 \times n + 18 + 23$$

where n is DP of the cellulose molecule. On the left side of the main peaks, the small peaks with a decrease in mass of 18 from the main peaks are ascribed to the dehydro-cellulose that might be produced from acid hydroysis. On the right side of the main peaks, the small peaks with a distance of 16 from the main peaks are attributed to cellulose molecule plus potassium ion. For spectra of carbanilated fraction B and fraction A, the main peaks are separated by m/z of 519, corresponding to a tricarbanilted anhydroglucose repeating unit. Again, the m/z values of the main peaks are the sum of the mass of one tricarbanilated cellulose molecule and one sodium ion, which can be expressed as follows,

$$M(n) = 519 \times n + 119 + 17 + 23$$

From this equation, it implied that there is one underivatized hydroxyl group in the cellulose molecule. The adjacent peaks with an increment of 119 from the main peak corresponds to the fully carbanilated cellulose, and the adjacent lines on the left from

the main lines with a reduction of m/z = 119 and 119×2 should correspond to cellulose molecules with two and three underivatized hydroxyl groups, respectively. These four peaks separated by a multiple of m/z of 119 all belonged to a cellulose molecule with the same DP value.

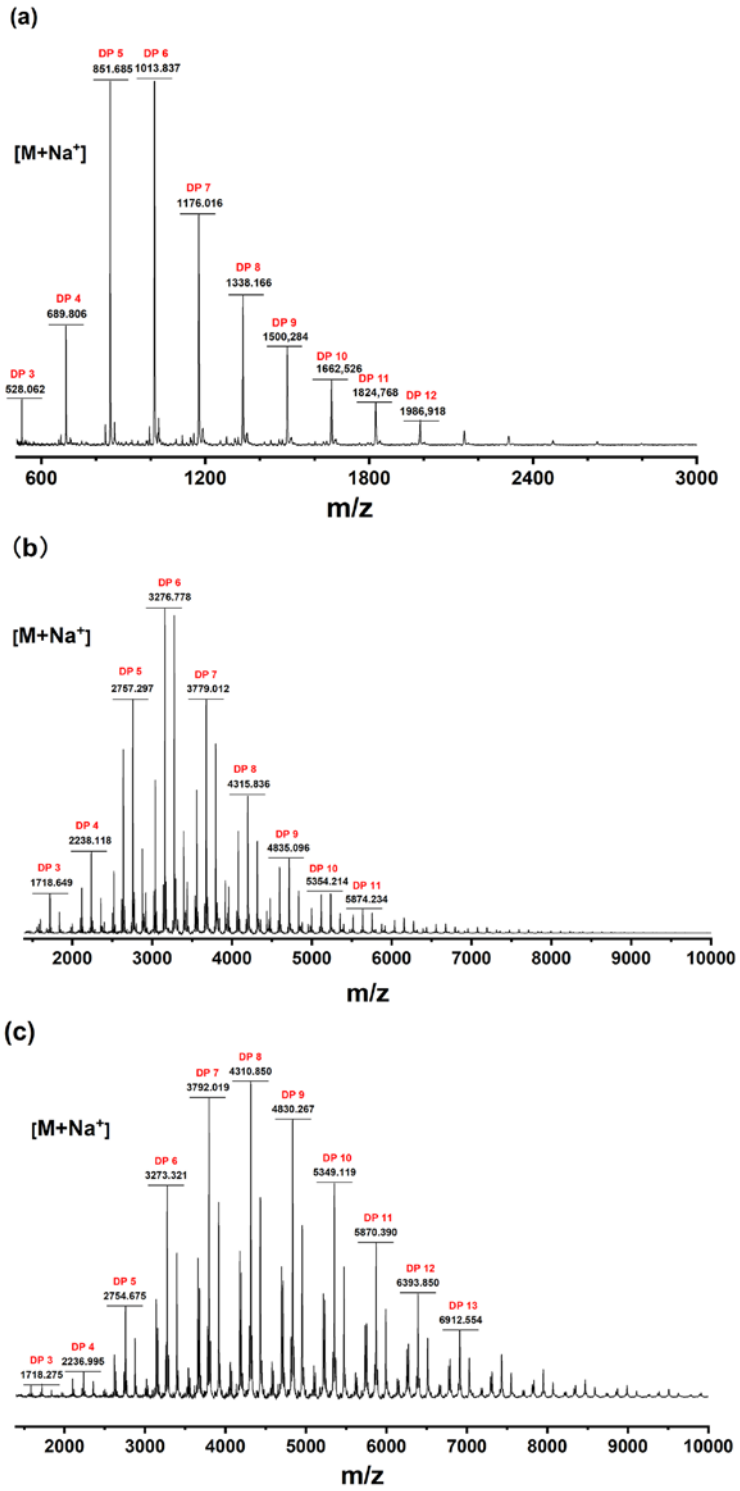

Figure V.4. *MALDI-TOF MS spectra of (a) the fraction B, (b) the carbanilated fraction B and (c) the carbanilated fraction A as a function of mass-to-charge (m/z) ratio in the positive-ion mode.*

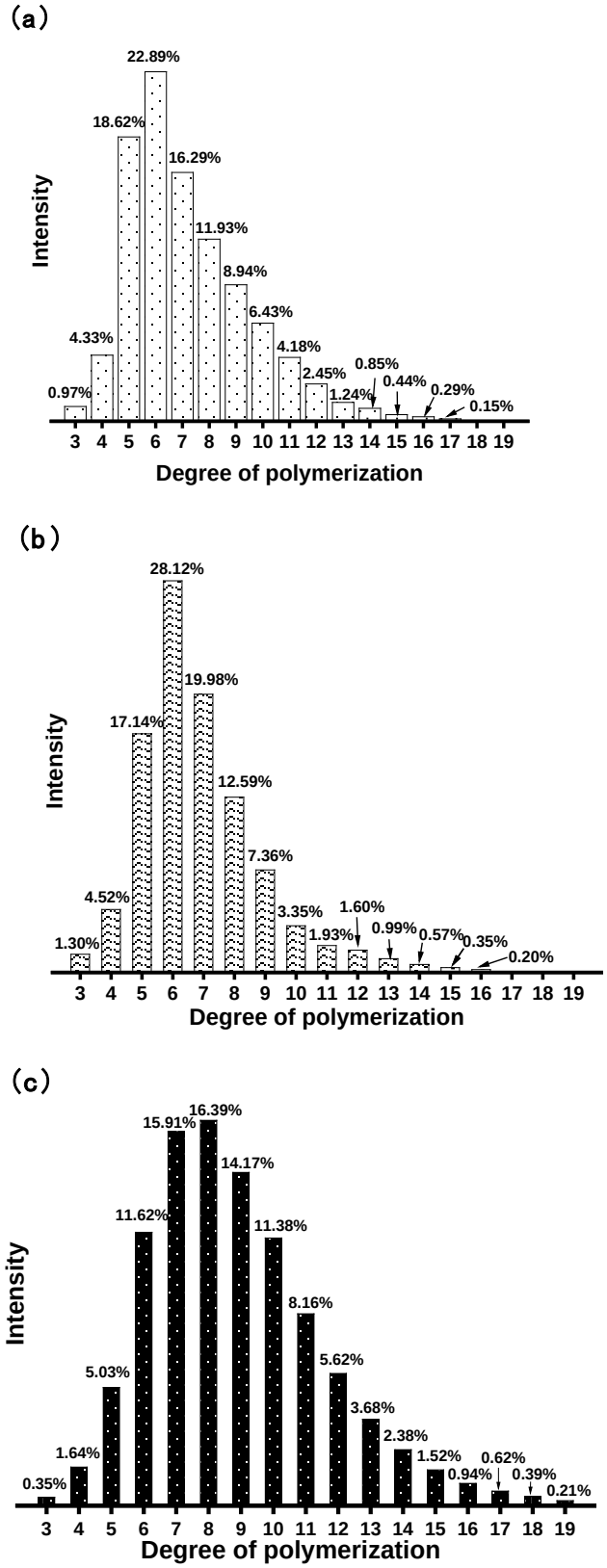

Figure V.5. *Integrated intensities of MALDI-ToF MS peaks from (a) fraction B, (b) carbanilated fraction B and (c) carbanilated fraction A with the same DP as a function of DP values. The proportions of each DP were calculated and denoted above each DP fraction.*

Based on the peak assignments, the sum of integrated peak areas that belongs to the same DP were calculated. Histograms of DP fractions are shown in Figure V.5. It displays that DP of 6 is predominant in the fraction B and the carbanilated fraction B. The population ranges over the DPs between 3 and 17 for fraction B and 3-16 for carbanilated fraction B. The number-averaged DP, weight-averaged DP and Đ value of the fraction B were calculated based on the histogram, yielding DP_n = 7.2, DP_w = 8.0 and Đ = 1.10, respectively. The DP_n and DP_w of the carbanilated fraction B are 0.3 and 0.5 smaller than that of the fraction B, respectively. This difference is likely due to different ionization efficiency between cellulose oligomers and carbanilated cellulose oligomers. The larger carbanilated cellulose molecule might have lower ionization tendency than the non-derivatized cellulose. The carbanilated fraction A gives a DP range of 3-19 with a dominant DP fraction at DP = 8. The DP_n and DP_w of carbanilated fraction A were 8.8 and 9.7, respectively. The calculated Đ values, 1.09, based on the MS result were almost the same for the carbanilated fraction A and carbanilated fraction B.

V.5. Size exclusion chromatography

The carbanilated fraction A and B in THF were injected into the SEC-2 (Chapter II.4.3.2), and the SEC data (RI and LALS) as a function of retention time are shown in Figure V.6. The pink areas are the analyzed region which corresponds to

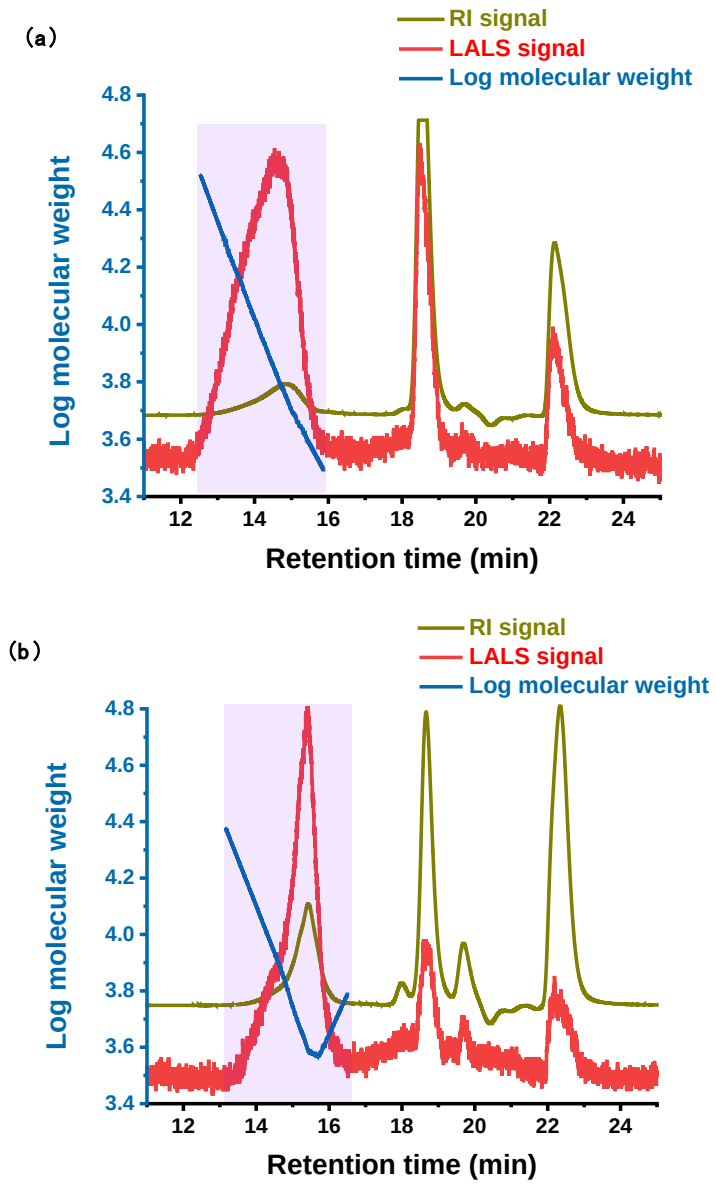

Figure V.6. *Refractive index (RI) signals, low-angle light scattering (LALS) signals and molecular weight of (a) carbanilated fraction A and (b) carbanilated fraction B as a function of retention time from the SEC-2.*

carbanilated cellulose oligomers. The other peaks outside of the pink areas are assigned to the side products of trimers, dimers, 1,3-dipenylurea and methyl carbanilates. The molecular weight of carbanilated fraction A linearly decreases with increasing retention time. However, in the case of carbanilated fraction B, the molecular weight goes down linearly until the retention time of 15.6 min and unusually increases after that point. This observation is against the principle of SEC: low molar mass molecules with smaller molecular size should elute after large molecules with higher molecular weight. There are two possible reasons to explain this phenomenon: (1) the carbanilated cellulose oligomers elute after retention time of 15.6 min have so small molecular size that they behaves as isotropic scatters (as illustrated in Figure II.2), then the calculated Rg values are not reliable, so is the molecular weight; (2) the LALS signal of carbanilated fraction B is so close to the signal of the PI trimer that the tail of the LALS signal of carbanilated cellulose oligomers includes the contribution from the trimer, which makes the detected LALS signal higher than the real value, resulting in higher calculated molecular weight. Nevertheless, the calculated molecular weight of carbailated fraction B is considered not reliable compared to that of the carbanilated fraction A.

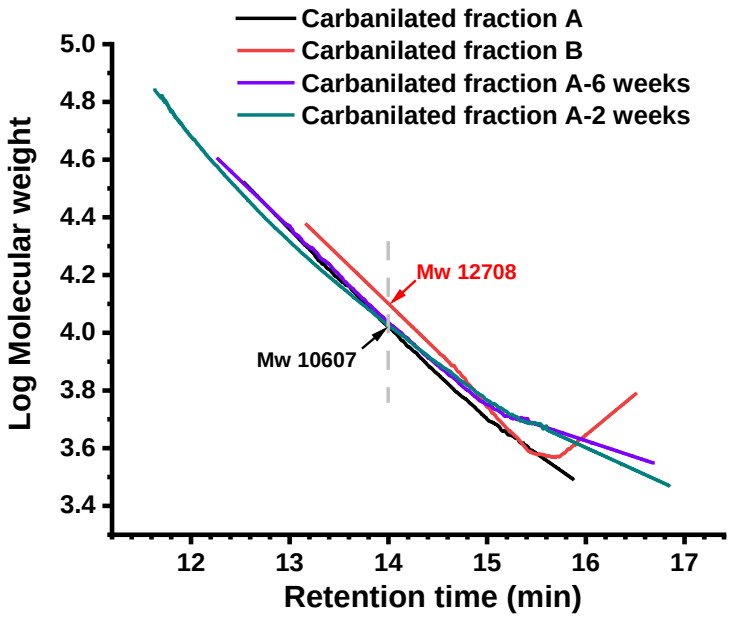

Figure V.7. *Overlaid molecular weight as a function of retention time for the carbanilated fraction A, fraction B, and cellulose oligomers that hydrolyzed at room temperature for 6 weeks and 2 weeks.*

Figure V.7 summarizes the relationship of retention time with the log molecular weight that from the results of carbanilated fraction A (black) and B (red), and the carbanilated fraction A hydrolyzed for 2 and 6 weeks at 23 ˚C. Surprisingly, the black and red curves only partially overlapped around the retention time of 15.6 min. Before the retention time of 14.7 min, the curves from carbanilated fraction A and B were nearly parallel. For example, at the retention time of 14.0 min, the molecular weights of carbanilated fraction A and B were 1.06×10^4 and 1.27×10^4 g mol^{-1}, respectively. The difference of about 2100 in molecular weight corresponds to about 4 tricarbanilated AGU units. The reason that caused this difference is unclear. To verify the relationship between retention time and molecular weight of tricarbanilates, the curves of two new samples (purple and green) were compared with that of carbanilated fraction A and B. Apparently, the black curve is more overlapped with the purple and green curves than the red curve. It indicates that the SEC result of the

carbanilated fraction A is more reliable than that of the carbanilated fraction B. The overlapped part of the three curves (black, purple and green) are mainly in the range of 13.5-14.5 min, the concentrations of the molecules in this range are higher than the concentrations of the other molecules in the samples. It implies that regardless of the molecular size, low concentration of carbanilated cellulose molecules can lead to inaccurate detection in molecular weight. The molecular weights of the carbanilated fraction B from SEC measurement are overestimated for about 80 % slices of elution time.

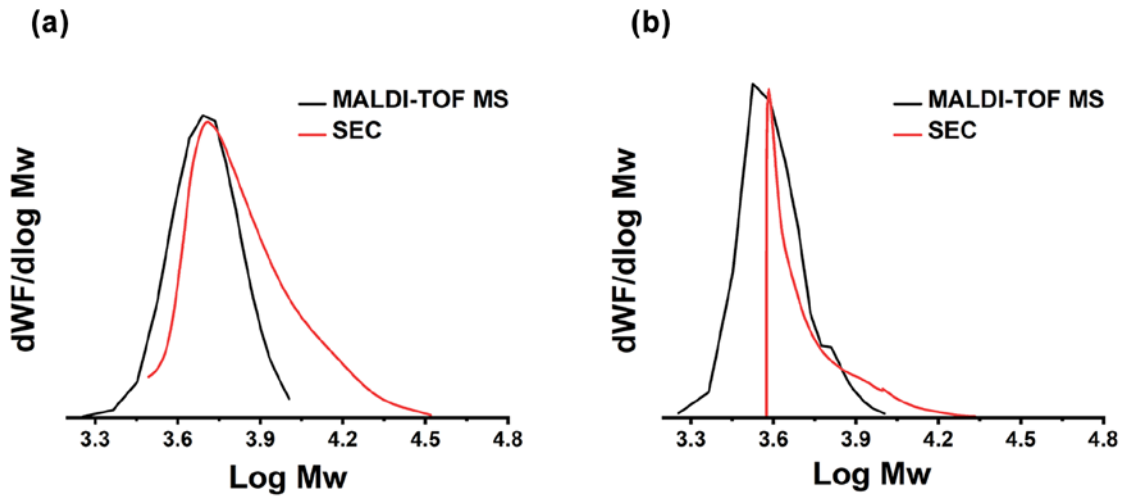

Figure V.8. *Overlaid molar mass distribution graphs of (a) carbanilated fraction A and (b)carbanilated fraction B from MALDI-TOF MS and SEC tests.*

The molar mass distribution of carbanilated fraction A and B from SEC and MALDI-TOF MS are compared in Figure V.8. The results of mass spectrometry give a histogram of number count for each fraction evenly spaced in molecular mass. The intensity is the integration of number count N and molecular weight Mw for each fraction. To plot the dWF/dlogMw as function of LogMw from MALDI-TOF MS results, the unit conversion is explained as follows,

$$\frac{dlogM_w}{dM_w} = \frac{1}{M_w}$$

$$dWF = d(N \times M_w)$$

$$\frac{dWF}{dlogM_w} = \frac{M_w \times d(N \times M_w)}{dM_w} = M_w \times Intensity$$

In the SEC molar mass distribution, the peak top positions of carbanilated fraction A and B are 5051 and 3956 g mol^{-1}, corresponding to DP_p of 9.7 and 7.6, respectively. The peak shapes of these two samples are both asymmetric with a long tail in the high-molecular-weight portion. Carbanilated fraction A has a relatively broader SEC molar mass distribution with DP_n = 12.2, DP_w = 14.9 and Đ = 1.2. The SEC molar mass distribution of carbanilated fraction B is much more assymetric and has no intensity below 3600 g mol^{-1}. This cut-off is most likely an artefact from the inaccurate molecular weight estimation. This is supported by the molar mass distribution of the carbanilated fraction B from MALDI-TOF MS, where there is a significant amount of oligomers with molecular weight below 3600 g mol^{-1}. Thus, the calculated DP_n and DP_w of fraction B based on SEC are not accurate. From the SEC-based distribution of the carbanilated fraction A, about 92 % of molecules have molecular weight larger than 4000 g mol^{-1}. However, such a proportion is only 65 % for the carbanilated fraction A based on MALDI-TOF MS. This indicates that there might be 20-30 % of high-molecular-weight molecules missing from the histogram of mass spectroscopy. It is presumably due to the differences in ionization efficiency between low- and high-mass oligomers. It also implies that the calculated number-averaged and weight-averaged DP values from carbanilated cellulose oligomers is likely biased toward the fractions with lower molecular weight.

The calculated DPs of fraction A and B from different characterization techniques are summarized in Table V.2. There are clear differences in the estimated valued between different characterization methods. The DP_n, DP_w and Đ of fraction A should

Table V.2. *Summary of molecular weight information of fraction A and B by different characterization techniques.*

Techniques		Fraction A	Fraction B
^{1}H NMR	DP_n	-	6.7
Solid-state ^{13}C CP/MAS NMR	DP_n	10.1	7.0
Mass spectroscopy	DP_n	8.8	7.2
	DP_w	9.7	8.0
	Đ	1.09	1.10
Size exclusion chromatography	DP_n	12.2	8.9
	DP_w	14.9	9.9
	Đ	1.22	1.11

be 12.2, 14.9 and 1.22, respectively. The DP_n of fraction A from solid-state ^{13}C CP/MAS NMR are slightly smaller than 12.2. For fraction B, the number-averaged DP from solid-state ^{13}C CP/MAS NMR was almost the same as the DP_n from ^{1}H NMR and mass spectroscopy.

As evident in Table V.2, none of the characterization techniques discussed can accurately determine a DP of cellulose oligomers with a wide DP distribution. SEC is reliable with relatively higher molecular weight oligomers such as the fraction A in this chapter. It is not the case with lower molecular weight oligomers as the molecular weight estimation based on light scattering is not trustable for small oligomers. The

DP information from the MALDI-TOF MS and NMR spectroscopies is more reliable for lower molecular-weight fractions. MALDI-TOF MS data might be biased towards the lower molecular weight oligomers as the ionization efficiency of oligomers is expected to have a negative correlation to its size. The NMR spectroscopy is a reliable method to determine the number-average molecular weight, but in general one cannot access to the DP distribution using NMR spectroscopy. It is unclear why the DP_n value of the fraction A is estimated smaller in the solid-state NMR than that from SEC.

V.6. Conclusions

In this chapter, characterization methods for DP determination of cellulose oligomers were compared. Liquid state ^{1}H NMR, solid-state ^{13}C CP/MAS NMR and MALDI-TOF MS spectroscopy are more suitable for characterizing cellulose oligomers with low molar mass and narrow DP distribution, such as the fraction B in this chapter. While for cellulose oligomers with relatively high molar mass and broad DP distribution, SEC is a preferred choice compared to the other spectroscopic methods.

Chapter VI

Chapter VI. Tunable DP and DP distribution of cellulose oligomers

VI.1. Introduction

The solubility-based fractionation proposed by Isogai and Usuda [1] is an effective and scalable method to produce oligomers with a narrow DP distribution as described in the Chapter I.4.3. While this method has merits of scalability and simplicity of manipulations, the obtained fractions are generally more polydisperse than those obtained via column chromatography fractionation. Furthermore, the method has been underexplored and it is unknown if the DP distribution of oligomers can be controlled more precisely via this method than in the first report.

In this chapter, therefore, I revisited each step of the oligomer preparation to improve this method based on the concentrated acid hydrolysis and the solubility-based fractionation. In particular, I investigated the possibility of controlling the DP

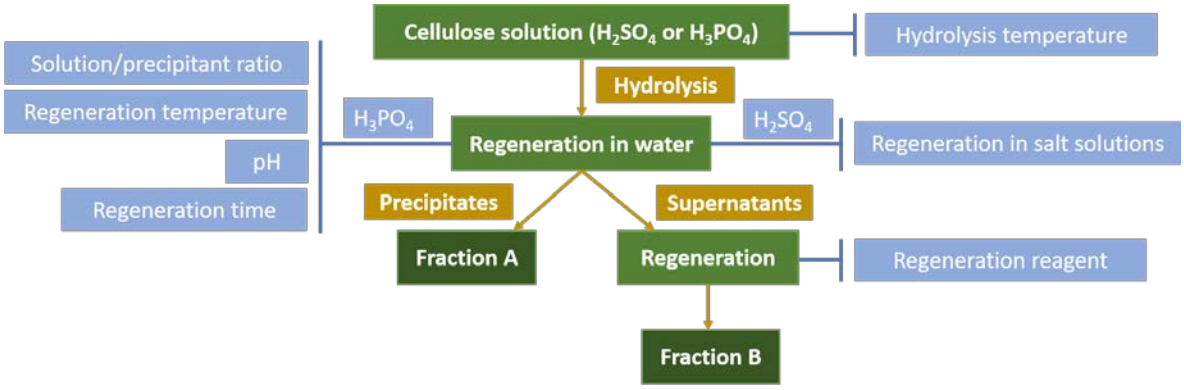

Scheme VI.1. *Scheme of preparing regenerated cellulose fraction A and B.*

and DP distribution of cellulose oligomers by changing the hydrolysis and regeneration conditions, which are summarized in Scheme VI.1 with light blue color

boxes. Sulfuric acid was also used together with phosphoric acid. The sulfuric acid-based method is industrially more relevant for its sustainability compared to the original phosphoric acid-based one: phosphorus is a critical global resource for food production, and the main source of phosphorus is non-renewable [216]. The DPs and DP distributions of obtained oligomers were characterized using the characterization methods described in the Chapter V. Based on the conclusions of Chapter V, the fraction A, the water-insoluble fraction, was characterized by SEC and the fraction B, the organic solvent insoluble fraction, was characterized by ^{1}H-NMR and MALDI-MS.

VI.2. Effect of hydrolysis conditions on fraction A

Experiments.

3.0 g of MCC were dissolved in about 96.6 g 83 wt% phosphoric acid at room temperature (Chapter II.2.1), and this dissolution process took 1 day. After 1 day, a transparent homogenous solution was obtained, and this point was set at the starting time of hydrolysis (0 day). For the cellulose solution that was put at 23 ˚C, after 7, 14, 21, 28, 35, 42, 49 and 56 days, about 5 g of the cellulose solutions were taken and mixed with the same weight of water, and decantated at 23 ˚C for 24 hours to obtain the fraction A. For the cellulose solution that was put at 40 ˚C, after 1, 2, 3 and 4 days, the cellulose solutions were regenerated to obtain the fraction A according to the Chapter II.2.3.1. The molecular weight distributions of the fraction A as a function of the hydrolysis time were investigated using SEC-2 (Chapter II.4.3.2) with light scattering detectors.

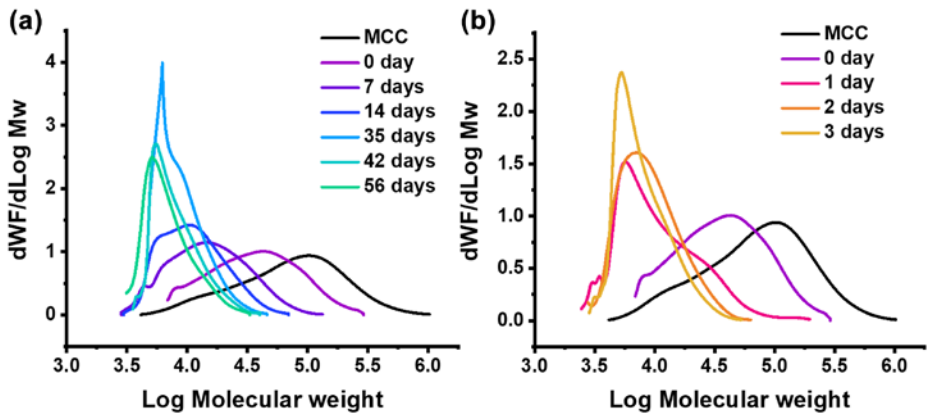

Figure VI.1. *Overlaid molar mass distribution graphs of MCC and the fraction A from the just dissolved cellulose solution (0 day) and the cellulose solutions that (a) hydrolyzed for 7 days, 14 days, 35 days, 42 days and 56 days at 23 ˚C, and (b) the fraction A from the cellulose solutions that hydrolyzed for 1 day, 2 days, 3 days and 4 days at 40 ˚C.*

Results and discussion.

The hydrolysis conditions in the literature of Isogai and Usuda [1] is hydrolyzing cellulose in a 83 wt% phosphoric acid aqueous solution at room temperature for 56 days (8 weeks). The average DP values of the fractions A and B were measured by viscometry, ^{1}H-NMR and SEC based on polystyrene standard. In this section, the hydrolysis was repeated in the same condition and the evolution of DP distributions was followed as a function of hydrolysis time.

Figure VI.1a shows SEC molecular weight distributions of the fraction A after different hydrolysis times (0, 7, 14, 35, 42, and 56 days) and Table VI.1 summarizes the DPs and Đ values. The starting material, MCC, has the broadest DP distribution ranging from DP 8 to DP 1900 and centered at a DP of 190. The 0-day specimen corresponds to the sample stored at room-temperature for 1 day to obtain a homogenous transparent solution. The dissolution makes the weight-averaged DP decrease by half with a narrower distribution. With hydrolysis proceeding, the

average DP continued to decrease as can be seen as a peak shift towards the lower-molecular weight region. During this process, the DP distribution becomes narrower. Interestingly, the DP distributions of the fraction A after 7, 14 and 35 days of hydrolysis shows one main peak with a shoulder. The shoulder peak seen in the 7- and 14-day samples becomes the main sharp peak in the 35-day sample. After 42 days, the

Table VI.1. *The weight-averaged DP, number-averaged DP and polydispersity index from SEC measurements of MCC and fraction A obtained after hydrolysis at 23 and 40 ˚C.*

	Hydrolysis time	DP_w	DP_n	Đ
	MCC	215.4	79.9	2.70
	0 day	96.6	50.6	1.91
Hydrolysis at 23 ˚C	7 days	37.8	22.5	1.68
	14 days	25.7	18.3	1.41
	35 days	19.8	16.8	1.18
	42 days	17.3	14.2	1.21
	56 days	14.9	12.2	1.22
Hydrolysis at 40 ˚C	1 day	28.9	15.8	1.83
	2 days	20.6	15.1	1.36
	3 days	17.5	13.6	1.29
	4 days	13.4	5.9	2.15

distributions are essentially monomodal with peak positions at DP 11 for the 42-day sample and DP 10 for the 56-day sample, respectively. The tails on the higher molecular weight side end approximately at DP 75 (42 days) and DP 60 (60 days).

To shorten the preparation time, the hydrolysis temperature was changed to 40 ˚C, and the other preparation conditions of the fraction A were kept the same with those

at 23 ˚C. The DP distributions of the fraction A as a function of hydrolysis time are shown in Figure VI.1b. After hydrolysis at 40 ˚C for only 1 day, the weight-averaged DP decreases to 29 from 215 of MCC, and the DP distribution is broad with the Đ value of 1.83. The peak is multimodal with a main peak at DP 11, a small but sharp doublet around DP 6 and a broad shoulder in the high DP range around DP 42. With

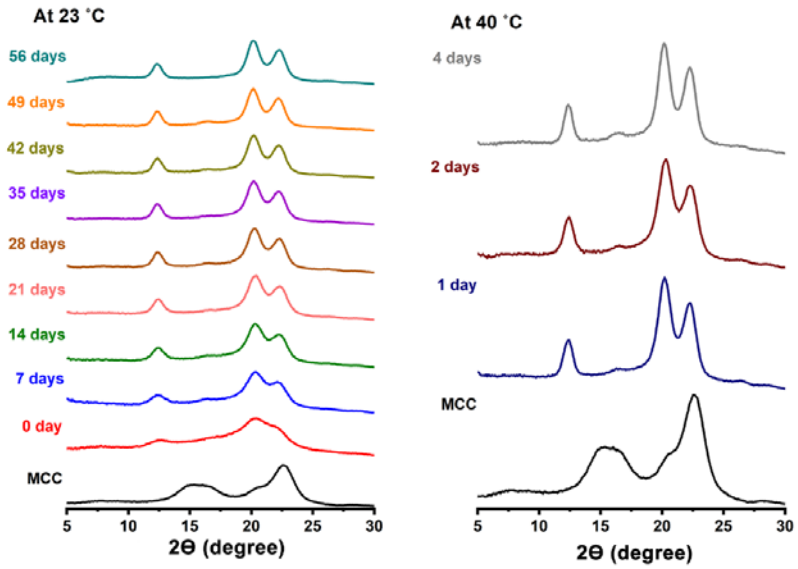

Figure VI.2. *X-ray diffraction profiles of MCC, the fraction A from the just dissolved cellulose solution (0 day) and the cellulose solutions that hydrolyzed for 7 days, 14 days, 35 days, 42 days and 56 days at 23 ˚C, and the fraction A from the cellulose solutions that hydrolyzed for 1 day, 2 days, 3 days and 4 days at 40 ˚C.*

hydrolysis proceeding, the average DP decreases much slower than on the first day of hydrolysis. The fraction A after hydrolysis for 2 and 3 days show narrow monomodal DP distributions with peak positions at DP 14 and DP 10, respectively. It is notable that the fraction A with hydrolysis at 40 ˚C for only 3 days has almost the same average DP and DP distribution as the fraction A with hydrolysis at 23 ˚C for 42 days.

Figure VI.2 shows the X-ray diffraction profiles of MCC and the fraction A with hydrolysis at 23 ˚C and 40 ˚C for different hydrolysis time. The MCC profile shows typical features of crystalline cellulose I, with three strong reflections, 1 ī 0 (15˚), 1 1 0 (16.5˚), 2 0 0 (22.5˚). After dissolved in phosphoric acid at 23 ˚C, the regenerated fraction A shows broad peaks with vague features of cellulose II. The characteristic peaks of cellulose II, 1 ī 0 (12.3˚), 1 1 0 (20.5˚), and 0 2 0 (22˚) become sharper, hence the crystallite sizes are larger as the hydrolysis time increases. This tendency where the diffraction peaks get sharper with decreasing DPs is also reported by Claisse [106]. It is most likely because crystallization of cellulose is more favorable with the shorter molecular chains than the longer chains that might have chain entanglements and other mechanical constraints. For the hydrolysis at 40 ˚C, this tendency is less obvious since the diffraction peaks of the fraction A with hydrolysis for 1 day is already very sharp, and the difference in the average DPs between 1-day and 4-day samples is less significant than that of the room temperature system.

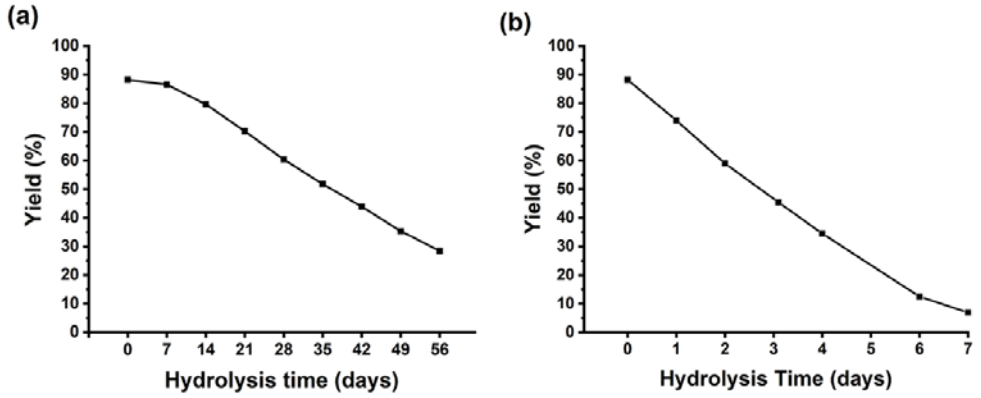

Figure VI.3. *The yield of the fraction A with different hydrolysis time at (a) 23 ˚C and (b) 40 ˚C.*

The yields as a function of hydrolysis time are shown in Figure VI.3. After the dissolution, the yield of the fraction A is 88 %. Both for the hydrolysis at 23 ˚C and 40 ˚C, the yields of the fraction A decrease with the increasing hydrolysis time. The

changes in yield and average DP of the fraction A are consistent with that in the literature by Isogai and Usuda [1]. With hydrolysis temperature at 40 ˚C for 1 day, the yield of the fraction A is 74 %. With hydrolysis proceeding, the yield decreased almost linearly to 7 % at 7 days. When comparing the fractions of 42 days at 23 ˚C and 3 days at 40 ˚C that have very similar DP distribution, the yields are roughly identical (44 % at 23 ˚C vs 45 % at 40 ˚C).

The higher temperature hydrolysis at 40 ˚C considerably shortens the preparation. For instance, a 3-day hydrolysis at 40 ˚C provided a fraction A in yield of 45 % with the weight-averaged DP and Đ of 17.5 and 1.29, that is essentially identical to the fraction A obtained via a 42-day hydrolysis at 23 ˚C.

VI.3. Effect of regeneration conditions on fraction B

In this section, the fraction B, an organic solvent-insoluble fraction, was investigated. In particular, the effects of different precipitants, isopropanol and methanol on the DP distribution of the fraction B were investigated.

VI.3.1. Fraction B from phosphoric acid hydrolysis

Experiments.

3.0 g of MCC were dissolved in about 96.6 g 83 wt% phosphoric acid at room temperature (Chapter II.2.1), and this dissolution process took about 1 day. Then the cellulose solution was put at 23 ˚C. After 7, 14, 21, 28, 35, 42, 49 and 56 days of hydrolysis, about 5 g of the cellulose solution were mixed with the same weight of

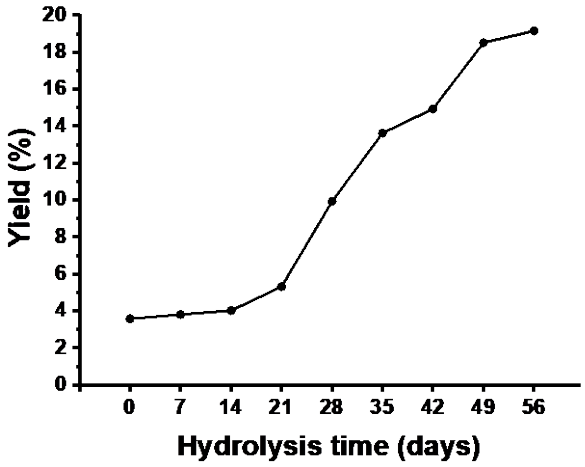

Figure VI.4. *The yield of the fraction B with different hydrolysis time at 23 ˚C.*

water, and the supernatant without filtration was mixed with three times its volume of isopropanol to obtain the fraction B. After washing with isopropanol until pH reached neutral, the fraction B was directly freeze-dried. The fraction B with hydrolysis time of 56 days was named as 56d-IP, and studied by X-ray diffraction, ^{1}H NMR and MALDI-TOF MS.

Results and discussion.

The yields of the fraction B are shown as a function of hydrolysis time in Figure VI.4. After dissolution, the yield of the fraction B is almost 4 %. With the increase of hydrolysis time, the yields of the fraction B keep increasing, up to approximately 19 % after hydrolysis at 23 ˚C for 56 days. Combining with the yield of the fraction A in Figure VI.3a, the overall yields (sum of the fractions A and B) are always not 100 %.

For instance, the overall yield of 0 day is about 92 %. It means that there was about 8% of cellulose oligomers that were lost during the washing process or unable to be recovered by isopropanol (e.g. glucose solubility in isopropanol at 22 ˚C is 0.66 g/L [217]). The overall yield is below 50 % after hydrolysis at 23 ˚C for 56 days. The unrecoverable fraction is most likely hydrolyzed into isopropanol soluble fraction (monomer, dimer, and/or degraded compounds).

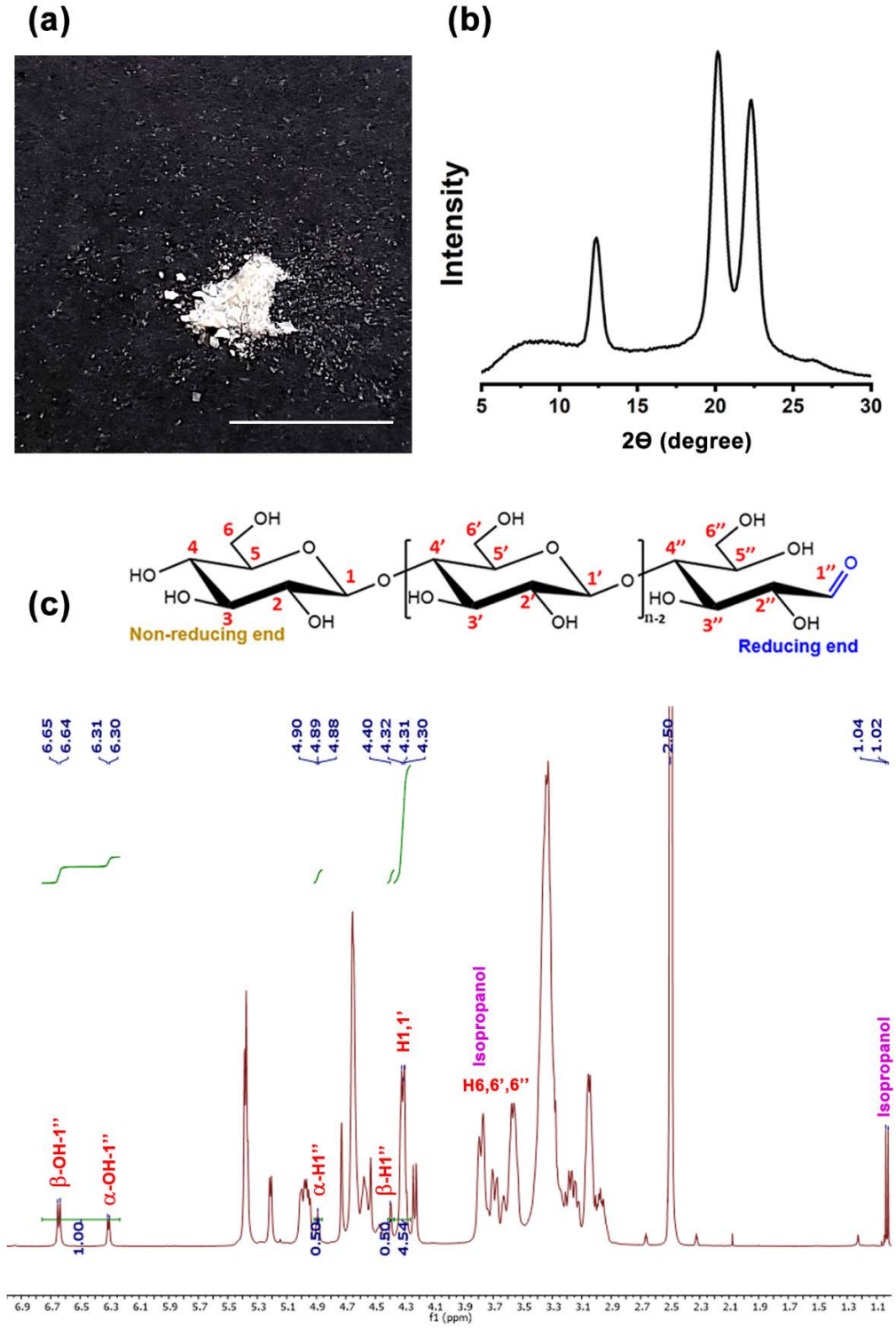

Figure VI.5. *(a)The photo of 5 mg of the fraction B (56d-IP) with the scale bar = 9 mm, (b) X-ray diffraction profile and (c) ^{1}H-NMR spectrum of the fraction B (56d-IP).*

Figure VI.5a shows the photo of the fraction B that hydrolyzed for 56 days at 23 ˚C (56d-IP) with the weight of 5 mg. The 56d-IP is densely packed white powder. The diffraction pattern (Figure VI.5b) indicates the 56d-IP consists of cellulose II. ^{1}H NMR spectrum of 56d-IP is shown in Fig. VI.5c. After integrating the peak areas assigned to OH-1'' or H1'' of the reducing ends and the peak area of the H1, 1' the number-averaged DPs are calculated as 5.5. In the spectrum, the contamination of isopropanol is seen: a peak at 1.04 ppm is due to the methyl protons of isopropanol;

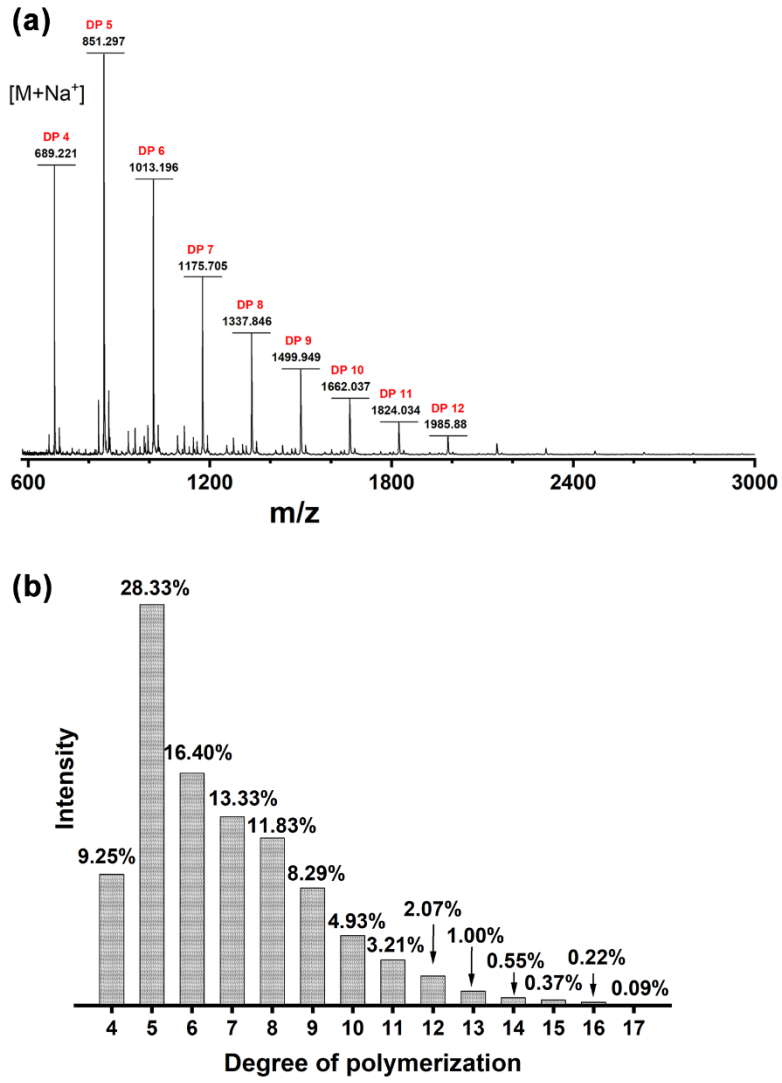

Figure VI.6. *(a) MALDI-TOF MS spectra of fraction B (56d-IP) as a function of mass-to-charge (m/z) ratio in the positive-ion mode. (b) Summation of integrated intensity from the same DP as a function of different DP in the fraction B (56d-IP).*

and the methanetriyl protons of isopropanol are seen at 3.78 ppm, which are merged with the peaks of H6,6',6'' on the cellulose rings.

The MALDI-TOF MS spectrum of the 56d-IP is shown in Figure VI.6a. The sum of the integrated peak areas that belongs to the same DP were calculated as decribed in Chapter V.4. The histogram as a function of different DPs is shown in Figure VI.6b. The dominant DP is 5 with the DP range of 4-17. Based on the integrated intensity from Figure VI.6b, the number-averaged DP, weight-averaged DP and Đ value are calculated as 6.8, 7.6 and 1.11, respectively. The number average DP from ^{1}H NMR is slightly lower in this report compared to the reported value in Isogai and Usuda's work. The current work shares the same hydrolysis condition with the original report, but the precipitants are different: isopropanol in this study and methanol in Isogai and Usuda.

VI.3.2. Fraction B precipitated from isopropanol and methanol

Experiments.

Two different samples were prepared as summarized in Table VI.2. Briefly, after six weeks of hydrolysis in 83 wt% phosphoric acid at 23 ˚C, the fraction B were regenerated by mixing methanol or isopropanol with the supernatant of fraction A according to the Chapter II.2.3.1. These fractions B were washed with respective

Table VI.2*. Difference between 42d-IP and 42d-Me in preparation conditions.*

	Hydrolysis time	Regeneration reagent	Mixing with water before freeze-drying
42d-IP	42 days	Isopropanol	Yes
42d-Me	42 days	Methanol	No

solvents until pH reached neutral. The methanol-regenerated fractions were directly freeze-dried (42d-Me), while the isopropanol-regenerated ones were first mixed with water and then freeze-dried (42d-IP). The addition of water here should not have any effect on its DP distribution.

Results and discussion.

Figure VI.7 shows photographs of the two fraction B with the same weight (5 mg). The samples directly freeze-dried from the organic solvent are more compact compared to the one freeze-dried from the water suspension (Figs. VI.5a and VI.7a vs

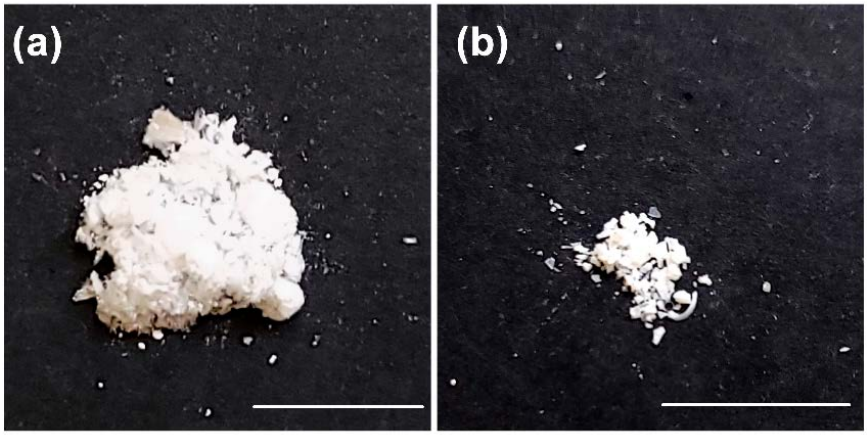

Figure VI.7. *The photos of 5 mg of (a) 42d-IP and (b) 42d-Me. The scale bar was 9 mm.*

VI.7b). The X-ray diffraction patterns (Figure VI.8) show that the two specimens are composed mainly of cellulose II. In the diffraction pattern of the isopropanol fraction, an additional peak at 16.4˚ is present, corresponding to a *d*-spacing of 5.4 Å. This small diffraction peak also appears in the X-ray patterns of the fraction A with other hydrolysis and regeneration conditions (Figure VI.2, Figure VI.12b, Figure VI.13b and Figure VI.14b). This peak is most likely from cellulose IV_{II} allomorph, but the reason of its formation is unclear. Because the fraction B are partially dissolved in

water, the fraction B might have experienced a different crystallization after suspended in water. Nevertheless, the proportion of the cellulose IV allomorph is small, and the main allomorph is crystalline cellulose II. Additional discussion on the

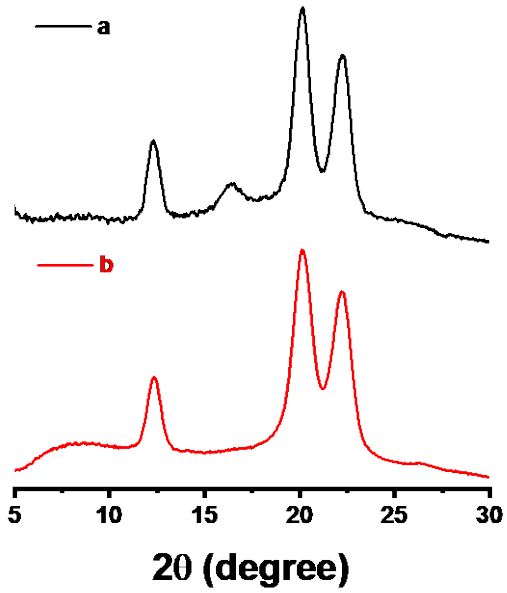

Figure VI.8. *X-ray diffraction profiles of the (a) 42d-IP and (b) 42d-Me.*

formation of cellulose IV_{II} are given in Appendix 4.1.

Figure VI.9 shows the ^{1}H NMR spectra of the two fractions B. After integrating the peak areas corresponding to OH-1'' or H1'' of the reducing ends and the peak area assigned to the H1, 1', the number-averaged DPs are calculated as 6.7 and 6.7 for 42d-IP and 42d-Me, respectively. Note that the spectrum of 42d-Me shows contamination peaks of methanol and acetone. The peak of the regeneration reagent (methanol) has significant intensity and is overlapping with peaks of cellulose. In the spectrum of 42d-IP, there is no obvious peak of isopropanol. This is not the case when the isopropanol fraction is freeze-dried directly from the solvent as shown in Figure VI.5c. Thus, suspending the fraction in water helps to thoroughly remove the solvent

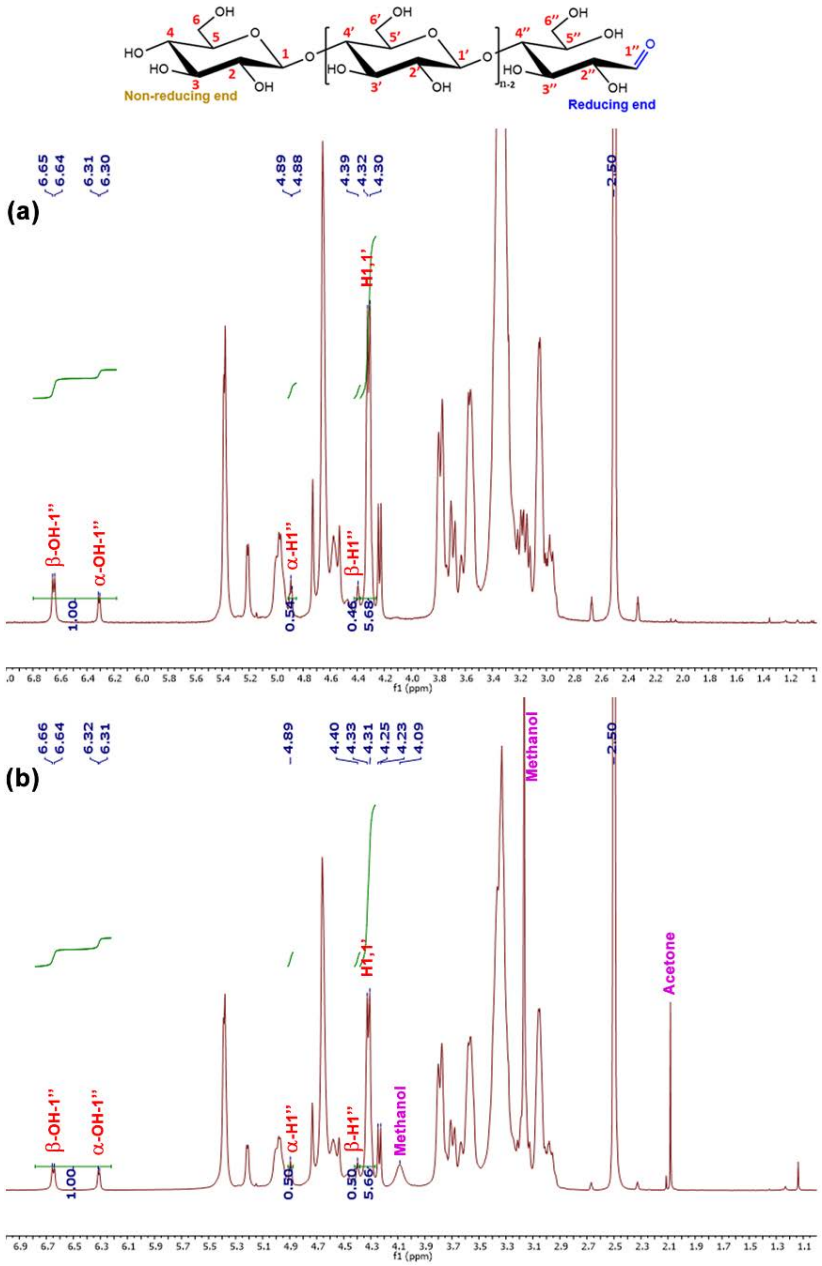

Figure VI.9. *^{1}H-NMR spectra of the (a) 42d-IP and (b) 42d-Me in deuterated DMSO.*

molecules.

The MALDI-TOF MS results of 42d-Me and 42d-IP are shown in Figure VI.10. The spectra were analyzed as described in Chapter V.4. The sum of integrated peak areas that belongs to the same DP was calculated, resulting in the DP histogram as

shown in Figure VI.11. The dominant DPs in 42d-IP and 42d-Me are 5 and 6, repectively. The intensities span over the DP range of 4-14 for 42d-IP and 4-17 for 42d-Me. Interestingly, when comparing the distrubutions, the isopropanol fraction has higher proportion of lower-molecular weight fraction below DP 6 than the isopropanol fraction. It indicates the lower solubility of cellotetraose and cellopentaose in isopropanol than in methanol. The number-average DP and weight-average DP and Đ value were calculated based on the data in Figure VI.10.

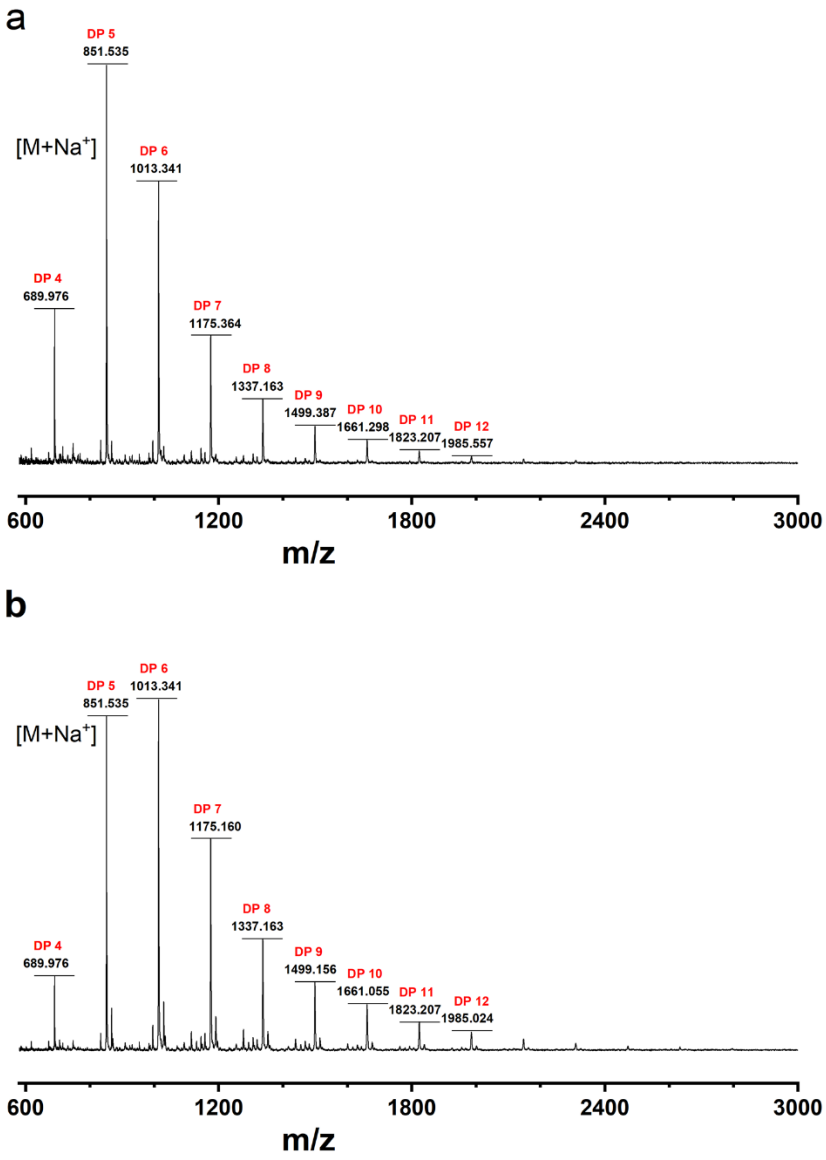

Figure VI.10. *MALDI-TOF MS spectra of (a) 42d-IP and (b) 42d-Me as a function of mass-to-charge (m/z) ratio in the positive-ion mode.*

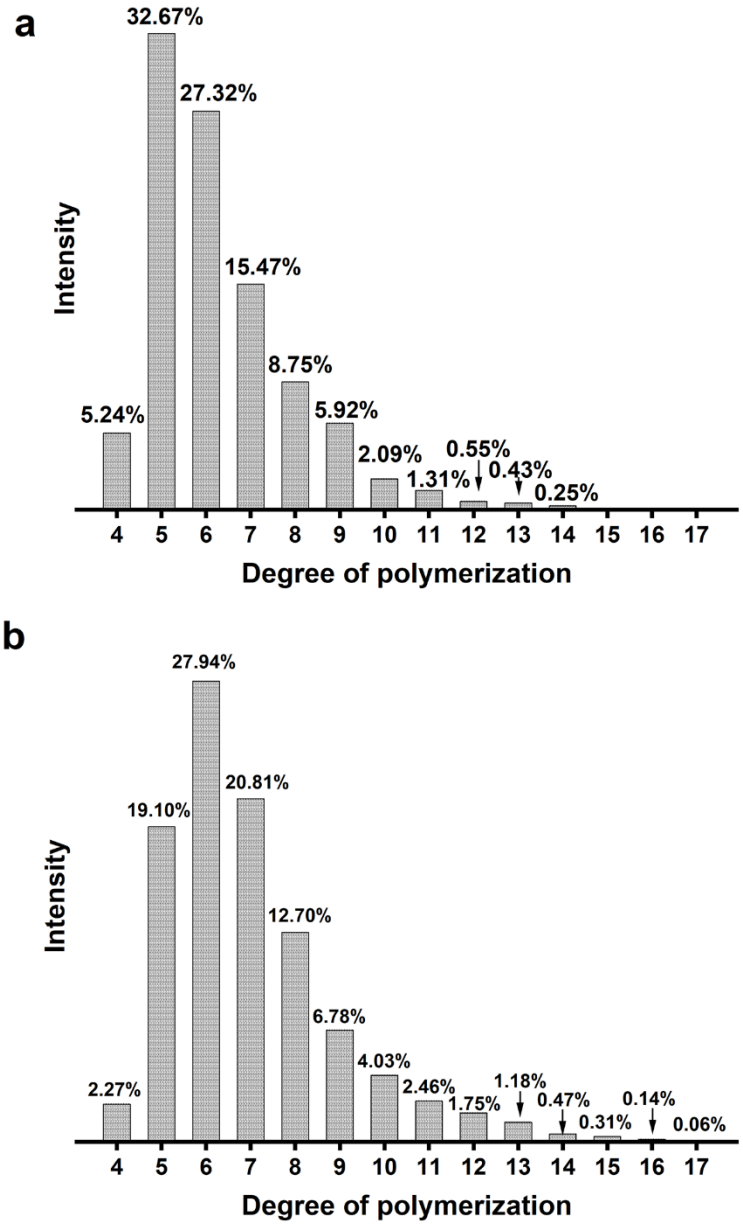

Figure VI.11. *Summation of integrated intensity from the same DP as a function of different DP in the (a) 42d-IP and (b) 42d-Me.*

Table VI.3 summarizes the average DPs, Đ values and yields of the three fraction B in this section. For 56d-IP, the number-average DP from ^{1}H NMR is significantly smaller than that from MALDI-TOF MS. The reason behind this difference is unknown. For 42d-IP and 42d-Me, the results are in better agreement between ^{1}H NMR and MALDI-TOF MS. 42d-IP has slightly lower average DPs and Đ value but higher yield than 42d-Me, likely due to the lower solubility of cellulose oligomers in

isopropanol than in methanol. Thus, isopropanol was used for the regeneration reagent for the fraction B in the following studies, and the precipitates were mixed with water before freeze-drying.

Table VI.3. *The weight-averaged DP, number-averaged DP and polydispersity index and yield of 42d-IP and 42d-Me.*

	^{1}H-NMR	MALDI-TOF MS			Yield (%)
	DP_n	DP_w	DP_n	Đ	
56d-IP	5.5	7.6	6.8	1.11	19
42d-IP	6.7	6.7	6.3	1.07	19
42d-Me	6.7	7.5	7.0	1.08	14

VI.4. Effect of regeneration conditions on fraction A

In the following, I investigated the effects of parameters involved in the regeneration on the DP distributions of the fraction A. Studied parameters include solution/precipitant ratio, temperature, pH, and regeneration time.

VI.4.1. Solution/precipitant ratio

Experiments.

0.5 g of MCC was dissolved in 16.8 g of 83 wt% phosphoric acid solution, and then hydrolyzed at 40 ˚C for 1 day. About 1 g of cellulose solution was mixed with 1 g or 10 g water. The mixtures were stored at 23 ˚C for 24 hours. Then the regenerated fractions A were washed and freeze-dried according to Chapter II.2.3.1, and investigated by lab source X-ray diffraction and SEC-2 (Chapter II.4.3.2).

Results and discussion.

The SEC molecular weight distributions of the obtained fractions A are shown in Figure VI.12a and the DPs and Đ are shown in Table VI.4. The main peak positions of the DP distributions were at DP 11 and DP 21 for 1:1 and 1:10, respectively. The fraction A from the 1:1 mixture contains more lower-DP cellulose oligomers with slightly narrower DP distribution compared to that from the 1:10 mixture. The fraction from the 1:1 mixture has a narrower main peak and a shoulder peak in the higher molecular-weight side. The X-ray diffraction patterns of two fractions are shown in Fig VI.12b. The one from the 1:1 mixture shows sharper diffraction peaks. This is reasonable considering that it contains more lower-molecular weight oligomers than that from the 1:10 mixture. As shown in Table IV.4 the yield of fraction A from the 1:1 mixture, 74 %, is 7 % higher than that from the 1:10 mixture.

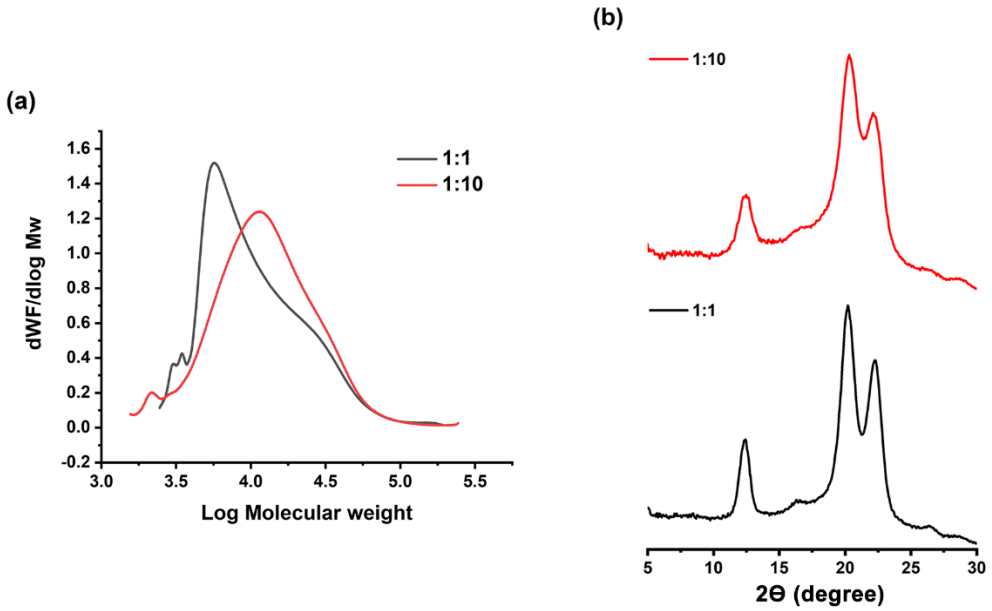

Figure VI.12. *(a) Overlaid differential molar mass graphs and (b) X-ray diffraction profiles of the fraction A from 1:1 and 1:10 cellulose phosphoric acid/water mixture.*

Table VI.4. *The weight-averaged DP, number-averaged DP and polydispersity index and yield of the fraction A from 1:1 and 1:10 cellulose phosphoric acid solution amd water mixture.*

	DP_w	DP_n	Đ	Yield (%)
1:1	28.9	15.8	1.83	74
1:10	32.8	17.4	1.89	67

These results indicate that lower precipitant/solution ratio, and hence higher cellulose content in the mixture, helps recover more low-molecular weight cellulose oligomers. This is presumably due to coprecipitation effect.

VI.4.2. Regeneration temperature and pH

Temperature and pH are critical factors affecting solubility. Thus, they should affect the regeneration behavior of cellulose oligomers from the solution.

Experiments.

0.5 g of MCC was dissolved in 16.8 g of 83 wt% phosphoric acid solution, then hydrolyzed at 40 ˚C for 2 day. About 1 g of cellulose solution was mixed with 1 g water. The mixtures were put at 23 ˚C or 70 ˚C in an acidic or neutralized (Chapter II.2.3.2) environment for 24 hours. Then the regenerated fraction A were washed and freeze-dried according to Chapter II.2.3.1, and then investigated by lab source X-ray diffraction and SEC-2 (Chapter II.4.3.2).

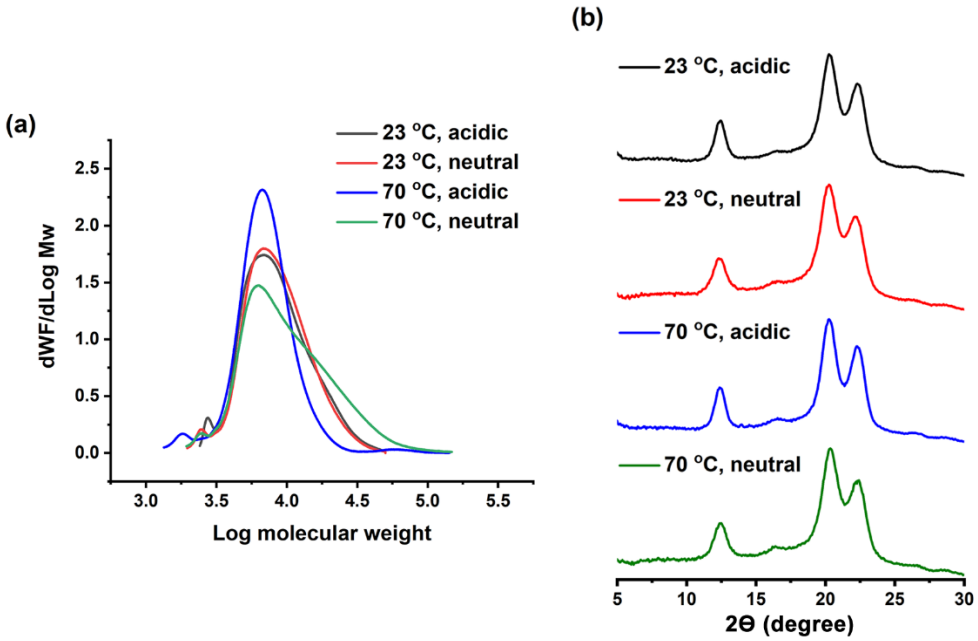

Figure VI.13. *(a) Overlaid molar mass distribution graphs and (b) X-ray diffraction profiles of the fraction A from regeneration conditions at four different conditions (23 ˚C in an acidic environment, 23 ˚C in a neutralized environment, 70 ˚C in an acidic environment and 70 ˚C in a neutralized environment).*

Results and discussion.

The SEC molecular weight distributions of the obtained fractions A are shown in Figure VI.13a and the molecular weight information is summarized in Table VI.5. The effect from pH is small on the DP distribution of the fraction A regenerated at 23 ˚C. Only a very slight shift of the distribution to the lower molecular weight side can

Table VI.5. *The weight-averaged DP, number-averaged DP and polydispersity index and yield of the of the fraction A from regeneration conditions at four different conditions (23 ˚C in an acidic environment, 23 ˚C in a neutralized environment, 70 ˚C in an acidic environment and 70 ˚C in a neutralized environment).*

	DP_w	DP_n	Đ	Yield (%)
23 ^oC, acidic	19.0	14.2	1.34	59
23 ^oC, neutral	18.8	14.2	1.32	58
70 ^oC, acidic	14.5	11.9	1.26	53
70 ^oC, neutral	26.0	15.4	1.69	51

be seen in the acidic condition compared to the neutral one. On the other hand, a significant effect of pH is seen when the regeneration temperature is set to 70 ˚C. When regenerated in the acidic environment, the DP distribution becomes much narrower with the weight-average DP of 14.5. When regenerated in the neutral environment, the DP distribution is much broader with the highest weight-averaged DP of 26.0. Note that the main peak positions for these four conditions are nearly identical. The X-ray diffraction peaks of the fraction A at 70 ˚C and acidic environment were the sharpest (Figure VI.13b), which is reasonable considering its DP distribution which contains more low-molecular weight fractions than the other three.

The drastic change between neutral and acidic environments at 70 ˚C indicates that the high molecular weight fractions observed in the neutral condition have been hydrolyzed during the regeneration in the acidic condition. This effect is almost negligible at 23 ˚C most likely because the hydrolysis is much slower at 23 ˚C than 70 ˚C. The lower yield of fraction A regenerated in the acidic condition at high temperature is reasonable considering that the hydrolysis proceeds during the regeneration time. On the other hand, the lower yield in neutral condition at the high

temperature is doubtful. As additional hydrolysis is not expected in that condition, it should be the same with the yield in the neutral condition at the room temperature. Thus, I compared these yields with the yields from another two batches of samples with the same regeneration conditions but hydrolyzed at 40 ˚C for 5 hours. From Table VI.6, for the samples hydrolyzed at 40 ˚C for 5 hours, the regeneration conditions at 70 ˚C in a neutral environment result in the highest yield when compared with other three regeneration conditions. The error in yield is in the range of 1-8 %. Thus, the yield of 51 % from neutral regeneration at 70 ˚C might be of an experimental error.

Table VI.6. *The yields of the fraction A that hydrolyzed at 40 for 5 hours and 48 hours from four different regeneration conditions (23 ˚C in an acidic environment, 23 ˚C in a neutralized environment, 70 ˚C in an acidic environment and 70 ˚C in a neutralized environment).*

Yield (%)	Hydrolysis time		
	5 hours	5 hours	48 hours
23 ºC, acidic	86	87	59
23 ºC, neutral	91	87	58
70 ºC, acidic	83	75	53
70 ºC, neutral	91	90	51

VI.4.3. Regeneration time

Experiments.

0.5 g of MCC was dissolved in 16.8 g of 83 wt% phosphoric acid solution, then hydrolyzed at 40 ˚C for 2 days. About 1 g of cellulose solution was mixed with 1 g

water. The precipitates from the mixture were washed immediately to prepare a 0-hour sample. Another mixture was stored at 23 ˚C for 24 hours before washing (24-hour sample). Then these fractions A were washed and freeze-dried according to Chapter II.2.3.1, and then investigated by lab source X-ray diffraction and SEC-2 (Chapter II.4.3.2).

Results and discussion.

The SEC molecular weight distributions of the obtained fractions A are shown in Figure VI.14a and the molecular weight information and yields are summarized in Table VI.7. The main peak of the fraction after 24 hours of regeneration was slightly shifted to the low DP range compared that of the 0-hour sample. This difference gives a slightly smaller average DPs for the regeneration time of 24 hours, while the Đ values are the same. The small shift of the molecular weight distribution indicates that the lower molecular weight fraction might take longer time to precipitate in water. This would be reasonable considering such a fraction is only partially insoluble in water. On the other hand, additional hydrolysis during the regeneration at room temperature is not fierce based on the previous section VI.4.2.

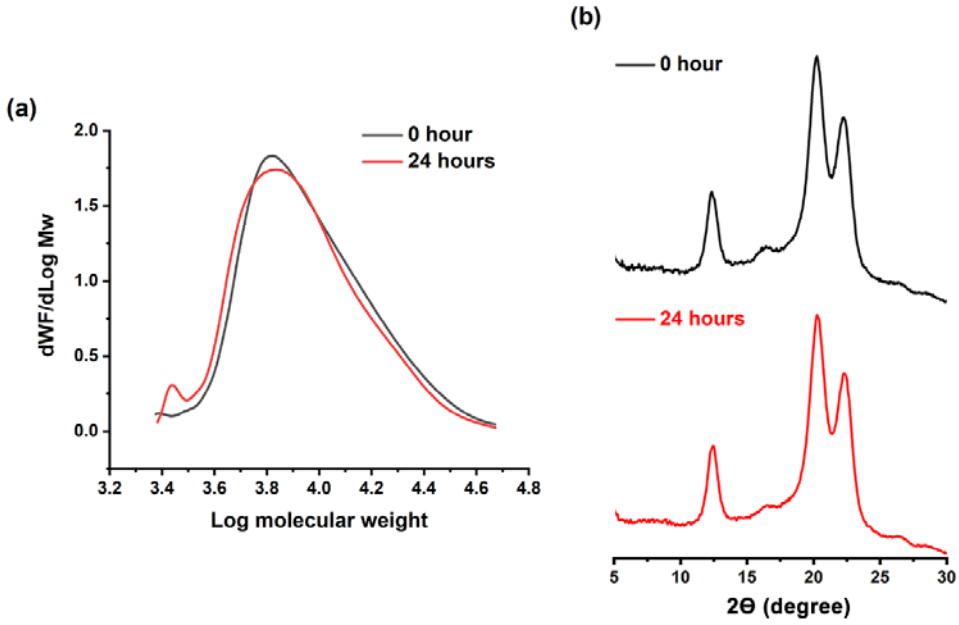

Figure VI.14. *(a) SEC molecular weight distributions and (b) X-ray diffraction profiles of the fraction A with regeneration time of 0 hour and 24 hours.*

Table VI.7. *The weight-averaged DP, number-averaged DP and polydispersity index and yield of the fraction A with the regeneration time of 0 hour and 24 hours.*

	DP_w	DP_n	Đ	Yield (%)
0 hour	20.4	15.2	1.34	55
24 hours	19.0	14.2	1.34	59

X-ray diffraction profiles of these two fractions are shown in Figure VI.14b. Interestingly, in the diffraction pattern of the fraction A with regeneration time of 0 hour, the small diffraction peak at 16.4˚, corresponding to cellulose IV_{II} allomorph as discussed above, are sharper than that with the regeneration time of 24 hours. The reason behind this phenomenon is unknown.

VI.5. Substitution of phosphoric acid by sulfuric acid

As described in the introduction of this chapter, in this section, sulfuric acid is

considered as a substitute for phosphoric acid due to sustainability reason.

VI.5.1. Fraction A from sulfuric acid hydrolysis

Experiments.

0.5 g of MCC was dissolved in 5 g of 63 wt% sulfuric acid (Chapter II.2.2) at room temperature. The cellulose solution was put at 40 ˚C. After 1, 2, 3 and 4.5 hours of hydrolysis, 1 g cellulose solution was taken and mixed with 1 g water, and kept at 23 ˚C for 24 hours, then directly washed by water until pH reached neutral.

1 g of MCC was dissolved in 10 g of 63 wt% sulfuric acid (Chapter II.2.2). The cellulose solution was put at 15 ˚C. After 2, 5, 8, 21, 26 and 30 hours of hydrolysis, 1 g cellulose solution was mixed with 1 g water, kept at 23 ˚C for 24 hours and then neutralized according to the Chapter II.2.3.2.

Results and discussion.

As shown in Figure VI.15a, the yield of the obtained fraction A from hydrolysis at 40 ˚C drops to near 0 % only after 3 hours of hydrolysis. The hydrolysis in sulfuric acid is much harsher at 40 ˚C than that in phosphoric acid.

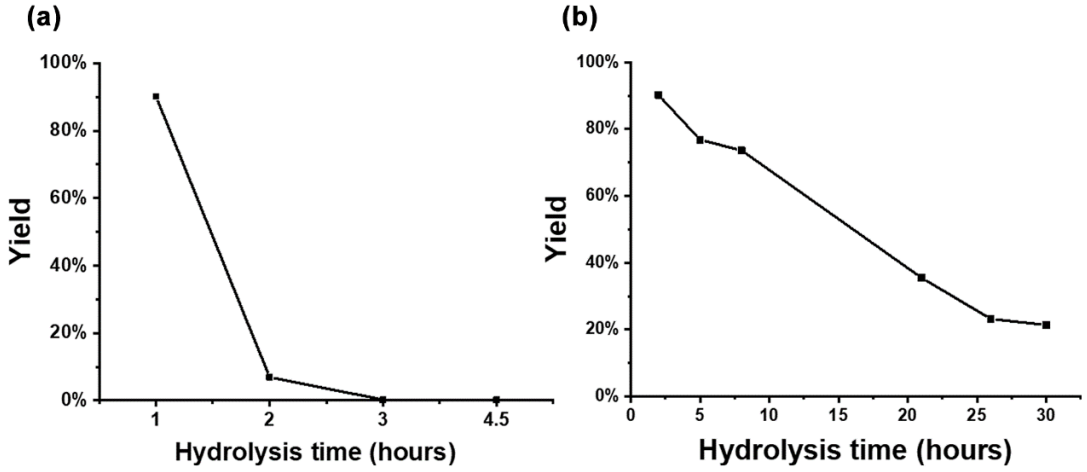

Figure VI.15. *Yields of the fraction A hydrolyzed by sulfuric acid at (a) 40 ˚C and (b) 15 ˚C with different hydrolysis time.*

To better control the hydrolysis and the yield of the fraction A, the hydrolysis temperature for sulfuric acid was changed to 15 ˚C. The yields of the obtained fraction A as function of hydrolysis time are shown in Figure VI.15b. When hydrolysis time is less than 8 hours, the yields of the obtained fraction A are above 70 %. As hydrolysis time increases beyond 20 hours, the yields of the fraction A decrease below 40 %.

Figure VI.16 showed the X-ray diffraction profiles of the fraction A hydrolyzed in sulfuric acid at 40 ˚C and 15 ˚C. For hydrolysis at 40 ˚C, the sample obtained after 1 hour of hydrolysis shows broad diffraction peaks. Diffraction features of cellulose II and cellulose IV_{II} are both visible. As the hydrolysis time increased to 2 hours, the peaks of cellulose II become sharper while the features of cellulose IV_{II} become less obvious. The same trend is observed for the hydrolysis at 15 ˚C. The sample obtained after 5 hours of hydrolysis shows broad diffraction peaks with cellulose II and cellulose IV_{II} features. With increasing hydrolysis time, the characteristic peaks of cellulose II become more obvious while the 16.4˚ peak is weakened. However, at the hydrolysis time of 30 hours, the characteristic peak of cellulose IV_{II} at 16.4˚ becomes

stronger again, against the general trend.

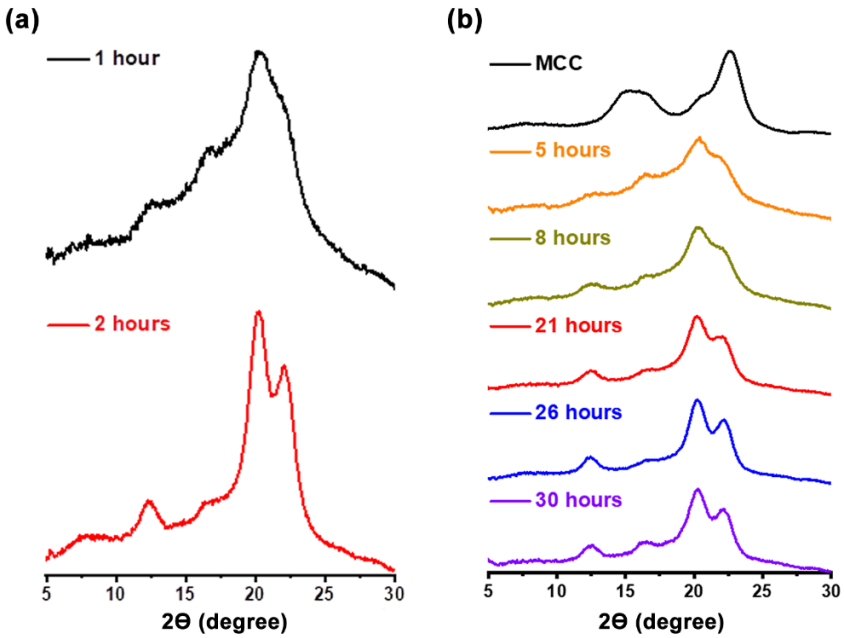

Figure VI.16. *X-ray diffraction profiles of the fraction A hydrolyzed by sulfuric acid at (a) 40 ˚C and (b) 15 ˚C with different hydrolysis time.*

From the ATR-FTIR spectra in Figure VI.17, the characteristic peak of sulfate group at 814 cm^{-1} is initially absent in the spectrum of MCC and increases as the hydrolysis time increases. This indicates a part of hydroxyl groups are sulfated during the hydrolysis. Due to the sulfate groups, the cellulose oligomers are carbonized after drying at 110 ˚C. However, when dried in a vacuum oven at 60 ˚C, carbanilation efficiency decreased, likely due to the presence of residual water. The resulting carbanilated fraction A were not soluble in THF or DMF. Thus, the molecular weight of these fractions A could not be obtained using SEC in this thesis. Solvent exchange with pyridine would be necessary for successful carbanilation of the cellulose oligomers from sulfuric acid hydrolysis.

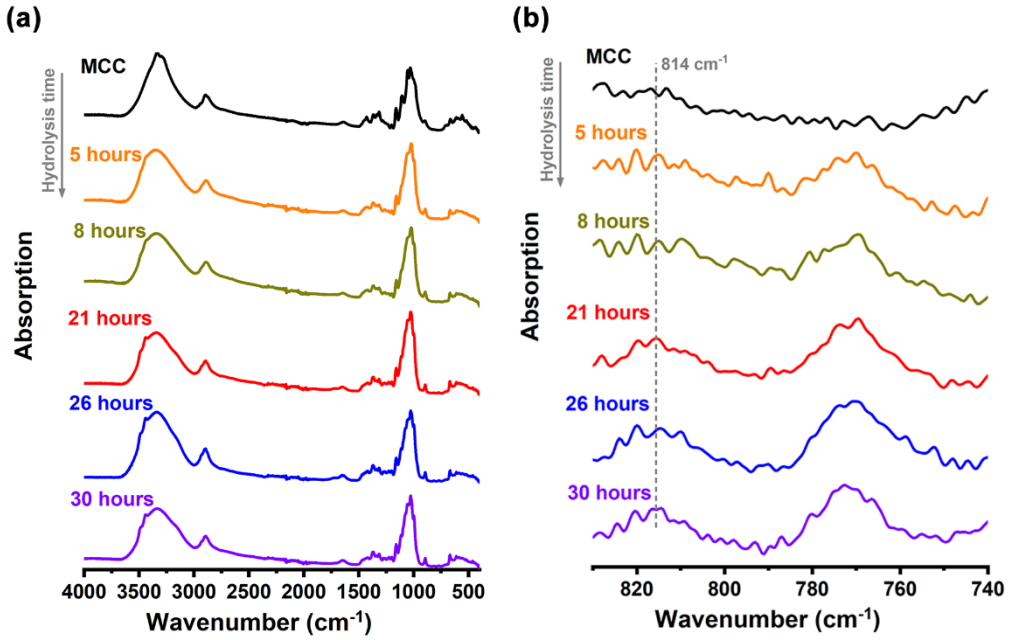

Figure VI.17. *(a) ATR-FTIR of the fraction A hydrolyzed by sulfuric acid at 15 ˚C with different hydrolysis time and (b) the zoom-in area from 830 cm^{-1} to 740 cm^{-1}.*

VI.5.2. Fraction B from sulfuric acid hydrolysis

Experiments.

5 g of MCC were dissolved in 50 g of 62 wt% sulfuric acid according to the Chapter II.2.2. After hydrolysis at 23 ˚C for 30 hours, the cellulose solution was mixed with 55 g water and stored at 4 ˚C for 24 hours. The supernatant of the mixture was filtered with filter water and mixed with 3 times its volume of isopropanol, then stored at 4 ˚C for 24 hours. The precipitates were washed with isopropanol to neutrality. Then the precipitate was suspended in water and then freeze-dried.

Results and discussion.

The obtained fraction B were fluffy like the phosphoric-acid hydrolyzed fraction B freeze dried from water suspension (42d-IP) in the section VI.3.2. The fraction B from sulfuric acid hydrolysis is named here as Fraction B-s, and 42d-IP was called as Fraction B-p in this section for comparison. Figure VI.18 compared the ATR-FTIR spectra of the Fractions B-p and B-s. The absorbance of sulfate group at 814 cm^{-1} is only visible in the spectrum of the Fraction B-s. The estimated sulfate content was about 1-2 %, and the estimation process was detailed in the Appendix 4.2.

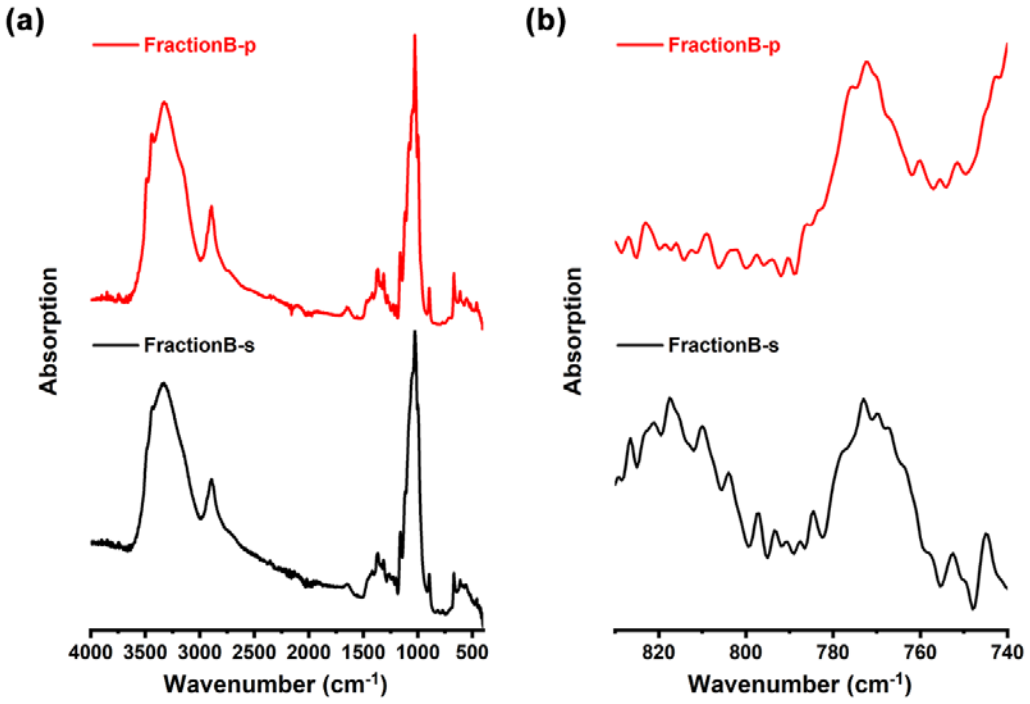

Figure VI.18. *(a) ATR-FTIR of the fraction B from phosphoric acid (Fraction B-p) and sulfuric acid (Fraction B-s) hydrolysis, and (b) the zoom-in area from 830 cm^{-1} to 740 cm^{-1}.*

The X-ray diffraction patterns (Figure VI.19) show that the major part of the both Fractions B-p and B-s is cellulose II. The diffraction peaks of the fraction B-p are sharper than that of Fraction B-s. The crystallite size is thus bigger in the fraction B-p than in the fraction B-s. Considering the comparable DP disbrutions described below,

this implies that the small number of sulfate groups on the cellulose molecules might interfere the crystallization in the fraction B-s. In addition, the peak at 16.4˚ is much weaker in the fraction B-s when compared to the Fraction B-p.

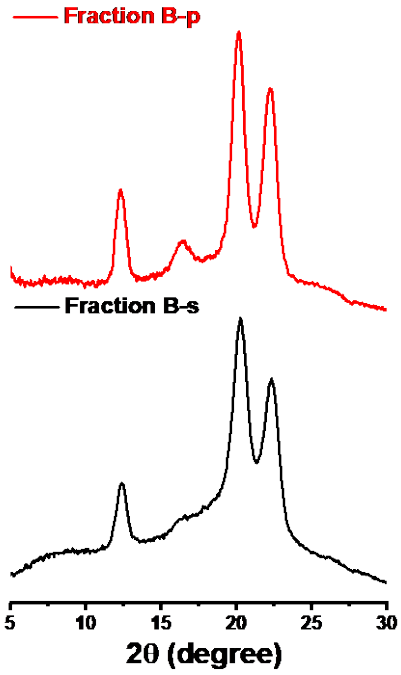

Figure VI.19. *X-ray diffraction profiles of the fraction B from phosphoric acid (Fraction B-p) and sulfuric acid (Fraction B-s) hydrolysis.*

Molecular weight distribution of the Fraction B-s was analyzed by the ^{1}H-NMR and MALDI-TOF MS techniques, and compared with Fraction B-p. In ^{1}H-NMR spectrum of Fraction B-s in deuterated DMSO most of the resonances that are assigned to -OH groups are absent (Appendix 4.3), and the reason is unknown. Thus, the FractionB-s and FractionB-p were dissolved in 2% NaOD/D_2O, and the ^{1}H-NMR spectra are shown in Figure VI.20. The chemical shifts around 5.29 ppm and 4.71 ppm are assigned to the α- and β-anomeric protons at the reducing ends, respectively. The peaks around 4.47 ppm are ascribed to the protons from H1 and H1'. Because the peaks of β-anomeric protons around 4.71 ppm are overlapped with the solvent peak at

4.80 ppm, the characteristic peaks of α-, β-anomeric protons and protons from H1 and H1' were deconvoluted to calculate the integrated intensity. The number-averaged DP was calculated as decribed in Chapter V.4. As shown in Table VI.8, the two fractions B have similar number-averaged DP values, 7.4 (B-p) and 7.5 (B-s).

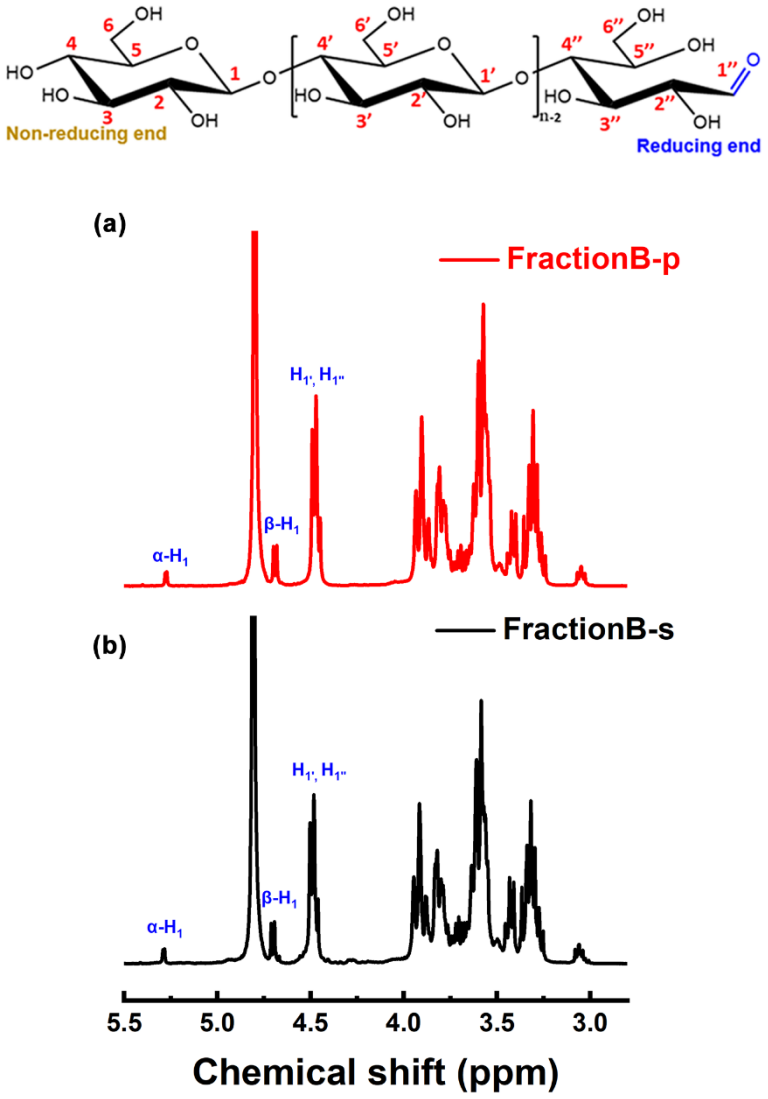

Figure VI.20. *^{1}H-NMR spectra of the Fraction B from (a) phosphoric acid and (b) sulfuric acid hydrolysis in 2 % NaOD/D_2O. Characteristic chemical shifts corresponding to specific bonds are annotated on the chemical structure of the cellulose molecule in the inset.*

Table VI.8. *The integrated area of the convoluted characteristic peaks assigned to a-, β-anomeric protons and protons from H1 and H1', and the calculated number-averaged DP of the fraction B from phosphoric acid (FractionB-p) and sulfuric acid (FractionB-s) hydrolysis.*

	Area(α-$H_{1''}$)	Area(β-$H_{1''}$)	Area (H_1, $H_{1'}$)	DP_n
Fraction B-p	1.29×10^4	3.52×10^4	3.08×10^5	7.4
Fraction B-s	1.22×10^4	2.64×10^4	2.51×10^5	7.5

The MALDI-TOF MS spectra of the Fraction B-p and the Fraction B-s as a function of mass-to-charge (m/z) ratio in the positive-ion mode are shown in Figure VI.21. The sum of integrated peak areas that belongs to the same DP are shown as histograms in Figure VI.22. The DP 6 fraction is dominant in the Fraction B-s, while the dominant DP in the Fraction B-p is 5. The intensities span over the DP range of 4-14 for the Fraction B-p and 4-15 for Fraction B-s. For DP larger than 6, the proportions are larger in the Fraction B-s than Fraction B-p. But the proportions of cellotetraose and cellopentaose in Fraction B-s are smaller than that in Fraction B-p.

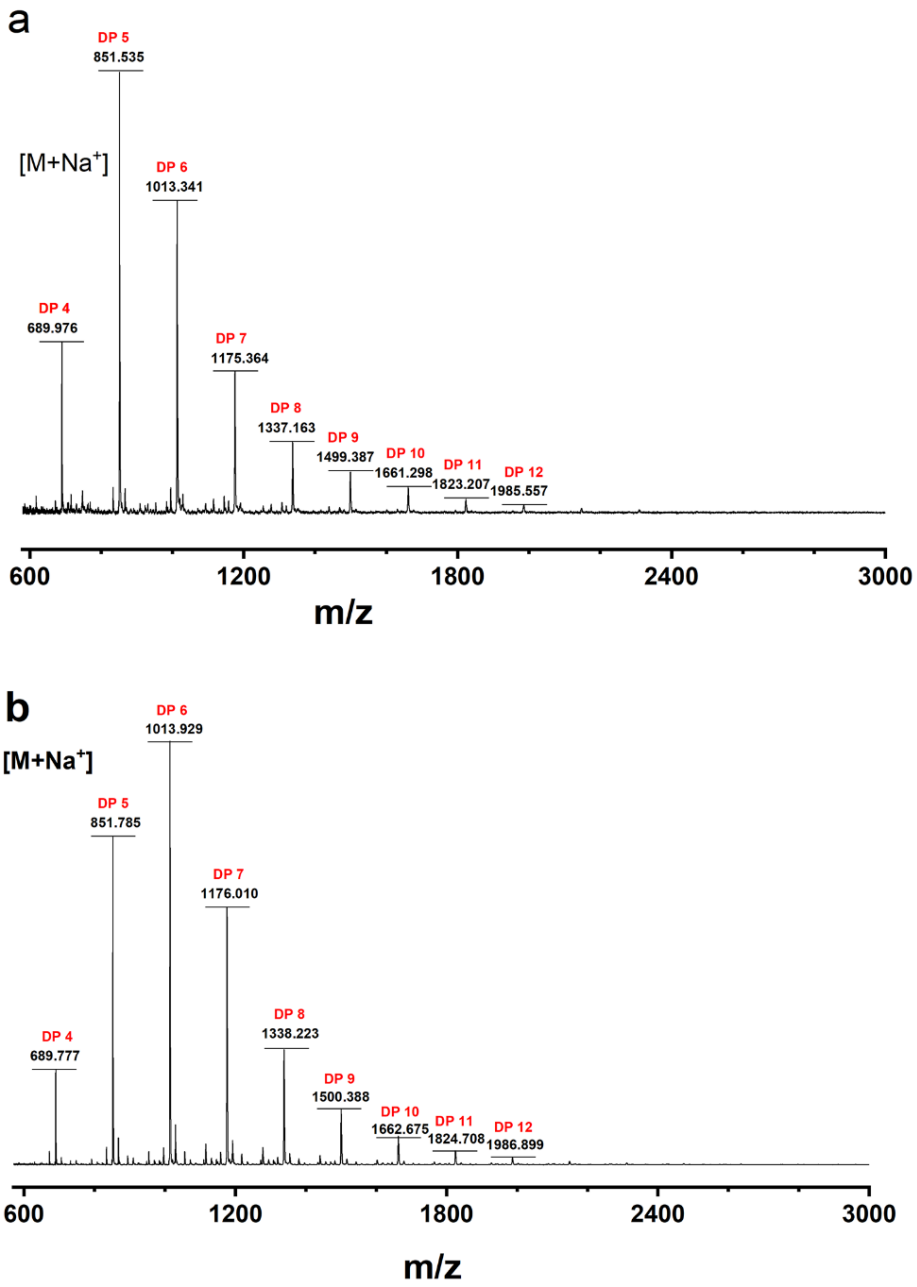

Figure VI.21. *MALDI-TOF MS spectra of the fraction B from (a) phosphoric acid and (b) sulfuric acid hydrolysis as a function of mass-to-charge (m/z) ratio in the positive-ion mode.*

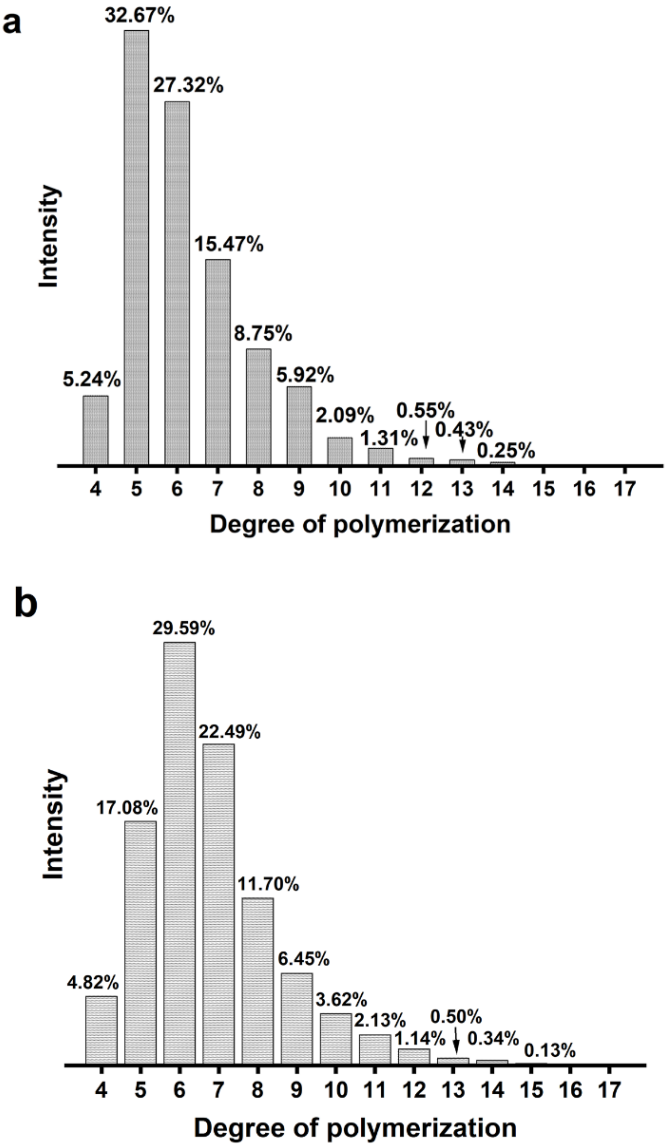

Figure VI.22. *The summation of integrated intensity from the same DP as a function of different DP in the fraction B from (a) phosphoric acid and (b) sulfuric acid hydrolysis.*

Table VI.9. *The weight-averaged DP, number-averaged DP, polydispersity index and yield of the fraction B from sulfuric and phosphoric hydrolysis.*

	^{1}H NMR	MALDI-TOF MS			Yield (%)
	DP_n	DP_n	DP_w	Đ	
Fraction B-p	7.4	6.3	6.7	1.07	19
Fraction B-s	7.5	6.8	7.3	1.07	26

Table VI.9 summarizes the average DPs, Đ and the yield of the fraction B-s and B-p. Both of the results from ^{1}H NMR and MALDI-TOF MS show that the Fraction B-s has slightly larger average DPs than the Fraction B-p with almost the same Đ. The yield of Fraction B-s was about 7 % more than that of Fraction B-p.

VI.5.3. Fraction A regenerated in salt solutions

Experiments.

5 g of MCC were dissolved in 50 g of 62 wt% sulfuric acid according to the Chapter II.2.2. After hydrolysis at 40 ˚C for 50 mins, 1 g of cellulose solution was mixed with 1 g of water, or 3.8 M HCl (aq) solution, or 3.8 M LiCl (aq) solution, or 3.8 M NaCl (aq) solution, or 3.8 M KCl (aq) solution, or 1.9 M Na_2SO_4 solution. Every mixture was repeated for three times. After decantation 4 ˚C for 24 hours, the precipitates were washed by water/ethanol (1:1 in volume) solution until pH reached neutral. Then

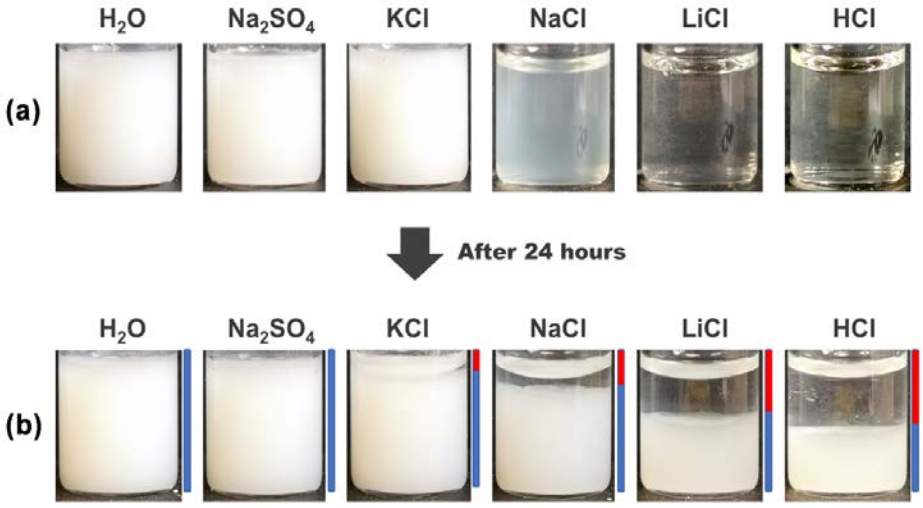

Figure VI.23. *The photograph of cellulose from sulfuric acid hydrolysis for 50 mins at 40 ^{o}C and regeneration in different solutions with the same molar concentration (half of the molar concentration for Na_2SO_4 solution), (a) the regeneration was in the beginning and (b) the regeneration was at room temperature for 24 hours, the blue bar was the height of precipitates and the red bar represented the height of supernatants.*

the precipitates were dried in a vacuum oven at 60 ˚C overnight.

Results and discussion.

Figure VI.23 shows the photos of regeneration mixtures with the regeneration time of 0 hour and 24 hours. The mixture with water, Na_2SO_4 and KCl are white, which means that plenty of regenerated cellulose oligomers were already precipitated just after adding the precipitants. The NaCl mixture are half-transparent, indicating there were less precipitates. The LiCl and HCl mixtures are almost transparent, implying that precipitation does not occur at that point. After stored at room temperature for 24 h, there appears precipitates in the mixtures with LiCl and HCl solutions. The heights of the precipitates, marked with the blue bars, are listed as Na_2SO_4 > KCl > NaCl > LiCl > HCl. The yields of precipitates from different regeneration reagents are presented in Figure VI.24. The yields are consistent with the heights of precipitates. The cations of KCl, NaCl, LiCl and HCl are all from the first column elements in the periodic table, and the ionization tendency is in a following order: H > Li > Na > K. It has a reverse correlation to the yield of the precipitates. The reason behind this interesting phenomenon is unclear.

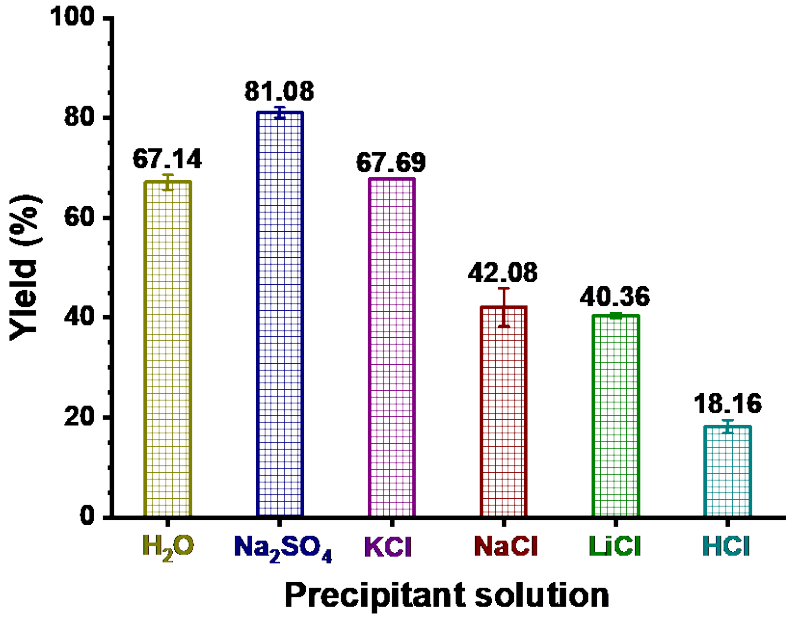

Figure VI.24. *The yields of the fraction A from sulfuric acid hydrolysis for 50 mins at 40 °C and regeneration in different solutions with the same molar concentration (half of the molar concentration for Na_2SO_4 solution).*

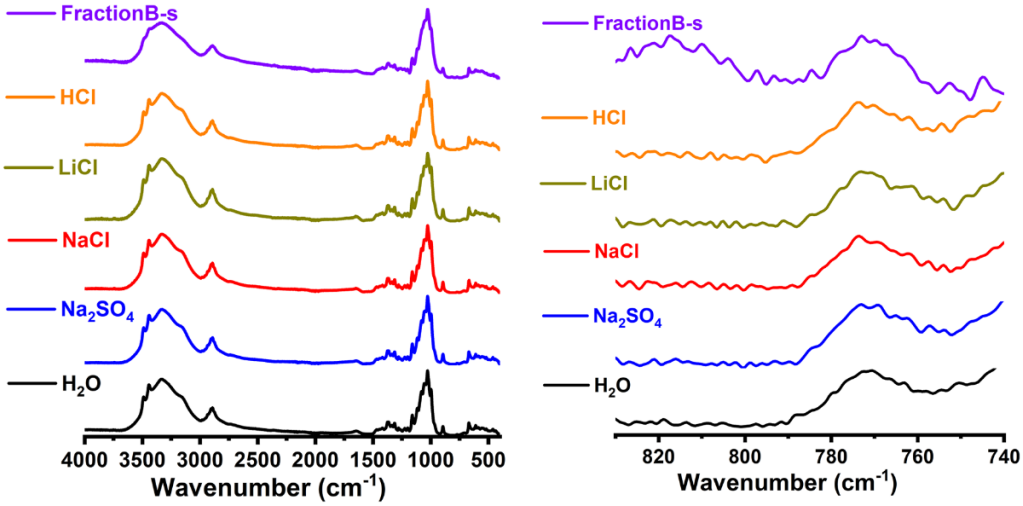

Figure VI.25. *ATR-FTIR of the fraction A from sulfuric acid hydrolysis for 50 mins at 40 °C and regeneration in different solutions with the same molar concentration (half of the molar concentration for Na_2SO_4 solution), and Fraction B from sulfuric acid hydrolysis was for comparison*

The ATR-FTIR spectra of the fraction A precipitated in salt solutions are shown in Figure VI.25. The Fraction B-s was used as the control sample to check the sulfate groups. It was shown that there was no sulfate group in all the fraction A from sulfuric acid hydrolysis at 40 ^{o}C for 50 mins. X-ray diffraction profiles of these fractions A are shown in Figure VI.26. They all have cellulose II allomorph. The small diffraction peak at 16.4˚ only appears in the diffraction pattern of fraction A from HCl solution, and the reason behind this observation is unknown.

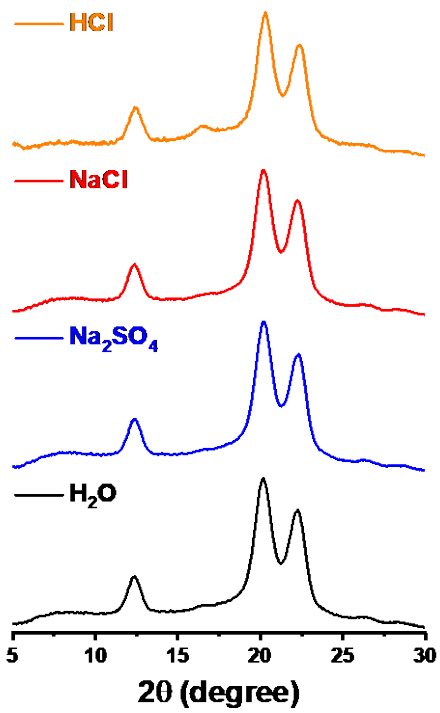

Figure VI.26. *X-ray diffraction profiles of the fraction A from sulfuric acid hydrolysis for 50 mins at 40 ^{o}C and regeneration in different solutions with the same molar concentration (half of the molar concentration for Na_2SO_4 solution).*

VI.6. Conclusions

In this chapter, various conditions, such as hydrolysis conditions, regeneration

conditions, and substitution of phosphoric acid by sulfuric acid, were conducted to investigate the effect on the DP and DP distributions of the fraction A and B. For phosphoric acid hydrolysis, increasing hydrolysis temperature from 23 ˚C to 40 ˚C could greatly shorten the preparation time. With hydrolysis temperature at 23 ˚C, it took 42 days to obtain fraction A in yield of 44 % with a DP_w of 17.3 and a Đ value of 1.21. However, it only required 3 days for the hydrolysis at 40 ˚C to obtain a similar fraction with a yield of 45 % with a DP_w of 17.5 and a Đ value of 1.29.

Compared with the weight ratio of cellulose solution vs. water in 1:10, the fraction A from the weight ratio in 1:1 had a 7 % higher yield with 13 % smaller average DP and slightly narrower DP distribution. For the fraction A hydrolyzed at 40 ˚C for 1 day, then regenerated at 23 ˚C, there was little change in the yield, average DP and DP distribution between the acidic and neutralized regeneration environments. However, at regeneration temperature of 70 ˚C, acidic environment in a smaller yield of 53 % presented a DP_w of 14.5 with a Đ value of 1.26, while neutralized regeneration environment in yield of 51 % exhibited a DP_w of 26.0 with a Đ value of 1.69. Regeneration time of 24 hours showed higher yield than regeneration time of 0 hour, but with little change in average DP and DP distribution. Sulfuric acid hydrolysis was more fiercely than phosphoric acid at the same temperature. However, the tricarbanilation of the fraction A hydrolyzed by sulfuric acid was unsuccessful. The challenges of dissolution in common solvents after low-efficient carbanilation made it difficult for DP analysis. The fraction B hydrolyzed by sulfuric acid could be dissolved in DMSO, and it showed almost the same average DP with the fraction B hydrolyzed by phosphoric acid with slightly higher yield and narrower DP distribution. The yields of fraction A that regenerated from different salt solutions

were listed as Na_2SO_4 > KCl > NaCl > LiCl > HCl.

Chapter VII

Chapter VII. Mechanism on producing monodisperse cellulose oligomers

VII.1. Introduction

In Chapter VI, the two fractions with DP of 15 and 7 were prepared according to the work of Isogai and Usuda [211]. The hydrolysis and regeneration conditions were varied to optimize the yields and investigate their effects on the obtained cellulose oligomers. Interestingly, the regeneration at high temperature in acidic environment was found to yield more monodisperse cellulose oligomers when compared with regeneration at room temperature or neutral environment (Figure VI.13). Even though it has been 30 years since the work of Isogai and Usuda was published, very few mechanistic studies have shed light on the question of how the regenerated cellulose get monodisperse. In this chapter, the hypotheses on the origin of the monodispersity are proposed, and the experiments and simulations for verifying the hypotheses are conducted and discussed.

VII.2. Hypothesis-1 about how regenerated cellulose become monodisperse

The hypothesis-1, proposed by Dr. Yoshiharu Nishiyama, is illustrated in Figure VII.2. Cellulose chains with different DP exit in the solution state, generated during the hydrolysis. After regeneration in water, the cellulose chains with different lengths are crystallized and precipitated in the acidic mixture. The cellulose chains that are not involved in the crystalline core are more accessible by the acid molecules in the mixture. They are hydrolyzed during the regeneration time. Assuming that the crystallite size along the chain direction has relatively small distribution, this crystallization-hydrolysis process should give the monodisperse molecular chains of

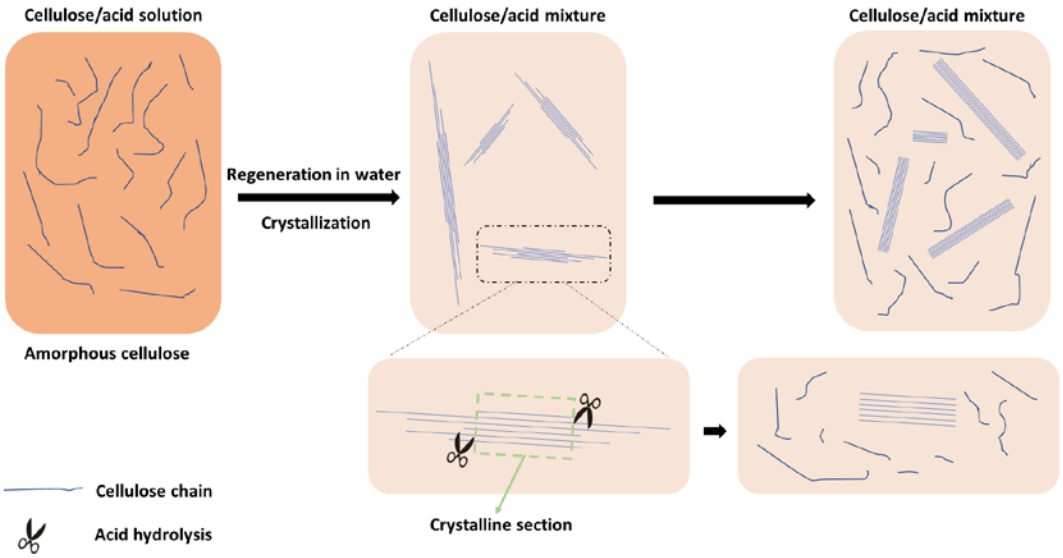

Figure VII.1. *Schematic representation of the hypothesis-1 about how the regenerated cellulose become monodisperse.*

which length is dominated by the crystallite size.

The hypothesis-1 has two crucial points. One is that cellulose chains should crystallize into cellulose II before the washing process. The acidic environment with sufficient regeneration time is another key point. The regeneration time was 24 hours for most of the cellulose oligomers that were studied in Chapter VI. According to the hypothesis-1, there should be some difference in polydispersity between samples regenerated in acidic and neutralized environments. However, the fraction A regenerated from acidic and neutral environment at 23 ˚C exhibited nearly the same molecular weight distribution as shown in Fig. IV.13. On the other hand, at 70 ˚C, acidic environment results in producing more monodisperse cellulose oligomers. Thus, the hypothesis-1 can explain the case at 70 ˚C, though it is not the case for the room temperature situation. Since most of the cellulose oligomers in this thesis were regenerated at 23 ˚C, the hypothesis-1 is not the reason behind the formation of

monodisperse cellulose oligomers in most cases.

VII.3. Crystalization of cellulose during regeneration

During the investigation of the hypothesis-1, I was interested in the question of when cellulose crystallizes after the cellulose solution is mixed with precipitant like water.

VII.3.1. Synchrotron X-ray scattering

Experiments.

An X-ray scattering experiment (Chapter II.4.2.2) in ESRF was designed to study the structure of the regenerated cellulose before the washing process. About 9 wt% cellulose/62 wt% H_2SO_4 solution and 3 wt% cellulose/83 wt% H_3PO_4 solution were hydrolyzed at 15 ^oC and 30 ^oC for 96 h, respectively. The simultaneous S/WAXS measurements were conducted with the two cellulose solutions. Then water was added from the top to the tubes containing the cellulose solutions at room temperature and let it diffuse without mixing. After decantation at 22 ^oC for 24 hours, the WAXS and SAXS tests were aimed at 10 mm away from the original interface between water and cellulose solution in the downward direction.

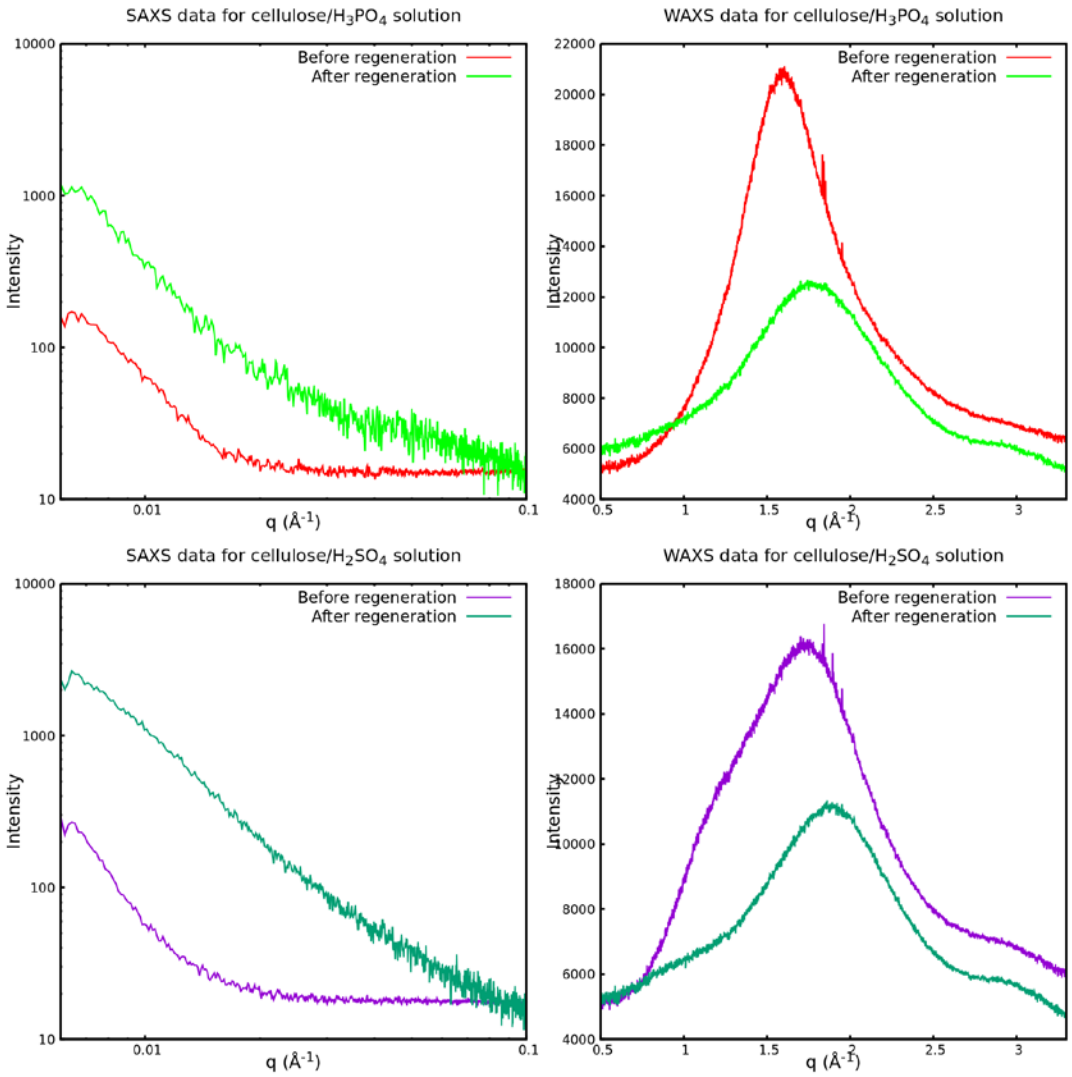

Figure VII.2. *SAXS and WAXS data of cellulose/H_3PO_4 and cellulose/H_2SO_4 solution before and after regenerated in water.*

Results and discussion.

As shown in Figure VII.2, the scattering intensities increases in the SAXS profile after the regeneration, which indicates the formation of aggregates. The WAXS data show mainly the scattering peaks of phosphoric acid and sulfuric acid with large signal-to-noise ratio. The peaks shifted to the right side after regeneration with lower intensity because of the dilution of the acid solutions with water. The WAXS data

after regeneration both show no diffraction peak of cellulose. There are two possible reasons: (1) the regenerated cellulose before washing is amorphous and (2) the regenerated cellulose in the beam is too little, and the diffraction peaks of cellulose II from the small amount of regenerated cellulose are buried in the noise. Indeed, in an experiment conducted with other acid concentration, small diffraction peaks of cellulose II are occasionally observed. Thus, the latter scenario might be the case in this situation.

VII.3.2. Lab source X-ray diffraction

I then used lab source X-ray diffraction to characterize the crystallinity of regenerated cellulose paste during the regeneration and washing process. For quantitative analysis, the X-ray beam intensity and the volume of cellulose in the paste needed to be normalized before the comparison of crystallinity between samples.

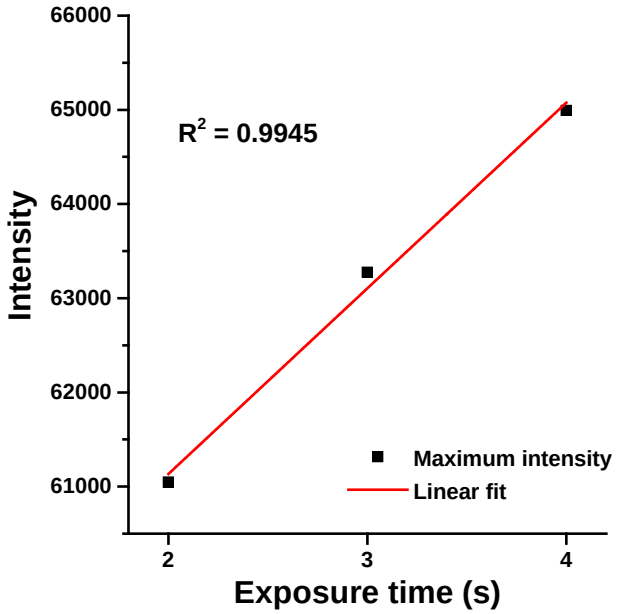

Figure VII.3. *The maximum XRD intensity of the supernatant of before-washing without beam stop as a function of exposure time.*

Experiments.

200 g of 3 wt% MCC/83 wt% H_3PO_4 cellulose solution was hydrolyzed at 40 ˚C for 72 hours. The cellulose solution was divided into 3 parts, and named as before-wash, 1st-wash, 2nd-wash, respectively. The cellulose solutions were mixed with equal volume of water and regenerated at 4 ˚C for 24 h. After centrifugation, the supernatant of before-wash was subjected to an XRD test (30 kV, 10 A) without beam stop for 2 s, 3 s and 4 s. The maximum intensity of the direct beam was read by ImageJ, and the plot was shown in Figure VII.3. It showed that the intensity was linear correlated with the exposure time, and the exposure time of 2 s was selected for the experiments to normalize the X-ray beam intensity.

The precipitates of the 1st-wash and 2nd-wash were washed with the same volume of water by centrifugation for once and twice, respectively. The pH of the final supernatant of before-wash, 1st-wash and 2nd-wash was measured by a pH meter, and the precipitates were concentrated by blotting with filter paper to obtain thick pastes. For each sample, some of the thick paste was filled in the round hole (diameter 2 mm, thickness 1 mm) of a plastic plate, and subjected to XRD measurements (30 kV, 20 A) with beam stop for 1 h. The XRD profiles of before-wash, 1st-wash and 2nd-wash were normalized with a cellulose content factor F_c and a beam intensity factor F_b as defined below. To normalize the signal intensities with respect to cellulose content on the X-ray path, the rest of the thick paste was put in an Eppendorf tube and centrifuged, then the height of the paste was marked. The paste was washed with acetone for three times by centrifugation, and the weight was measured as m_1 after drying. The Eppendorf tubes were emptied and filled with water until reaching the marker, and the weight of the water was measured as m_2. To normalize the X-ray beam intensity,

every sample was subjected to an XRD measurement (30 kV, 10 A) without beam stop for 2 s after the XRD measurement, and the intensity of the direct beam, I_n, was read by ImageJ. The beam intensity factor F_b, the cellulose content V_c and the cellulose content factor F_c were calculated as follows,

$$F_b = \frac{I_0(\text{before-wash})}{I_0}$$

$$V_c(\%) = \frac{m_1/\rho(cellulose)}{m_2/\rho(H_2O)} \times 100\%$$

$$F_c = \frac{V_c(\text{before-wash})}{V_c}$$

where ρ(cellulose) is 1.5 g/cm^3, and ρ(H_2O) is 1.0 g/cm^3.

About 100 g of 9 wt% MCC/62 wt% H_2SO_4 solution was hydrolyzed at 23 ˚C for 30 hours. The cellulose solution was divided into 2 parts, and named as before-wash-1 and 8th-wash-1. The cellulose solutions were mixed with equal volume of water and regenerated at 4 ˚C for 24 h. The precipitates of the 8th-wash-1 were washed for 8 times until pH reached neutral. The precipitates of before-wash-1 and 8th-wash-1 were concentrated by blotting with filter paper to obtain thick pastes, and then subjected to the XRD analysis as described above. ^{13}C CP/MAS NMR experiments were conducted on the pastes of the before-wash-1 and 8th-wash-1 with the MAS rate at 6 kHz.

Results and discussion.

The normalized XRD profiles are shown in Figure VII.4a. The pastes of before-wash, 1st-wash and 2nd-wash all show the diffraction peaks at 2θ = 12˚, 20˚ and 22˚, which are indexed as 1 $\bar{1}$ 0, 1 1 0, and 0 2 0 of cellulose II, respectively. The profiles of the before-wash, 1st-wash and 2nd-wash exhibit a broad scattering around 10˚. The X-rays used in this section is lab-source X-ray with Ni filter and without

monochromation, and thus contain characteristic X-rays (CuKα, 8 keV) and continuous X-rays (up to 30 keV in the operation condition). The continuous X-rays are normally not an issue as they are of lower intensity compared to the CuKα X-rays. When a sample contains highly attenuating atoms like sulfur and phosphorus,

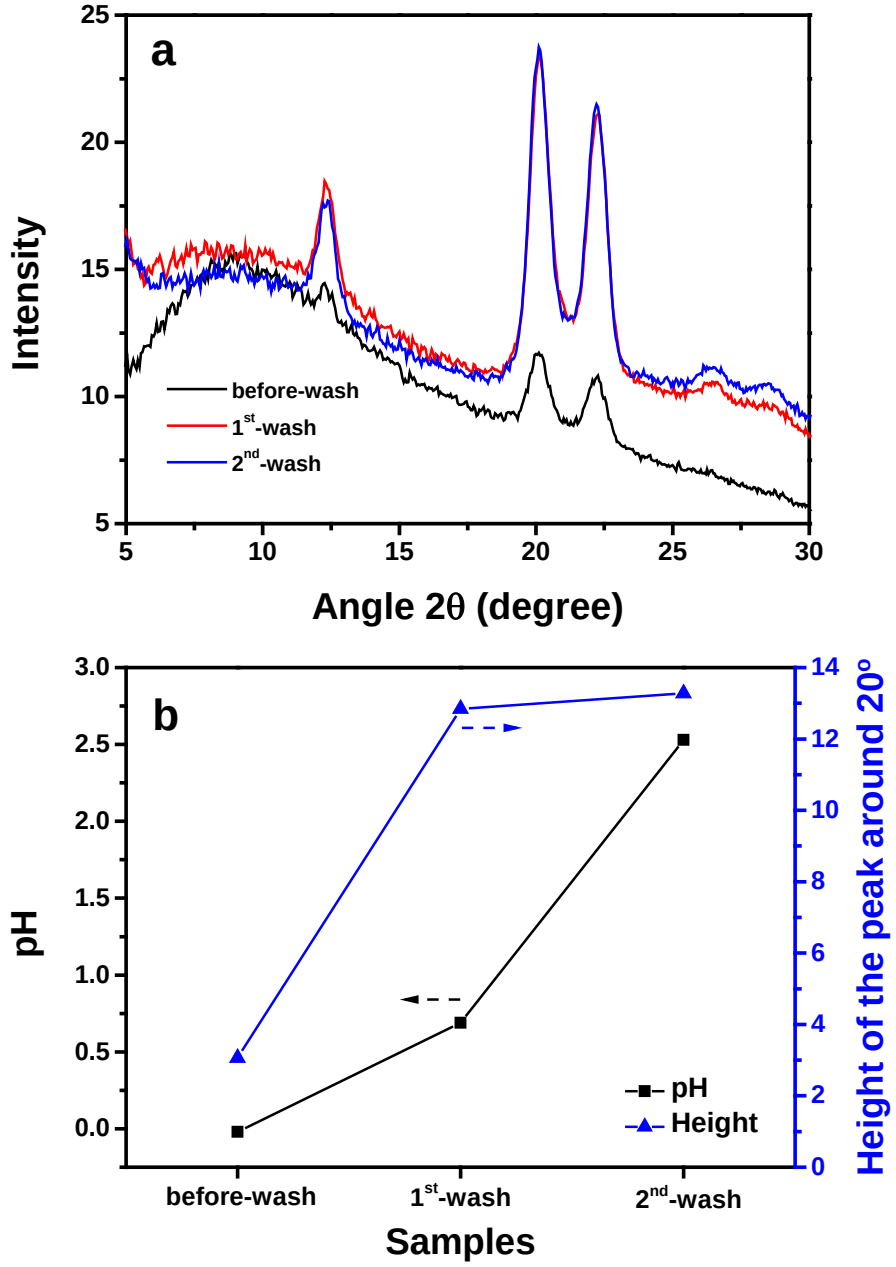

Figure VII.4. *(a) The normalized XRD profiles of before-wash,1st-wash and 2nd-wash with the exposure time of 1 h; (b) The pH of the supernatant of before-wash,1st-wash and 2nd-wash and the height of the peak around 20° in the normalized XRD profiles.*

however, the low energy CuKα beam is more absorbed than the high energy continuous X-rays, and the contribution from continuous X-ray increases in scattering intensities relative to that of CuKα X-rays. This effect results in increase in the lower angle scattering intensity seen at around 10˚ in the before-wash sample. The height of this broad peak decreased with the increase of washing times. Because the concentrations of H^+ and PO_4^{3-} in the paste decrease with increasing the washing times, which is verified by the pH of the supernatants of the cellulose pastes in Figure VII.4b. The apparent low intensities of cellulose II peaks before washing process are likely an artefact due to the strong attenuation from phosphorus.

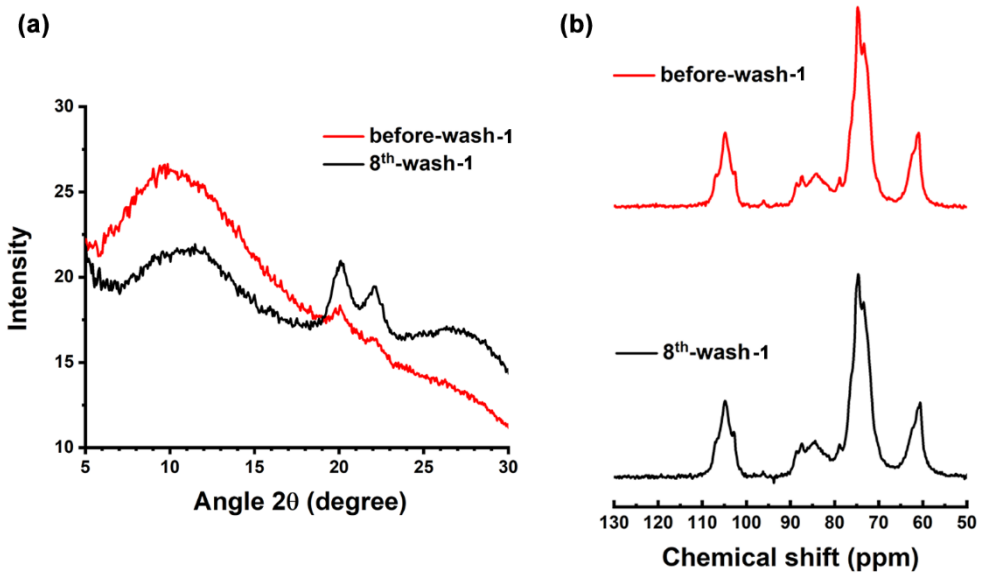

Figure VII.5. *(a) The normalized XRD profiles of the H_2SO_4-hydrolyzed cellulose pastes of before-wash-1 and 8^{th}-wash-1 with the exposure time of 1 h; (b) ^{13}C CP/MAS NMR of the H_2SO_4-hydrolyzed cellulose pastes of before-wash-1 and 8^{th}-wash-1 with the MAS spin at 6 kHz.*

Figure VII.5a shows the normalized XRD profiles of the H_2SO_4-hydrolyzed cellulose pastes before and after the whole washing process. Both the samples exhibit the broad peak around 10˚. It indicates there are still sulfur in the pastes. Because the pH of the supernatant of 8^{th}-wash-1 reaches neutral. The sulfur in the 8^{th}-wash-1

should be mainly from the sulfate group on cellulose. When compared with H_3PO_4-hydrolyzed cellulose pastes in Figure VII.4, the heights of the diffraction peak at 20˚ have much smaller difference between the H_2SO_4-hydrolyzed cellulose pastes before and after the washing process. The little difference in crystallinity between before-wash-1 and 8^{th}-wash-1 is also verified by the ^{13}C CP/MAS NMR spectra (Figure VII.5b), which shows nearly the same proportions of the crystalline C4 and amorphous C4 in the range of 81-91 ppm.

Based on these preliminary observations, the crystallization of cellulose happens at least partially in the solution/precipitant mixture before the first washing process. This agrees with the observation of the regeneration in the acidic condition at high temperature. Further experiments would be needed if additional crystallization occurs during the washing process.

VII.4. Hypothesis-2 about how regenerated cellulose become monodisperse

The question of why regenerated cellulose become monodisperse at room temperature remains unclear, and in this section another hypothesis, the hypothesis-2 is proposed. Here, as illustrated in Figure VII.6, cellulose in a cellulose/acid solution after hydrolysis is assumed to have a Gaussian DP distribution with a large polydispersity. The addition of precipitant divides this distribution into two, below and above the cutoff value as shown in the scheme. On the left side of the cutoff, it represents the short- ıin cellulose oligomers that are soluble and remain in the solution. On the rigıı side of the cutoff, it represents the regenerated cellulose oligomers that precipitate in the regeneration mixture. Due to the existence of the cutoff, the polydispersity of the regenerated cellulose becomes smaller.

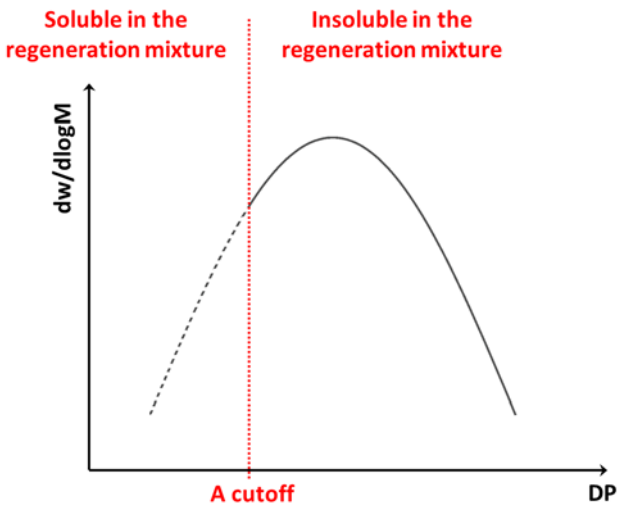

Figure VII.6. *Schematic representation of the hypothesis-2 about how the regenerated cellulose become monodisperse.*

An in-house program originally written by Dr. Yoshiharu Nishiyama, was used to simulate the hydrolysis and regeneration process. It assumes there is a cellulose chain with an initial DP of one hundred million, and this cellulose chain is cut randomly different times. After cutting, only the cellulose chains with DP larger than 8 are used for the calculation to simulate the molecular weight distribution of the fraction A. The number-average DP (DP_n), weight-average DP (DP_w), Đ and yield are calculated as follows,

$$DP_n = \frac{\sum c_i}{\sum c_i / DP_i}$$

$$DP_w = \frac{\sum DP_i \cdot c_i}{\sum c_i}$$

$$Đ = \frac{DP_w}{DP_n}$$

$$Yield\ (\%) = \frac{N_8}{N_c + 1} \times 100\%$$

where c_i represents the populations of chains with the DP of i, N_8 is the number of chains with the DP larger than 8, and N_c is the number of scissions applied in a simulation. My contribution to the design of the program is the proposition of adding the cut-off at DP 8. The calculation results were shown in Table VII.1. With

Table VII.1. The simulation results of hydrolysis and regeneration based on the hypothesis-2.

Cut times	DP_n	DP_w	Đ	Yield (%)
1000	99858	189296	2.00	100
9000	10004	20014	2.00	100
90000	1009	2000	2.00	100
900000	109	201	1.85	100
9000000	19	24	1.29	79
10000000	14	15	1.14	49

increasing number of scissions, the average DP and the yield both decreased. When the cut times was ten million, the DP_n, Đ and yield were 13.5, 1.14 and 49 %, respectively. In the paper of Isogai et al. [1], the DP_n, Đ and yield of the cellulose oligomers that regenerated from water were 15, 1.15 and 40 %, respectively. Although simulated values are in an apparent agreement with the experimental results, there are several major problems to be addressed. First, the validity of random scission model is uncertain. This can be checked by monitoring the population of

glucose in organic solvent fraction. Secondly, the initial molecular distribution is not monodispersing unlike in the simulation. Finally, the cutoff at DP 8 might not be right. DP 8 is considered as a solubility limit of cellulose in water, but the fraction B, organic solvent soluble fraction contains certain amounts of oligomers with a DP larger than 8. From the MALDI-MS results in the Chapter V and Chapter VI, low DPs like DP 4-7 exist in both the fraction A and B. Thus, the solubility-based fractionation only gives a soft cutoff unlike the simulated hard cutoff.

VII.5. Conclusions

In this chapter, I studied how the regenerated cellulose becomes monodisperse in the paper of Isogai and Usuda [211]. The hypothesis-1 could explain the reason why cellulose get monodisperse when regenerated at 70 ˚C in an acidic environment, but it is not the answer to the regeneration at room temperature. The simulation results based on the random chain scission (hypothesis-2) were close to the average DPs, Đ value and yield of fraction A in the literature from Isogai and Usuda [211]. Thus, I tentatively consider that this model explains the DP distribution of cellulose oligomers regenerated in water, although several assumptions in the simulation might not be correct and need to be further investigated. In addition, X-ray scattering and diffraction experiments were used to explore when cellulose crystallize during regeneration.

Chapter VIII

Chapter VIII. Conclusions and perspectives

VIII.1. General conclusions

This project aimed at preparing cellulose oligomers with controlled average molecular weight and molecular weight distribution by acid hydrolysis. The goal of the study was to understand the molecular mechanisms in the swelling, dissolution, hydrolysis and regeneration processes, in the meantime, to well characterize the obtained cellulose oligomers.

Firstly, we followed the swelling behaviors of cellulose in sulfuric acid at -20 ˚C using X-ray diffraction and found a cellulose-acid crystallosolvate. This crystalline complex had an orthorhombic unit cell with dimensions of a = 18.24 Å, b = 25.98 Å, c = 25.05 Å. This unit cell was composed of 4 cellulose chains, 48 sulfuric acid molecules and 144 water molecules. The fiber repeat of 25 Å suggested the rare occurrence of five-fold helical conformation of cellulose molecules. Sulfuric acid molecules were organized in a similar manner to that in the sulfuric acid tetrahydrate crystal. The complexation appeared only with the acid concentration above 62 wt%. This concentration dependence implied that the lack of water molecules in the system drove the complexation to form a stable hydration state of sulfuric acid. The observed complexation behaviors bring some knowledge on the low temperature swelling and dissolution of cellulose in sulfuric acid and give the first example of cellulose-acid crystallosolvate.

To well characterize the molecular weight of cellulose oligomers, the derivatization methods of cellulose were compared and optimized, then different characterization methods were evaluated. Carbanilated cellulose oligomers presented more distinct

light scattering signals than the nitrated cellulose oligomers due to their larger molecular size and dn/dc value. For determining the DS values of carbanilated cellulose, liquid state ^{1}H NMR by using NH/H_1 method suffered less influence from the side products than the aromatic H/H_1 method and elemental analysis. Solid-state ^{13}C SP/MAS NMR and FT-IR spectroscopies were effective in estimating DS values of carbanilated cellulose in solid-state. The carbanilation in DMF resulted in tricarbanilated cellulose with the usage of argon gas and fresh phenylisocyanate. As for characterization methods in DP determination, liquid state ^{1}H NMR, solid-state ^{13}C CP/MAS NMR and MALDI-TOF MS spectroscopy are more suitable than SEC for cellulose oligomers with low molar mass and soluble in DMSO at room temperature. While for cellulose oligomers with relatively high molecular weight and insoluble in DMSO at room temperature, SEC is preferred compared to the other spectroscopic methods. The evaluation of analytical methods in the DS and DP measurements clarifies the applicable conditions and serves a basis for more efficient and accurate analysis.

Finally, different conditions, such as hydrolysis temperature, regeneration temperature, pH, time and reagents, and substitution of phosphoric acid by sulfuric acid, were varied to investigate the molecular weight and molecular weight distribution of cellulose oligomers. Cellulose oligomers with different weight-average DP and Đ values, as summarized in Figure VIII.1.1, were obtained by varying these conditions. More detailed preparation conditions were in Chapter VI. Two hypotheses for revealing how regenerated cellulose become monodisperse were elucidated in Chapter VII. The hypothesis-1 could explain how cellulose oligomers became monodisperse when regenerated in an acidic environment at 70 ˚C, but it is not the

answer to the regeneration at room temperature. The simulation results based on the random chain scission (hypothesis-2) were close to the average DPs, Đ value and

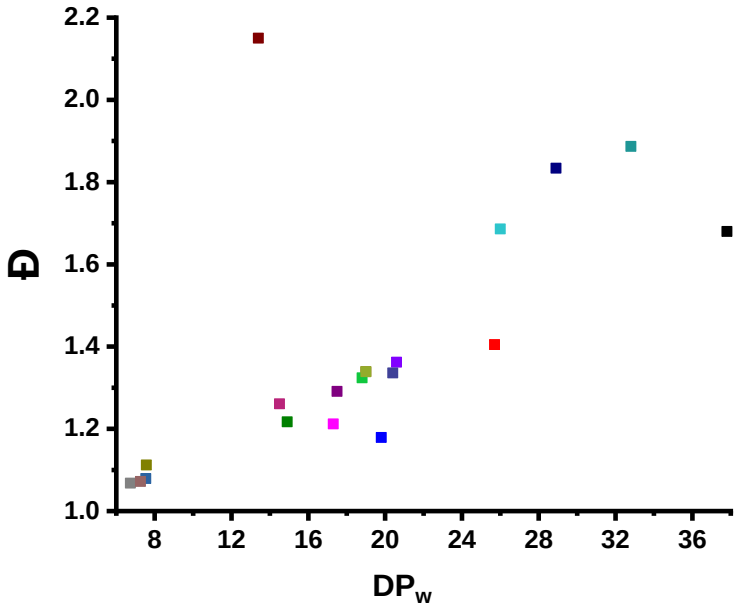

Figure VIII.1.1. *DP_w and Đ values of the cellulose oligomers that were obtained in this thesis.*

yield of the cellulose fractions (DP_w = 15) in the paper from Isogai and Usuda [1]. The hypothesis-2 offers a plausible explanation to the question of how regenerated cellulose became monodisperse, and sheds light on further control of molecular weight and molecular weight distribution.

VIII.2. Perspectives

The swelling behavior of cellulose in phosphoric acid at low temperature will be investigated to check if cellulose and phosphoric acid will form a novel crystalline complex. By comparing the two cellulose/acid systems, we may have better understanding of the interactions between cellulose and acid molecules, and then

optimize the processing of acid-based cellulose solvent systems.

The activation energies of carbanilation of cellulose in different solvents can be studied. Efforts also can be put on increasing the yield of carbanilated cellulose oligomers during purification.

Establishing an accurate relationship between the molecular weight of tricarbanilated cellulose and the retention time of SEC can make the molecular weight analysis of cellulose oligomers simpler. In this case, accurate molecular weight of cellulose oligomers can be obtained by RI or UV signals, regardless of the molecular size of the tested cellulose oligomers.

The solid-state ^{13}C CP/MAS NMR method for DP determination needs to be repeated for more samples in order to establish an accurate M_0/M_s coefficient.

The difficulty in measuring the molecular weight of sulfated cellulose oligomers needs to be solved. Other conditions, for instance, cellulose content in acid solution, regeneration in more different reagents, can be varied to control the molecular weight and molecular weight distribution of cellulose oligomers. In addition, some results that are not logical in the thesis need to be repeated.

Preparation of cellulose oligomers by enzyme hydrolysis can be investigated.

Regeneration in salt solution needs further investigation, such as the conformation of regenerated cellulose in the mixtures, morphology of the regenerated cellulose, interactions between cellulose molecules and salt ions, molecular weight and molecular weight distributions.

The formation of cellulose IV_{II} in the regenerated cellulose (Chapter VI) is interesting. The relationship between the intensity of this diffraction peak and the

respective preparation conditions can be further investigated.

To achieve quantitative analysis of crystallinity, the question whether the crystallinity of the regenerated cellulose changes before and after washing process can be studied by an X-ray diffraction instrument with monochromator with high energy X-rays. Solid state ^{13}C CP/MAS will be conducted on the H_3PO_4-hydrolyzed regenerated cellulose before and after washing process.

For the in-house program based on the hypothesis-2, the cutoff will be estimated by comparing the DP distributions of the fraction A (SEC results) and the fraction B (MALDI MS results) with the simulation results of the fraction A and B, on the condition of other assumptions unchanged.

As mentioned in Chapter I.3, with the merits of abundant reducing ends and molecular directionality, monodisperse cellulose oligomers have great potential in making new types of functional nano-objects by crystallization and self-assembly processes. I have done some preliminary trials in crystallization of tricarbanilated cellulose. However, due to the low yield of tricarbanilated cellulose oligomers after

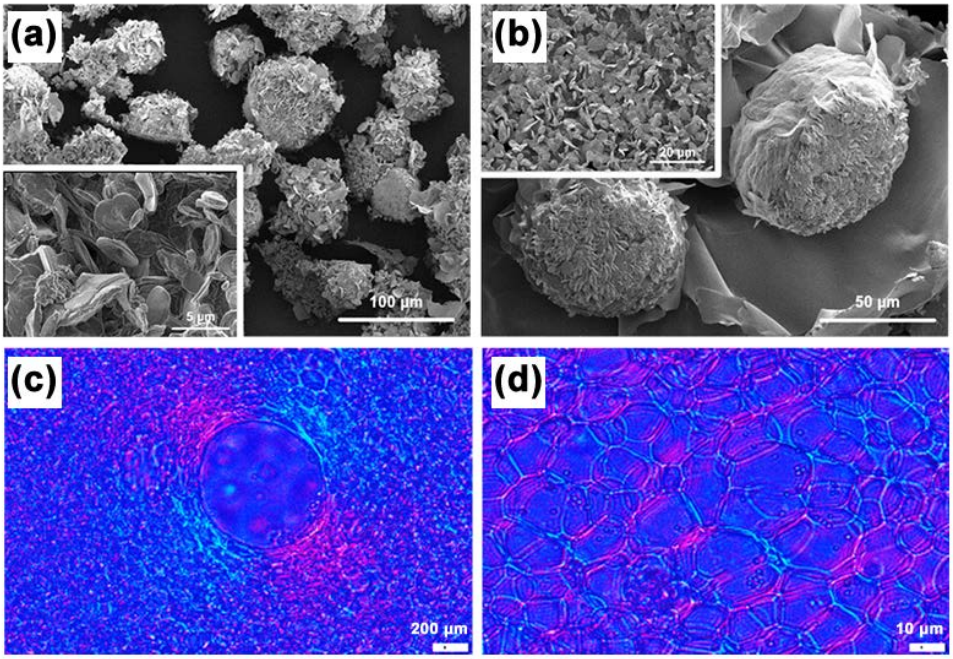

Figure VIII.2.1. *(a, b) Scanning electron microscopy images of tricarbanilated MCC air-dried from acetone. (c, d) Polarized microscopy images of tricarbanilated MCC obtained by cooling down 100 mg/mL DMSO solution from 90 ˚C to 23 ˚C, observed with a λ plate.*

purification, the main results are about tricarbanilated MCC.

From Figure VIII.2.1a and b, the tricarbanilated MCC that were air-dried from acetone solution shows various morphologies, for instance flower-like and plate-like. The polarized microscopy images of the tricarbanilated MCC obtained by cooling down 100 mg/mL DMSO solution from 90 ˚C to 23 ˚C show a fishing net shape. The red and blue colors indicate inversed orientations.

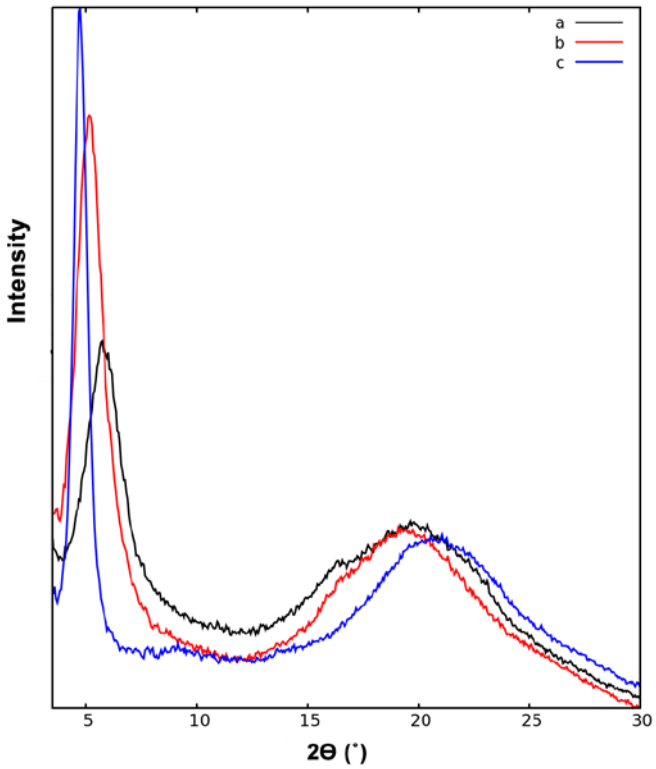

Figure VIII.2.2. *X-ray diffraction profiles of (a) tricarbanilated MCC (b) the sample a after annealing at 180 ˚C with vacuum for half an hour, and (c) the sample b after annealing at 180 ˚C with water vapor for half an hour.*

The X-ray diffraction profiles of tricarbanilated MCC before and after annealing are shown in Figure VIII.2.2. All of them present two main diffraction peaks but with different positions. Before annealing, the two diffraction peaks located at 5.6˚ and 19.8˚. After annealing at 180 ˚C with vacuum, the peak at 5.6˚ shifts to 5.1˚ with much higher intensity and almost the same peak width, while the peak at 19.8˚ shifts to 19.5˚ with almost the same intensity but slightly narrower peak width. After further annealing at 180 ˚C with water vapor, the peak at 5.1˚ shifts to 4.7˚ with even higher intensity and half of the width, and the peak at 19.8˚ shifts to 21˚ with almost the same height and peak width. The annealing with water vapor can increase the crystallinity and crystal size.

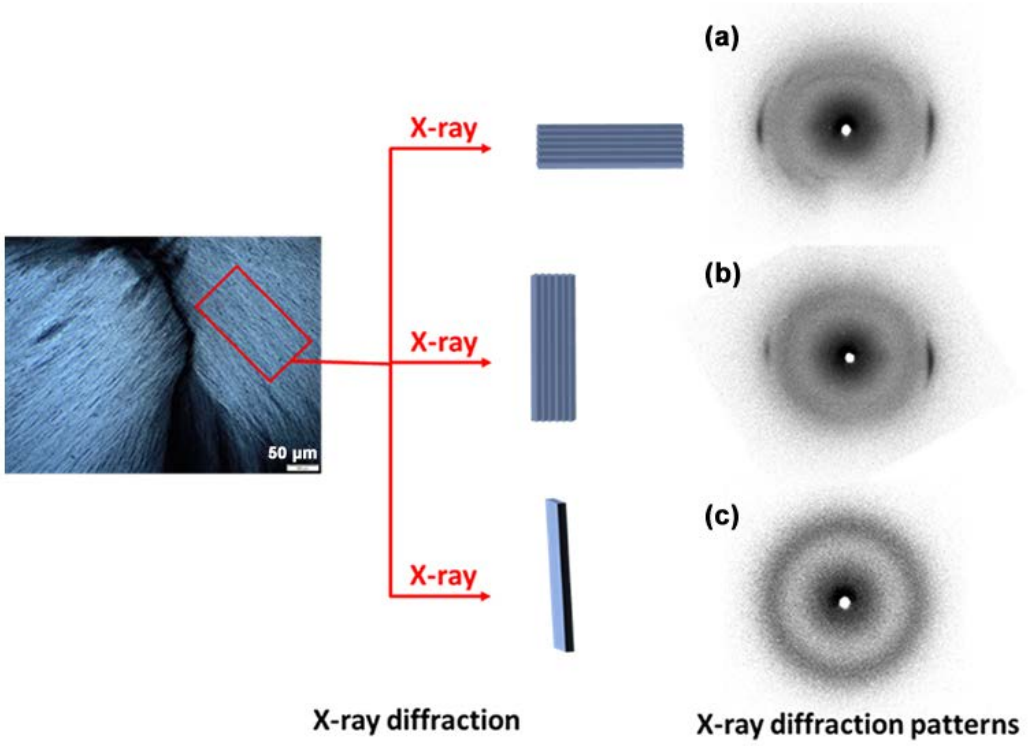

Figure VIII.2.3. *Polarized microscopy image and X-ray diffraction profiles of tricarbanilated MCC obtained by cooling down 10 mg/mL DMSO solution from 55 ˚C to 4 ˚C.*

By cooling down 10 mg/mL of tricarbanilated MCC in DMSO solution from 55 ˚C to 4 ˚C, there appears fibers with the same molecular orientations from the polarized microscopy images in Figure VIII.2.3 and Figure VIII.2.4. When these oriented fibers were placed in three different ways as illustrated in Figure VIII.2.3, different diffraction patterns can be seen. Figure VIII.2.3a and b both show strong arcs with 2Θ around 25˚, corresponding to a *d*-spacing of 3.5 Å, while Figure VIII.2.3c presents a powder diffraction pattern. In addition, from Figure VIII.2.4a and b, vacuum during X-ray diffraction measurement can make the resulting diffraction pattern lose most of the orientations but generate more sharp peaks. This phenomenon should be due to the elimination of DMSO and recrystallization of tricarbanilated MCC during the vacuum process.

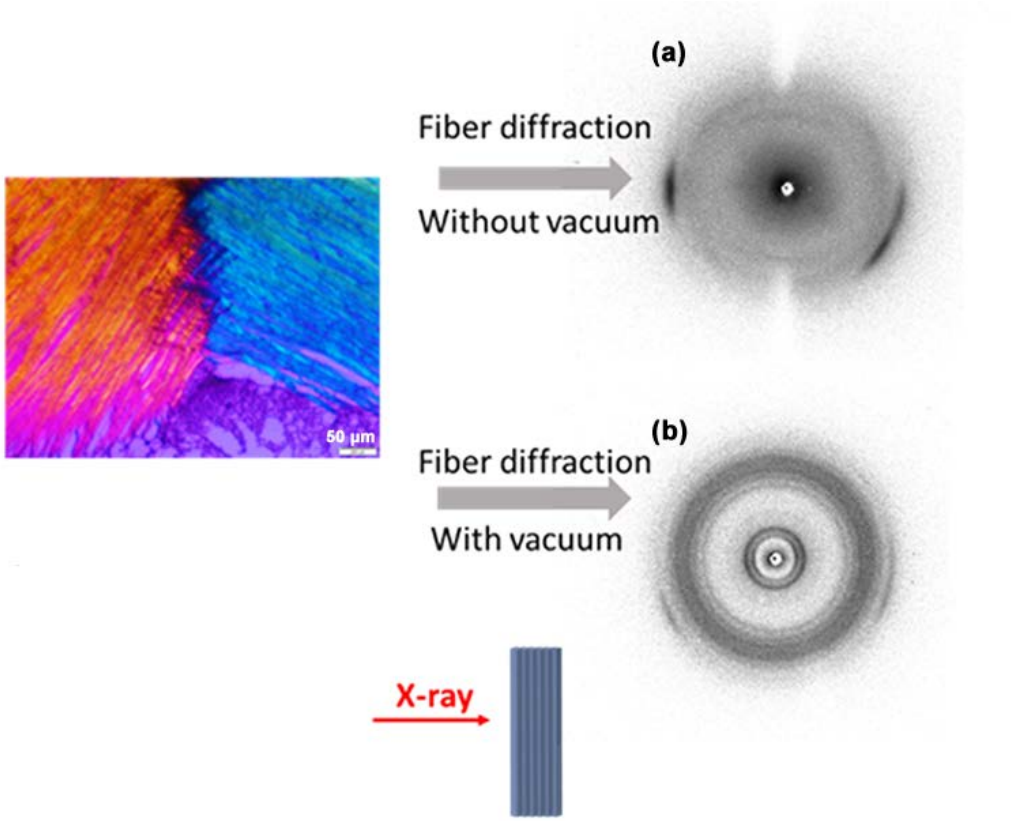

Figure VIII.2.4. *Polarized microscopy image observed with a λ plate and X-ray diffraction profiles of tricarbanilated MCC obtained by cooling down 10 mg/mL DMSO solution from 55 ˚C to 4 ˚C.*

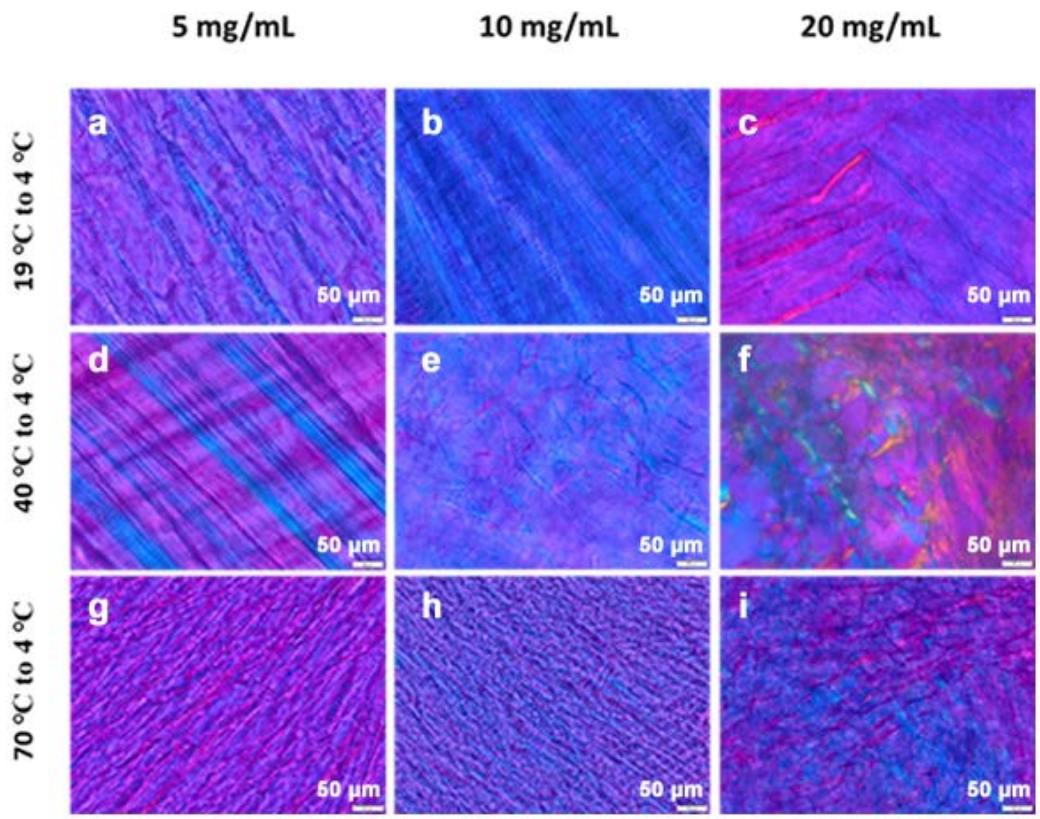

Figure VIII.2.5. *Polarized microscopy image observed with a λ plate of tricarbanilated MCC obtained by cooling down 5, 10 and 20 mg/mL DMSO solution from 70, 40 and 19 ˚C to 4 ˚C.*

Three concentrations, 5, 10 and 20 mg/mL, of tricarbanilated MCC in DMSO were cooled from three initial temperatures at 70, 40 and 19 ˚C to 4 ˚C. With high concentration of 20 mg/mL or initial temperature at 70 ˚C, the morphologies of the precipitates are less uniform. From 40 ˚C to 4 ˚C, the morphology of the precipitates is the most uniform for the concentration of 5 mg/mL. From 19 ˚C to 4 ˚C, concentration of 10 mg/mL results in the most uniform morphology and almost the same orientations for all fibers.

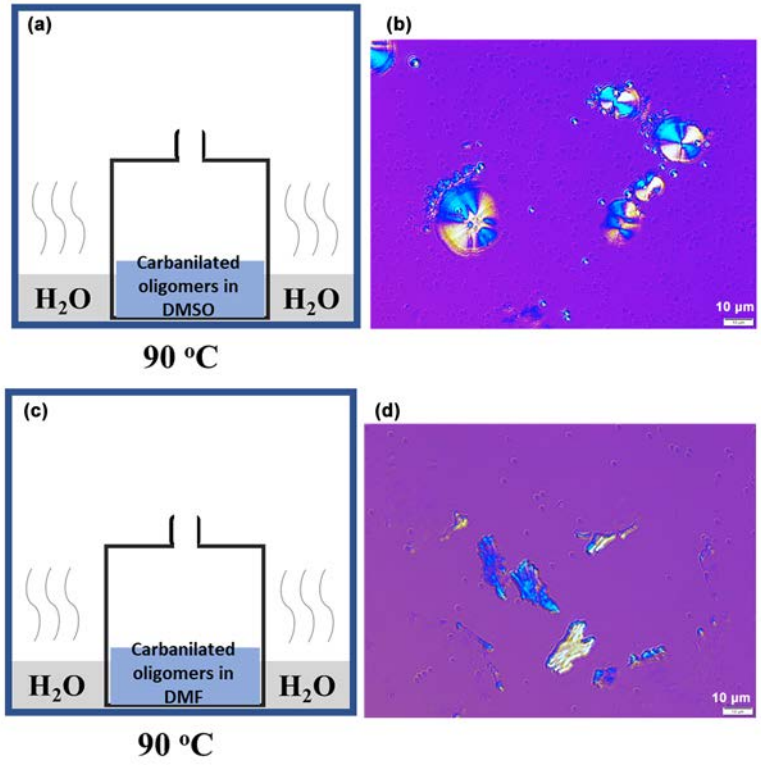

Figure VIII.2.6. *Illustration of crystallization process of tricarbanilated cellulose oligomers in (a) DMSO and (c) DMF. Polarized microscopy image observed with a λ plate of the (b) tricarbanilated cellulose oligomers/DMSO mixture and (d)) tricarbanilated cellulose oligomers/DMF mixture after crystallization process.*

Cellulose oligomers (the fraction A) hydrolyzed at room temperature for 56 days were tricarbanilated and purified by dialysis in acetone (Chapter II.3.3). 1 wt% tricarbanilated cellulose oligomers in DMSO was put in an open container, and this open container was in a sealed container with water insider. The sealed container was put in an oven at 90 ˚C for 2 days, as illustrated in Figure VIII.2.6a. The obtained precipitates were observed under a polarized microscopy with a λ plate and shown in Figure VIII.2.6b. The spherulites exhibit a strong birefringence. 1 wt% tricarbanilated cellulose oligomers in DMF were subjected to the same conditions but results in plate-like objects (Figure VIII.2.6d).

The precipitates from the tricarbanilated cellulose oligomers in DMF mixture (Figure VIII.2.6d) were observed by transmission electron microscopy and electron diffraction. Most of the precipitates do not have diffraction pattern. But we still found two objects (Figure VIII.2.7b and d) in the precipitates have nice diffraction patterns.

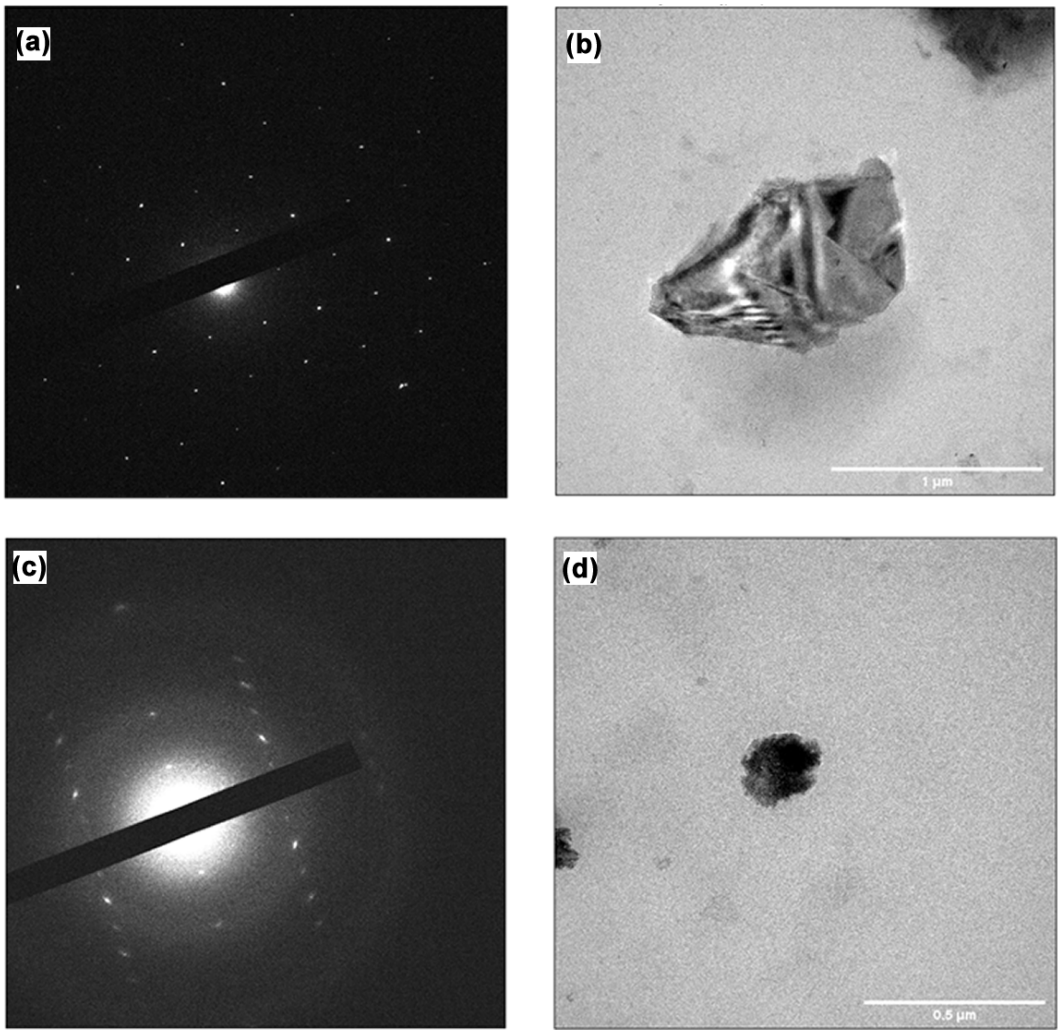

Figure VIII.2.7. *(a, c) Two-dimensional electron diffraction and (b, d) transmission electron microscopy images of the mixture from the crystallization process in Figure VIII.6d.*

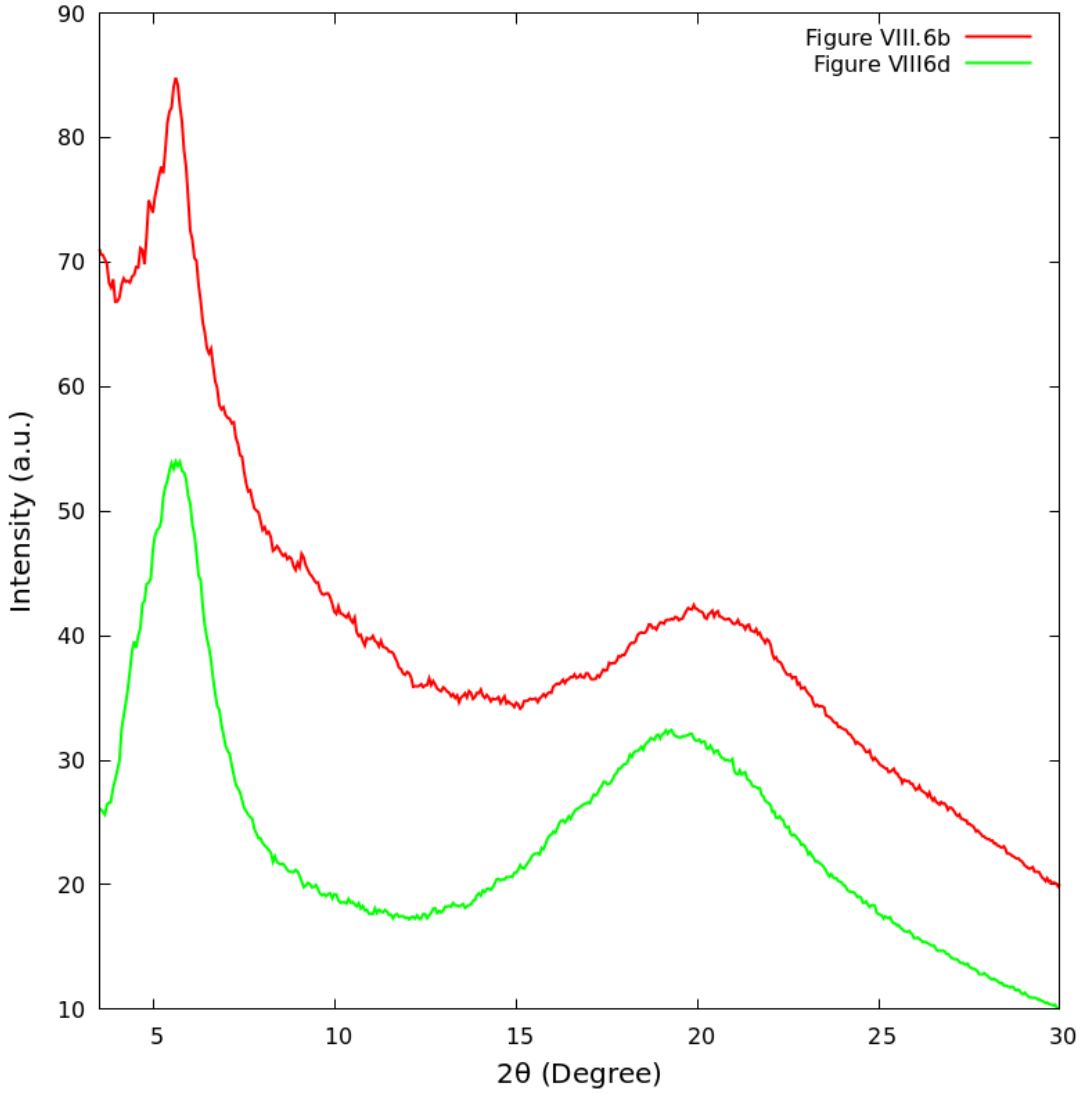

Figure VIII.2.8. *X-ray diffraction profiles of the precipitates from the crystallization process in Figure VIII.6b and Figure VIII.6d.*

However, X-ray diffraction patterns of the two precipitates in Figure VIII.2.8 only show two main peaks with similar positions. It indicates most of the precipitates might be amorphous.

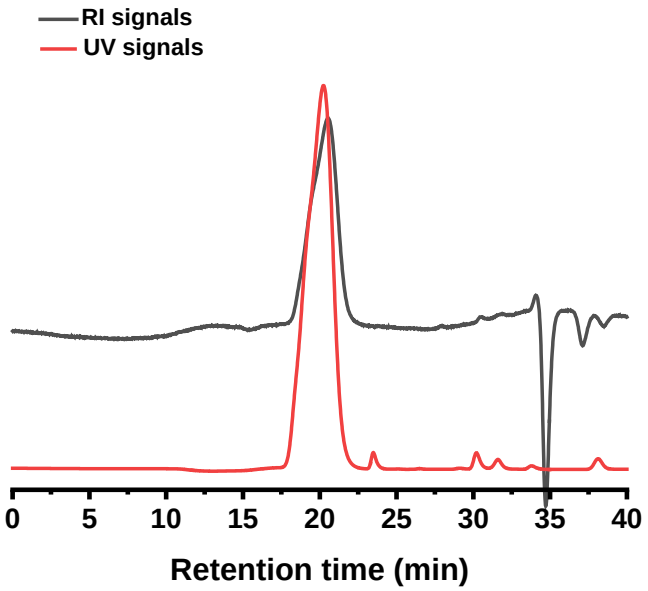

Figure VIII.2.9. *RI and UV signals of the carbanilated cellulose oligomers as function of the retention time by SEC-1.*

From Figure VIII.2.9, the UV signals of the carbanilated cellulose oligomers imply there are still some residual side products in the carbanilated cellulose oligomers. The crystals in Figure VIII.2.7 are more likely to come from the residual side products or contaminations.

The main application of cellulose carbanilates is for determining molecular weight of cellulose. Other chemical modifications of cellulose with broader application prospects will be tried on cellulose oligomers, and the crystallization can be studied to fabricate functional nano-objects with defined structures and morphologies.

Appendices

Appendix 1. Supporting information of Chapter II & IV

Appendix 1.1. Comparison between two phenylisocyanate

In the Chapter IV, I used two different bottles of phenylisocyanate: one (PI-old) was stored in a lab shelf at least for a year after it was open, and another was newly purchased and opened (PI-new). As shown in Table IV.5, they have different reactivities when used for carbanilation reaction of MCC, where the use of PI-new results in DS of 3.0 while that with PI-old only reaches to 2.7. I thus characterized the two PIs to understand the origin of this different.

PI-old and PI-new were dissolved in deuterated chloroform and subjected to ^{1}H and ^{13}C NMR measurements. Figure S1.1a shows ^{1}H NMR spectra of two PIs. It is clear that the peaks of PI-new are significantly broadened compared to those of PI-old. However, no clear difference is observed between two PIs in ^{13}C NMR spectra. Thus, the reason of different reactivities of these two PIs is unknown. It is possible to have chloroform-insoluble impurity that might cause the difference.

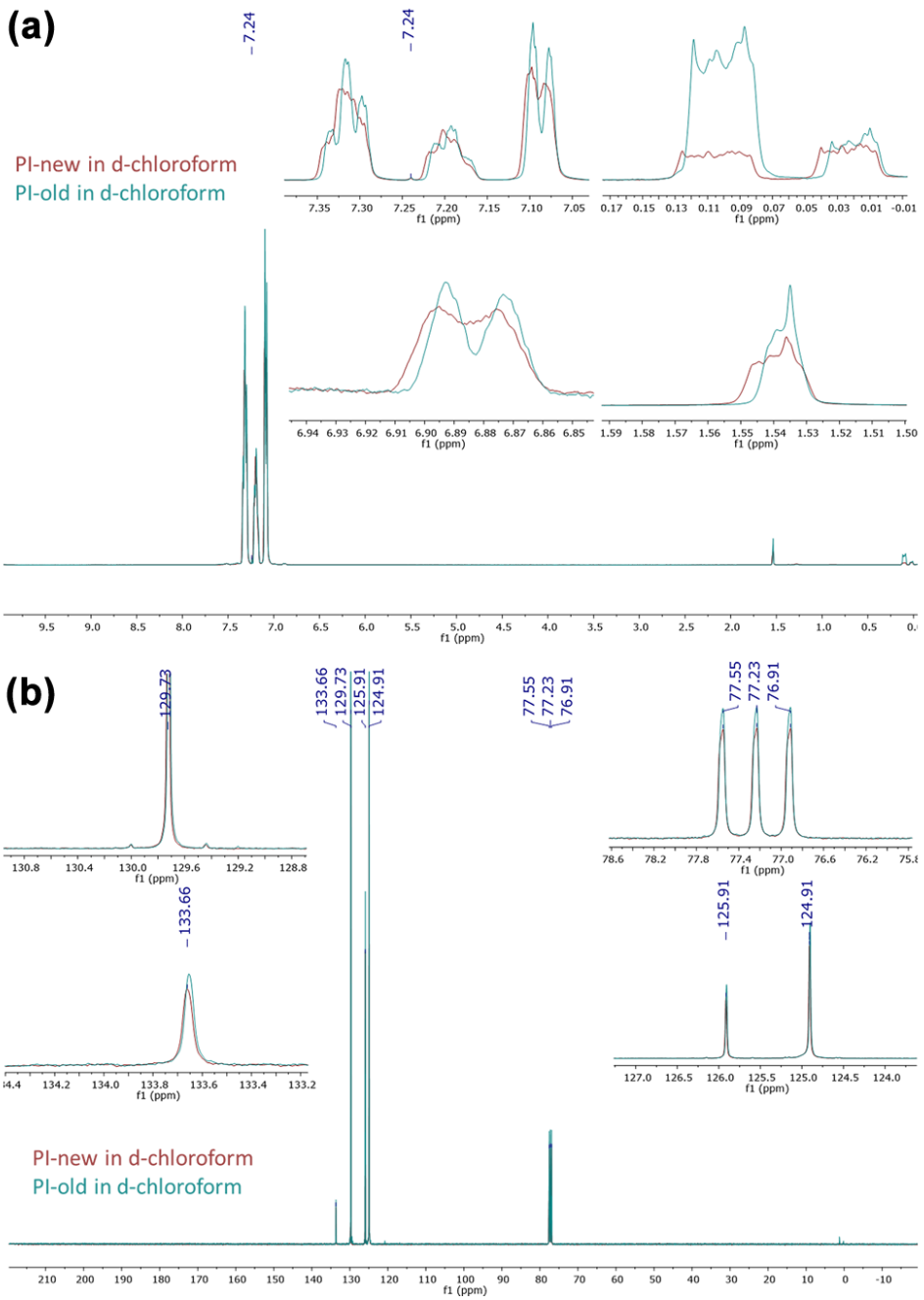

Figure S1.1. *Liquid state (a) ^{1}H NMR and (b) ^{13}C NMR of PI-new and PI-old in deuterated chloroform.*

Appendix 2. Supporting information of Chapter III

Appendix 2.1. Exhaustive search of unit cell parameters

We carried out an exhaustive search of the unit cell parameters by assuming an orthorhombic unit cell. The unit cell parameter, *a*, is allowed to vary from 4 Å to 20 Å, nad *b* is constrained to be larger than *a* and smaller than 20 Å, both with steps of 0.01 Å. The *d*-spacing, d_{hkl}, was calculated as follow,

$$d_{hkl} = \frac{h^2}{a^2} + \frac{k^2}{b^2} + \frac{l^2}{c^2}$$

where h ($0 \leq h \leq 10$), k ($0 \leq k \leq 10$) and l ($0 \leq k \leq 6$) were Miller indices.

The sum of the difference between d_{obs} and d_{hkl} of the 12 reflections (marked in Figure 1), φ_s, was calculated as:

$$\varphi_s = \sum_{i=1}^{12} \min_{\substack{0 \leq h \leq 10 \\ 0 \leq k \leq 10}} \frac{(d_{hkl}(i) - d_{obs}(i))^2}{\varepsilon(i)}$$

where $\varepsilon(i)$ was the error of the $d_{obs}(i)$.

Figure S1a shows a φ_s map as a function of unit cell parameters, a and b. Red spots indicated good agreement between d_{obs} and d_{hkl} for the 12 reflections. There were more red spots when the unit cell parameters *a* and *b*, hence the unit cell volume were large (Fig. S1). This is reasonable as a larger unit cell is more likely to get smaller φ_s due to its denser reciprocal lattice. To eliminate the influence of the unit cell volume, the φ_{Vu} was calculated as follows:

$$\varphi_{Vu} = \varphi_s \times V_u \times V_u$$

It was found the tendency of φ_{Vu} with increasing volume was nearly flat, so the volume effect was considered roughly cancelled. The smallest φ_{Vu} corresponded to the unit cell parameters a = 9.12 Å, b = 12.99 Å, c = 25.08 Å.

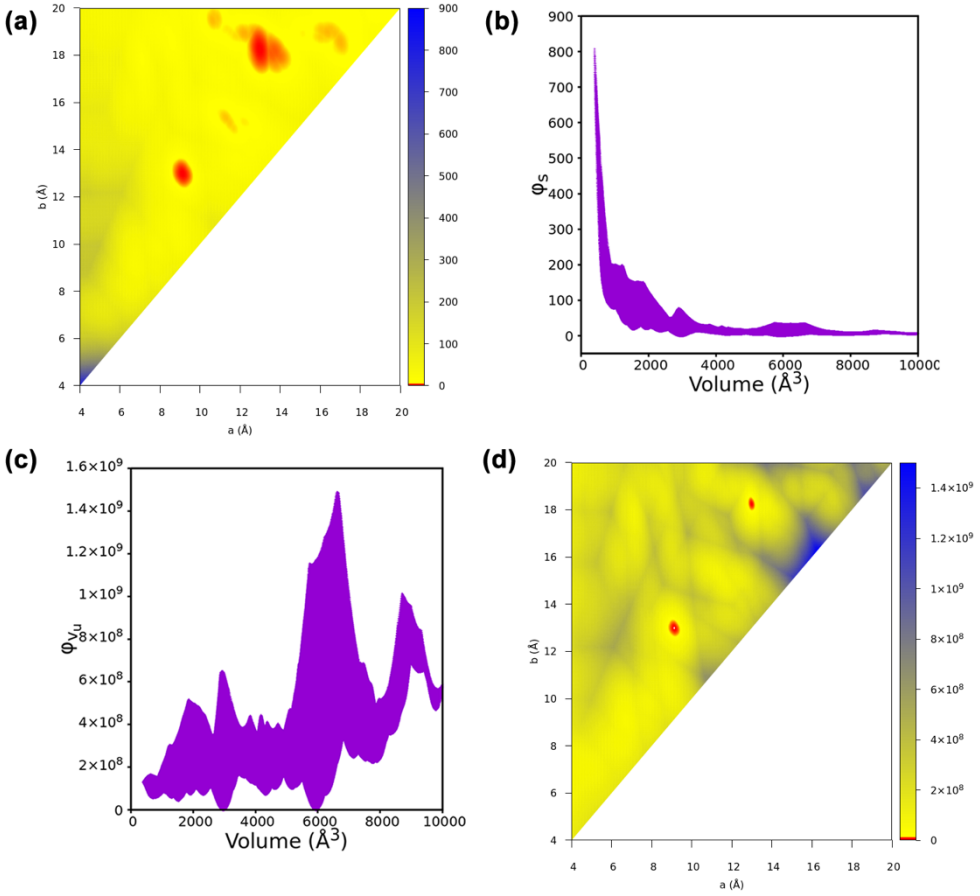

Figure S2.1. *(a) φ_S map as a function of unit cell parameters, a and b. Red regions represent φ_S below 10. (b) φ_S as a function of unit cell volume. (c) φ_{Vu} as a function of unit cell volume. (d) φ_{Vu} map as a function of unit cell parameters, a and b.*

Table S2.1. *The d-spacings (d_{obs}), errors of d-spacings (ε), the possible l values of Miller indices of the 12 reflections marked in Figure III.3b.*

Reflections	d_{obs} (Å)	*Error of* d_{obs} ε (Å)	d_{cal} (Å)	$\lvert d_{obs}-d_{cal}\rvert/d_{obs}$ (%)	Miller indices
No. 1	3.92	0.03	3.91	-0.22	130
No. 2	4.30	0.04	4.30	0.06	210
No. 3	5.29	0.05	5.29	0.01	120
No. 4	6.50	0.06	6.50	-0.08	020
No. 5	7.46	0.07	7.46	0.05	110
No. 6	9.13	0.08	9.12	-0.11	100
No. 7	5.77	0.05	5.77	-0.05	022
No. 8	5.12	0.05	5.13	0.18	023
No. 9	4.51	0.04	4.51	0.02	024
No. 10	5.63	0.05	5.64	0.30	014
No. 11	4.66	0.05	4.68	0.41	015
No. 12	3.98	0.03	3.98	0.08	016

Appendix 3. Supporting information of Chapter V

Appendix 3.1 Kinetics of cross-polarization between ^{1}H and ^{13}C

As described in Chapter II.4.5.1 and Chapter V, the CP/MAS NMR measurement is semiquantitative due to the kinetic effects involved in the cross polarization event. Again, the ^{13}C magintization, $M_s(t)$ can be expressed as:

$$M_s(t) = \frac{M_0}{T_{CH}} \times \left(\frac{1}{T_{CH}} + \frac{1}{T_{1C}} - \frac{1}{T_{1H}}\right) \times \left(e^{-\frac{t}{T_{1H}}} - e^{-t\times\left(\frac{1}{T_{CH}}+\frac{1}{T_{1C}}\right)}\right) \ldots\text{(i)}$$

where M_0 is the initial ^{1}H spin temperature, corresponding to the maximum magnetization value without signal decay due to the kinetics effect. Generally, T_{1C} is very long compared with T_{1H} and T_{CH}, as well as CP contact time, and its influence on the relaxation dynamics during the cross-polarization can be ignored. If the conditions of (1) T_{1C} » T_{1H} and (2) T_{1H} » T_{CH} can be satisfied, the above equation can be simplified as follows,

$$M_s(t) = M_0 \times \left(e^{-\frac{t}{T_{1H}}} - e^{-\frac{t}{T_{CH}}}\right). \ldots\text{(ii)}$$

To estimate these time constants in the equation (i), two sets of solid-state NMR measurements were conducted. First one is with a normal CP pulse sequence with a variable CP contact time from 0.001 ms to 10 ms. Another one is for ^{13}C T1 measurement described by Torchia [218].

The evolution of peak intensities of different C1 contributions as a function of CP contact time (left column of each figure) and delay time for ^{13}C T1 (right column) are shown in Figures S3.1-3. The fitted curves are shown as green lines together with fitted parameters. As described by Hill et al., The ^{13}C T1 decay could not be expressed by a single exponential function. There are two relaxations, fast (in the order of c.a. 100 ms) and slow ones (in the order of tens to a hundred of seconds). Nevertheless, even the shorter T1 is significantly larger than the T_{CH} and CP contact time.

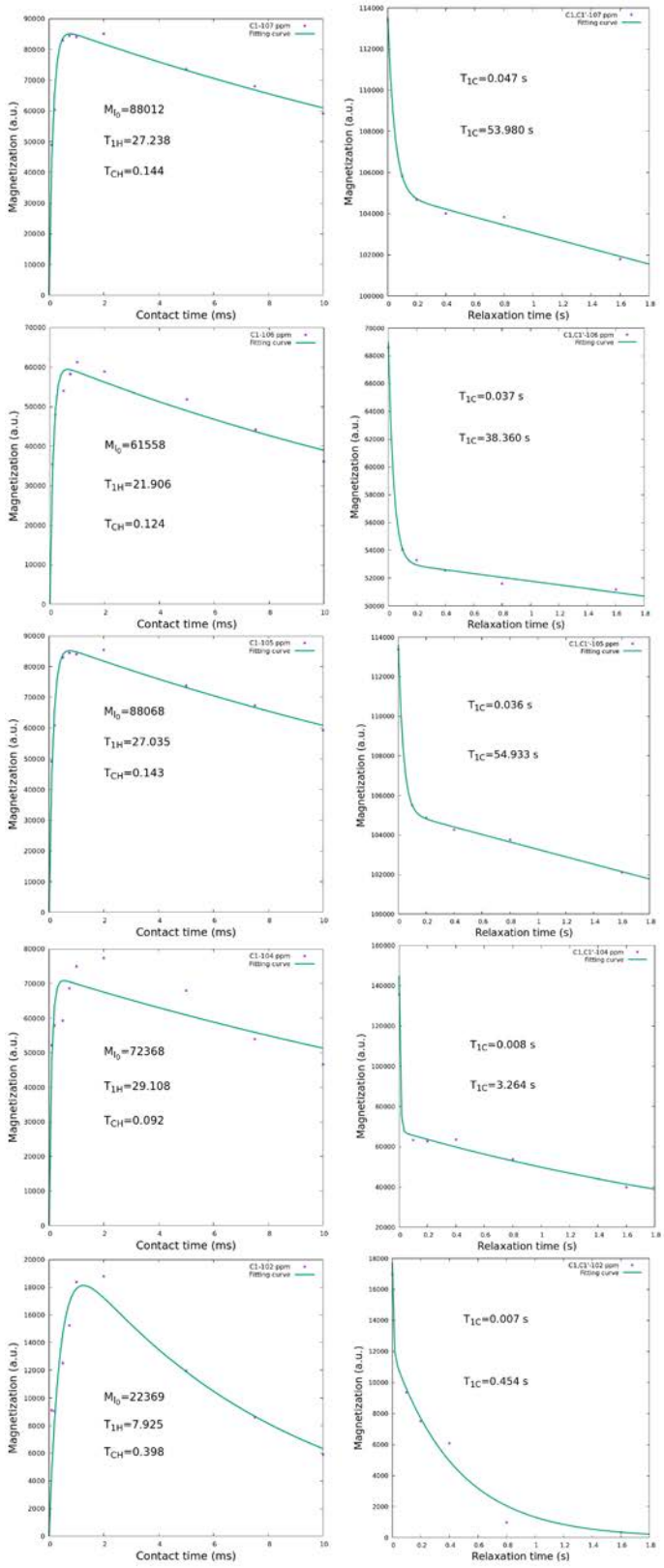

Figure S3.1. *Variation of ^{13}C signal intensity with CP contact time (left) and ^{13}C spin-lock time (right) for the C1 & C1' region of rehydrated fraction A.*

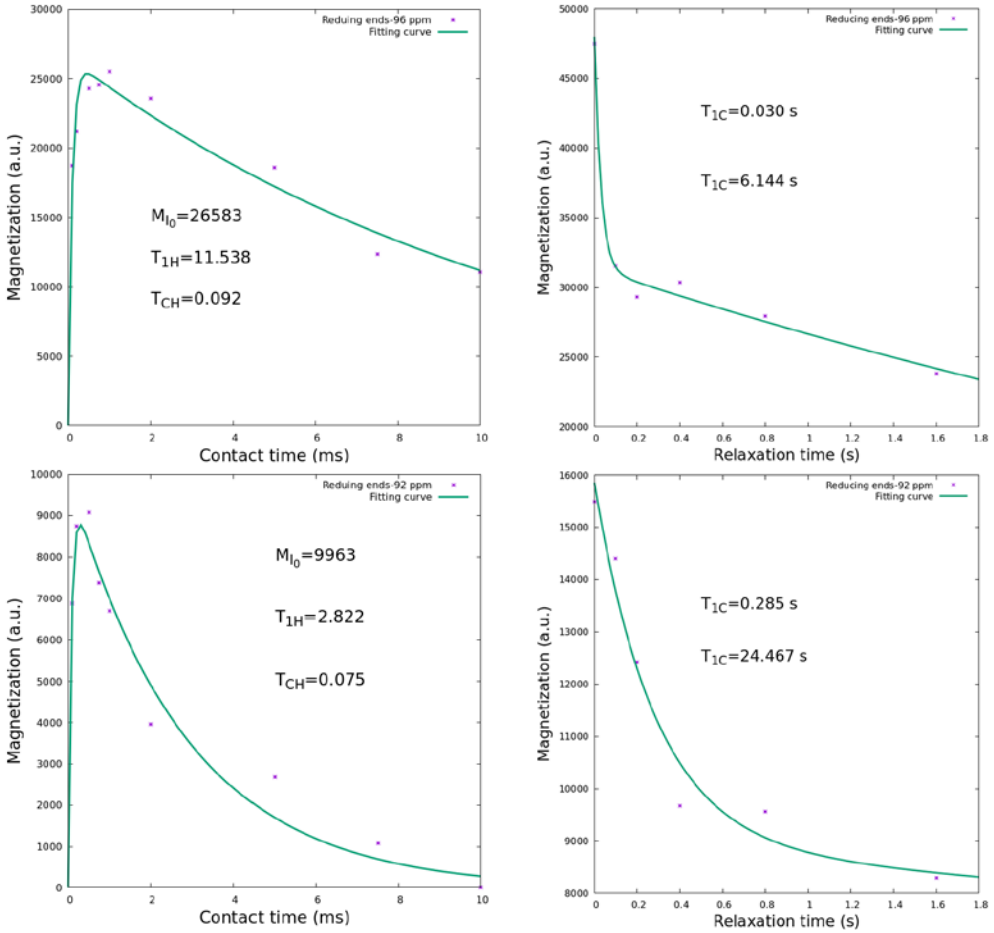

Figure S3.2. *Variation of ^{13}C signal intensity with CP contact time (left) and ^{13}C spin-lock time (right) for the reducing end (C1'') region of rehydrated fraction A.*

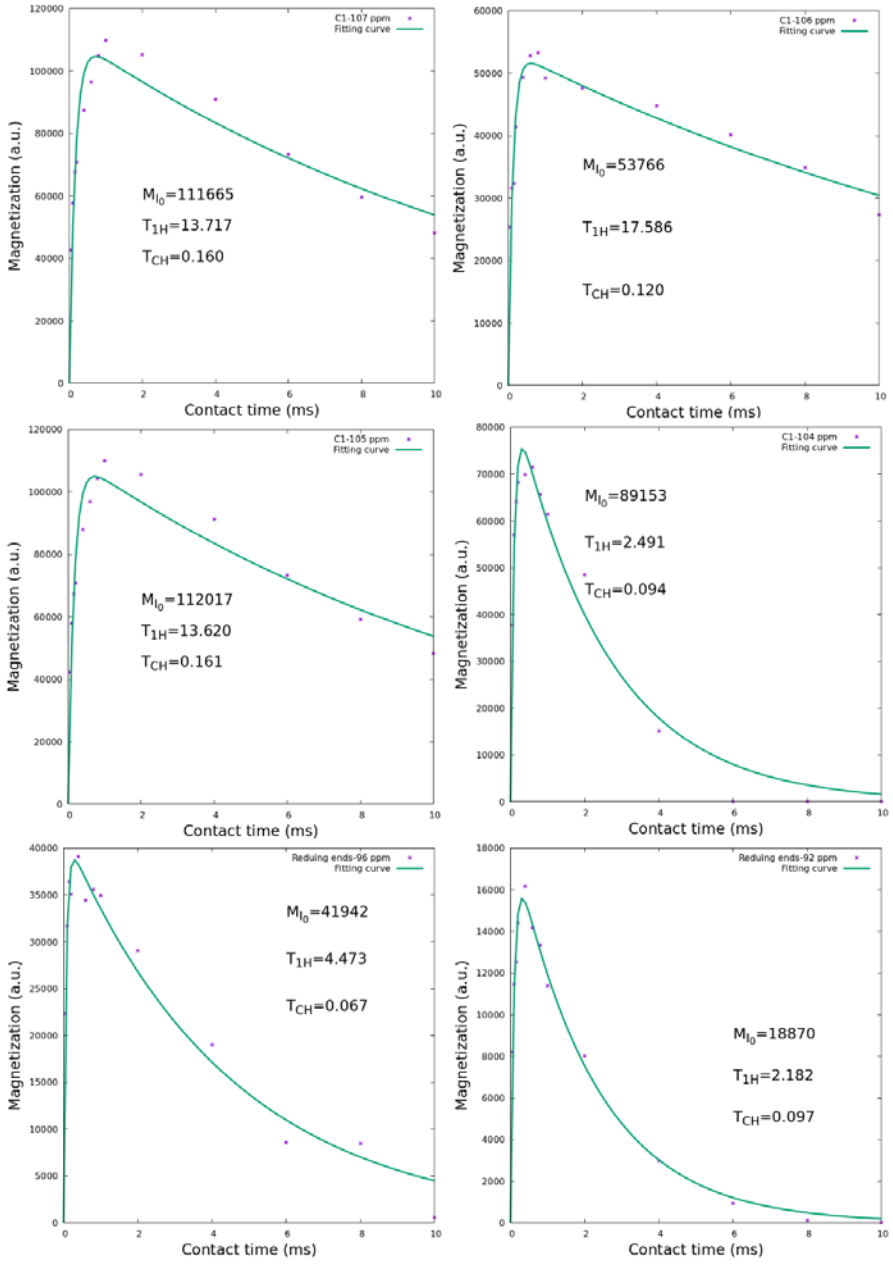

Figure S3.3. *Variation of ^{13}C signal intensity with CP contact time for the C1 & C1' region and reducing end (C1'') region of rehydrated fraction B.*

Appendix 4. Supporting information of Chapter VI

Appendix 4.1. Formation of cellulose IV_{II}

The X-ray diffraction patterns of regenerated cellulose oligomers show the diffraction features of cellulose II without exception in this thesis work. However, as described in Chapter VI, there is often an additional peak at 2θ of 16.4°. This peak position does not correspond to predicted reflection positions based on the unit cell proposed by Langan et al. This reflection corresponds most likely to 1 1 0 reflection of orthorhombic cellulose IV_{II} allomorph [219]. Another strong reflection of cellulose IV_{II}, 0 2 0, predicted at around 21.9° might be hidden below 0 2 0 of cellulose II.

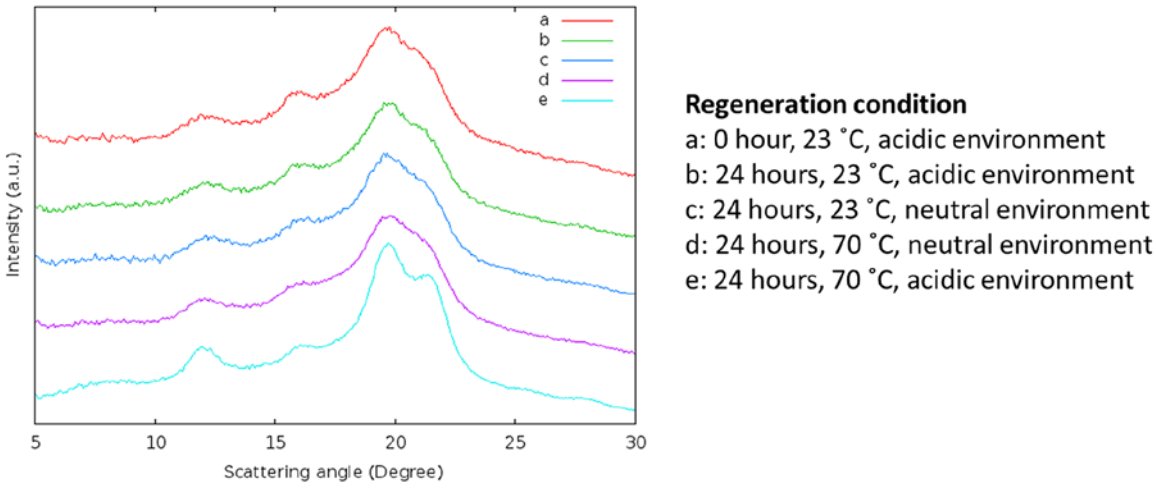

Figure S4.1. *X-ray diffraction profiles of the cellulose/H_3PO_4 solution hydrolyzed at 40 ˚C for 5 hours with different regeneration conditions.*

While in the report by Buleon & Chanzy [219], they a single crystal of cellulose IV_{II} composed of low molecular weight cellulose (number average DP of 18), the crystallization condition was very different as they used cellulose triacetate as a starting material for crystallization. It is not clear in this study why cellulose IV_{II} is formed in only specific conditions. Since the crystal structure of cellulose IV_{II} is not established yet, the crystallization of cellulose IV_{II} based on oligomers is of interest

for the crystallography of cellulose. Further investigations are needed to better control the crystallization process of obtained cellulose oligomers.

Appendix 4.2. Estimation of sulfur content based on ATR-FTIR.

The sulfur content was estimated for cellulose oligomers hydrolyzed in sulfuric acid using ATR-FTIR spectroscopy. As described in the main text, the band at 813 cm^{-1} is an absorbance of C-O-S vibration of sulfate half ester. I estimated the sulfur content based on the intensity ratio between this sulfate band and the C-O-C bending bands between 1140-1180 cm^{-1}. As calibrants, I used two cellulose nanocrystal (CNC) samples with known sulfur contents based on conductometric titration. They were provided by Dr Emily Cranston and Dr Fangbo Lin, respectively.

Figure S4.2 shows the peak fitting results of two band areas for sulfate and C-O-C vibrations of two CNC samples and the fraction B-s. the peak areas of each band are summarized in Table S4.1. The sulfur content was estimated as follows:

$$S\ content\ (dp7s) = \frac{S_T(CNC) * \frac{a_s(dp7s)}{a_{coc}(dp7s)}}{\frac{a_s(CNC)}{a_{coc}(CNC)}}$$

The estimated sulfur content of the Fraction B-s is 2 % based on Dr Lin's value and 1 % based on Dr Cranston's value. The reason of the large difference between two estimations are unknown for the moment.

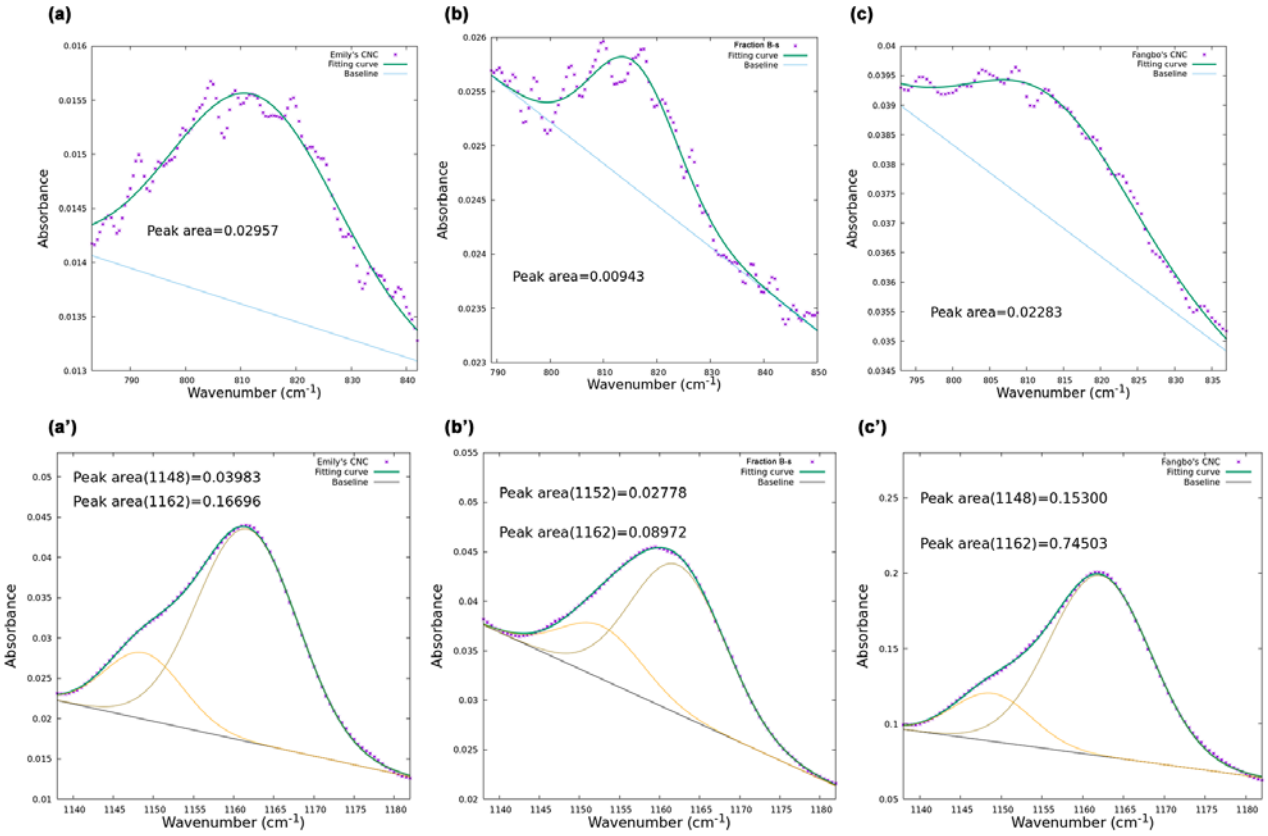

Figure S4.2. *Peak fitting of the peaks assigned to (a,b,c) sulfate groups and (a',b',c') C-O-C of cellulose in ATR-FTIR from three samples, (a,a') CNC provided by Dr Emily Cranston (University British Columbia), (b,b') Fraction B-s and (c,c') CNC provided by Dr Fangbo Lin (Cermav).*

Table SI.3.1. *Integrated Peak areas of the peaks assigned to sulfate groups and C-O-C of cellulose in ATR-FTIR from three samples, Dr. Cranston's CNC, Fraction B-s and Dr. Lin's CNC.*

	C-O-C (1148+1162)	Sulfate group (814)	Sulfur content by titration
Dr Cranston's CNC	0.207	0.030	1.19 %
Dr. Lin's CNC	0.898	0.023	0.7 %
Fraction B-s	0.118	0.009	

Appendix 4.3. ^{1}H-NMR of Fraction B-p and Fraction B-s in DMSO-d6

Figure S4.3 shows ^{1}H NMR spectra of the fractions B in DMSO-d6. The peaks in the chemical shift range from 5.5-4.5 ppm appear very different between fractions B-s and B-p. The origin of this difference is unknown at this moment. Thus, I changed the solvent from DMSO-d6 to NaOH/D_2O for the DP estimation of these fractions.

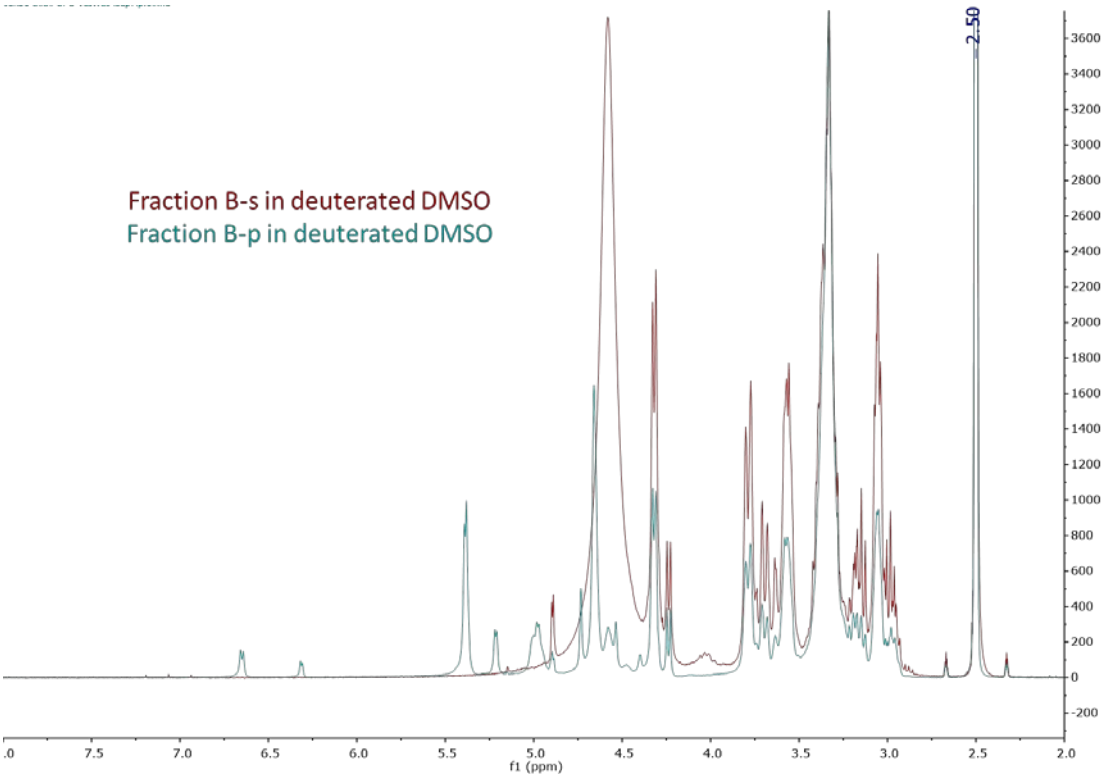

Figure S4.3. *^{1}H NMR of Fraction B-s and Fraction B-p in deuterated DMSO.*

Appendix 4.4. DP information of fraction A regenerated from salt solutions

The H_2SO_4-hydrolyzed fraction A regenerated from salt solutions could be dissolved in DMSO at 60 ˚C, so these samples were subjected to MALDI MS measurements. As shown in Figure S4.4, the DP information of the fraction A was estimated from ^{13}C CP/MAS NMR and MALDI MS spectroscopies. There are big differences between the DP_n estimated from ^{13}C CP/MAS NMR and MALDI MS for the same smaples. As discussed in Chapter V, the DP information of the Fraction A estimated from ^{13}C CP/MAS NMR and MALDI MS should not be reliable. Thus, the DP information of the H_2SO_4-hydrolyzed fraction A regenerated from salt solutions is still uncertain.

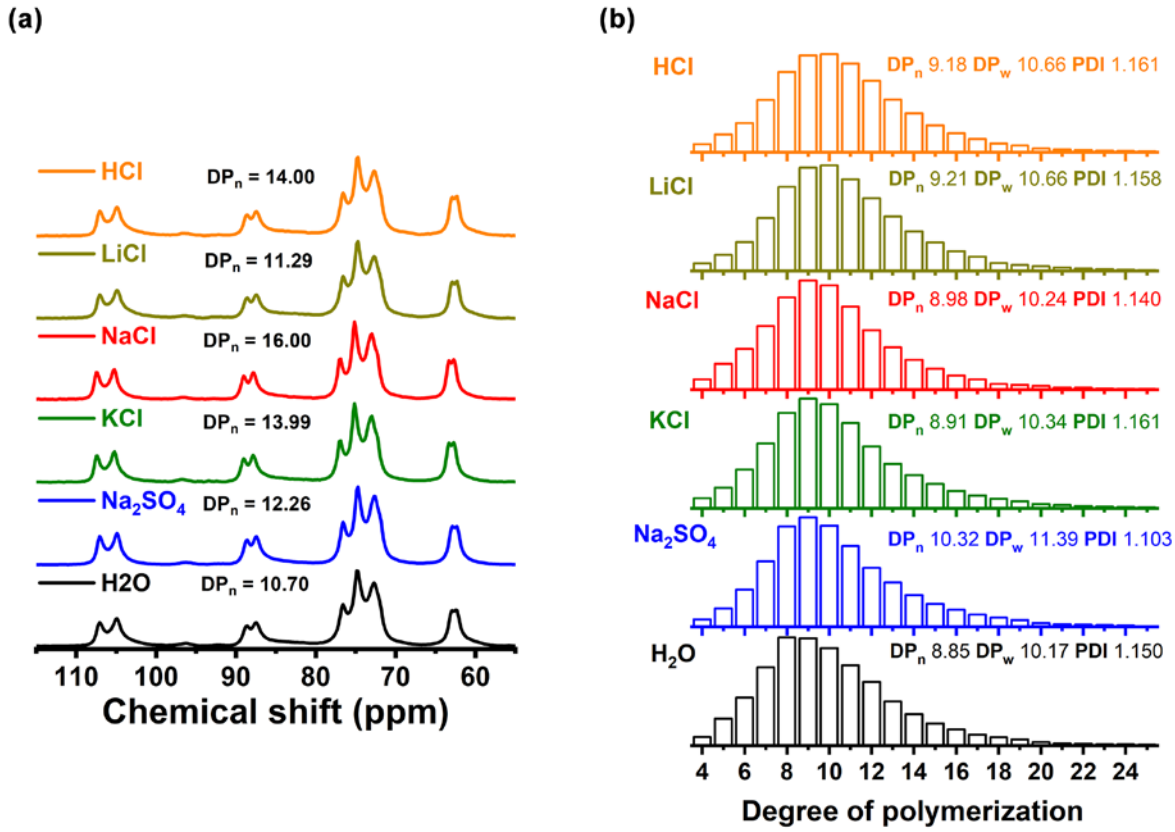

Figure S4.4. *DP information of the fraction A from sulfuric acid hydrolysis for 50 mins at 40 °C and regeneration in different solutions with the same molar concentration (half of the molar concentration for Na_2SO_4 solution) from (a) solid-state ^{13}C CP/MAS NMR and (b) MALDI-TOF MS.*

References

References

1. Isogai, A.; Usuda, M., Preparation of low-molecular weight celluloses using phosphoric acid. *Mokuzai Gakkaishi* **1991,** *37*, 339-344.

2. Payen, A., Mémoire sur la composition du tissu propre des plantes et du ligneux. *Comptes rendus* **1838,** *7*, 1052-1056.

3. Brongniart, A.; Pelouze, T.; Dumas, A., Rapport sur un mémoire de M. Payen, relatif à la composition de la matière ligneuse. *CR Hebd Seances Acad Sci* **1839,** *8*, 51-53.

4. Habibi, Y.; Lucia, L. A.; Rojas, O. J., Cellulose Nanocrystals: Chemistry, Self-Assembly, and Applications. *Chemical Reviews* **2010,** *110*, 3479-3500.

5. Małachowska, E.; Dubowik, M.; Lipkiewicz, A.; Przybysz, K.; Przybysz, P., Analysis of cellulose pulp characteristics and processing parameters for efficient paper production. *Sustainability* **2020,** *12*, 7219.

6. Xie, H.; Du, H.; Yang, X.; Si, C., Recent strategies in preparation of cellulose nanocrystals and cellulose nanofibrils derived from raw cellulose materials. *International Journal of Polymer Science* **2018,** *2018*.

7. Zihare, L.; Blumberga, D., Market opportunities for cellulose products from combined renewable resources. *Environmental and Climate Technologies* **2017,** *19*, 33-38.

8. Trache, D.; Hussin, M. H.; Chuin, C. T. H.; Sabar, S.; Fazita, M. N.; Taiwo, O. F.; Hassan, T.; Haafiz, M. M., Microcrystalline cellulose: Isolation, characterization and bio-composites application—A review. *International Journal of Biological Macromolecules* **2016,** *93*, 789-804.

9. Nsor-Atindana, J.; Chen, M.; Goff, H. D.; Zhong, F.; Sharif, H. R.; Li, Y., Functionality and nutritional aspects of microcrystalline cellulose in food. *Carbohydrate polymers* **2017,** *172*, 159-174.

10. Shatkin, J. A.; Wegner, T. H.; Bilek, E. T.; Cowie, J., Market projections of cellulose nanomaterial-enabled products-Part 1: Applications. *TAPPI JOURNAL, Volume 13, Number 5, 2014; pp. 9-16.* **2014,** *13*, 9-16.

11. Edgar, K. J.; Buchanan, C. M.; Debenham, J. S.; Rundquist, P. A.; Seiler, B. D.; Shelton, M. C.; Tindall, D., Advances in cellulose ester performance and application. *Progress in polymer science* **2001,** *26*, 1605-1688.

12. Muvhiiwa, R.; Mawere, E.; Moyo, L. B.; Tshuma, L., Utilization of cellulose in tobacco (Nicotiana tobacum) stalks for nitrocellulose production. *Heliyon* **2021,** *7*, e07598.

13. Ko, D.; Kim, S.-H.; Shin, C.-H.; Lee, Y.-T.; Kim, C. R.; Kim, J.-Y., Study on bio-degradation of cigarette filter rods with filter materials. *Journal of the Korean Society of Tobacco Science* **2005,** *27*, 75-82.

14. Rustemeyer, P. In *1. History of CA and evolution of the markets*, Macromolecular Symposia, 2004; Wiley Online Library: 2004; pp 1-6.

15. Coulson, A.; Lyne, D., The dynamic friction between cellulose acetate yarn and a cylindrical metal surface. *Journal of the Textile Institute Proceedings* **1955,** *46*, P112-P122.

16. Posey-Dowty, J.; Seo, K.; Walker, K.; Wilson, A., Carboxymethylcellulose acetate butyrate in water-based automotive paints. *Surface Coatings International Part B: Coatings Transactions* **2002,** *85*, 203-208.

17. Freudenberg, K.; Braun, E., Mitteilung über Lignin und Cellulose Ann.

Methylcellulose **1928,** *460*, 288.

18. Nishiyama, Y.; Langan, P.; Chanzy, H., Crystal structure and hydrogen-bonding system in cellulose Iβ from synchrotron X-ray and neutron fiber diffraction. *Journal of the American Chemical Society* **2002,** *124*, 9074-9082.

19. Nishiyama, Y.; Sugiyama, J.; Chanzy, H.; Langan, P., Crystal structure and hydrogen bonding system in cellulose Iα from synchrotron X-ray and neutron fiber diffraction. *Journal of the American Chemical Society* **2003,** *125*, 14300-14306.

20. Kroon-Batenburg, L.; Bouma, B.; Kroon, J., Stability of cellulose structures studied by MD simulations. Could mercerized cellulose II be parallel? *Macromolecules* **1996,** *29*, 5695-5699.

21. Pereira, A.; Mobedshahi, M.; Ladisch, M., Preparation of cellodextrins. *Methods in Enzymology* **1988,** *160*, 26-38.

22. Billès, E.; Onwukamike, K. N.; Coma, V.; Grelier, S.; Peruch, F., Cellulose oligomers production and separation for the synthesis of new fully bio-based amphiphilic compounds. *Carbohydrate polymers* **2016,** *154*, 121-128.

23. Seifollahi, M.; Amiri, H., Enzymatic post-hydrolysis of water-soluble cellulose oligomers released by chemical hydrolysis for cellulosic butanol production. *Cellulose* **2019,** *26*, 4479-4494.

24. Seifollahi, M.; Amiri, H., Enhanced production of cellulosic butanol by simultaneous co-saccharification and fermentation of water-soluble cellulose oligomers obtained by chemical hydrolysis. *Fuel* **2020,** *263*, 116759.

25. Serizawa, T.; Maeda, T.; Yamaguchi, S.; Sawada, T., Aqueous Suspensions of Cellulose Oligomer Nanoribbons for Growth and Natural Filtration-Based Separation of Cancer Spheroids. *Langmuir* **2020,** *36*, 13890-13898.

26. Ma, Z.; Li, Q.; Wang, B.; Feng, X.; Xu, H.; Mao, Z.; You, C.; Sui, X., Synthetic semicrystalline cellulose oligomers as efficient Pickering emulsion stabilizers. *Carbohydrate polymers* **2021,** *254*, 117445.

27. Queyroy, S.; Müller‐Plathe, F.; Brown, D., Molecular dynamics simulations of cellulose oligomers: conformational analysis. *Macromolecular theory and simulations* **2004,** *13*, 427-440.

28. Shen, T.; Langan, P.; French, A. D.; Johnson, G. P.; Gnanakaran, S., Conformational flexibility of soluble cellulose oligomers: chain length and temperature dependence. *Journal of the American Chemical Society* **2009,** *131*, 14786-14794.

29. Yin, J.; Raegen, A.; Idziak, S. H.; Forrest, J. A., Crystallization and melting of highly monodisperse poly (ethylene-oxide). *Soft Matter* **2020,** *16*, 7958-7969.

30. Alt, H. G.; Eichner, M. E., Preparation of an ethylene (hydrido) tungsten complex by photo-induced. beta.-elimination. *Angew. Chem.;(Germany, Federal Republic of)* **1982,** *21*.

31. Okushio, K.; Fukuyama, K.; Kuge, T., Synthesis of cellobiose, cellotriose, cellotetraose, and lactose. *Carbohydrate research* **1983,** *121*, 163-173.

32. Nakatsubo, F.; Kamitakahara, H.; Hori, M., Cationic ring-opening polymerization of 3, 6-di-O-benzyl-α-D-glucose 1, 2, 4-orthopivalate and the first chemical synthesis of cellulose. *Journal of the American Chemical Society* **1996,** *118*, 1677-1681.

33. Galan, M. C.; Jones, R. A.; Tran, A.-T., Recent developments of ionic liquids in oligosaccharide synthesis: the sweet side of ionic liquids. *Carbohydrate research* **2013,** *375*, 35-46.

34. Zhu, X.; Schmidt, R. R., New principles for glycoside‐bond formation.

Angewandte Chemie International Edition **2009,** *48*, 1900-1934.

35. Ritter, T. K.; Mong, K. K. T.; Liu, H.; Nakatani, T.; Wong, C. H., A programmable one‐pot oligosaccharide synthesis for diversifying the sugar domains of natural products: A case study of vancomycin. *Angewandte Chemie* **2003,** *115*, 4805-4808.

36. Peng, P.; Xiong, D.-C.; Ye, X.-S., ortho-Methylphenylthioglycosides as glycosyl building blocks for preactivation-based oligosaccharide synthesis. *Carbohydrate research* **2014,** *384*, 1-8.

37. Kaji, E.; Yamamoto, D.; Shirai, Y.; Ishige, K.; Arai, Y.; Shirahata, T.; Makino, K.; Nishino, T., Thermodynamically controlled regioselective glycosylation of fully unprotected sugars through Bis (boronate) intermediates. *European Journal of Organic Chemistry* **2014,** *2014*, 3536-3539.

38. Kaji, E.; Nishino, T.; Ishige, K.; Ohya, Y.; Shirai, Y., Regioselective glycosylation of fully unprotected methyl hexopyranosides by means of transient masking of hydroxy groups with arylboronic acids. *Tetrahedron Letters* **2010,** *51*, 1570-1573.

39. Kamitakahara, H.; Nakatsubo, F.; Klemm, D., Block co-oligomers of tri-O-methylated and unmodified cello-oligosaccharides as model compounds for methylcellulose and its dissolution/gelation behavior. *Cellulose* **2006,** *13*, 375-392.

40. Nishimura, T.; Nakatsubo, F., First synthesis of cellooctaose by a convergent synthetic method. *Carbohydrate research* **1996,** *294*, 53-64.

41. Monsan, P.; Paul, F., Enzymatic synthesis of oligosaccharides. *FEMS Microbiology Reviews* **1995,** *16*, 187-192.

42. Nilsson, K. G., Enzymatic synthesis of oligosaccharides. *Trends in Biotechnology*

1988, *6*, 256-264.

43. Kobayashi, S., Challenge of synthetic cellulose. *Journal of Polymer Science Part A: Polymer Chemistry* **2005,** *43*, 693-710.

44. Kadokawa, J.-i., Precision polysaccharide synthesis catalyzed by enzymes. *Chemical reviews* **2011,** *111*, 4308-4345.

45. Shoda, S.-i.; Uyama, H.; Kadokawa, J.-i.; Kimura, S.; Kobayashi, S., Enzymes as green catalysts for precision macromolecular synthesis. *Chemical reviews* **2016,** *116*, 2307-2413.

46. Kobayashi, S.; Kashiwa, K.; Kawasaki, T.; Shoda, S., Novel method for polysaccharide synthesis using an enzyme: the first in vitro synthesis of cellulose via a nonbiosynthetic path utilizing cellulase as catalyst. *Journal of the American Chemical Society* **1991,** *113*, 3079-3084.

47. Kobayashi, S.; Shoda, S.-i., Chemical synthesis of cellulose and cello-oligomers using a hydrolysis enzyme as a catalyst. *International journal of biological macromolecules* **1995,** *17*, 373-379.

48. Kobayashi, S.; Kawasaki, T.; Obata, K.; Shoda, S.-i., A novel method for synthesis of cellooligosaccharide derivatives by using enzyme catalyst. *Chemistry letters* **1993,** *22*, 685-686.

49. Nakai, H.; Abou Hachem, M.; Petersen, B. O.; Westphal, Y.; Mannerstedt, K.; Baumann, M. J.; Dilokpimol, A.; Schols, H. A.; Duus, J. Ø.; Svensson, B., Efficient chemoenzymatic oligosaccharide synthesis by reverse phosphorolysis using cellobiose phosphorylase and cellodextrin phosphorylase from Clostridium thermocellum. *Biochimie* **2010,** *92*, 1818-1826.

50. Petrović, D. M.; Kok, I.; Woortman, A. J.; Ćirić, J.; Loos, K., Characterization of

oligocellulose synthesized by reverse phosphorolysis using different cellodextrin phosphorylases. *Analytical chemistry* **2015,** *87*, 9639-9646.

51. Hattori, T.; Ogata, M.; Kameshima, Y.; Totani, K.; Nikaido, M.; Nakamura, T.; Koshino, H.; Usui, T., Enzymatic synthesis of cellulose II-like substance via cellulolytic enzyme-mediated transglycosylation in an aqueous medium. *Carbohydrate research* **2012,** *353*, 22-26.

52. Fort, S.; Christiansen, L.; Schülein, M.; Cottaz, S.; Drigueza, H., Stepwise synthesis of cellodextrins assisted by a mutant cellulase. *Israel Journal of Chemistry* **2000,** *40*, 217-221.

53. Pringsheim, H., Über den fermentativen Abbau der Cellulose. *Biological Chemistry* **1912,** *78*, 266-291.

54. Mielenz, J. R., Ethanol production from biomass: technology and commercialization status. *Current opinion in microbiology* **2001,** *4*, 324-329.

55. Lee, Y.-H.; Fan, L., Properties and mode of action of cellulase. In *Advances in Biochemical Engineering, Volume 17*, Springer: 1980; pp 101-129.

56. Kuhad, R. C.; Singh, A.; Eriksson, K.-E. L., Microorganisms and enzymes involved in the degradation of plant fiber cell walls. *Biotechnology in the pulp and paper industry* **1997**, 45-125.

57. Kluge, S.; Bonhage, B.; Viell, J.; Granström, M.; Kindler, A.; Spiess, A. C., Enzymatic production of cello-oligomers with endoglucanases. *Cellulose* **2019,** *26*, 4279-4290.

58. Teeri, T. T., Crystalline cellulose degradation: new insight into the function of cellobiohydrolases. *Trends in biotechnology* **1997,** *15*, 160-167.

59. Gunata, Y. Z.; Bayonove, C. L.; Tapiero, C.; Cordonnier, R. E., Hydrolysis of

grape monoterpenyl. beta.-D-glucosides by various. beta.-glucosidases. *Journal of Agricultural and Food Chemistry* **1990,** *38*, 1232-1236.

60. Dadi, A. P.; Varanasi, S.; Schall, C. A., Enhancement of cellulose saccharification kinetics using an ionic liquid pretreatment step. *Biotechnology and bioengineering* **2006,** *95*, 904-910.

61. Swatloski, R. P.; Spear, S. K.; Holbrey, J. D.; Rogers, R. D., Dissolution of cellose with ionic liquids. *Journal of the American chemical society* **2002,** *124*, 4974-4975.

62. Baboukani, B. S.; Vossoughi, M.; Alemzadeh, I., Optimisation of dilute-acid pretreatment conditions for enhancement sugar recovery and enzymatic hydrolysis of wheat straw. *Biosystems engineering* **2012,** *111*, 166-174.

63. Hu, Z.; Wen, Z., Enhancing enzymatic digestibility of switchgrass by microwave-assisted alkali pretreatment. *Biochemical Engineering Journal* **2008,** *38*, 369-378.

64. Zhao, Y.; Wang, Y.; Zhu, J.; Ragauskas, A.; Deng, Y., Enhanced enzymatic hydrolysis of spruce by alkaline pretreatment at low temperature. *Biotechnology and bioengineering* **2008,** *99*, 1320-1328.

65. Kim, S.; Holtzapple, M. T., Lime pretreatment and enzymatic hydrolysis of corn stover. *Bioresource technology* **2005,** *96*, 1994-2006.

66. Hall, M.; Bansal, P.; Lee, J. H.; Realff, M. J.; Bommarius, A. S., Biological pretreatment of cellulose: Enhancing enzymatic hydrolysis rate using cellulose-binding domains from cellulases. *Bioresource technology* **2011,** *102*, 2910-2915.

67. Peng, H.; Li, H.; Luo, H.; Xu, J., A novel combined pretreatment of ball milling and microwave irradiation for enhancing enzymatic hydrolysis of microcrystalline cellulose. *Bioresource technology* **2013,** *130*, 81-87.

68. Barakat, A.; Mayer-Laigle, C.; Solhy, A.; Arancon, R. A.; De Vries, H.; Luque, R., Mechanical pretreatments of lignocellulosic biomass: towards facile and environmentally sound technologies for biofuels production. *Rsc Advances* **2014,** *4*, 48109-48127.

69. Bak, J. S.; Ko, J. K.; Han, Y. H.; Lee, B. C.; Choi, I.-G.; Kim, K. H., Improved enzymatic hydrolysis yield of rice straw using electron beam irradiation pretreatment. *Bioresource Technology* **2009,** *100*, 1285-1290.

70. Zhang, C.; Pang, F.; Li, B.; Xue, S.; Kang, Y., Recycled aqueous ammonia expansion (RAAE) pretreatment to improve enzymatic digestibility of corn stalks. *Bioresource technology* **2013,** *138*, 314-320.

71. Brandt, A.; Gräsvik, J.; Hallett, J. P.; Welton, T., Deconstruction of lignocellulosic biomass with ionic liquids. *Green chemistry* **2013,** *15*, 550-583.

72. Zhao, H.; Jones, C. L.; Baker, G. A.; Xia, S.; Olubajo, O.; Person, V. N., Regenerating cellulose from ionic liquids for an accelerated enzymatic hydrolysis. *Journal of biotechnology* **2009,** *139*, 47-54.

73. Tadesse, H.; Luque, R., Advances on biomass pretreatment using ionic liquids: an overview. *Energy & Environmental Science* **2011,** *4*, 3913-3929.

74. Sun, Y.-C.; Xu, J.-K.; Xu, F.; Sun, R.-C., Structural comparison and enhanced enzymatic hydrolysis of eucalyptus cellulose via pretreatment with different ionic liquids and catalysts. *Process Biochemistry* **2013,** *48*, 844-852.

75. Samayam, I. P.; Hanson, B. L.; Langan, P.; Schall, C. A., Ionic-liquid induced changes in cellulose structure associated with enhanced biomass hydrolysis. *Biomacromolecules* **2011,** *12*, 3091-3098.

76. Turner, M. B.; Spear, S. K.; Huddleston, J. G.; Holbrey, J. D.; Rogers, R. D., Ionic

liquid salt-induced inactivation and unfolding of cellulase from Trichoderma reesei. *Green Chemistry* **2003,** *5*, 443-447.

77. Zhang, Q.; Benoit, M.; De Oliveira Vigier, K.; Barrault, J.; Jérôme, F., Green and inexpensive choline - derived solvents for cellulose decrystallization. *Chemistry – A European Journal* **2012,** *18*, 1043-1046.

78. Bose, S.; Barnes, C. A.; Petrich, J. W., Enhanced stability and activity of cellulase in an ionic liquid and the effect of pretreatment on cellulose hydrolysis. *Biotechnology and bioengineering* **2012,** *109*, 434-443.

79. Hess, K.; Dziengel, K., Über Cellotriose und ihre Derivate. *Berichte der deutschen chemischen Gesellschaft (A and B Series)* **1935,** *68*, 1594-1605.

80. Arndt, P.; Bockholt, K.; Gerdes, R.; Huschens, S.; Pyplo, J.; Redlich, H.; Samm, K., Cellulose oligomers: preparation from cellulose triacetate, chemical transformations and reactions. *Cellulose* **2003,** *10*, 75-83.

81. Arndt, P.; Gerdes, R.; Huschens, S.; Pyplo-Schnieders, J.; Redlich, H., Preparation of cellulose oligomers from cellulose triacetate (standard procedure). *Cellulose* **2005,** *12*, 317-326.

82. Miller, G. L.; Dean, J.; Blum, R., A study of methods for preparing oligosaccharides from cellulose. *Archives of Biochemistry and Biophysics* **1960,** *91*, 21-26.

83. Akpinar, O.; Penner, M. H., Preparation of cellooligosaccharides: Comparative study. **2008**.

84. Shafizadeh, F.; Furneaux, R. H.; Cochran, T. G.; Scholl, J. P.; Sakai, Y., Production of levoglucosan and glucose from pyrolysis of cellulosic materials.

Journal of Applied Polymer Science **1979,** *23*, 3525-3539.

85. Piskorz, J.; Majerski, P.; Radlein, D.; Vladars-Usas, A.; Scott, D., Flash pyrolysis of cellulose for production of anhydro-oligomers. *Journal of Analytical and Applied Pyrolysis* **2000,** *56*, 145-166.

86. Yu, Y.; Liu, D.; Wu, H., Characterization of water-soluble intermediates from slow pyrolysis of cellulose at low temperatures. *Energy & fuels* **2012,** *26*, 7331-7339.

87. Shrotri, A.; Lambert, L. K.; Tanksale, A.; Beltramini, J., Mechanical depolymerisation of acidulated cellulose: understanding the solubility of high molecular weight oligomers. *Green chemistry* **2013,** *15*, 2761-2768.

88. Dornath, P.; Cho, H. J.; Paulsen, A.; Dauenhauer, P.; Fan, W., Efficient mechano-catalytic depolymerization of crystalline cellulose by formation of branched glucan chains. *Green Chemistry* **2015,** *17*, 769-775.

89. Li, C.; Zhao, Z. K., Efficient acid-catalyzed hydrolysis of cellulose in ionic liquid. *Advanced Synthesis & Catalysis* **2007,** *349*, 1847-1850.

90. Voloch, M.; Ladisch, M.; Cantarella, M.; Tsao, G., Preparation of cellodextrins using sulfuric acid. *Biotechnology and bioengineering* **1984,** *26*, 557-559.

91. Zhang, Y.-H. P.; Lynd, L. R., Cellodextrin preparation by mixed-acid hydrolysis and chromatographic separation. *Analytical biochemistry* **2003,** *322*, 225-232.

92. Brown, W., The separation of cellodextrins by gel permeation chromatography. *Journal of Chromatography A* **1970,** *52*, 273-284.

93. Hamacher, K.; Schmid, G.; Sahm, H.; Wandrey, C., Structural heterogeneity of cellooligomers homogeneous according to high-resolution size-exclusion chromatography. *Journal of Chromatography A* **1985,** *319*, 311-318.

94. Akpinar, O.; McGorrin, R. J.; Penner, M. H., Cellulose-based chromatography for

cellooligosaccharide production. *Journal of agricultural and food chemistry* **2004,** *52*, 4144-4148.

95. Liebert, T.; Seifert, M.; Heinze, T. In *Efficient Method for the Preparation of Pure, Water - Soluble Cellodextrines*, Macromolecular symposia, 2008; Wiley Online Library: 2008; pp 140-149.

96. Kasuya, N.; Kusaka, Y.; Habu, N.; Ohnishi, A., Development of chiral stationary phases consisting of low-molecular-weight cellulose derivatives covalently bonded to silica gel. *Cellulose* **2002,** *9*, 263-269.

97. Zweckmair, T.; Oberlerchner, J. T.; Böhmdorfer, S.; Bacher, M.; Sauerland, V.; Rosenau, T.; Potthast, A., Preparation and analytical characterisation of pure fractions of cellooligosaccharides. *Journal of Chromatography A* **2016,** *1431*, 47-54.

98. Flugge, L. A.; Blank, J. T.; Petillo, P. A., Isolation, modification, and NMR assignments of a series of cellulose oligomers. *Journal of the American Chemical Society* **1999,** *121*, 7228-7238.

99. Chilamkurthi, S.; Willemsen, J.-H.; van der Wielen, L. A.; Poiesz, E.; Ottens, M., High-throughput determination of adsorption equilibria for chromatographic oligosaccharide separations. *Journal of Chromatography A* **2012,** *1239*, 22-34.

100. Schmidt, J.; John, M.; Wandrey, C., Rapid separation of malto-, xylo-and cello-oligosaccharides (DP 2–9) on cation-exchange resin using water as eluent. *Journal of Chromatography A* **1981,** *213*, 151-155.

101. Scobell, H.; Brobst, K., Rapid high-resolution separation of oligosaccharides on silver form cation-exchange resins. *Journal of Chromatography A* **1981,** *212*, 51-64.

102. Hostomská-Chytilová, Z.; Mikes, O.; Vrátý, P.; Smrž, M., Chromatography of cellodextrins and enzymatic hydrolysates of cellulose on ion-exchange derivatives of

spheron. *Journal of Chromatography A* **1982,** *235*, 229-236.

103. Isogai, A.; Usuda, M., Preparation of low-molecular weight celluloses using phosphoric acid. *Journal of the Japan Wood Research Society (Japan)* **1991**.

104. Berl, E., Viscosity determination of cellulose. *Industrial & Engineering Chemistry Analytical Edition* **1941,** *13*, 322-326.

105. Alexander, W.; Mitchell, R., Rapid measurement of cellulose viscosity by nitration methods. *Analytical Chemistry* **1949,** *21*, 1497-1500.

106. Claisse, N. Préparation et modification d'oligosaccharides de cellulose par chimie douce bio-inspirée. Université de Grenoble, 2012.

107. McManus, J. B.; Wilson, L.; Yang, H.; Kubicki, J. D.; Tien, M., Kinetic analysis of cellulose synthase of Gluconacetobacter hansenii in whole cells and in purified form. *Enzyme and microbial technology* **2018,** *119*, 24-29.

108. Villares, A.; Moreau, C.; Bennati-Granier, C.; Garajova, S.; Foucat, L.; Falourd, X.; Saake, B.; Berrin, J.-G.; Cathala, B., Lytic polysaccharide monooxygenases disrupt the cellulose fibers structure. *Scientific reports* **2017,** *7*, 1-9.

109. Bouchard, J.; Méthot, M.; Fraschini, C.; Beck, S., Effect of oligosaccharide deposition on the surface of cellulose nanocrystals as a function of acid hydrolysis temperature. *Cellulose* **2016,** *23*, 3555-3567.

110. Mormann, W.; Michel, U., Improved synthesis of cellulose carbamates without by-products. *Carbohydrate polymers* **2002,** *50*, 201-208.

111. Fischer, M.; Fischer, K. In *Polymer - Analogous Preparation of Cellulose Tricarbanilates: Mechanisms of Degradation in Dimethylsulfoxide*, Macromolecular Symposia, 2005; Wiley Online Library: 2005; pp 121-136.

112. Evans, R.; Wearne, R. H.; Wallis, A. F., Pyridine-catalyzed depolymerization of cellulose during carbanilation with phenylisocyanate in dimethylsulfoxide. *Journal of applied polymer science* **1991,** *42*, 821-827.

113. Henniges, U.; Kloser, E.; Patel, A.; Potthast, A.; Kosma, P.; Fischer, M.; Fischer, K.; Rosenau, T., Studies on DMSO-containing carbanilation mixtures: chemistry, oxidations and cellulose integrity. *Cellulose* **2007,** *14*, 497-511.

114. Hearon, W.; Hiatt, G. D.; Fordyce, C. R., Carbamates of Cellulose and Cellulose Acetate. I. Preparation1. *Journal of the American Chemical Society* **1943,** *65*, 829-833.

115. Hearon, W.; Hiatt, G. D.; Fordyce, C. R., Carbamates of Cellulose and Cellulose Acetate. II. Stability toward Hydrolysis1. *Journal of the American Chemical Society* **1943,** *65*, 833-836.

116. Barthel, S.; Heinze, T., Acylation and carbanilation of cellulose in ionic liquids. *Green Chemistry* **2006,** *8*, 301-306.

117. Miyagi, Y.; Young, R. A., Carbanilation of cellulose in the paraformaldehyde–dimethyl sulfoxide solvent system. *Journal of Applied Polymer Science* **1982,** *27*, 673-685.

118. Wenzel, M.; Burchard, W.; Schätzel, K., Dynamic light scattering from semidilute cellulose-tri-carbanilate solutions. *Polymer* **1986,** *27*, 195-201.

119. Schlufter, K.; Schmauder, H. P.; Dorn, S.; Heinze, T., Efficient homogeneous chemical modification of bacterial cellulose in the ionic liquid 1 - N - butyl - 3 - methylimidazolium chloride. *Macromolecular rapid communications* **2006,** *27*, 1670-1676.

120. Hall, D. M.; Horne, J. R., Preparation of cellulose triacetate and cellulose

tricarbanilate by nondegradative methods. *Journal of Applied Polymer Science* **1973,** *17*, 3727-3732.

121. Evans, R.; Wearne, R. H.; Wallis, A. F., Molecular weight distribution of cellulose as its tricarbanilate by high performance size exclusion chromatography. *Journal of applied polymer science* **1989,** *37*, 3291-3303.

122. Terbojevich, M.; Cosani, A.; Camilot, M.; Focher, B., Solution studies of cellulose tricarbanilates obtained in homogeneous phase. *Journal of applied polymer science* **1995,** *55*, 1663-1671.

123. Yanagisawa, M.; Isogai, A., SEC− MALS− QELS study on the molecular conformation of cellulose in LiCl/amide solutions. *Biomacromolecules* **2005,** *6*, 1258-1265.

124. Chen, W.; Zhang, M.; Feng, Y.; Wu, J.; Gao, X.; Zhang, J.; He, J.; Zhang, J., Homogeneous synthesis of partially substituted cellulose phenylcarbamates aiming at chiral recognition. *Polymer International* **2015,** *64*, 1037-1044.

125. Staudinger, H.; Eder, K., Über das Viskositätsgesetz für Fadenmoleküle. *Naturwissenschaften* **1941,** *29*, 221-221.

126. Chen, H.; Guo, B., Use of Binary Solvent Systems in the MALDI-TOF Analysis of Poly (methyl methacrylate). *Analytical chemistry* **1997,** *69*, 4399-4404.

127. Rashidzadeh, H.; Guo, B., Use of MALDI-TOF to measure molecular weight distributions of polydisperse poly (methyl methacrylate). *Analytical chemistry* **1998,** *70*, 131-135.

128. Schriemer, D. C.; Li, L., Mass discrimination in the analysis of polydisperse polymers by MALDI time-of-flight mass spectrometry. 1. Sample preparation and desorption/ionization issues. *Analytical Chemistry* **1997,** *69*, 4169-4175.

129. Crompton, T. R., *Chromatography Mass Spectroscopy in Polymer Analysis*. Smithers Rapra: 2010.

130. Staudinger, H.; Schweitzer, O., Über hochpolymere Verbindungen, 48. Mitteil.: Über die Molekülgröße der Cellulose. *Berichte der deutschen chemischen Gesellschaft (A and B Series)* **1930,** *63*, 3132-3154.

131. Flory, P. J., *Principles of polymer chemistry*. Cornell University Press: 1953.

132. Evans, R.; Wallis, A. F., Cellulose molecular weights determined by viscometry. *Journal of applied polymer science* **1989,** *37*, 2331-2340.

133. Oberlerchner, J. T.; Rosenau, T.; Potthast, A., Overview of methods for the direct molar mass determination of cellulose. *Molecules* **2015,** *20*, 10313-10341.

134. Lindman, B.; Karlström, G.; Stigsson, L., On the mechanism of dissolution of cellulose. *Journal of molecular liquids* **2010,** *156*, 76-81.

135. Glasser, W. G.; Atalla, R. H.; Blackwell, J.; Brown, R. M.; Burchard, W.; French, A. D.; Klemm, D. O.; Nishiyama, Y., About the structure of cellulose: debating the Lindman hypothesis. *Cellulose* **2012,** *19*, 589-598.

136. Alves, L.; Medronho, B.; Antunes, F. E.; Topgaard, D.; Lindman, B., Dissolution state of cellulose in aqueous systems. 2. Acidic solvents. *Carbohydrate polymers* **2016,** *151*, 707-715.

137. Mohd, N.; Draman, S.; Salleh, M.; Yusof, N. In *Dissolution of cellulose in ionic liquid: A review*, AIP conference proceedings, 2017; AIP Publishing LLC: 2017; p 020035.

138. Isogai, A.; Atalla, R., Dissolution of cellulose in aqueous NaOH solutions. *Cellulose* **1998,** *5*, 309-319.

139. Ioelovich, M., Study of cellulose interaction with concentrated solutions of

sulfuric acid. *International Scholarly Research Notices* **2012,** *2012*.

140. Meyer, K.; Mark, H., For the crystallizable part of cellulose. *Chemische Berichte* **1928,** *61*, 593-614.

141. Kuhn, W., Hydrolysis of polysaccharides. *Ber* **1930,** *63*, 1510.

142. Celanese, B. Improvements in phosphoric acid solutions of cellulose. 1925.

143. Navard, P.; Wendler, F.; Meister, F.; Bercea, M.; Budtova, T., Preparation and properties of cellulose solutions. In *The European Polysaccharide network of excellence (EPNOE)*, Springer: 2012; pp 91-152.

144. de Carolles, B., Ueber die Holzfaser und einige ihrer Verbindungen. *Journal für Praktische Chemie* **1844,** *32*, 427-441.

145. Camacho, F.; González-Tello, P.; Jurado, E.; Robles, A., Microcrystalline-cellulose hydrolysis with concentrated sulphuric acid. *Journal of Chemical Technology & Biotechnology: International Research in Process, Environmental AND Clean Technology* **1996,** *67*, 350-356.

146. Boerstoel, H.; Maatman, H.; Westerink, J.; Koenders, B., Liquid crystalline solutions of cellulose in phosphoric acid. *Polymer* **2001,** *42*, 7371-7379.

147. Bhandari, N.; Macdonald, D. G.; Bakhshi, N. N., Kinetic studies of corn stover saccharification using sulphuric acid. *Biotechnology and bioengineering* **1984,** *26*, 320-327.

148. Church, J. A.; Wooldridge, D., Continuous high-solids acid hydrolysis of biomass in a 1 1/2-in. plug flow reactor. *Industrial & Engineering Chemistry Product Research and Development* **1981,** *20*, 371-378.

149. Huang, W.; Wang, Y.; Zhang, L.; Chen, L., Rapid dissolution of spruce cellulose

in H2SO4 aqueous solution at low temperature. *Cellulose* **2016,** *23*, 3463-3473.

150. Dong, X. M.; Revol, J.-F.; Gray, D. G., Effect of microcrystallite preparation conditions on the formation of colloid crystals of cellulose. *Cellulose* **1998,** *5*, 19-32.

151. Roman, M.; Winter, W. T., Effect of sulfate groups from sulfuric acid hydrolysis on the thermal degradation behavior of bacterial cellulose. *Biomacromolecules* **2004,** *5*, 1671-1677.

152. Selim, I.; Zikry, A.; Gaber, S., Physicochemical properties of prepared cellulose sulfates: II. From linen pulp bleached by the H2O2 method. *Polymer-plastics technology and engineering* **2005,** *43*, 1387-1402.

153. Song, G.; Zhang, J.; Nishiyama, Y., Twisted pseudo-tetragonal orthorhombic lamellar crystal in cellulose/ionic liquid spherulite. *Cellulose* **2020,** *27*, 5449-5455.

154. Hess, K.; Trogus, C., Information about alkali cellulose. *Zeitschrift fur Phisikalische Chemie-Abteilung B-Chemie der Elementarprozesse Aufbau der Materie* **1931,** *11*, 381-408.

155. Sobue, H.; Kiessig, H.; Hess, K., Das System Cellulose–Natriumhydroxyd–Wasser in Abhängigkeit von der Temperatur. *Zeitschrift für Physikalische Chemie* **1939,** *43*, 309-328.

156. Nishimura, H.; Okano, T.; Sarko, A., Mercerization of cellulose. 5. Crystal and molecular structure of Na-cellulose I. *Macromolecules* **1991,** *24*, 759-770.

157. Okano, T.; Sarko, A., Mercerization of cellulose. II. Alkali–cellulose intermediates and a possible mercerization mechanism. *Journal of Applied Polymer Science* **1985,** *30*, 325-332.

158. Okano, T.; Kim, N.-H.; Sugiyama, J., Supermolecular structure of alkali-swollen cellulose. *Cellulose: Structural and Functional Aspects* **1989**, 93.

159. Nishimura, H.; Sarko, A., Mercerization of cellulose. 6. Crystal and molecular structure of Na-cellulose IV. *Macromolecules* **1991,** *24*, 771-778.

160. Hess, K.; Gundermann, J., Über die Einwirkung von flüssigem Ammoniak auf Cellulosefasern (Bildung von Ammoniak-Cellulose I, Ammoniak-Gellulose II und Cellulose III). *Berichte der deutschen chemischen Gesellschaft (A and B Series)* **1937,** *70*, 1788-1799.

161. Barry, A.; Peterson, F.; King, A., X-ray studies of reactions of cellulose in non-aqueous systems. I. Interaction of cellulose and liquid ammonia1. *Journal of the American Chemical Society* **1936,** *58*, 333-337.

162. Hess, K.; Trogus, C., Über Ammoniak-Cellulose (Vorläuf. Mitteil.). *Berichte der deutschen chemischen Gesellschaft (A and B Series)* **1935,** *68*, 1986-1988.

163. Wada, M.; Nishiyama, Y.; Langan, P., X-ray structure of ammonia− cellulose I: New insights into the conversion of cellulose I to cellulose IIII. *Macromolecules* **2006,** *39*, 2947-2952.

164. Clark, G.; Parker, E., An X-ray diffraction study of the action of liquid ammonia on cellulose and its derivatives. *Journal of Physical Chemistry* **1937,** *41*, 777-786.

165. Schweizer, E., Das kupferoxyd - ammoniak, ein auflösungsmittel für die pflanzenfaser. *Journal für praktische Chemie* **1857,** *72*, 109-111.

166. Miyamoto, I.; Matsuoka, Y.; Matsui, T.; Okajima, K., Studies on Structure of Cuprammonium Cellulose II. Structural Change of Cellulose–Cuprammonium Complex as a Function of Hydroxyl Ion Concentration. *Polymer journal* **1995,** *27*, 1123-1131.

167. Sisson, W. A.; Saner, W. R., An X-ray Diffraction Study of the Swelling Action

of Several Quaternary Ammonium Hydroxides on Cellulose Fibers. *Journal of Physical Chemistry* **1939,** *43*, 687-699.

168. Trogus, C.; Hess, K., Concerning Addition Compounds of Cellulose with Hydrazine, Ethylenediamine, and Tetra-methylenediamine. *Z. Physik. Chem.(Leipzig) B* **1931,** *14*, 387-395.

169. Loeb, L.; Segal, L., Studies of the ethylenediamine - cellulose complex. I. Decomposition of the complex by solvents. *Journal of Polymer Science* **1955,** *15*, 343-354.

170. Segal, L.; Nelson, M. L.; Conrad, C. M., Experiments on the Reduction of the Crystallinity of Cotton Cellulose. *The Journal of Physical Chemistry* **1951,** *55*, 325-336.

171. Segal, L.; Nelson, M. L.; Conrad, C. M., Further studies on cotton cellulose with reduced crystallinity. *Textile research journal* **1953,** *23*, 428-435.

172. Creely, J. J.; Segal, L.; Loeb, L., An x-ray study of new cellulose complexes with diamines containing three, five, six, seven, and eight carbon atoms. *Journal of Polymer Science* **1959,** *36*, 205-214.

173. Lee, D. M.; Burnfield, K. E.; Blackwell, J., Structure of a cellulose I–ethylenediamine complex. *Biopolymers: Original Research on Biomolecules* **1984,** *23*, 111-126.

174. Numata, Y.; Kono, H.; Kawano, S.; Erata, T.; Takai, M., Cross-polarization/magic-angle spinning 13C nuclear magnetic resonance study of cellulose I–ethylenediamine complex. *Journal of bioscience and bioengineering* **2003,** *96*, 461-466.

175. Wada, M.; Kwon, G. J.; Nishiyama, Y., Structure and thermal behavior of a

cellulose I− ethylenediamine complex. *Biomacromolecules* **2008,** *9*, 2898-2904.

176. Sawada, D.; Nishiyama, Y.; Petridis, L.; Parthasarathi, R.; Gnanakaran, S.; Forsyth, V. T.; Wada, M.; Langan, P., Structure and dynamics of a complex of cellulose with EDA: insights into the action of amines on cellulose. *Cellulose* **2013,** *20*, 1563-1571.

177. Su, X.; Kimura, S.; Wada, M.; Kuga, S., Stoichiometry and stability of cellulose-hydrazine complexes. *Cellulose* **2011,** *18*, 531-537.

178. Lee, D. M.; Blackwell, J.; Litt, M., Structure of a cellulose II‐hydrazine complex. *Biopolymers: Original Research on Biomolecules* **1983,** *22*, 1383-1399.

179. Sakurada, I.; Hutino, K., Über die intramizellare quellung der zellulose durch wasser. *kolloid-zeitschrift* **1936,** *77*, 346-351.

180. Hermans, P.; Weidinger, A., The hydrates of cellulose. *Journal of Colloid Science* **1946,** *1*, 185-193.

181. Lee, D. M.; Blackwell, J., Structure of cellulose II hydrate. *Biopolymers: Original Research on Biomolecules* **1981,** *20*, 2165-2179.

182. Kobayashi, K.; Kimura, S.; Togawa, E.; Wada, M., Crystal transition from cellulose II hydrate to cellulose II. *Carbohydrate polymers* **2011,** *86*, 975-981.

183. Song, G.; Yu, J.; Ding, M.; Zhang, J., A novel cellulose/ionic liquid complex crystal. *Crystal Growth & Design* **2018,** *18*, 4260-4264.

184. Endo, T.; Yoshida, S.; Kimura, Y., Self-Assembly and Complexation of Cellulose/Ionic Liquid at High Cellulose Concentration: Anion Dependence. *Crystal Growth & Design* **2020,** *20*, 6267-6271.

185. Nishiyama, Y.; Asaadi, S.; Ahvenainen, P.; Sixta, H., Water-induced

crystallization and nano-scale spinodal decomposition of cellulose in NMMO and ionic liquid dope. *Cellulose* **2019,** *26*, 281-289.

186. Jiang, F.; Zhang, X.; Hwang, W.; Nishiyama, Y.; Briber, R. M.; Wang, H., Oligocellulose from acid hydrolysis: A revisit. *Applied Surface Science* **2021,** *537*, 147783.

187. Zhang, X.; Jiang, F.; Mao, Y.; Henderson, D.; Nishiyama, Y.; Briber, R.; Wang, H. In *Oligomeric Cellulose Co-Crystallization with DMSO*, APS March Meeting Abstracts, 2019; 2019; p L70. 160.

188. Warwicker, J.; Wright, A. C., Function of sheets of cellulose chains in swelling reactions on cellulose. *Journal of applied polymer science* **1967,** *11*, 659-671.

189. http://www.microscopyu.com/articles/polarized/polarizedintro.html

190. Malvern Static Light Scattering technologies for GPC - SEC explained.

191. Lesot, P., Vladimir I. Bakhmutov: NMR spectroscopy in liquids and solids. In Springer: 2015.

192. Andrew, E.; Bradbury, A.; Eades, R., NMR spectra recorded from a crystal rotated at high speed. *Nature* **1958,** *182*, 1659.

193. Hill, D. J.; Le, T. T.; Whittaker, A. K., A technique for the quantitative measurements of signal intensities in cellulose-based transformer insulators by 13 C CPMAS NMR. *Cellulose* **1994,** *1*, 237-247.

194. Hess, K.; Trogus, C., Zur Kenntnis der Vorgänge bei der Auflösung von Cellulose in Kupferoxydammoniak. *Zeitschrift für Physikalische Chemie* **1929,** *145*, 401-450.

195. Trogus, C.; Hess, K., Über Additionsverbindungen der Cellulose mit Hydrazin, Äthylendiamin und Tetramethylendiamin. *Zeitschrift für Physikalische Chemie* **1931,**

14, 387-395.

196. Wada, M.; Nishiyama, Y.; Bellesia, G.; Forsyth, T.; Gnanakaran, S.; Langan, P., Neutron crystallographic and molecular dynamics studies of the structure of ammonia-cellulose I: rearrangement of hydrogen bonding during the treatment of cellulose with ammonia. *Cellulose* **2011,** *18*, 191-206.

197. Poumarede, J.; Figuier, L., 'Mémoire sur le ligneux et sur les produits qui l'accompagnent dans le bois'. *Académie des Sciences de Paris* **1846,** *23*, pp. 918-19.

198. Heinrich, F.; Richard, H., Process for the manufacture of solutions of cellulose in sulphuric acid. In Google Patents: 1944.

199. Nishiyama, Y.; Langan, P.; O'Neill, H.; Pingali, S. V.; Harton, S., Structural coarsening of aspen wood by hydrothermal pretreatment monitored by small-and wide-angle scattering of X-rays and neutrons on oriented specimens. *Cellulose* **2014,** *21*, 1015-1024.

200. Nishiyama, Y.; Johnson, G. P.; French, A. D., Diffraction from nonperiodic models of cellulose crystals. *Cellulose* **2012,** *19*, 319-336.

201. Kjällman, T.; Olovsson, I., Hydrogen bond studies. LVIII. The crystal structures of normal and deuterated sulphuric acid tetrahydrate,(H5O2+) 2SO42− and (D5O2+) 2SO42−. *Acta Crystallographica Section B: Structural Crystallography and Crystal Chemistry* **1972,** *28*, 1692-1697.

202. Meader, D.; Atkins, E.; Happey, F., Cellulose trinitrate: molecular conformation and packing considerations. *Polymer* **1978,** *19*, 1371-1374.

203. Beyer, K. D.; Hansen, A. R.; Poston, M., The search for sulfuric acid octahydrate: experimental evidence. *The Journal of Physical Chemistry A* **2003,** *107*, 2025-2032.

204. Kobayashi, K.; Kimura, S.; Togawa, E.; Wada, M., Crystal transition from Na–

cellulose IV to cellulose II monitored using synchrotron X-ray diffraction. *Carbohydrate polymers* **2011,** *83*, 483-488.

205. Liu, X.; Zhou, T.; Wang, X.; Zhang, J., Investigation of selective molecular interactions using two-dimensional Fourier transform IR spectroscopy. *Analytical and bioanalytical chemistry* **2010,** *397*, 339-343.

206. Mikroyannidis, J. A., Synthesis and characterization of nadimidized 1 - [(dialkoxyphosphinyl) methyl1] - 2, 4 - and - 2, 6 - diaminobenzenes and their polymerization to fire - resistant laminating resins. *Journal of Polymer Science: Polymer Chemistry Edition* **1984,** *22*, 3535-3548.

207. Zhang, J. B.; Zhang, P. Y.; Chen, G. H.; Han, F.; Wei, X. H., Photochemical reaction between magnesium tetraphenyl porphyrin and oxygen. *Chinese Chemical Letters* **2008,** *19*, 1190-1192.

208. Bernet, B.; Vasella, A., Intra - and Intermolecular H - Bonds of Alcohols in DMSO, 1H - NMR Analysis of Inter - Residue H - Bonds in Selected Oligosaccharides: Cellobiose, Lactose, N, N′ - Diacetylchitobiose, Maltose, Sucrose, Agarose, and Hyaluronates. *Helvetica Chimica Acta* **2000,** *83*, 2055-2071.

209. Sugiyama, H.; Hisamichi, K.; Usui, T.; Sakai, K., A study of the conformation of β-1, 4-linked glucose oligomers, cellobiose to cellohexaose, in solution. *Journal of Molecular Structure* **2000,** *556*, 173-177.

210. Moulthrop, J. S.; Swatloski, R. P.; Moyna, G.; Rogers, R. D., High-resolution 13C NMR studies of cellulose and cellulose oligomers in ionic liquid solutions. *Chemical communications* **2005**, 1557-1559.

211. Isogai, A.; Usuda, M.; Kato, T.; Uryu, T.; Atalla, R. H., Solid-state CP/MAS

carbon-13 NMR study of cellulose polymorphs. *Macromolecules* **1989,** *22,* 3168-3172.

212. Horii, F.; Hirai, A.; Kitamaru, R.; Sakurada, I., Cross-polarization/magic-angle spinning 13C NMR studies of cotton and cupra rayon with different water contents. *Cellulose chemistry and technology* **1985,** *19,* 513-523.

213. Idström, A.; Schantz, S.; Sundberg, J.; Chmelka, B. F.; Gatenholm, P.; Nordstierna, L., 13C NMR assignments of regenerated cellulose from solid-state 2D NMR spectroscopy. *Carbohydrate polymers* **2016,** *151,* 480-487.

214. Zuckerstätter, G.; Terinte, N.; Sixta, H.; Schuster, K. C., Novel insight into cellulose supramolecular structure through 13C CP-MAS NMR spectroscopy and paramagnetic relaxation enhancement. *Carbohydrate polymers* **2013,** *93,* 122-128.

215. Kita, Y.; Kusumi, R.; Kimura, T.; Kitaoka, M.; Nishiyama, Y.; Wada, M., Surface structural analysis of selectively 13 C-labeled cellulose II by solid-state NMR spectroscopy. *Cellulose* **2020,** *27,* 1899-1907.

216. Cordell, D.; Neset, T.-S., Phosphorus vulnerability: a qualitative framework for assessing the vulnerability of national and regional food systems to the multi-dimensional stressors of phosphorus scarcity. *Global Environmental Change* **2014,** *24,* 108-122.

217. Montañés, F.; Olano, A.; Ibáñez, E.; Fornari, T., Modeling solubilities of sugars in alcohols based on original experimental data. *AIChE journal* **2007,** *53,* 2411-2418.

218. Torchia, D. A., The measurement of proton-enhanced carbon-13 T1 values by a method which suppresses artifacts. *Journal of Magnetic Resonance (1969)* **1978,** *30,* 613-616.

219. Buleon, A.; Chanzy, H., Single crystals of cellulose IVII: preparation and

properties. *Journal of Polymer Science: Polymer Physics Edition* **1980,** *18*, 1209-1217.